ACETYLENIC TETRATHIAFULVALENES AND RELATED MACROCYCLIC SYSTEMS

GUANG CHEN

Acetylenic Tetrathiafulvalenes and Related Macrocyclic Systems

by

A thesis submitted to the

School of Graduate Studies

in partial fulfilment of the

requirements for the degree of

Doctor of Philosophy

Department of Chemistry

Memorial University of Newfoundland

April 2011

St. John's Newfoundland

Abstract

This thesis reports the study of a series of novel acetylenic π-extended tetrathiafulvalene derivatives (exTTFs). The detailed research is divided into two major projects. In the first project, acetylenic anthraquinoid-type exTTFs (referred to as TTFAQs) were synthesized and characterized. The target compounds have rigid macrocyclic enyne conjugated π-frameworks which can be constructed by a one-pot, 4-fold Sonogashira coupling strategy. The molecules show interesting solid-state stacking in single crystals, and rich electronic and redox properties as characterized by UV-vis and fluorescence spectroscopy, cyclic voltammetry, and spectroelectrochemistry. In the second project, a series of acetylenic tetrathiafulvalene vinylogues (TTFVs) and their structural analogues, oligoyne-derived TTFs, were synthesized and studied. Two routes are explored for the selective formation of macrocyclic TTFV and acyclic TTFV oligomers. Electronic and redox properties of these molecules were characterized by various instrumental analyses. Oligoyne-TTFs undergo electropolymerization to form stable TTFV-containing polymer films which show electrochromic behavior. Solid-state reactivity of oligoyne-TTFs were studied by differential scanning calorimetric and thermogravimetric analysis. Finally, in a side project, a series of TTFV-centered tweezer-like molecules and TTFV-crown ether hybrids were designed and synthesized as supramolecular hosts for [60]fullerene and metal cations.

Acknowledgements

I would like to express sincere thanks to my supervisor, Prof. Yuming Zhao, for his inspirational guildance, generous help, and constant encouragement during my graduate program at Memorial University. His broad knowledge, creative ideas, and amiable personality set up an excellent example of an extraordinary young scientist from which I have learnt a lot and which I will never forget.

I would also like to thank Prof. Peter Pickup and Prof. Christina Bottaro for being my supervisory committee members and giving me helpful suggestions.

I would like to further express my heartful thanks to my collaborators, Dr. Ilias Mahmud and Mr. Stephan Bouzan for their support in parts of the synthetic work, Prof. David Thompson and Dr. Li Wang for helpful discussions on photochemical properties of some compounds, and Prof. Louise Dawe for nicely solving single crystal structures. Special thanks are given to Mrs. Linda Winsor and Mrs. Lidan Tao for mass spectrometric analysis.

I would like to extend my thanks to all the professors and staff in the Department of Chemistry, Memorial University, especially professors from the organic chemistry division, Prof. Graham Bodwell, Prof. Paris Georghiou and Prof. Sunil Pansare, for their kind help during my study.

Last but not the least, I would like to thank my parents and my wife. Their love, encouragement and support are very important to my success.

Contents

List of Figures

List of Schemes

List of Tables

List of Abbreviations and Symbols

A	acceptor
Å	angstrom
APCI	atmospheric pressure chemical ionization
aq	aqueous
Bu	butyl
BEDT-TTF	bis(ethylenedithio)terathiafulvalene
ca	circa
calcd	calculated
CBPQT	cyclobis(paraquat-*p*-phenylene)
cm	centimeter
CPE	controlled potential electrolysis
C-S	charge-separated
CV	cyclic voltammetry

D	donor
d	doublet
D-A	donor-acceptor
DBU	1,8-diazabicyclo[5.4.0]undec-7-ene
DDQ	2,3-dichloro-5,6-dicyanobenzoquinone
dec	decomposed
DMF	N,N-dimethyl formamide
DMS	dimethyl sulfate
DNA	deoxyribonucleic acid
DPV	differential pulse voltammetry
DSC	differential scanning calorimetry
DTF	dithiafulvene
E_g	bandgap energy
Et	ethyl
exTTF	π-extended tetrathiafulvalene
FTIR	Fourier transform infrared
g	gram(s)

h	hour(s)
HOMO	highest occupied molecular orbital
HQ	hydroquinone
HRMS	high resolution mass spectrometry
HRP	horseradish peroxidase
HWE	Horner-Wadsworth-Emmons
IR	infrared
ITO	indium tin oxide
J	coupling constant
LCMS	liquid chromatography-mass spectrometry
LDA	lithium diisopropylamide
LUMO	lowest unoccupied molecular orbital
m	multiplet
m/z	mass to charge ratio
mA	milliampere
MALDI-TOF	matrix assisted laser desorption/ionization–time of flight
Me	methyl

mg	milligram(s)
MHz	megahertz
min	minute(s)
mL	milliliter
mmol	millimole
mol	mole
m.p.	melting point
MS	mass spectrometry
mW	milliwatt
MWNT	multi-walled carbon nanotubes
NLO	nonlinear optical
nm	nanometer
NMR	nuclear magnetic resonance
NP	naphthalene
ns	nanosecond
ODCB	*ortho*-dichlorobenzene
OFET	organic field effect transistor

p	*para*
PAE	poly(*p*-aryleneethynylene)
PCC	pyridinium chlorochromate
Ph	phenyl
ppm	parts per million
PVC	polyvinyl chloride
rbf	round-bottom flask
s	second or singlet
satd	saturated
S/D	source/drain
SWNT	single-walled carbon nanotubes
t	triplet
TBABr	tetra-*n*-butylammonium bromide
TBAF	tetra-*n*-butylammonium fluoride
T_c	superconducting transition temperature
TCNE	tetracyanoethylene
TCNQ	tetracyanoquinodimethane

TGA	thermogravimetric analysis
THF	tetrahydrofuran
TIPS	triisopropylsilyl
TLC	thin-layer chromotography
TMEDA	tetramethylethylenediamine
TMS	trimethylsilyl
TMSA	trimethylsilylacetylene
TNB	1,3,5-trinitrobenzene
TNP	2,4,6-trinitrophenol
TNT	2,4,6-trinitrotoluene
TTF	tetrathiafulvalene
TTFAQ	antraquinoid-type tetrathiafulvalene
TTFV	tetrathiafulvalene vinylogue
UV-Vis	ultraviolet-visible
UV-Vis-NIR	ultraviolet-visible-near infrared
V	volt
XRD	X-ray diffraction

δ	chemical shift
λ_{em}	maximum emission wavelength
λ_{max}	maximum absorption wavelength

Chapter 1

Introduction

1.1 A Brief Overview of Tetrathiafulvalene and π-Extended Tetrathiafulvalene Derivatives

1.1.1 Structures of Tetrathiafulvalenes

Tetrathiafulvalene (TTF) is a sulfur-containing heterocyclic compound, the structure of which consists of two 1,3-dithiole rings connected via a carbon-carbon double bond. Structure **1** shown in Figure 1.1 is the simplest TTF, from which much more complex TTF analogues can be derived by expanding its π-conjugated molecular skeleton.

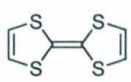

1

Figure 1.1: Structure of tetrathiafulvalene.

π-Extended TTFs (exTTFs) generally refer to larger TTF analogues with various

conjugated moieties attached to either the side chain positions or placed in between the two dithiole rings. For example, compounds **2-4** in Figure 1.2 illustrate exTTFs with fused aromatic structures on the side chain positions of dithiole rings,[1–6] and compounds **5-8** are exTTFs containing different $\pi-$bridges between the two dithiole rings of TTF.[7–10]

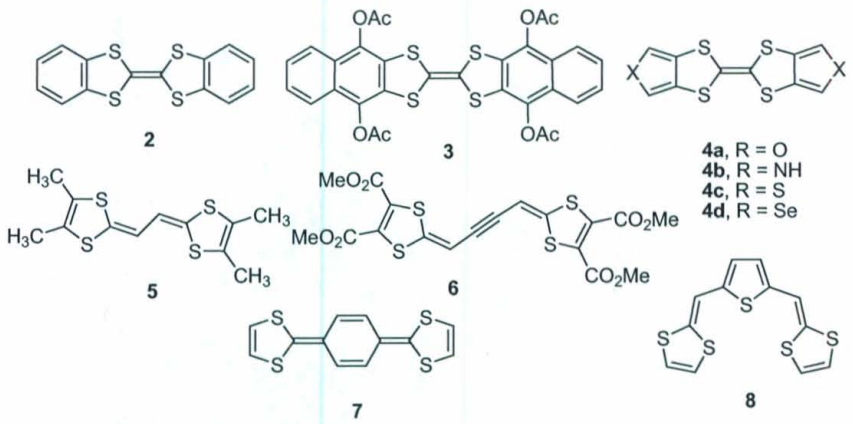

Figure 1.2: Selected structures of π-extended tetrathiafulvalenes.

1.1.2 General Properties of TTFs

TTFs and exTTFs are well known for their excellent electron donating abilities that stem from the remarkable stability of their oxidized cationic products. Unsubstituted TTF **1** can readily donate up to two electrons through two successive reversible single-electron transfer processes, with $E^{\circ}_{1ox} = 0.34$ V, $E^{\circ}_{2ox} = 0.78$ V vs Ag/AgCl in MeCN.[11] The dithiole ring of TTF upon oxidation becomes a 6-π electron aromatic system, and the gained aromaticity greatly stabilizes the resulting cationic and dicationic species. The second oxidation potential (E°_{2ox}) of TTF is higher than the first one (E°_{1ox}). This is partially due to the destabilizing Coulombic repulsion between the

two close-lying positive charges in the dications $[TTF]^{2+}$ (Scheme 1.1). For TTF derivatives featuring a sufficient degree of electron delocalization through extended $\pi-$conjugated frameworks, the Coulomb repulsion however can be effectively reduced. As a result, the gap between the two oxidation potentials may decrease or even reverse due to the enhanced stability of the TTF dication. For instance, the second oxidation of exTTF **9** (Figure 1.3) was found to be so much easier than the first oxidation step that **9** actually underwent a simultaneous two-electron transfer upon oxidation. Such electrochemical behavior, referred to as the "inverted potential" scenario, is a commonly seen property among numerous exTTFs. The electron donating property of a substituted TTF is also significantly affected by the nature of its substituent groups. As a general trend, an electron-withdrawing substituent would reduce the electron-donating ability of TTF, therefore resulting in increased oxidation potentials, and vice versa for an electron-donating group.[12] The electronic substitution effect thus offers a useful approach to finely tune the electronic properties of TTFs to be suitable for device applications.

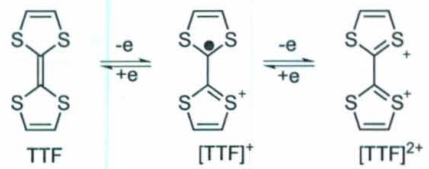

Scheme 1.1: Stepwise two-electron oxidation of unsubstituted TTF.

1.1.3 Recent Applications of TTFs

TTFs have found many applications, most of which are based on their electron donating abilities. In the latter part of this section, an overview of these applications

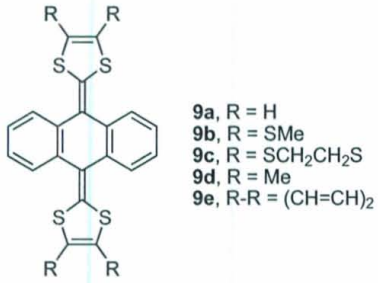

Figure 1.3: Examples of exTTFs bearing an anthraquinoid central unit.

is given with the emphasis on the most recent breakthroughs. The purpose of this section is to show the broad applications of TTF that are enabled and benefited from rational molecular design and engineering.

1.1.3.1 Applications of TTFs in Organic Conductors and Superconductors

The first and most important application of TTFs is in the field of organic conductors and superconductors. As early as 1972, the first organic conductor $[TTF]^{+}Cl^{-}$ was reported by Wudl.[13] In the solid structure of this charge-transfer salt, the π-donors (TTFs) had their central double bonds effectively stacked to allow sufficient intermolecular orbital interactions. This salt was found to show metallic electrical conductivity along the direction of molecular stacking. In the following year, another remarkable charge-transfer compound, TTF-TCNQ (TCNQ stands for tetracyanoquinodimethane), was reported to exhibit a high conductivity value of ca. 400 S cm^{-1} at room temperature.[14] In the TTF-TCNQ complex, delocalized electrons were readily generated by intermolecular charge transfer from TTF to TCNQ, which accounted for the excellent conductivity of the materials.[15] Since then, a large number of TTF-based organic metals have been synthesized and some of

them have shown superior superconductivity.[16] One excellent example is κ-(BEDT-TTF)$_2$Cu(N(CN)$_2$)Cl (BEDT-TTF stands for bis(ethylenedithio)terathiafulvalene). First discovered in 1990, this material still holds the record of highest transition temperature T_c = 12.8 K at ambient pressure.[17] Nowadays, TTF-based conductors and superconductors are still topics of active and growing research interest. Besides single crystals of charge transfer complex,[18–20] TTF-based materials prepared in other micromorphologies such as thin films,[21–23] organogels,[24] oligomers,[25] polymers,[26–28] and neutral coordination polymers[29] have also been found to show conductivity or superconductivity upon doping. In general, the conductivity of a solid material can be improved by facilitating charge carrier generation. For TTF-based materials, this can be achieved by lowering the energy gap between the TTF donor and associated acceptor units. In addition, the formation of conduction path within the solid also plays a critical role in affecting conductivity.[30] In this light, optimal molecular solid-state packing that allows for efficient intermolecular overlap of π or d orbitals is often desirable. Molecular structural tailoring and modification therefore present an important and indispensable approach for tuning the conductivity of TTF-based materials. Some examples of TTF-based molecular and macromolecular conductors are given in Figure 1.4.

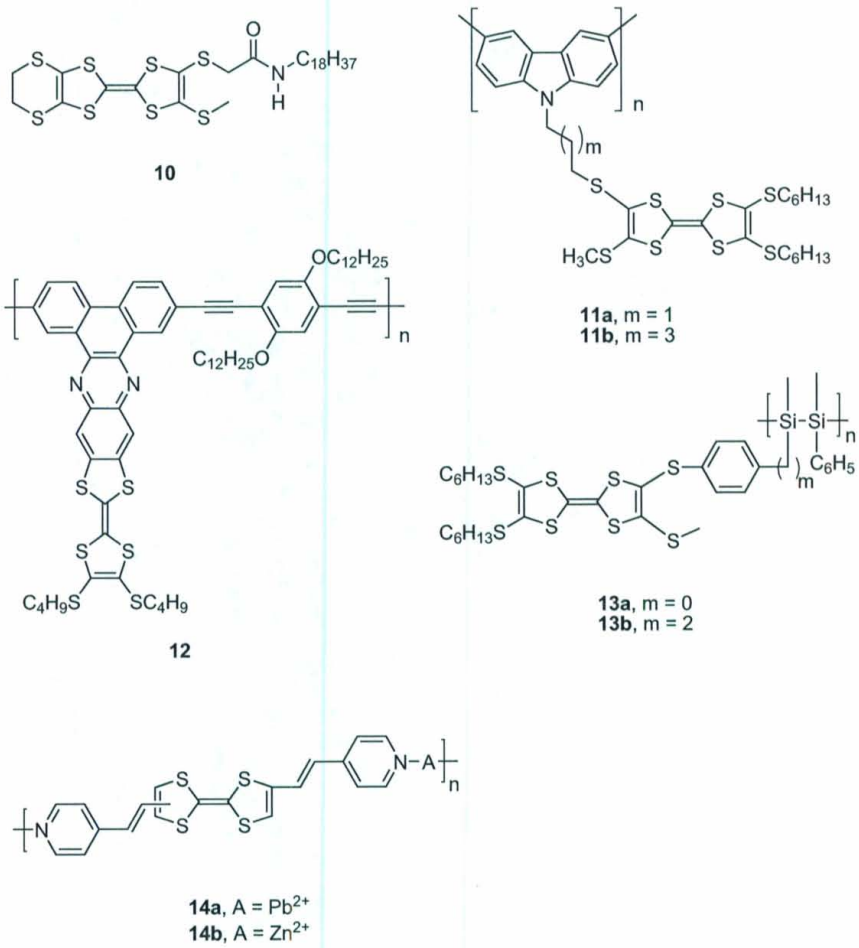

Figure 1.4: Selected examples of TTFs showing conductivity or superconductivity.

1.1.3.2 Applications of TTFs in Organic Field Effect Transistors

TTF and derivatives have been frequently employed as the active components in organic field effect transistors (OFETs), mostly acting as *p*-type semiconductors.[31–34] In contrast to the properties needed for conductors, less efficient intermolecular interactions is a prerequisite for TTF materials in OFETs in order to retain semiconductivity. For example, benzene-fused bis(tetrathiafulvalene) **15** with 2-ethylhexyl chains (see Figure 1.5) was used as the *p*-channel semiconductors in a solution-processed OFET.[32] The device achieved a mobility of 5.6×10^{-4} $cm^2V^{-1}s^{-1}$ with an on/off ratio of 1.6×10^4. The presence of branched alkyl chains in **15** was believed to contribute to the excellent OFET performance, since they led to reduced conductivity of the thin flim by prohibiting tight intermolecular packing and enhanced solubility (processability). In 2009, Roncali studied a series of TTFs with different spacers, including *N*-methylpyrrole, furan, thiophene, and *meta*- or *para*-phenylene linkages.[33] It was reported that the TTF bearing a *meta*-phenylene spacer gave the highest mobility and on/off ratio. Such a good performance was ascribed to the spacer effects that modulated the vertical self-assembly of molecules and increased the first oxidation potential of the TTF. TTFs have also been used as source/drain (S/D) electrodes in OFETs.[35,36] It was demonstrated that organic bottom-contact transistors using TTF-TCNQ with metallic conductivity as S/D electrodes provided smaller contact resistance and larger overall mobility by more than one order of magnitude than those using Au electrodes.[35]

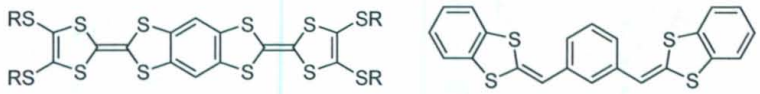

15 R = 2-ethylhexyl **16**

Figure 1.5: Two TTF derivatives that have found use in the fabrication of high performance OFETs.

1.1.3.3 Applications of TTFs in Plastic Solar Cells

TTFs are good candidates for making solar cell materials as well.[37] One way to increase the efficiency of solar energy conversion is to generate a stabilized charge-separated (C-S) state upon light irradiation in a donor-acceptor system. TTFs are suitable electron donors for this purpose because they can be easily oxidized, and the resulting cations and dications are stabilized by aromaticity. Upon interaction with a suitable acceptor such as C_{60}, facile charge transfer from TTF to the acceptor unit can be promoted by photon excitation, generating stabilized radical ion pairs. This is the basic working principle for TTF-based organic solar cells. To achieve long-lived photoinduced C-S states, tuning of the linkers between the acceptor and TTF groups is a molecular approach frequently sought after in order to decelerate charge recombination that follows photoinduced charge separation. In addition to prolonged lifetime of charge-separated species, sufficiently high charge transfer mobility is another important factor governing the performance of organic solar cells. With the high mobilities observed in TTF-based OFETs, it is widely believed that TTF-based donor materials should facilitate the active layer of organic solar cell to attain good charge transfer mobility.

There have been a large number of TTF-based donor-acceptor materials developed

for solar cell fabrication. Among them the TTFAQ-C_{60}/NT system has recently attracted enormous interest and it is discussed at length in Section 1.2. Herein we first focus on several representatives of TTF-based D-A molecular and macromolecular systems that have been extensively investigated as solar cell materials in recent years. In 2007 a TTF-C_{60}-TTF triad **17** (Figure 1.6) was reported.[38] The structure of **17** is composed of a pyrozoline-attached C_{60} acceptor and two TTF donors connected via amide linkages. This compound was characterized with a very fast photoinduced C-S rate ($> 3.8 \times 10^9$ s^{-1}) and a high efficiency ($\Phi > 0.85$). In addition, the C-S state was remarkably stable with a lifetime of 230 ns in CH_2Cl_2. It was suggested that the pyrozoline ring participates in the photoinduced electron transfer process and accounts for its much longer lifetime than other analogous TTF-C_{60}-TTF triads. TTF-based polymers have also found usefulness in solar cell devices. For example, polymer TTF-PAE **18** shown in Figure 1.6 (where PAE refers to poly(*p*-aryleneethynylene)s) was designed to exhibit enhanced photovoltaic properties.[39] The conjugated PAE backbone of **18** acted as electron acceptor, while the coplanarity of the main chain with TTF side groups allowed continuous π-stacking between molecules. This molecular design motif appears to be significantly advantageous over other types of TTF-fused polymers .

1.1.3.4 Applications of TTFs in Chemical Sensors

TTFs have been widely used in the field of chemical sensing, either functioning as electron mediators[40–44] or as agents to translate binding events into detectable signals such as UV-Vis absorption and fluorescence spectral changes or electrochemical responses.[45] For example, a TTF-TCNQ/MWNT modified Au electrode immobilized

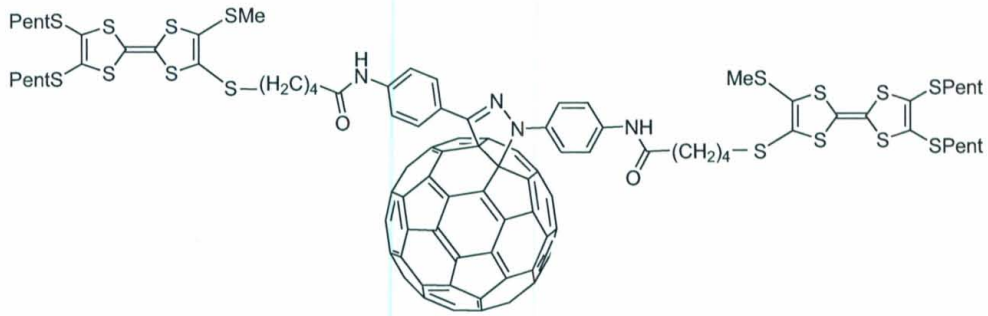

17

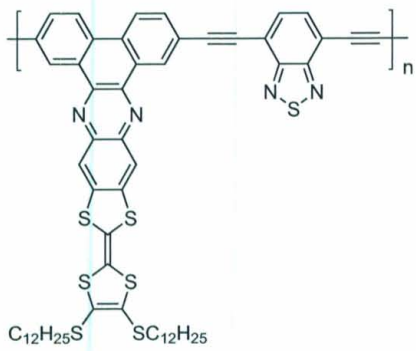

18

Figure 1.6: Two examples of TTF derivatives for solar cell applications.

with horseradish peroxidase (HRP) was used for the detection of H_2O_2 at 0 V.[41] TTF-TCNQ served as an electron mediator to facilitate the electron transfer from the active centre of HRP to the electrode, thus catalyzing the reduction of H_2O_2 by HRP. Taking advantage of the electrocatalytic beahaviors of TTF-TCNQ, a PVC/TTF-TCNQ (PVC, polyvinyl chloride) composite electrode was fabricated for simultaneous detection of ascorbic acid and uric acid in a flow injection system.[42]

TTF-based chemosensors generally consist of various receptor groups linked to TTF unit(s). The receptor is capable of binding to analytes of interest in a selective manner, while the binding event induces detectable changes in the electronic properties of the TTF core.[46] For example, crown ether appended TTFs **19** and **20** in Figure 1.7 were found to show good sensing properties for Pd^{2+}.[47] In these molecules, the crown ether moieties acted as metal receptors, and they communicated with the TTF cores via conjugated linkages. When the binding event occurred, two types of signals would be translated. First, the binding of Pd^{2+} with the crown ether increased its electron accepting ability, leading to an observable redshift of the charge-transfer band in the UV-Vis absorption spectrum. Second, the electron density on the TTF core was decreased, which resulted in a positive shift of the first oxidation potential. The second oxidation potential was shifted as well because the binding metal ion was not released by repulsion from the TTF cation due to the remoteness of the binding site.

Aside from cation sensors, TTF-based anion sensors have also been developed. Calix[4]arene is a commonly employed anion receptor to be combined with TTF units, for example, compounds **21-24** in Figure 1.8.[48] In these sensors, the rigid molecular structure of calix[4]arene allows for preorganization of TTF side chains

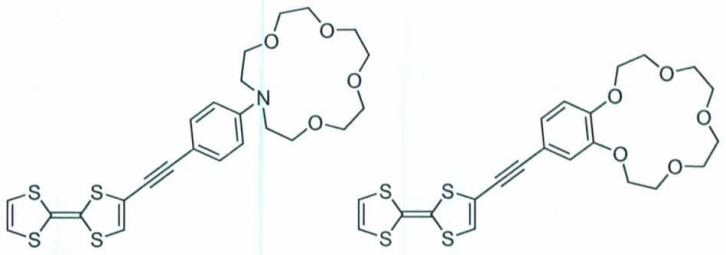

19 20

Figure 1.7: TTF-crown ether hybrids as cation sensors.

that work together with the calix[4]arene to produce a suitable cavity for selective binding. Moreover the amide linker groups were designed to effect H-bonding to enhance affinity for anions. Nevertheless, only compound **21** showed electrochemical sensory behavior for anions, whereas the other molecules did not afford significant cyclic voltammetric (CV) changes on binding with anions. It was reasoned that the intramolecular H-bonds taking place in compound **22** and **24** hindered their binding with anions, and the molecular rigidity of compounds **23** and **25** disfavored anion binding as well.

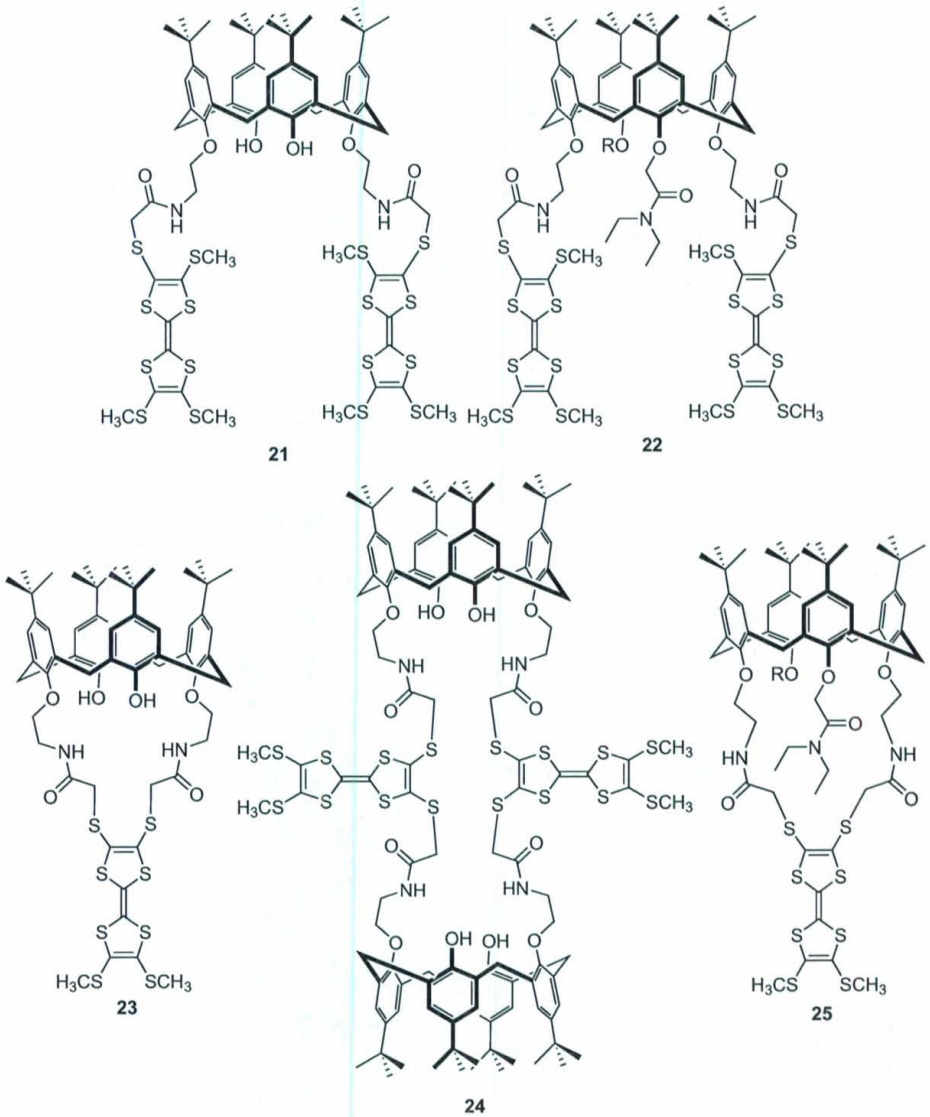

Figure 1.8: Examples of TTF-calix[4]arenes as anion sensors.

TTFs are also useful building components in the design of sensors for neutral compounds and supramolecules. For instance, TTFs bearing a calix[4]pyrrole receptor was found to show good sensory performance for nitroaromatic explosives including 1,3,5-trinitrobenzene (TNB), 2,4,6-trinitrophenol (TNP), and 2,4,6-trinitrotoluene (TNT).[49] The calix[4]pyrroles in compounds **26** and **27** (Figure 1.9) formed defined cavities with annulated TTF subunits as binding pockets. Two non-covalent forces are operative in binding with nitroaromatic analytes: (1) H-bonding interactions effected by the pyrrolic N-H protons, and (2) extra π surfaces provided by annulated aromatic systems on the TTF side chains. The complexation of the TTF-calix[4]pyrroles with nitroaromatic compounds led to a dramatic color change that was observable by the naked eye. Recently, TTFs were applied to DNA sensing. For example, a TTF-anthracene **28** encapsulated SWNT nanocomposite was found to adsorb DNA to give electrochemical sensing properties.[50]

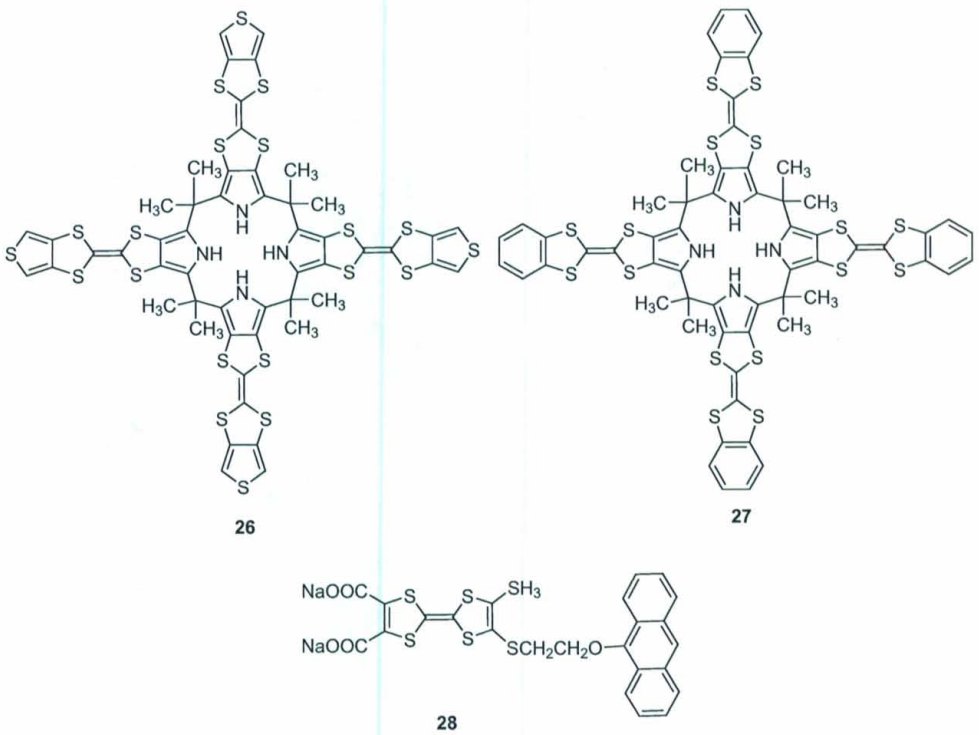

Figure 1.9: Structures of TTFs capable of sensing neutral analytes.

1.1.3.5 Applications of TTFs in Redox-Controlled Molecular Switches

TTFs are important building blocks for the construction of redox-controlled molecular switches, owing to their excellent redox behaviors and readily tunable electronic properties.[51–53] First, most TTFs show reversible redox properties, a must for the stability of redox switches. Second, different oxidation states of TTFs can be produced by either chemical or electrochemical means, allowing for two convenient approaches to exert inputs. Third, TTFs in different oxidation states exhibit different electronic properties, which in turn affords straightforward output signals such as UV-Vis absorption, fluorescence, and conductivity. Of particular interest is that in numerous cases TTFs in different oxidation states were found to exhibit very prominent electrochromic effects, such that the dramatic color changes became visibly detectable. Figure 1.10 lists a few selected structures of TTF-based molecules displaying intriguing redox switching properties. For instance, compound **33** was attached to the surfaces of metal electrodes via the terminal thiolacetyl anchors. The conductance of this molecule was measured to be high at low voltage with significant dependence on the oxidation state of TTF. In 2009, a type of TTF-porphyrin based redox fluorescent switch was reported.[54] In the neutral state, the fluorescence of the porphyrin units was almost quenched by electron transfer from TTF to porphyrin. Upon oxidation this electron transfer process was attenuated and the fluorescence of the porphyrin was hence restored.

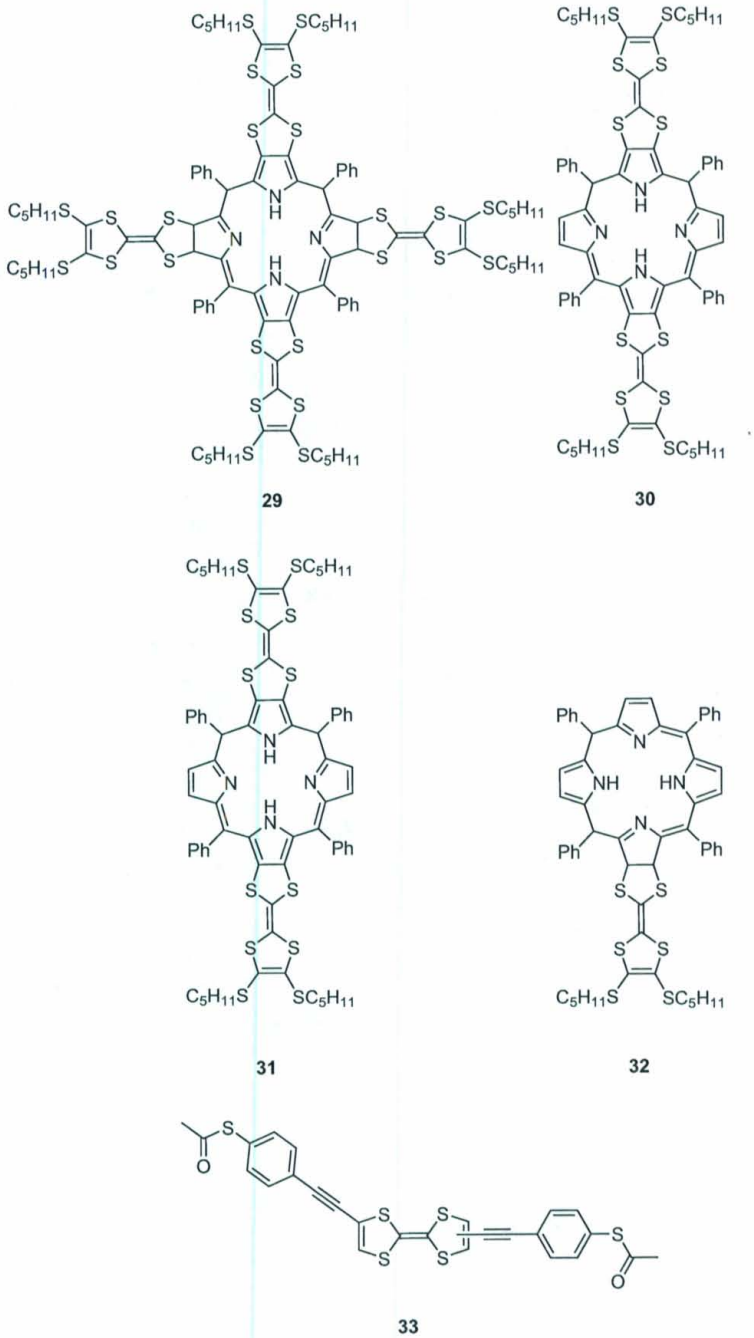

Figure 1.10: Examples of TTF-based redox-controlled molecular switches.

The input/output windows of TTF-based redox switches can be further expanded when TTF cores in different oxidation states interact with other molecules. A three-pole supramolecular switch was devised in 1999, which showed three stages controllable by different voltage inputs.[55] As shown in Figure 1.11, in the neutral state, TTF was bound to $CBPQT^{4+}$ (CBPQT, cyclobis(paraquat-*p*-phenylene)) by charge-transfer and $\pi - \pi$ interactions. Upon oxidation to the radical cation, TTF was released as a free species due to electrostatic repulsion. When further oxidized to the dication, TTF complexed with the cation receptor–crown ether 1/5DN38C10. The three stages shown in Figure 1.11 were associated with distinct colors and the system was therefore proposed to be useful in electrochromic display devices.

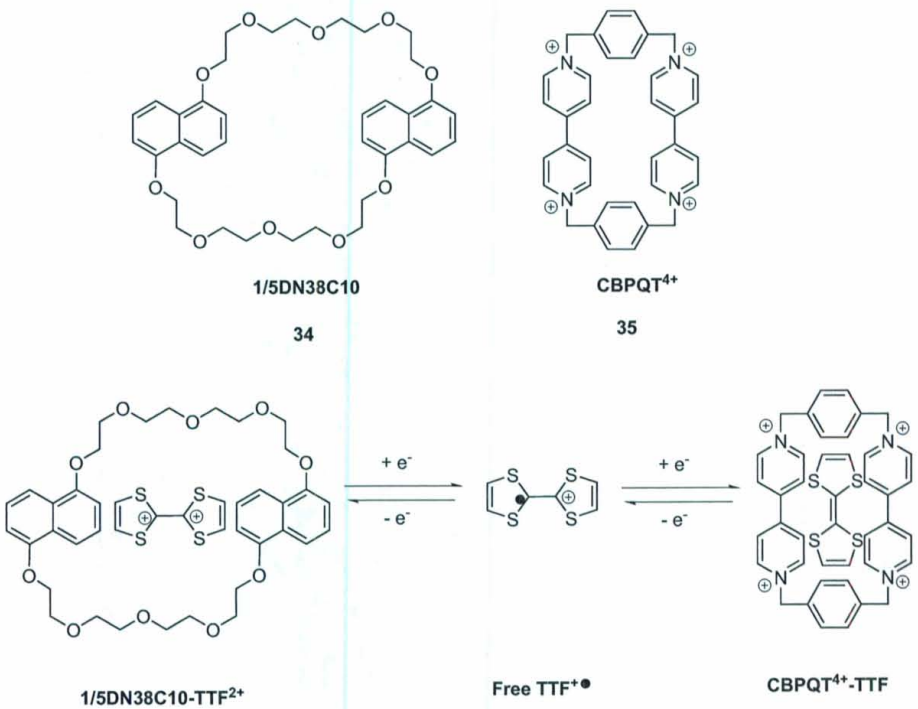

Figure 1.11: Mechanism of a three-hole TTF redox switch.

TTF-based redox switches can also be used as the integral components for various molecular machines, especially the "shuttle-like" devices.[56–58] In general, such systems require three essential parts to be functional–a ring component and two stationary platforms. Figure 1.12 shows a number of examples of molecular machines containing TTF as the active unit. Of these compounds, the ring component is a cyclic compound that can move along the molecular axis, such as $CBPQT^{4+}$ or β-cyclodextrin.[58] The two stationary platforms show affinity for the ring component through non-covalent forces. One of them is TTF which interacts strongly with the ring component in the neutral state; however, the attraction can be reversed to repulsion when TTF is oxidized. Another stationary part is usually an aromatic group that is less susceptible to oxidation; for example, naphthalene (NP), hydroquinone (HQ), or triazole. Such a group can also attract the ring component through $\pi-$stacking, but not as strongly as does the neutral TTF. The mechanism of these machines is as follows. In the neutral stage, the electron deficient ring component $CBPQT^{4+}$ prefers to be associated with the strong electron donor TTF. The binding is evident by the observation of a low energy charge transfer band in the UV-Vis spectrum. When TTF is oxidized, the coulombic repulsion between the TTF cation and $CBPQT^{4+}$ ring moves the ring away from the TTF and relocates it to the other stationary site. This process is accompanied by a high energy charge transfer band. When TTF is reduced, the system returns to its original state. Despite the straightforward mechanism, in real molecular designs there are still many other factors that need to be considered. The first factor is the rigidity of the molecular structure. Although a rigid system can reduce the complex conformers arising from flexible structures,[57] it may also prevent the movement of the ring component.[59,60] If such is the case, the machine will fail to

function properly. Another factor that should be considered is the relative strengths of possible interactions within the system. Sometimes an undesired interaction could overwhelm the interaction between the TTF and the ring component.[61] Secondary and tertiary structures of the systems also impose critical effects. For example, the molecular machine **36** with power systems installed failed to work.[62] Although porphyrin-C_{60} was supposed to generate oxidized TTF species via charge transfer upon photoexcitation, complete oxidation of TTF was hindered presumably due to the shielding by surrounding units. Molecular machines with electrical bistability have also been reported in the recent literature.[63] Representative examples are given in Figure 1.13.

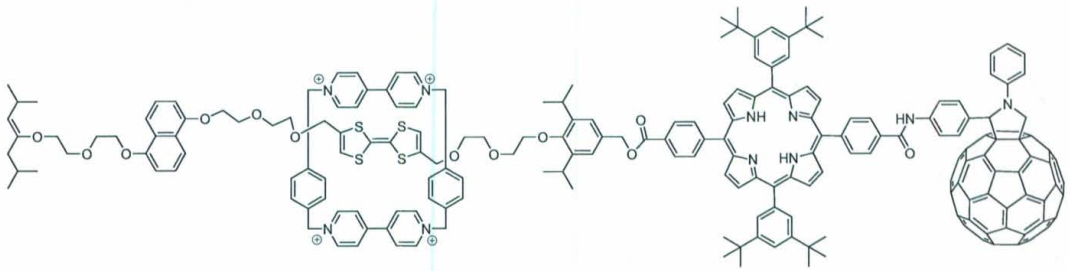

36

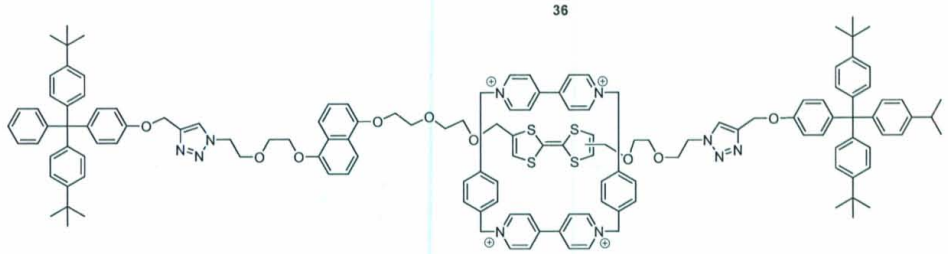

37

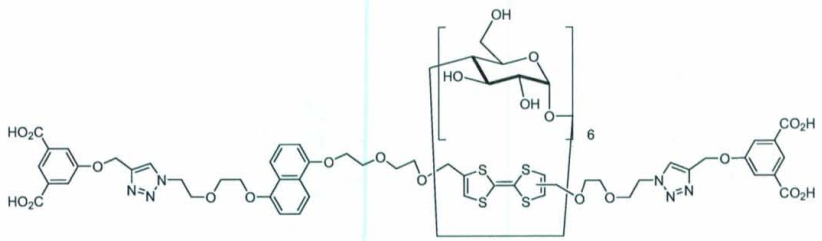

38

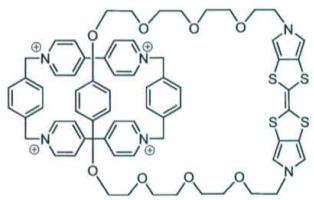

39

40

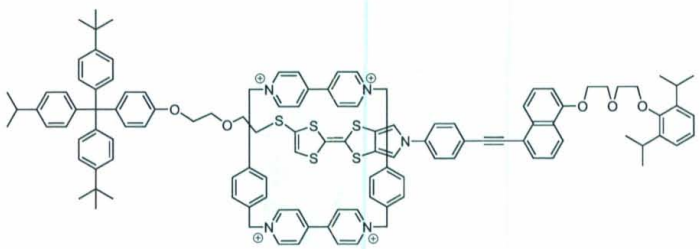

41

Figure 1.12: Examples of TTF-based molecular machines.

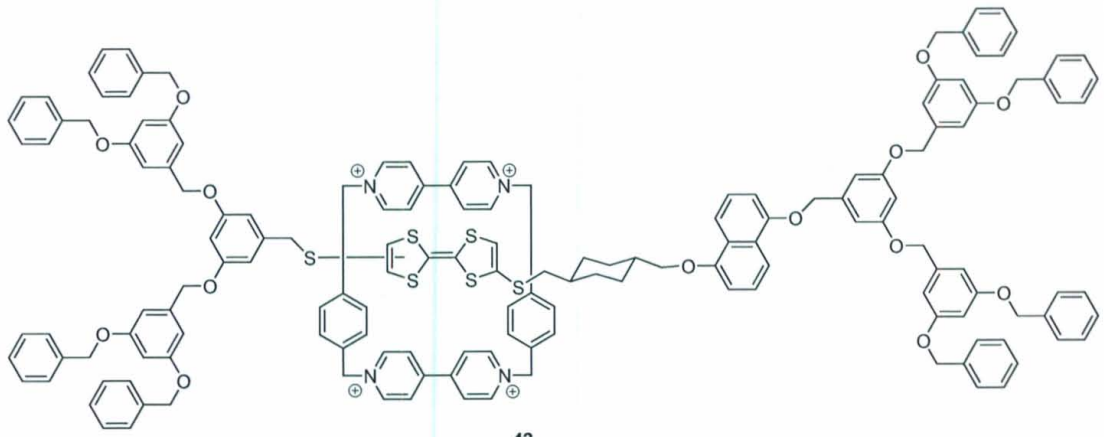

42

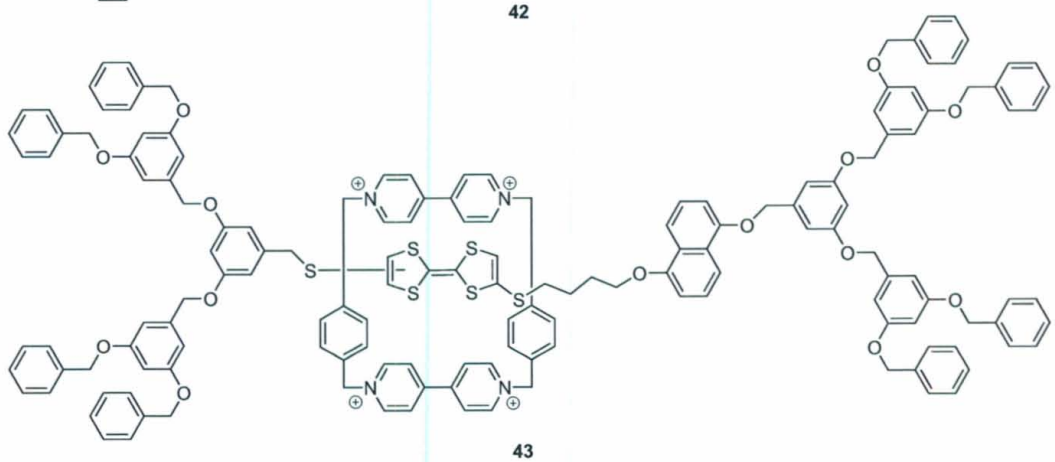

43

Figure 1.13: TTF molecular machines with electrical bistability.

1.1.3.6 Applications of TTFs in Other Fields

In addition to the applications discussed above, TTFs have also been used in other fields of materials science, such as magnetic materials,[64,65] nonlinear optical materials,[66,67] liquid crystals,[68,69] metal ligands,[70–72] MALDI matrix,[73] and so on. In order to meet the different requirements for various applications, the molecular structures of TTFs have to be tailored and modified flexibly and diversely. Thanks to the great effort of synthetic chemists over the past decades, a large number of synthetic methods have become available for the preparation of various TTF-based molecular and macromolecular structures.

1.2 Synthesis Methods for TTF and TTF Derivatives

Briefly speaking, the synthesis of TTFs falls into two catagories: (i) the synthesis of simple TTFs and exTTFs with conjugated extension on the side chain position of dithiole rings, and (ii) the synthesis of exTTFs with conjugated spacers between two dithiole rings. For the first type of synthesis, the construction of the TTF moiety is the key. This topic has been reviewed in several articles,[74–76] while the general synthetic routes for the TTF skeleton and the two important precursors, thione and dithiolium salt, are summarized in Schemes 1.2 and 1.3.

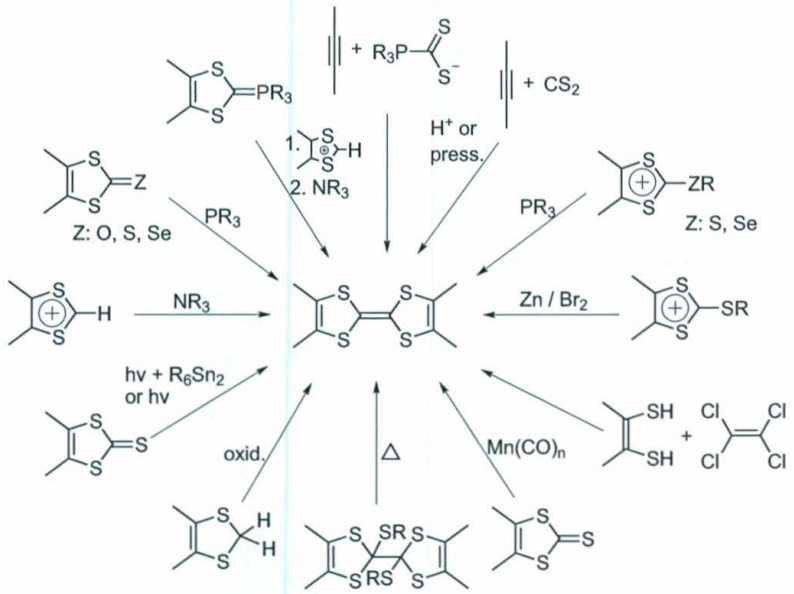

Scheme 1.2: Synthetic methods for preparing the TTF skeleton (adapted from reference 65).

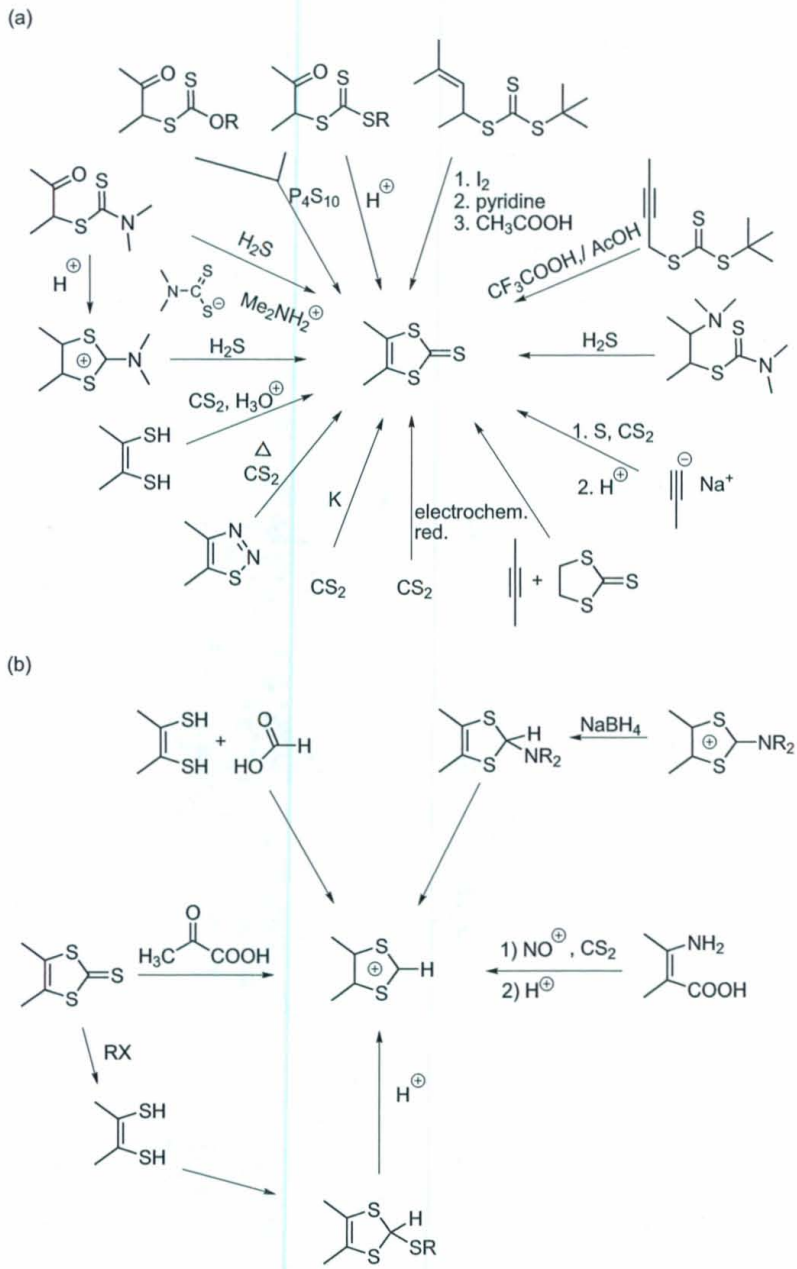

Scheme 1.3: Synthetic methods for (a) thione and (b) dithiolium salt (adapted from reference 65).

Among the numerous synthetic routes for the construction of simple TTF cores, three methods are most popular as summarized in Scheme 1.4: (a) phosphate-promoted coupling of thiones **44**, (b) base-catalyzed coupling of dithiolium salts **45**, and (c) coupling reaction between a dithiolium salt **45** and ylide **46** or phosphonate **47** in the presence of a strong base. In general, methods (a) and (b) are suitable for preparing symmetrical TTFs, while method (c) is particularly efficient in synthesizing unsymmetrical TTFs. It is worth noting that cross coupling of a mixture of 1,3-dithiole-2-thiones and 1,3-dithiole-2-ones with different substituents in neat triethylphosphate can afford the unsymmetrical product in good yields, such as those demonstrated in Scheme 1.5.[77]

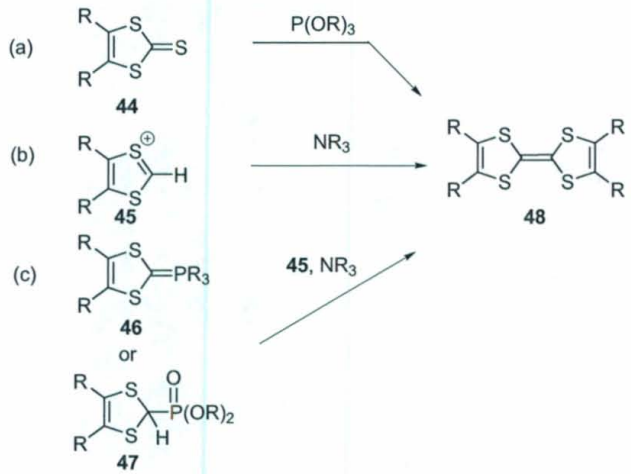

Scheme 1.4: Three important synthetic routes to TTF.

Scheme 1.5: Asymmetrical coupling in neat triethylphosphate.

The precursor thione **44** can be prepared on a large scale from readily available CS_2 and alkali metals such as K or Na (Scheme 1.6) This method was developed by Hoyer's group in 1979.[78] Reduction of CS_2 with K or Na produced 1,3-dithiole-2-thione-4,5-dithiolate (dimercaptoisotrithione, dmit), the proposed mechanism of which is outlined in Scheme 1.7.[79] The resulting dithiolate was separated from Na_2CS_3 as the tetraethylammonium salts of its zinc chelate. Subsequent reaction of the zinc complex with suitable electrophilic agents would afford thione products with desired substituents. The commonly used electrophiles for such reactions include alkyl halides, vinyl halides, propargyl bromides, acyl chlorides, and alike.

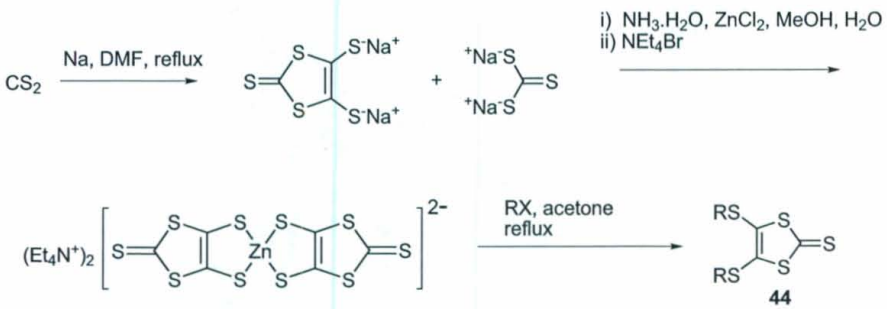

Scheme 1.6: Preparation of thione **44** by reduction of CS_2 with Na.

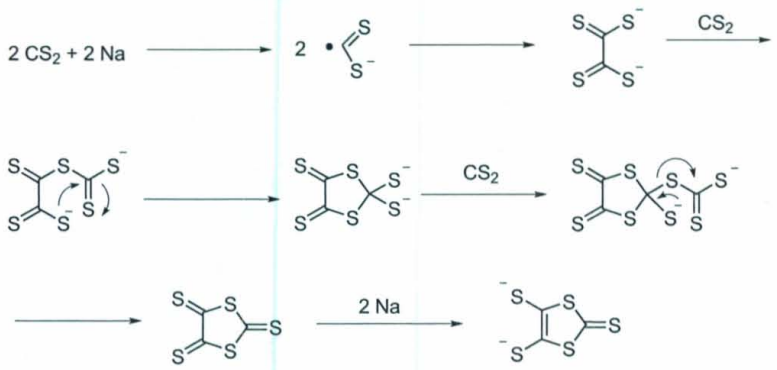

Scheme 1.7: Mechanism of the reduction of CS_2 with Na.

With thione **44** in hand, another important precursor, dithiolium salt **45**, can be readily prepared via an addition-reduction-elimination sequence as shown in Scheme 1.8. Although alkylation of the thione is favored by aromatization of the dithiole ring, methyl iodide is not reactive enough to effect such a reaction. The preferable choices of alkylating reagents are methyl fluorosulfate, methyl tirfluorosulfonate, triethyloxonium tetrafluoroborate and others. Alkylation of thione **44** can also be done by heating with dimethyl sulfate at 100 °C. The corresponding dithiolium tetrafluoroborate **52** can be obtained smoothly as a precipitate after addition of HBF_4 (Scheme 1.9).[80] Subsequent reduction of **52** with $NaBH_4$, followed by elimination under acidic conditions furnishes the desired product, dithiolium salt **45**.

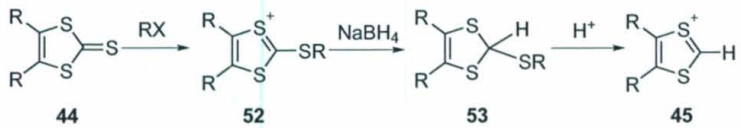

44 **52** **53** **45**

Scheme 1.8: Synthesis of dithiolium salts **45**.

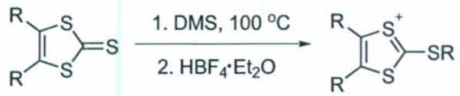

44 **52**

Scheme 1.9: Methylation of thione **44** by dimethyl sulfate.

Dithiolium salt **45** can be further converted into Wittig reagent **46** or phosphonate **47** by reacting with either phosphine or phosphite (Scheme 1.10). Compound **46** and **47** can then be used for the preparation of simple TTFs by coupling reaction with dithiolium salt **45**, or they can be used as precursors for the Horner-Wadsworth-Emmons (HWE) reaction to generate exTTF with large conjugated structure.

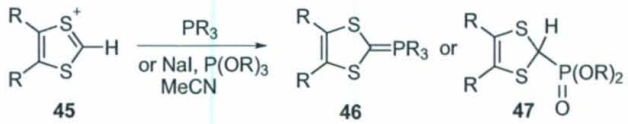

Scheme 1.10: Preparation of Wittig reagent **46** or phosphonate **47** from dithiolium salt **45**.

Under highly dilution, 4,5-bis(alkylthio)-1,3-dithiole-2-thione **44** can react with excess trialkyl phosphites to yield phosphonate **47** as the major product (Scheme 1.11). Meanwhile, a trace amount of tetrathiafulvalene resulting from a coupling reaction is also produced in the synthesis.[79,81] In comparison to the multistep route outlined in Scheme 1.10, this one-step approach is more economical; however, the use of excess $P(OEt)_3$ generates problems in purification and prevents its execution on large scale.

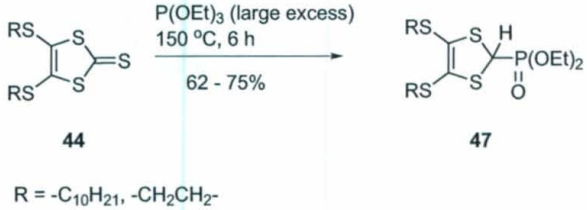

Scheme 1.11: Direct preparation of phosphonate **47** from thione **44**.

Another synthetic method for construction of simple TTF is the reaction of an electrophilic alkyne, such as dimethyl acetylenedicarboxylate (DMAD), with a 1,3-dipole **54** which is the adduct of Bu_3P and CS_2 (Scheme 1.12). The reaction affords the ylide intermediate **55**, which can be directly dimerized into TTF product **56**. However, the direct transformation from **55** to TTF **56** suffers from very low yields. To avert this problem, ylide intermediate **55** is usually trapped by addition of HBF_4 to form a stable phosphonium salt **57**,[82] which has been proven to be a good precursor

for olefination reaction with various carbonyl compounds.

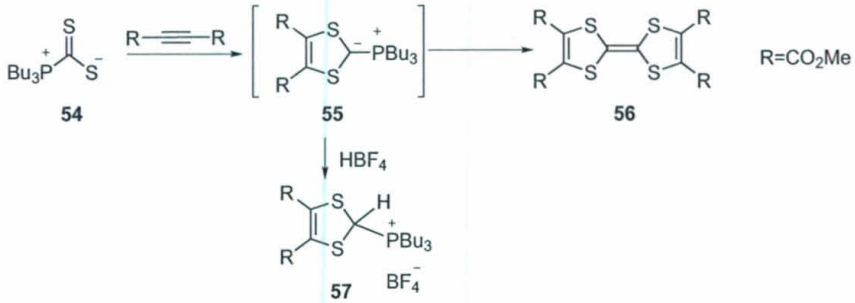

Scheme 1.12: Synthesis of phosphonium salt **57** by 1,3-dipolar cycloaddition.

Once the TTF skeleton is formed, it can be further modified through a number of well-established methodologies to create functionalized TTFs and exTTFs. An important route is by lithiation of TTF with an organolithium reagent such as LDA at -78 °C, followed by reactions with various available electrophiles (Scheme 1.13). The various products shown in the scheme are useful for further synthetic elaboration. The aldehyde TTF derivatives are especially suitable for preparing π-extended systems via Wittig reactions, while the alcohol and acid derivatized TTFs can be readily linked to other functional groups via esterification reactions. When there is an electron donating substituent (e.g. Me) attached to one of the dithiole rings, the acidity of the adjacent proton on the very same dithiole ring decreases. This drives lithiation to occur preferentially on the other dithiole ring. In contrast, an electron withdrawing group will direct the lithiation on the same dithiole ring. Such directing effects by substituents bring regioselectively to this methodology, enabling the preparation of multisubstituted TTFs.[83]

Another important methodology for TTF functionalization is based on the use of a β-cyanoethyl protecting group.[81,84,85] The β-cyanoethyl group can be introduced via

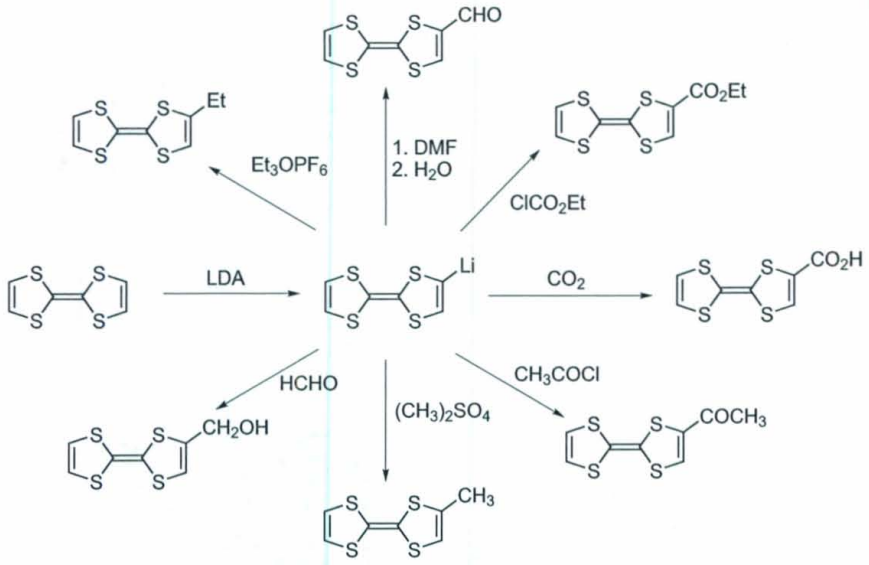

Scheme 1.13: Lithiation of TTF and further reactions with different electrophiles (adapted from reference 72).

the reaction of dmit (1,3-dithiole-2-thione-4,5-dithiolate) with 3-bromopropionitrile.[81] The removal of the β-cyanoethyl group occurs smoothly in the presence of a base such as MeONa.[84] The resulting thiolate reacts with suitable electrophiles to yield various TTF derivatives (Scheme 1.14).[85] In addition, monodeprotection of a bisprotected precursor can be easily achieved by using one equiv of $CsOH{\cdot}H_2O$ in $MeOH/CHCl_3$. The cesium thiolate is stable and precipitates out of the reaction mixture.[84]

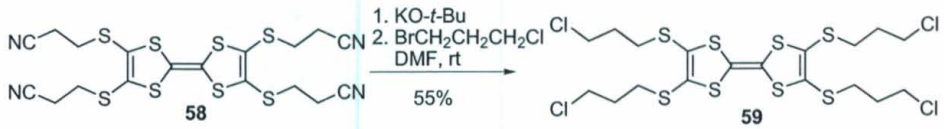

Scheme 1.14: Removal of β-cyanoethyl group and further reaction with electrophiles.

For the preparation of various annulated exTTFs, Diels-Alder reactions have been widely used (Scheme 1.15).[82] The highly reactive diene intermediate **61** was generated

in situ to stereoselectively react with a dienophile. However, the relatively high temperature for the diene generation may cause problems in cases where thermal stability of the product is an issue.

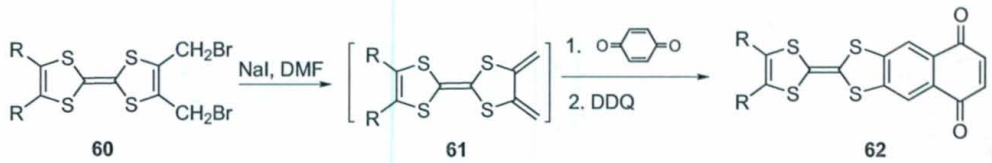

60 61 62

Scheme 1.15: Synthesis of an annulated TTF via the Diels-Alder reaction.

For the synthesis of exTTFs with large π-conjugated spacers between the two dithiole rings, two major synthetic methodologies are frequently adopted. The first one is to prepare a diketone or dialdehyde with extended conjugation, which is then converted to the exTTF by Wittig olefination or coupling with thione. Wittig olefination of the ketone or aldehyde using phosphonium salts proceeds under relatively mild conditions, and normally affords clean products. However, this reaction may not be suitable for compounds which are not compatible with basic conditions, and the preparation of phosphonate is time-consuming and costly. In the meantime, direct coupling of the ketone or aldehyde with thione in the presence of a large excess of trialkyl phosphite requires high temperatures. This method is fast and economical, but may not be suitable for the synthesis of products with relatively low thermal stability. Also, the use of large amounts of phosphite may cause problems in purifications. Scheme 1.16 illustrates these two routes for the synthesis of TTFAQ starting from anthraquinone.[86]

Another methodology for the synthesis of exTTFs is to prepare monomers with dithiole rings, which then undergo further reactions to extend its conjugated

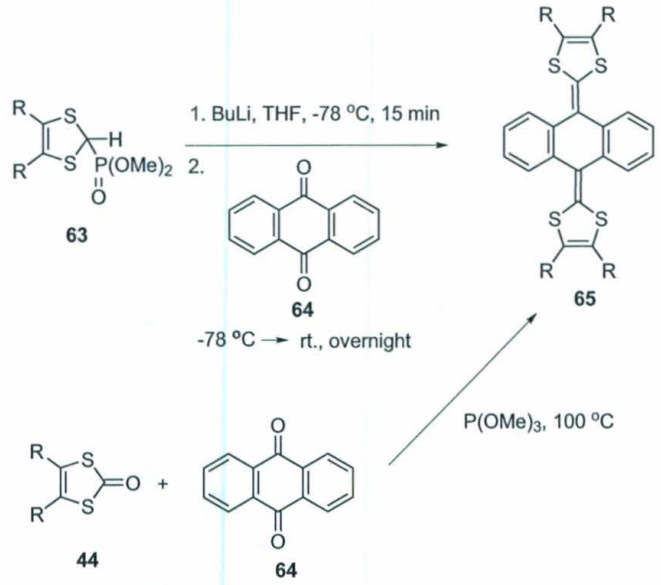

Scheme 1.16: Two synthetic routes to exTTFs with antraquinoid structures.

framework. For example, an extended TTFV derivative **67** with two triple bonds between two dithiole rings was synthesized from monomer **66** using the Hay coupling reaction (Scheme 1.17).[87]

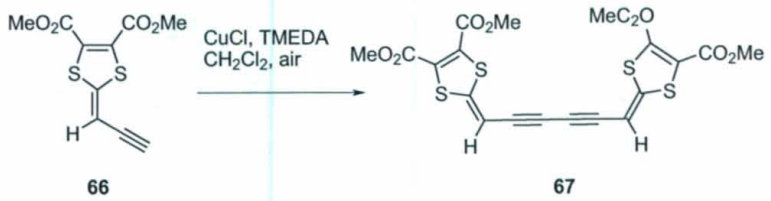

Scheme 1.17: Synthesis of exTTF **67** by Hay coupling of alkynyl dithiofulvalene.

Besides these conventional routes to TTF and exTTF, other synthetic methods are available for making novel exTTF structures. For example, a TTF-TCNE (TCNE, tetracyanoethylene) push-and-pull chromophore **69** was prepared by a one-pot reaction involving successive additions of TTF and TCNE to a polyyne precursor **68** (Scheme 1.18). The first mechanistic step is the addition of TCNE to the electron-

rich C≡C triple bond immediately next to the electron-rich dimethylaminobenzene moiety. The resulting intermediate features an electron-deficient triple bond adjacent to the TCNE adduct, which then directs a subsequent addition of TTF onto it. After the second addition, the electron density on adjacent triple bond becomes enriched to favor another iteration of TCNE addition. This cycle is repeated until all the triple bonds of the polyyne segment are reacted.[88]

68 69

Scheme 1.18: Synthesis of novel TTF-TCNQ push-and-pull chromophore.

1.3 TTFAQs: exTTFs Bearing an Anthraquinoid $\pi-$Spacer

TTFAQ is an important class of exTTFs with an anthraquinoid conjugated $\pi-$linkage located between the two dithiole rings. Compared to simple TTFs and other types of exTTFs, TTFAQs feature dramatic conformational changes during redox processes and their dications have significantly enhanced stability (see Figure 1.14). In the neutral state, TTFAQs adopt a saddle-like molecular shape to minimize the repulsions between sulfur atoms in the dithiole rings and the adjacent hydrogens on the central anthraquinoid moiety. Upon oxidation to dication species, the central part becomes planar, and the dithiole rings rotate to be perpendicular to the central plane. The

aromaticity gained in the central moiety further stabilizes the TTFAQ dication, making TTFAQ favor simultaneous rather than stepwise two-electron transfer.

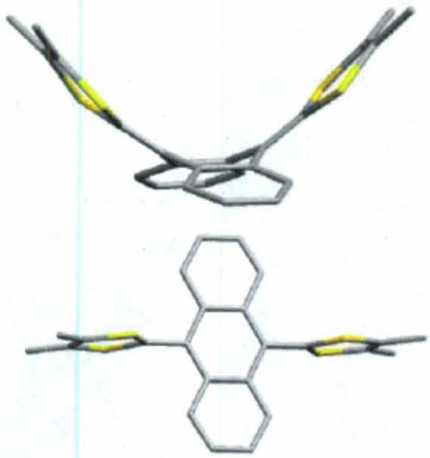

Figure 1.14: Conformations of TTFAQ in neutral (top) and dication (bottom) states (adapted from reference 65).

Like other exTTFs, TTFAQs can be prepared by the olefination strategy as discussed in the previous section. Commonly, an anthraquinone derivative is chosen as the starting material to be subjected to an HWE reaction with corresponding phosphonate, or heated with thione in the presence of excess trialkyl phosphite. These synthetic routes usually afford TTFAQs with good yields and scarcely encounters problems. Because of their low oxidation potentials and stabilized dication states, TTFAQs can serve as good electron donors in various donor-acceptor molecular ensembles to facilitate the generation of long-lived charge-separated states upon photoexcitation. For this reason, TTFAQs have been widely used in preparing photoinduced charge-transfer donor-acceptor (D-A) systems and solar cells. In the recent literature, a plethora of TTFAQ-C_{60} dyads and triads have been reported,

which showed promising photovoltaic and charge-transfer properties.[37] For example, two multi-donor-acceptor systems TTFAQ-TTFAQ-C_{60} **70** and TTF-TTFAQ-C_{60} **71** were reported in 2009 (Figure 1.15).[89] These systems give lifetimes of charge-separate states on the μs scale. The remarkable stability of the charge-separated state is due to the excellent electronic properties of TTFAQ and delicately designed molecular structure. First, the pyrrolidine ring not only acts as the linkage between C_{60} and the $\pi-$conjugated system, but also exerts some effects to enhance the stability of the charge-separated state. Second, the *p*-phenyleneethynylene bridge, in addition to its facile synthesis, allowed reasonable electronic communication between electroactive moieties. Third, the incorporation of multiple donor groups enabled further charge transfer from the adjacent radical ion pair state (D—$D^{+\cdot}A^{-\cdot}$) to the remote radical ion pair state ($D^{+\cdot}$—D-$A^{-\cdot}$), which further stabilized the charge-transfer state.

Recently, it has been demonstrated that the concave shapes of anthraquinoid-type structures provide suitable binding sites for the convex surface of C_{60}.[90,91] For example, a TTFAQ-based crown ether **72** (Figure 1.16) was reported to show 1:1 binding with ammonium-functionalized C_{60} derivative **73** with a large association constant $K_a = 10^6$ M^{-1}.[92] The strong binding was attributed to the preorganization of TTFAQ and C_{60} through H-bonding between the crown ether moiety and the ammonium group, which facilitated the interaction between TTFAQ and C_{60}.

The favored TTFAQ–C_{60} binding offers a useful approach for the design of organic photovoltaic materials. For example, a type of TTFAQ-based tweezers **74** and **75** was reported to show affinity for C_{60} in aromatic solvents (Figure 1.17).[92] Upon photoexcitation, these complexes generate charge-separated states. Although the lifetimes were measured to be on the ps scale in the solution phase, the solid state

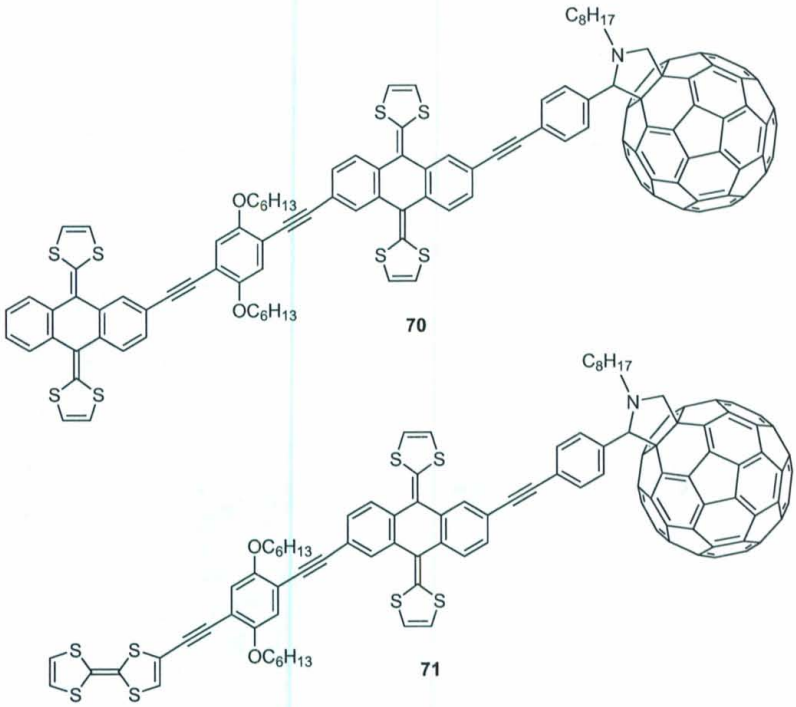

Figure 1.15: Structures of TTFAQ-C_{60} donor-acceptor systems.

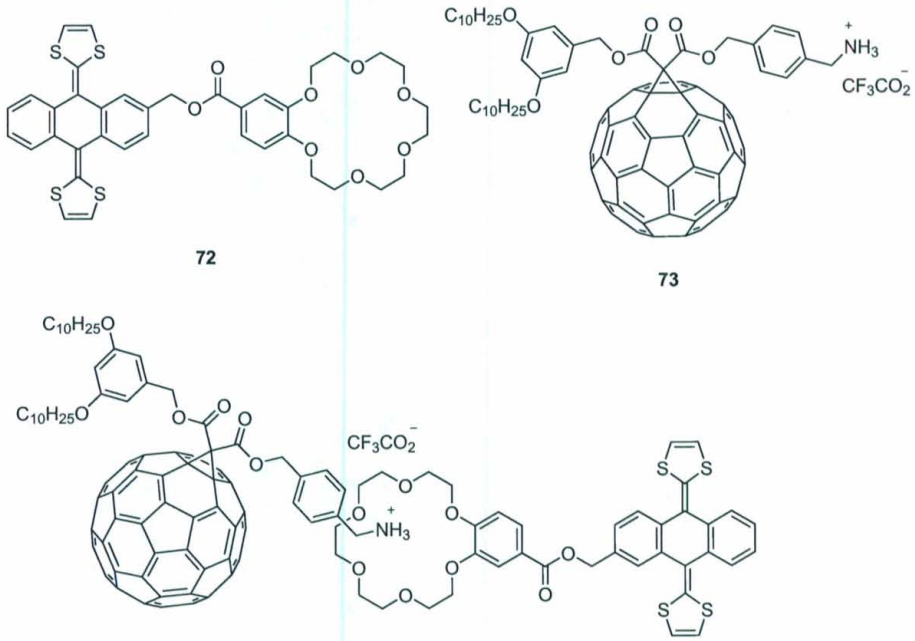

Figure 1.16: Complexation of TTFAQ and C_{60} derivatives.

properties were proposed to be very different and useful for photovoltaic devices.

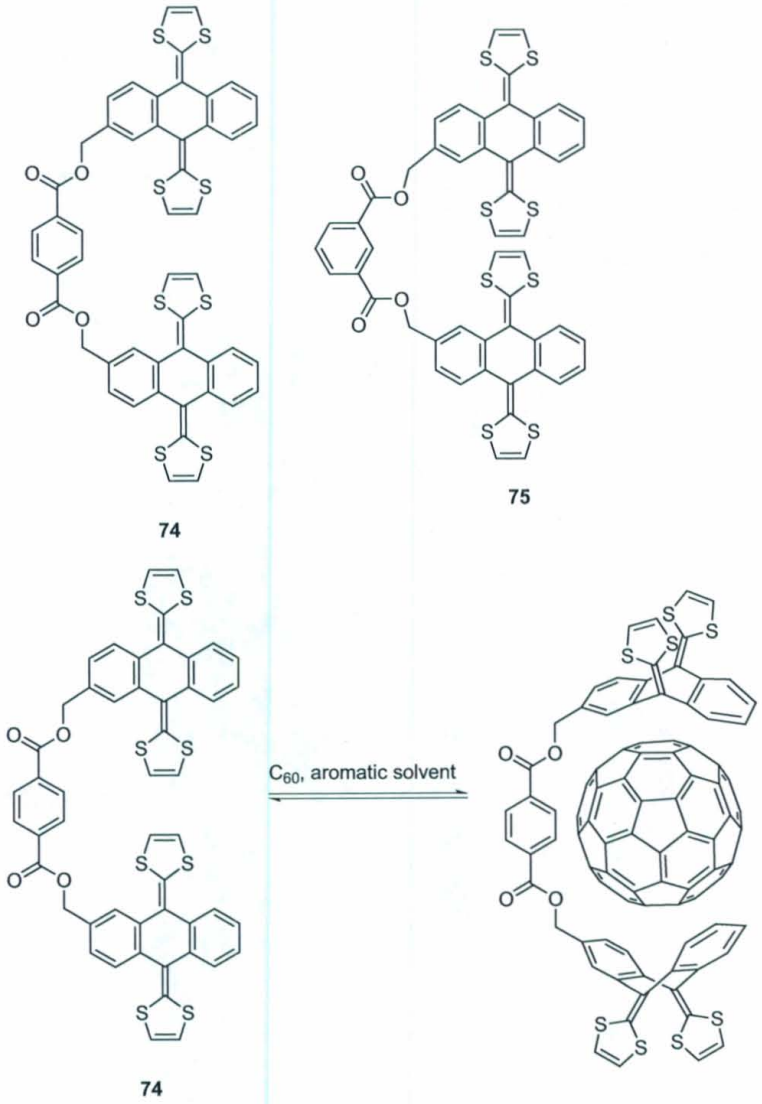

Figure 1.17: TTFAQ tweezers binding to C_{60}.

Our group has recently been interested in the construction of TTFAQ-based donor-acceptor systems and exploration of their potential applications as advanced organic optoelectronic materials.[93–96] For example, TTFAQ-boronic acid derivative **76** was

synthesized as an electrochemical sugar sensor (Figure 1.18).[94] In this compound, the boronic acid moieties were designed to bind with sugars and the binding led to altered electrochemical redox potentials of the TTFAQ core. Indeed, compound **76** has shown preferential binding to fructose and ribose, and significant anodic shifts in the oxidation potentials were observed. As another example, TTFAQ-crown ether **77** (Figure 1.18) was prepared and found to be a sensitive fluorescent probe for Ba^{2+} ion.[96] The crown ether moieties on the side chain of dithiole rings created a cavity for metal ion binding. The electron donating ability of TTFAQ core was decreased after the molecule was bound to metal ions. In this way, photoinduced electron transfer from TTFAQ to anthracene was effectively quenched to restore the fluorescence of the anthracene groups.

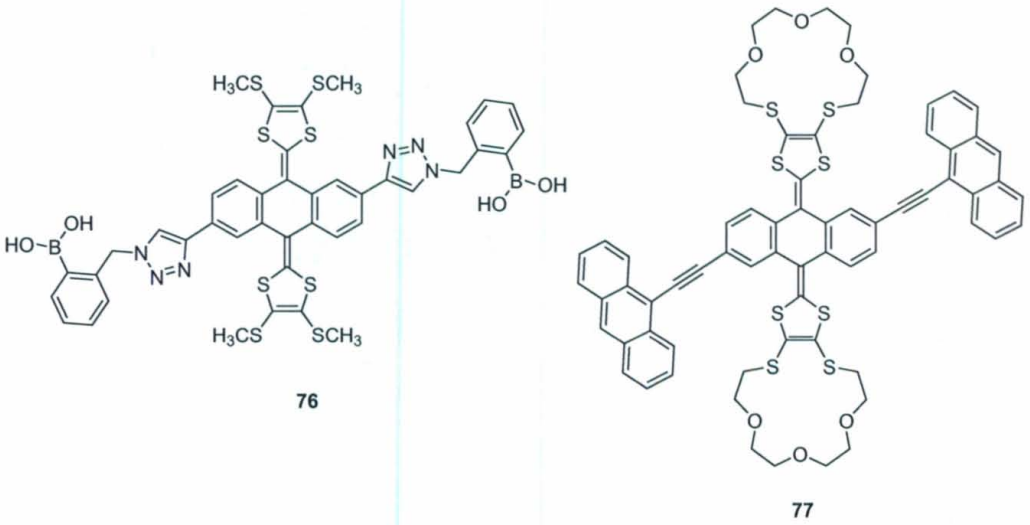

Figure 1.18: TTFAQ-based molecular sensors prepared by our group.

1.4 Tetrathiafulvalene Vinylogues (TTFV)

Tetrathiafulvalene vinylogues refers to exTTFs with two C=C bonds between the dithiole rings. Figure 1.19 lists some representatives of TTFV derivatives.[97–99] Like other TTFs, TTFVs are good electron donors, which can undergo substantial conformational changes upon oxidation (Figure 1.20). In the neutral state, TTFVs adopt non-planar conformations to lower the repulsion between the dithiole rings and substituents congested around the vinyl position. The dihedral angles increase with the sizes of the substituents, while monosubstituted TTFVs are nearly planar in shape. Upon oxidation, the molecules rotate to make the TTFV skeleton planar. The substituents are now orthogonal to the plane with a dihedral angle close to 90°. The reduced steric interactions favor the formation of dications, thus simultaneous two-electron oxidation is frequently observed for TTFVs.[99]

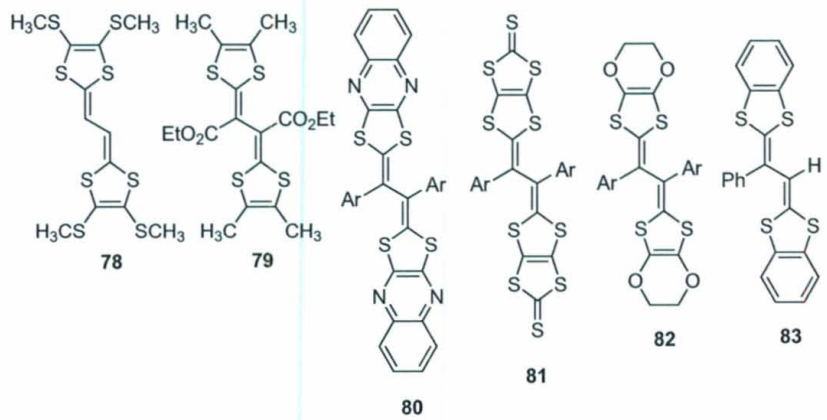

Figure 1.19: Structures of tetrathiafulvalene vinylogues.

TTFVs can be prepared by synthetic protocols different from other exTTFs. The synthesis usually begins with an oxidative dimerization of dithiafulvene (DTF),

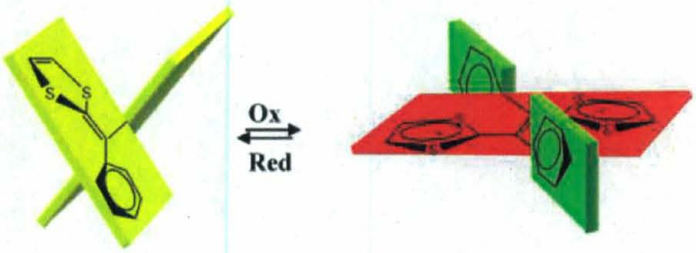

Figure 1.20: Structures of TTFV in the neutral and oxidized states (adapted from reference 94).

followed by reduction. This process can be done chemically or electrochemically. The mechanism of the dimerization reaction is described in Scheme 1.19. The first step is the oxidation of DTF to generate a radical cation, which then dimerizes to form a protonated dicationic TTFV. After deprotonation, neutral TTFV is formed and immediately oxidized to the dication in situ, due to the lower oxidation potential of TTFV relative to DTF. Hence, to finalize the synthesis a reduction step is used to afford neutral TTFV. Common oxidants for the dimerization include $AgBF_4$, Br_2, and I_2, while in some cases sunlight can also initiate the dimerization.[100] Besides these chemical methods, bulk electrolysis provides another efficient method to produce TTFVs from respective DTF precursors.[101,102] The dimerization usually proceeds smoothly to furnish products in moderate to good yields. However, in the absence of substituents that could greatly stabilize the radical cation of DTF, dimerization either did not occur[103] or required the assistance of a metal template, such as the case for compound **89** (Figure 1.21).[104] When a monomer containing two DTF groups was subjected to dimerization, TTFV macrocycles or polymers were formed.[101,105]

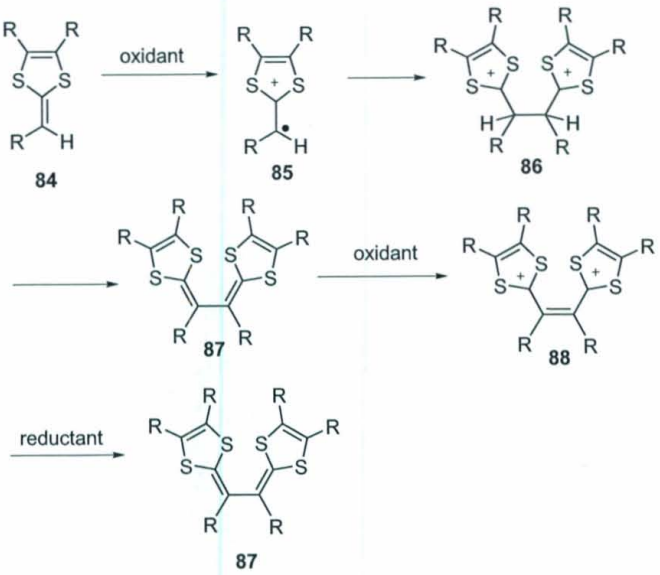

Scheme 1.19: Mechanism for oxidative DTF dimerization.

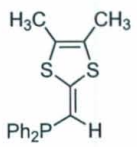

Figure 1.21: DTF that requires template for dimerization.

TTFVs can also be made in a stepwise manner from DTFs. As shown in Scheme 1.20, compound **90** reacted with phosphorous oxychloride in DMF, leading to the formation of compound **91**, which was then subjected to an HWE reaction with phosphonate to give TTFV **92**.[103]

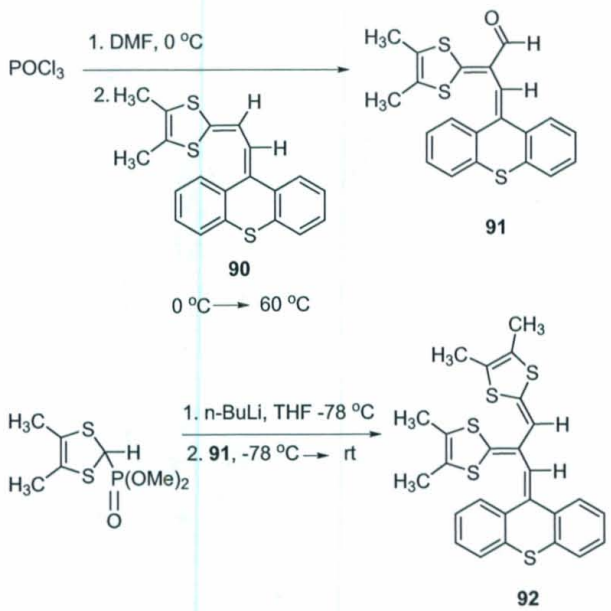

Scheme 1.20: Stepwise synthesis of TTFV **92** from monomer **90**.

The applications of TTFVs are somewhat limited, because in many cases TTFVs in both the neutral and oxidized state are nonplanar in structure. This feature disfavors efficient intermolecular interactions in the solid state, resulting in poor conductivity. However, like other TTFs, TTFVs are very good electron donors, and the ease of preparation, and more importantly, the substituent-dependant conformational changes upon oxidation make them good building blocks for the construction of redox-active chemosensors. In 2003, a series of cyclic TTFVs **35** with alkyl linkers on the side chain of dithiole rings were synthesized and proposed for use as molecular clips (Figure

1.22).[106] It was found that the linkers barely changed the electron donating ability of TTFV. A short linker indeed prevented the stretching of molecules upon oxidation to dications, resulting in a clip movement. In addition, this movement seemed to be insensitive to the electronic nature and steric hindrance of the substituents on the central spacer. Based on these results, a TTFV derivative **94** with thiolepicoline side chains was prepared and investigated (Scheme 1.21). When binding with Zn^{2+}, the conformational change during oxidation was constrained. In this situation, it was proposed a clip motion would occur instead of normal stretch motion, which was supported by the positive shift of oxidation potentials and coalescence of two one-electron oxidations to a two-electron oxidation in the cyclic voltammetric analysis.[107]

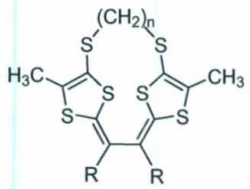

93

Figure 1.22: TTFV clips with linkage connecting two dithiole rings at side chain position.

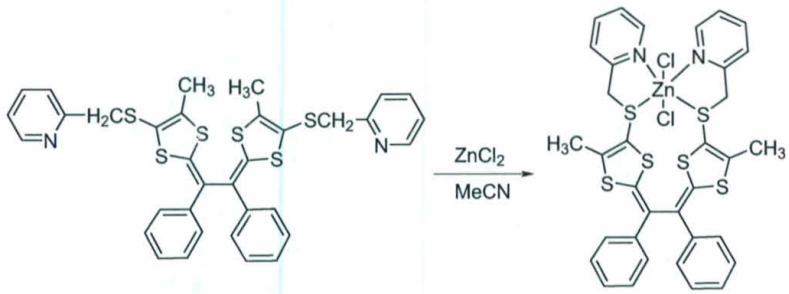

94 (ZZ/EE/ZE) **94·$ZnCl_2$**

Scheme 1.21: Binding of thiolepicoline-appended TTFV **94** with Zn^{2+}.

Another series of cyclic TTFVs **95a-c** with crown ether linkers in the substituent positions were synthesized and studied in 2007 (Figure 1.23). It was found that a crown ether chain with six oxygens was necessary to maintain the stretch motion. The crown ether unit provided the binding site for Pd^{2+} ion.[108]

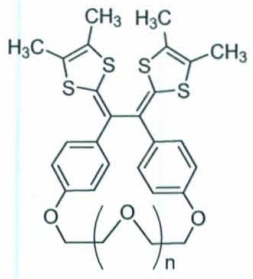

95a, n = 2
95b, n = 3
95c, n = 4

Figure 1.23: Structures of crown ether-type TTFVs **95**.

Recently a TTFV-metal coordination macrocycle **96** was synthesized (Figure 1.24).[107] The pyridyl substituents attached to TTFV provided the binding sites to Mo. Upon complexation, the electron density of TTFV was decreased and the first oxidation potential of TTFV was shifted negatively. The Mo(0) center gained electron density to show a lower oxidation potential.

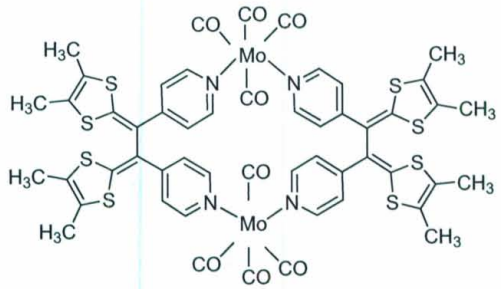

96

Figure 1.24: Structure of a TTFV-Mo coordination macrocycle.

1.5 Outline of this Thesis

This PhD dissertation has accomplished two major projects in the development of exTTF-based organic conjugated materials. A brief overview on TTFs and exTTFs is given in Chapter 1 with emphasis on two themes: (i) the recent applications and synthetic methodologies of various TTF-based organic materials, and (ii) the relationship between molecular structure and electronic/photonic properties.

Chapter 2 describes the synthesis and characterization of two series of $\pi-$extended TTFAQ analogues. Large conjugated systems in these TTFAQ analogues are expected to maintain their high stability and alter their electronic properties as well as solid state packing. The synthetic routes involved the use of a one-pot, 4-fold Sonogashira macrocyclization as the key step to construct large shape-persistent macrocylic conjugated systems between two dithiole rings. The structures of these TTFAQ analogues were clearly determined by X-ray crystallographic analysis. Their electronic properties were studied by UV-Vis, fluorescence, cyclic voltammetry, and spectroelectrochemistry. Comparison of these two series of TTFAQ analogues with corresponding dithiofulvalene monomers and TTFAQ were made.

Chapter 3 focuses on the synthesis and characterization of a series of TTF-oligoynes and TTFV derivatives including macrocyclic TTFVs, TTFV tweezers and a crown ether-tethered TTFV. The development of suitable synthetic methodologies and understanding of essential structure-property relationships for these TTFV ananlogues will contribute to further design of TTFV materials and molecular devices. The syntheses employed Sonogashira coupling, Hay coupling, and click chemistry. The electronic properties were studied by UV-Vis, fluorescence, cyclic voltammetry,

and spectroelectrochemistry. Electropolymerization and solid-state polymerization of TTFV-oligoyne based macromolecules were also investigated.

In Chapter 4, a summary and conclusions of this thesis work are given. Based on the results acquired, potential solutions to the difficulties and problems encountered in the current work are suggested. In addition, perspective remarks are provided in this chapter to foresee some appealing directions worth pursuing in the future work.

Chapter 2

Synthesis and Characterization of π-Extended TTFAQ Anologues

2.1 Introduction

Anthraquinoid-type TTF analogues (*i.e.* TTFAQs) constitute an important branch in the family of exTTFs owing to their intriguing electronic, redox, and photophysical properties. As discussed in Section 1.2.1, the unique molecular properties of TTFAQs are primarily associated with their central anthraquinone $\pi-$core. In the recent TTF literature, the strategy of incorporating large $\pi-$conjugated structures in between the two dithiole rings of TTF has been frequently used and proven to be fruitful in generating novel optoelectronic organic materials. Indeed, the insertion of $\pi-$units bestows two major benefits in terms of material design at the molecular level. First, the extended $\pi-$conjugation improves the stability of cationic species, which in turn enhances the donor ability of the TTF and enriches its redox activity. Second, the

intrinsic electronic properties of inserted $\pi-$ spacers may be coupled with the TTF unit to bring about new optoelectronic properties to the hybrid systems. For example, a truxene-TTF hybrid **97** was recently reported, the structure of which comprises a truxene core and three dithialfulvene units (Figure 2.1). This exTTF showed a significant redshift of its long-wavelength absorption in the UV-vis spectrum, and afforded non-planar aromatic $\pi-$surface to favor binding with [60]fullerene through non-covalent forces.[109]

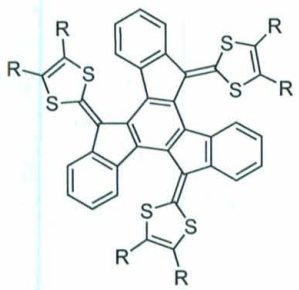

97

Figure 2.1: Chemical structure of truxene-TTF hybrid **97**.

One of the objectives of this thesis work was to develop new TTFAQ analogues with highly $\pi-$extended structures. To this end, two types of TTFAQ anologues were designed as illustrated in Figure 2.2. The structures of these TTFAQ analogues contain a conjugated bisbenzo-enyne macrocycle central unit between the two dithiole rings. Novel molecular properties were anticipated from the highly conjugated systems, while a systematic survey of structure-property relationships should deliver knowledge beneficial to the future design of new TTF derivatives that are of both theoretical and practical values to supramolecular and materials sciences. The following sections describe the synthetic methods for these TTFAQ analogues

and electronic and electrochemical redox properties characterized by UV-Vis absorption and fluorescence spectroscopic, voltammetric, and spectroelectrochemistry analyses.[110,111]

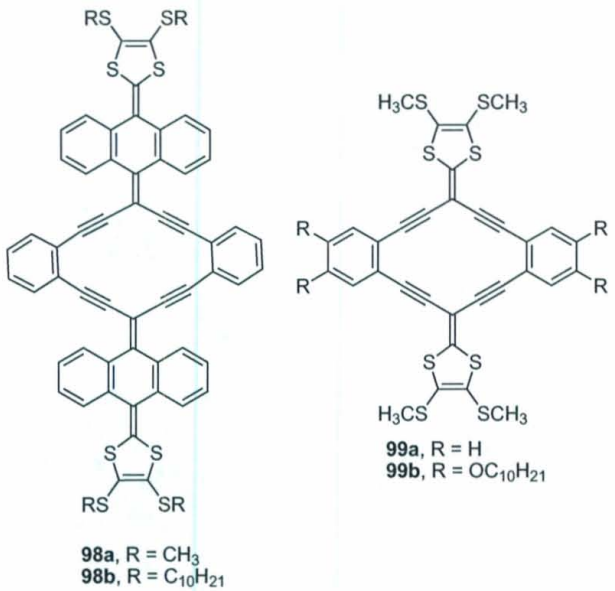

Figure 2.2: Structures of target $\pi-$extended TTFAQ analogues **98a,b** and **99a,b**.

2.2 Results and Discussion

2.2.1 Synthesis and Characterization of TTFAQ Analogue 98

2.2.1.1 Retrosynthetic Analysis

The retrosynthetic analysis of TTFAQ analogue **98** is outlined in Scheme 2.1. The core structure of the target compound **98** contains a shape-persistent enyne macrocycle that can be disconnected into two synthons through the Sonogashira reaction, *o*-diiodobenzene and desilylated **100**. This step can be performed by either

a one-pot or a stepwise approach. Precursor **100** can be generated from dibromo compound **101** from Sonogashira coupling of dibromo compound **101** with TMSA. Dibromo compound **101** contains two key functional groups, a dithiole ring and a dibromovinylidene unit. The dibromo functionality can be installed via a Corey-Fuchs reaction on ketone **102** which carries a dithiole ring, while ketone **102** can be obtained from a selective olefination reaction on anthraquinone **103**, either by a phosphite-mediated coupling reaction with thione **104**, or by an HWE reaction with one molar equiv of phosphonate **105**. Both thione **104** and phosphonate **105** are readily accessible through well-established procedures reported in the literature.

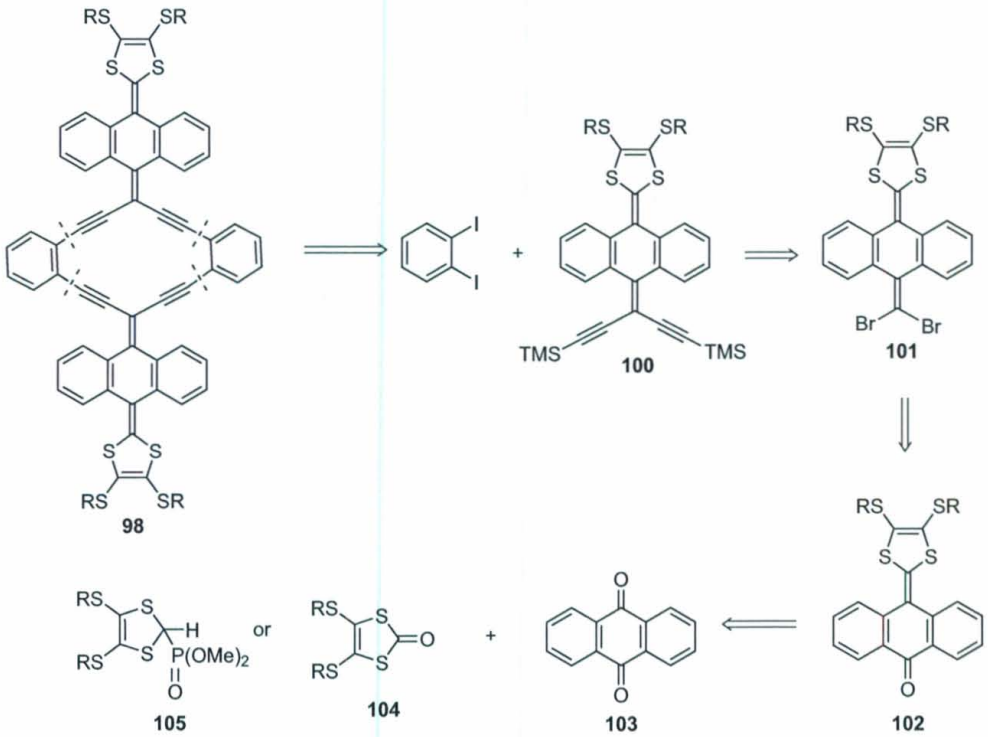

Scheme 2.1: Retrosynthesis of TTFAQ analogue **98**.

2.2.1.2 Synthesis of *S*-Methyl Thione 104a and *S*-Decyl Thione 104b

S-Methyl thione **104a** and *S*-decyl thione **104b** were first prepared using known procedures.[78,112] As shown in Scheme 2.2, the synthesis of *S*-Decyl thione **104a** started with a reaction between Na and CS_2 using DMF as the solvent. The resulting dithiolate was chelated with Zn^{2+} upon addition of $ZnCl_2$ and $NH_3 \cdot H_2O$, and precipitated out as a stable red colored salt **106** in the presence of tetraethylammonium bromide. The overall yield of this sequence of reactions was 88%. Salt **106** was then dissociated into free dithiolate in refluxing acetone, and the resulting intermediate was subsequently alkylated with MeI to afford *S*-methyl thione **104a** in 74% yield, or with decyl bromide to afford *S*-decyl thione **104b** in 60% yield.

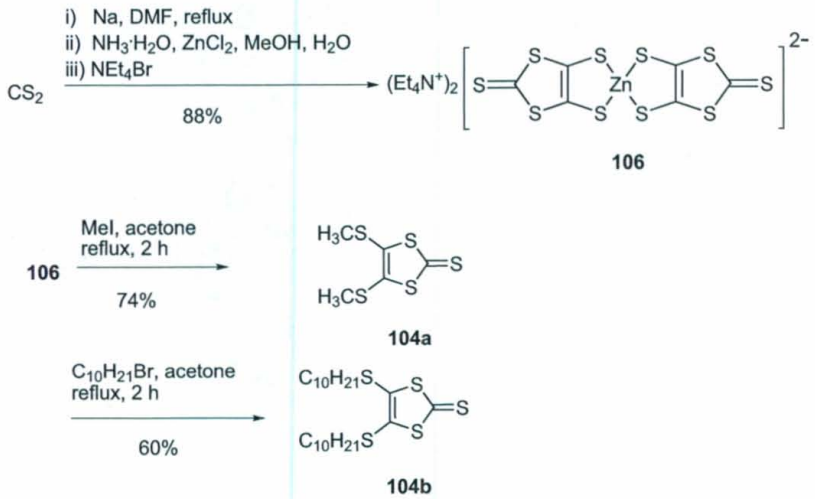

Scheme 2.2: Synthesis of *S*-decyl thione **104a** and *S*-methyl thione **104b**.

2.2.1.3 Synthesis of *S*-Decyl Phosphonate 105a and *S*-Methyl Phosphonate 105b

Phosphonates **105a,b** were synthesized according to known procedures as outlined in Scheme 2.3.[112] Thiones **104a,b** were first alkylated with dimethyl sulfate (DMS) at 90 ^{o}C. The resulting products were then treated with $HBF_4{\cdot}Et_2O$, and precipitated out as salts **107a,b** respectively upon addition of diethyl ether. As these salts were moisture-sensitive, they were immediately subjected to reduction with $NaBH_4$ in EtOH to afford thiols **108a,b** as stable solids. Thiols **108a,b** were converted to salts **109a,b** by treatment with first Ac_2O then $HBF_4{\cdot}Et_2O$. The products **109a,b** were again unstable and directly converted to phosphonates **105a,b** by reaction with $P(OMe)_3$ in the presence of NaI in MeCN. The lower yields of *S*-decyl derivatives compared to *S*-methyl ones were the result of increased solubilities that resulted in more product losses in the filtration steps. Phosphonates **105a,b** are important precursors and were frequently used for the synthesis of TTFs in this work.

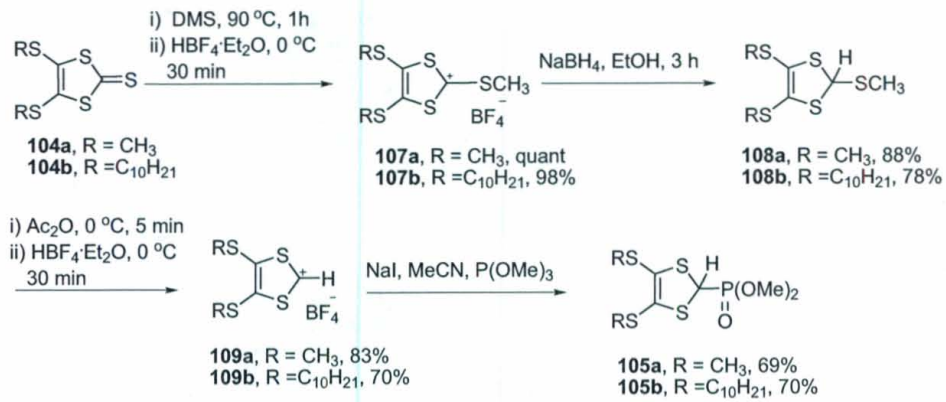

Scheme 2.3: Synthesis of *S*-decyl phosphonate **105a** and *S*-methyl phosphonate **105b**.

2.2.1.4 Synthesis of Dibromo Precursor 101

The synthesis of compound **101** can be carried out using anthraquinone as the starting material, with two direct functional group interconversions: (1) the dithiole ring formation and (2) the introduction of dibromovinylidene functionality. Two synthetic routes can be used with different sequences of reactions as outlined in Scheme 2.4.

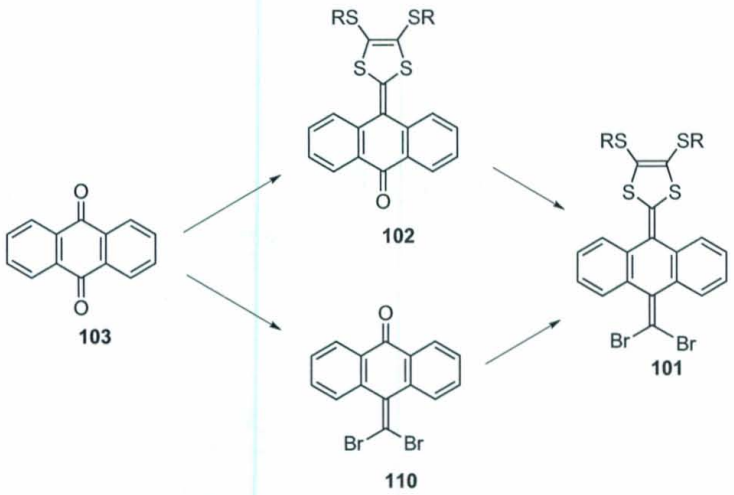

Scheme 2.4: Two synthetic routes to DTF dibromo compound **101**.

In the synthetic work, the route that begins with the incorporation of the dibromovinylidene group followed by olefination to install DTF was attempted first. The addition of one dibromovinylidene group to anthraquinone was presumably achievable via a Corey-Fuchs reaction using excess anthraquinone **103**. Nevertheless, the reaction yielded only disubstituted product (see Scheme 2.5), despite the fact that small amounts of CBr_4 (as low as 0.1 equiv) were used.[113] Obviously, the Corey-Fuchs reaction could not be stopped at the mono-substituted stage, since dibromovinylidene is so good an electron-withdrawing group that, once formed,

it further increases the electrophilicity of the keto group at its *para*-position and speeds up the second Corey-Fuchs reaction. The enhanced reactivity hence thwarted the attempt to obtain mono-dibromovinylidene anthraquinone from anthraquinone directly.

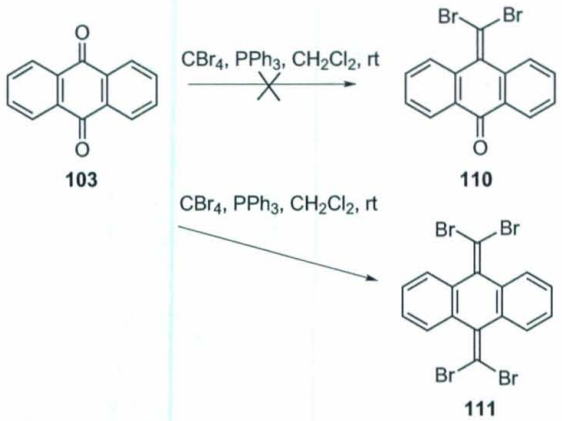

Scheme 2.5: Corey-Fuchs reaction of anthraquinone **103**.

Alternatively, route 2 as proposed in Scheme 2.4 was explored. In this synthetic route, DTF ketone **102** was planned to be made first and then converted to DTF dibromo compound **101**. In a previous study by our group, mono-substituted DTF-anthraquinone **113** was obtained as a minor product in 20% yield in an HWE reaction in which diethynylated anthraquinone **112** was reacted with 2 equiv of phosphonate **105a** in the presence of base (Scheme 2.6).[114] Based on this result, it was assumed that a similar HWE reaction between anthraquinone **103** and only 1 equiv of phosphonate **105a** should yield mono-DTF substituted product **102** in an acceptable yield. However, as shown in Scheme 2.7, contrary to the reaction in Scheme 2.6 this reaction only gave di-olefinated product, TTFAQ **114**, even when only 0.6 equiv of phosphonate **105a** was used. This result was unexpected and seemingly

counterintuitive, since the intermediate of this reaction, **102a**, should be less reactive than anthraquinone due to the electron-donating nature of the DTF group.

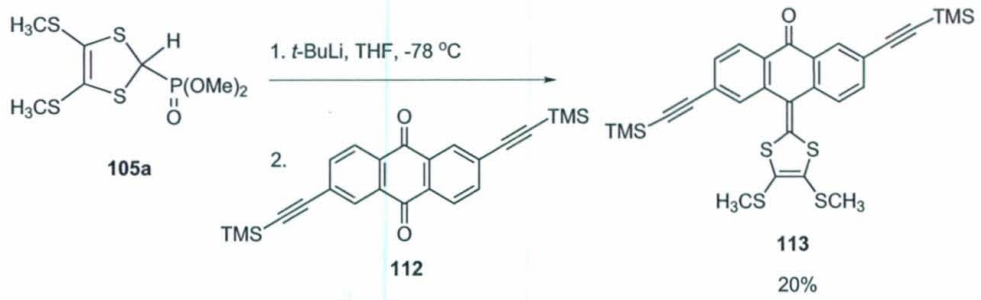

Scheme 2.6: Formation of mono-DTF anthraquinone **113** in an HWE reaction.

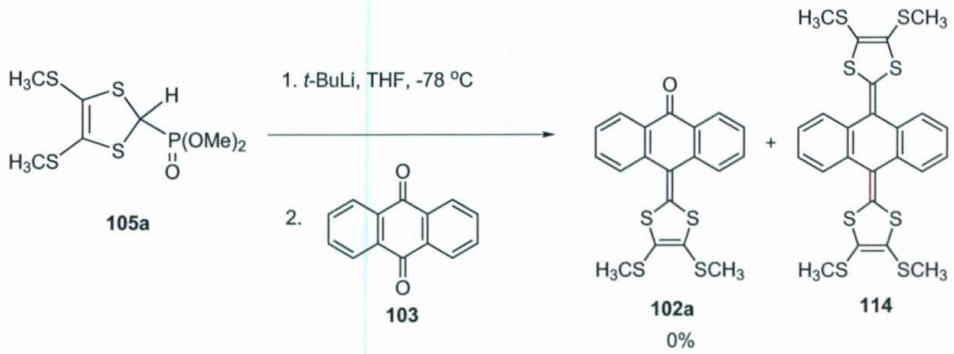

Scheme 2.7: Attempted synthesis of mono-DTF anthraquinone **102a** via an HWE reaction.

To circumvent the problems encountered in the above two synthetic routes, a phosphite-mediated coupling strategy was investigated as depicted in Scheme 2.8.[79] In the presence of triethyl phosphite, thiones **104a,b** reacted with excess anthraquinone at high temperature to give DTF ketones **102a,b**. Although the purification step was somewhat tedious due to the presence of a large amount of triethyl phosphite, ketones **102a,b** were successfully produced by this reaction in moderate to good yields. Compounds **102a,b** were then readily converted to DTF dibromides **101a,b** by Corey-Fuchs reactions. It is worth noting that the reagents and glassware used for these reactions must be thoroughly dried to ensure high yields.

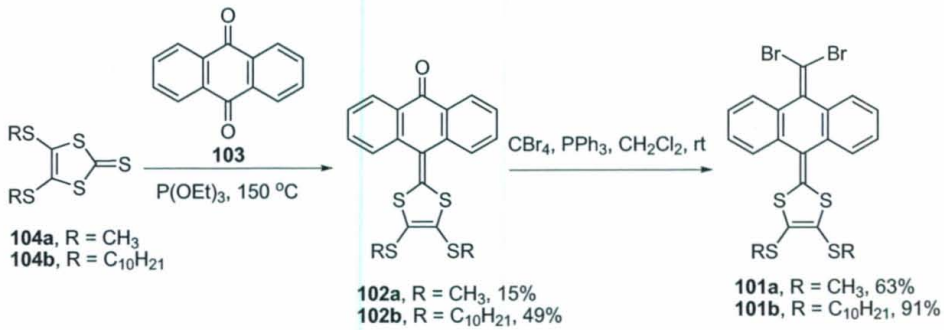

Scheme 2.8: Synthesis of DTF-dibromides **101a,b**.

2.2.1.5 Synthesis of Dialkynes 115a,b and Macrocyclic TTFAQ Analogue 98b

With compounds **101a,b** in hand, the syntheses of dialkynes **115a,b** were straightforward. Sonogashira coupling reactions between compounds **101a,b** and TMSA at 60 °C afforded diethynylated products **100a,b** in good to excellent yields (Scheme 2.9). The successful synthesis of compounds **100a,b** enabled the construction

of macrocyclic TTFAQ analogues **98a,b** and other related acyclic exTTFs.

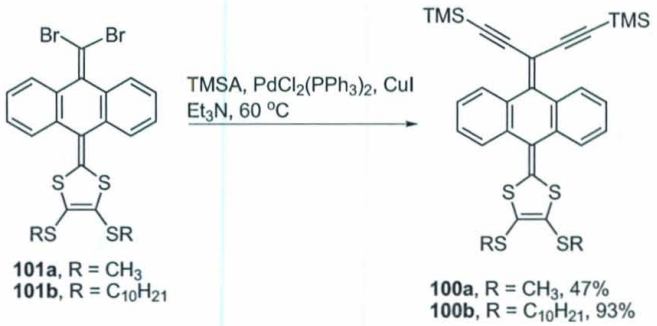

101a, R = CH_3
101b, R = $C_{10}H_{21}$

100a, R = CH_3, 47%
100b, R = $C_{10}H_{21}$, 93%

Scheme 2.9: Synthesis of DTF diethynylated compound **100a,b**.

Removal of the TMS groups of **100a,b** by K_2CO_3 in THF/MeOH furnished free dialkynes **115a,b**. On account of their relatively low stability, the desilylated intermediates were immediately subjected to macrocyclization reactions without extended storage. The macrocyclic enyne frameworks of the target TTFAQ analogues were planned to be constructed by Sonogashira couplings. *S*-decyl substituted macrocyclic TTFAQ analogue **98b** was chosen as the first target, considering its good solubility and the observation that Sonogashira couplings involving related *S*-decyl substituted TTFAQs tended to give higher yields than did *S*-methyl substituted TTFAQs. In principle, the target compound **98b** could be prepared by a two-fold Sonogashira reaction between dialkyne **115b** and a pre-made aryldihalide counterpart **116b**, or by a one-pot 4-fold Sonogashira reaction between two molecules of dialkyne **115b** and two molecules of aryldihalide **117** (see Scheme 2.10). Each of the strategies has pros and cons. While the first macrocyclization strategy, owing to its lower entropic demand, is expected to afford a better yield, the second one-pot strategy features superior synthetic conciseness.

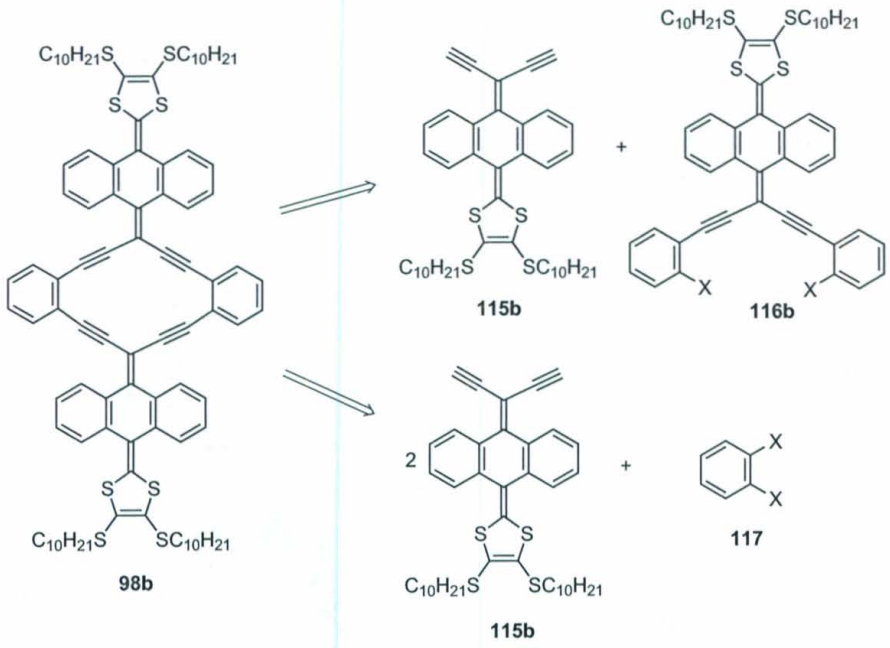

Scheme 2.10: Two strategies for the synthesis of macrocyclic exTTF **98b**.

To explore the first route, 1-bromo-2-iodobenzene was selected as the aryldihalide building block, as the the iodo group of 1-bromo-2-iodobenzene was expected to undergo selective Sonogashira coupling due to its higher reactivity than the bromo group. As outlined in Scheme 2.11, dialkyne **115b** generated in situ from desilylation of compound **100b** was reacted with 1-bromo-2-iodobenzene in Et_3N using $Pd(PPh_3)_2Cl_2/CuI$ as catalyst. After **100b** was consumed as verified by TLC analysis, the mixture was purified by flash column chromatography. The crude products from different chromatographic fractions were then subjected to MALDI-TOF MS analysis. According to the MS data, the reaction yielded no cyclic product **98b** but two acylic products, dihalide **118b** and dimer **119b** (see Scheme 2.11). By conducting the reaction at different temperatures (0 to 60 °C), a trend was found that the yield of dimer **119** increased with increasing reaction

temperatures. Cyclized products, however, were not observed in the temperature range investigated. To test the reactivity of **118b** for Sonogashira coupling, a model reaction between TMSA and **118b** was tried under typical Sonogashira conditions at 60 °C overnight. Unfortunately, no coupling reaction was observed to take place. The test reaction revealed the inertness of **118b** to Sonagashira coupling, and the 1-bromo-2-iodobenzene strategy for macrocyclization was therefore abandoned.

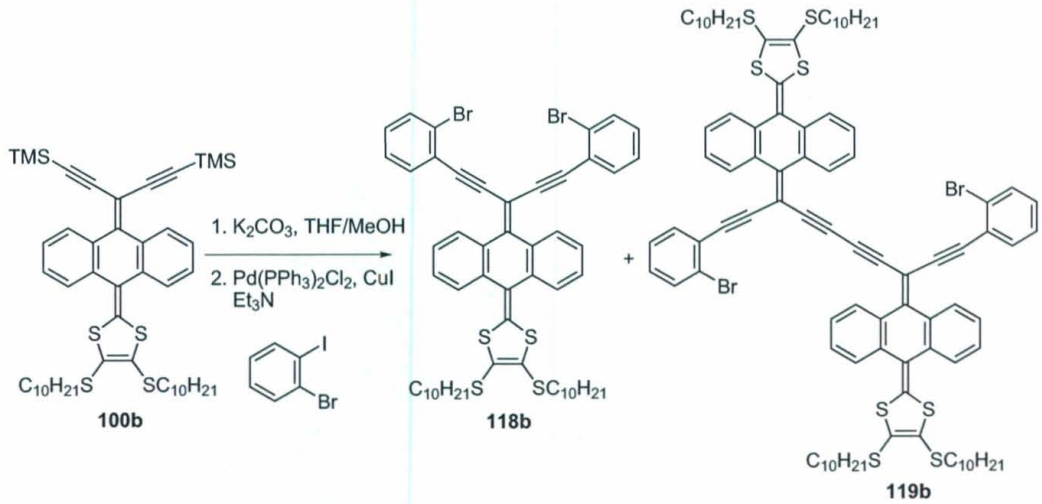

Scheme 2.11: Sonogashira reaction of desilylated **100b** with 1-bromo-2-iodo benzene.

The unsuccessful outcome of the first stepwise macrocyclization route justified the need for a more reactive arylhalide precursor. 1,2-Diiodobenzene was then selected to cross couple with desilylated **100b**. The reaction was done at rt with other conditions the same as those for the reaction described in Scheme 2.11. The outcome was promising as MALDI-TOF MS analysis of one of the fractions from column chromatographic separation clearly showed the formation of TTFAQ macrocycle **98b**. Although the crude product contained some inextricable byproducts and the yield of **98b** was rather low, the result of this reaction was promising. Further

optimization of the reaction conditions indeed led to satisfactory results. As shown in Scheme 2.12, when a Et_2O solution of desilylated **100b** was slowly added into a mixture containing 1,2-diiodobenzene, Et_3N, and catalyst $CuI/Pd(PPh_3)_4$ at 60 °C, pure product **98b** was obtained in 27% yield from crystallization after column chromatographic separation.

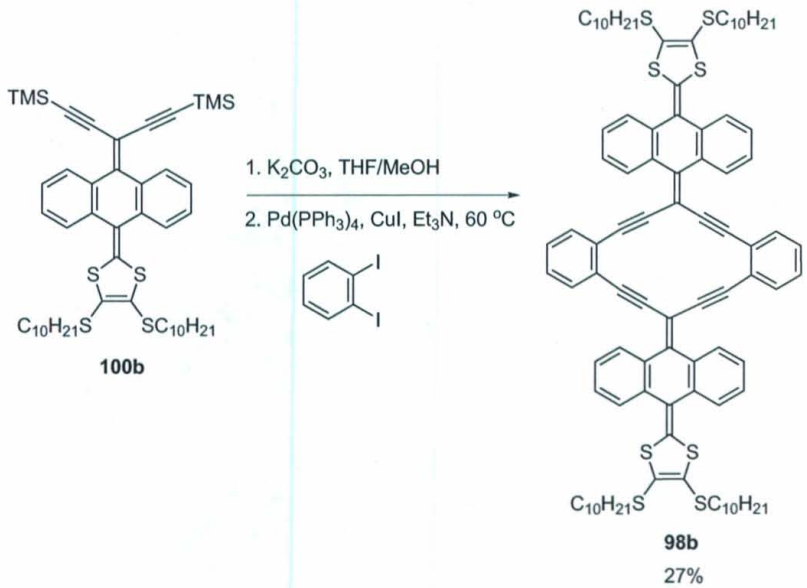

Scheme 2.12: Synthesis of macrocyclic exTTF **98b** by Sonagashira reaction with 1,2-diiodobenzene.

Optimization of the one-pot macrocyclization reaction is not a short story and worth some comments here. Theoretically, there are a number of side reactions in competition with the cyclization. Two major rivalries included: (1) linear chain elongation versus cyclization, and (2) cross-coupling versus homo-coupling reactions. Thus effort was focused on maximizing cyclization and minimizing homocoupling. First, different solvent/base systems were tested. It was found that only in pure

Et_3N was the cyclic product formed. In other solvent systems, such as Et_3N/THF (1:2, 1:4, 1:8) and DBU/benzene, diyne **115b** (desilylated **100b**) quickly polymerized to form a black-red solution which was composed of mostly homo-coupling products as evidenced by a fragmentation ion at m/z 639 in the MALDI-TOF MS. Second, the concentration effect of starting materials was examined. With a fixed diyne concentration, the amount of diiodobenzene was varied from 0.7 to 1.3 equiv, but the reaction gave no observable difference in the yield of cyclic product. This was unexpected because the amount of diiodo benzene for an ideal reaction should be less than 1.0 equiv due to the slight loss of diyne in the desilylation step. When more than 1.0 equiv of diiodobenzene was added, the yield of dihalide **116b** increased as expected. It is known that high dilution favor cyclization over polymerization. Thus, a solution of diyne **115b** and 1,2-diiodobenzene was added dropwise into a Et_3N mixture containing the catalysts. Surprisingly, only homo-coupling products were formed. It is not clear why homo-coupling became so much faster than cross-coupling under high dilution. Third, the temperature effect was investigated. At low temperatures (0 °C, -15 °C) mainly homo-coupling products were produced, whereas at a high temperature (60 °C) a complicated mixture of oligomers was formed, resulting from both cross-coupling and homo-coupling reactions. No significant difference was observed in the yield of cyclic product between reactions conducted at rt and 60 °C. This observation can be explained as follows. On the one hand, the molecule requires a certain temperature to overcome the energy barrier in the cyclization stage. On the another hand, high temperature accelerates homo-coupling reactions, which in turn lowers the yield of the cyclization, because the activation energy of the cyclization is higher than the linear oligomerization. According to these arguments, the key to improving the

yield of cyclization is to lower the activation energy barrier for cross coupling by using a more efficient catalyst. As such, the cyclization reaction can efficiently proceed at a low temperature that does not greatly increase unwanted homo-coupling. In addition, because the reaction rate of cyclization is more sensitive to the diyne concentration than the linear oligomerization, it is possible to minimize homo-coupling by using a low concentration of diyne during the reaction. On this consideration, a solution of diyne **115b** was added slowly into a mixture containing 1,2-diiodobenzene and a more reactive catalyst, $Pd(PPh_3)_4$, at 60 °C. The yield of product increased significantly as indicated by TLC. According to MALDI-TOF MS, other byproducts were mainly oligomers formed by cross-coupling. It should be noted that slow addition of diyne to the reaction mixture was critical to achieving improved yields. In fact, yield of cyclization was not significantly improved when $Pd(PPh_3)_4$ was added in one portion at rt. Moreover, improvement of yield was observed for the reaction using $PdCl_2(PPh_3)_2$ where diyne was slowly added at 60 °C.

Based on the experimental results, it was proposed that the reaction proceeds through three major stages as described in Scheme 2.13. *Stage 1*: cross-coupling of diyne **115b** with the large excess of diiodobenzene to form **116b** through compound **120b**. Homo-coupling of **100b** and **120b** took place in a diminutive degree due to their low concentrations. During the process, the concentration of **116b** increases and the concentration of diiodobenzene decreases. *Stage 2*: once the concentration of **116b** increases to a comparable level to diiodobenzene, diyne **115b** starts to react with **116b** to form **122b**. In the meantime, **120b** could react with **116b** to form **121b**. *Stage 3*: **122b** cyclizes to form **98b**, or undergoes cross-coupling with alkynes or iodo compounds to afford acyclic oligomers. The chance for **122b** to undergo

homo-coupling is small due to its low concentration during this process.

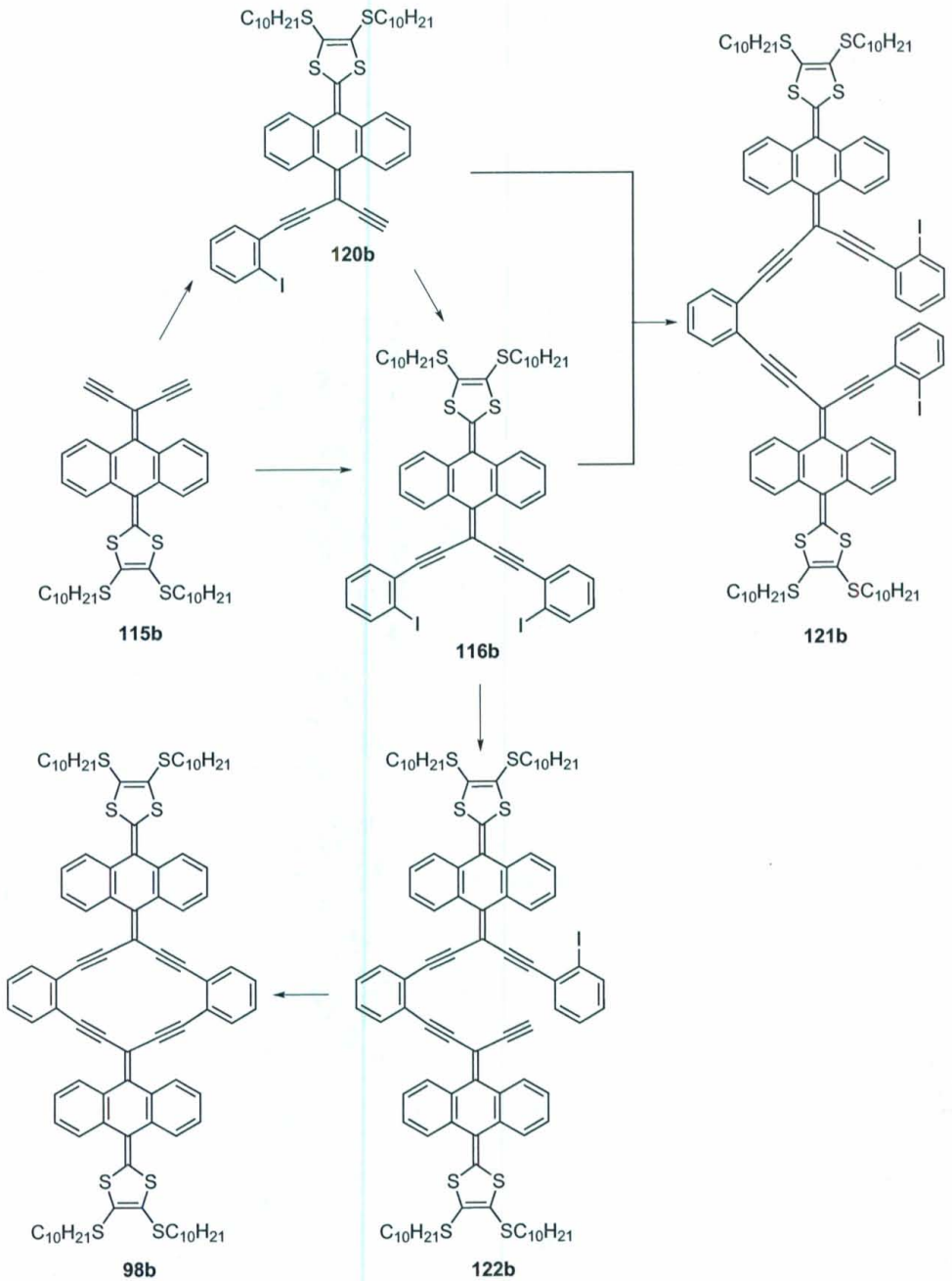

Scheme 2.13: Proposed steps for the formation of macrocyclic exTTF **98b**.

The purification of the macrocyclic TTFAQ product **98b** was achieved by flash column chromatography with a long column length and slow elution rate due to the complex composition of the crude product. One major difficulty encountered was that the macrocycle product had a very similar R_f value to one of the byproducts as revealed by TLC. Based on MALDI-TOF MS analysis, this troublesome byproduct was identified to be diiodo oligomer **121b** (Figure 2.3). To solve this problem, TMSA was added to the reaction mixture in the presence of Pd/Cu catalyst to convert this byproduct into a cross-coupled compound that was more easily separable from the cyclic product by column chromatography. Later, it was found that the byproduct could be simply removed by recrystallization of the crude product from a 1:1 $CHCl_3$/MeOH solution.

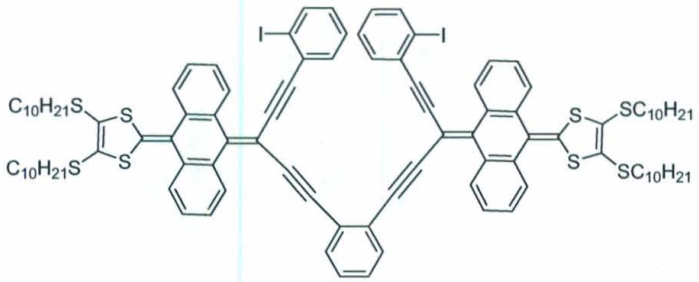

121b

Figure 2.3: Structure of byproduct **121b** formed in the macrocyclization reaction.

2.2.1.6 Attempted Synthesis of Macrocyclic TTFAQ Analogues 98a,c

After the successful synthesis of macrocyclic exTTF **98b**, two analogous macrocylic TTFAQ derivatives **98a**,**c** (Figure 2.4) were then pursued. However, the synthesis of these two targets was not successful for the reasons given below. For compound **98a**,

the short side chains, methyl groups, on the dithiole rings were designed to enhance intermolecular $\pi-$stacking in the solid state. Unfortunately, the incorporation of methyl groups was found to significantly decrease the solubility of relevant intermediates and the product in organic solvents, which in turn substantially lowered the yields of certain synthetic steps; in particular, the Sonogashira macrocyclization reaction. If one cross-coupling step is assumed to have a moderate yield of 40%, then the overall yield of the macrocyclization which involves four successive steps of cross couplings will be only 2.6%. This accounts for the unsuccessful attempted synthesis of **98a**. In TTFAQ derivative **98c**, a diiodobenzene building block bearing two decyloxy groups was used for constructing the macrocycle. The decyl side chains were expected to increase the solubility of the product and improve the yield. The macrocyclization reaction intended to make **98c** was tried, but failed to produce any desired cyclic product as evidenced by MALDI-TOF MS analysis.

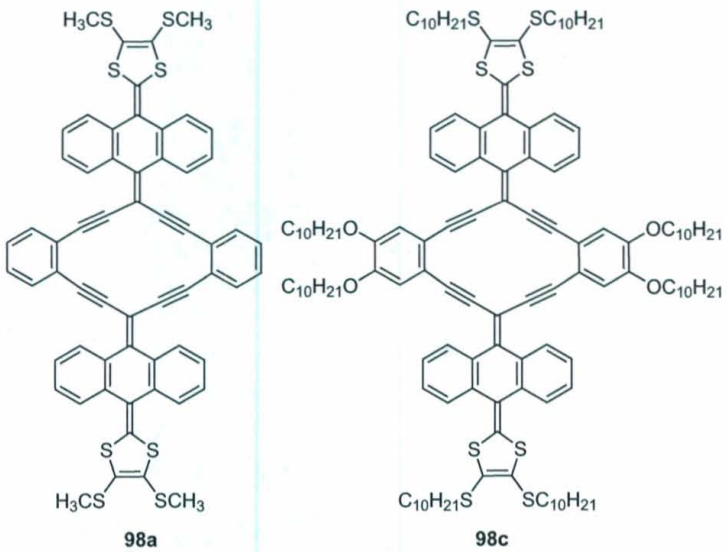

Figure 2.4: Structure of macrocyclic exTTF derivatives **98a,c**.

2.2.1.7 Synthesis of Related Acyclic $\pi-$Extended TTF and DTF Analogues

After the synthesis of macrocyclic TTFAQ analogues, related acyclic exTTF **123** and monomer **124** were synthesized for the purpose of a comparative study. The synthesis was done by a Sonogashira reaction of desilylated **100b** with 1 equiv of iodobenzene, yielding both **123** and **124** in reasonable yields (Scheme 2.14). The formation of **123** resulted from a cross coupling between diyne **115b** and 1 equiv of iodobenzene, followed by a homo-coupling. Likely, the rate of homo-coupling was comparable to that of cross-coupling in this synthetic case. The use of only 1 equiv of iodobenzene was based on the known conditions for a homo-cross-coupling reaction.[114]

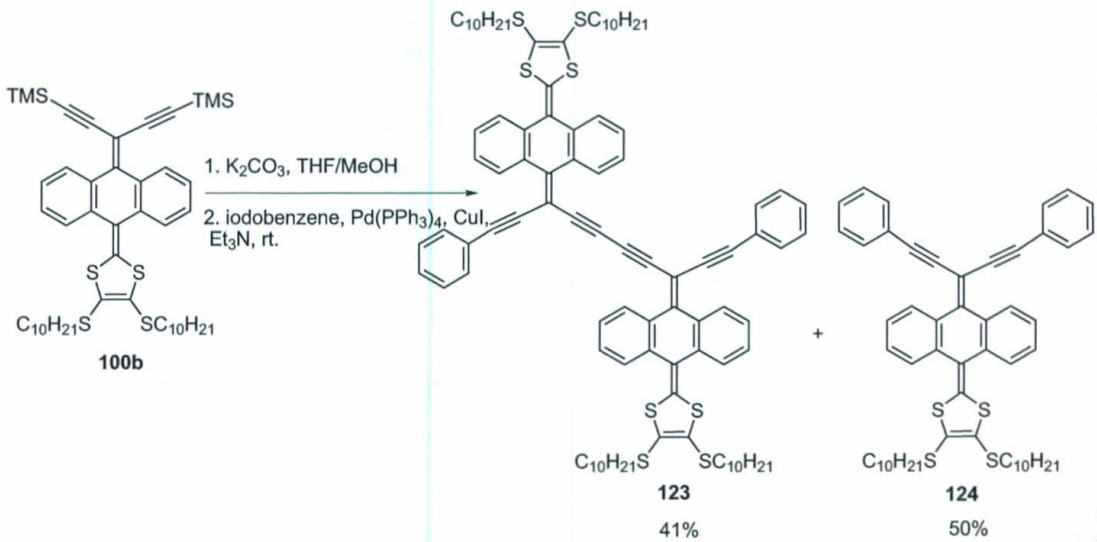

Scheme 2.14: Synthesis of acyclic $\pi-$extended TTFAQ **123** and DTF **124**.

2.2.1.8 Synthetic Strategies for $\pi-$Extended TTFAQ Analogues with Endcapping Functionality

Compound **123** shown in Scheme 2.14 can be regarded as a TTFAQ analogue expanded by an anthracene-diyne-anthracene $\pi-$spacer. Conceivably, attachment of various substituents to the terminal positions of **123** should lead to a variety of intriguing donor/acceptor polyads that may find application in charge-transfer and electroactive organic materials. To further explore this synthetic potential, a target compound **126** was investigated using the same synthetic strategy as Scheme 2.14. As shown in Scheme 2.15, iodoarene **125** was used in lieu of iodobenzene in order to get ex-TTFAQ **126**. If this reaction was successful, donor/acceptor endcapping groups would be easily introduced via a desilylation-Sonogashira coupling sequence. However, this reaction afforded the two-fold cross-coupling product as the major one, whereas the rate of homo-coupling reaction appeared to be much slower in this case. Since the homo-cross-coupling reaction appears to be substrate dependant and somewhat unpredictable, it is therefore believed to be an unsuitable approach for the synthesis of the endcapped ex-TTFAQ derivativtives.

During the synthesis of compound **100b** by a Sonagashira reaction of dibromo compound **101b** with TMSA (Scheme 2.9), it was noticed that the reaction did not go to completion after 2 days at rt. Besides **100b** and starting materials, an unknown compound was separated as a minor product. Although its instability prevented further characterization, MALDI-TOF MS analysis suggested it could be a mono-substituted product **127** (see Figure 2.5). If this byproduct was indeed **127**, it would serve as a facile starting material for the synthesis of endcapped ex-TTFAQs targeted

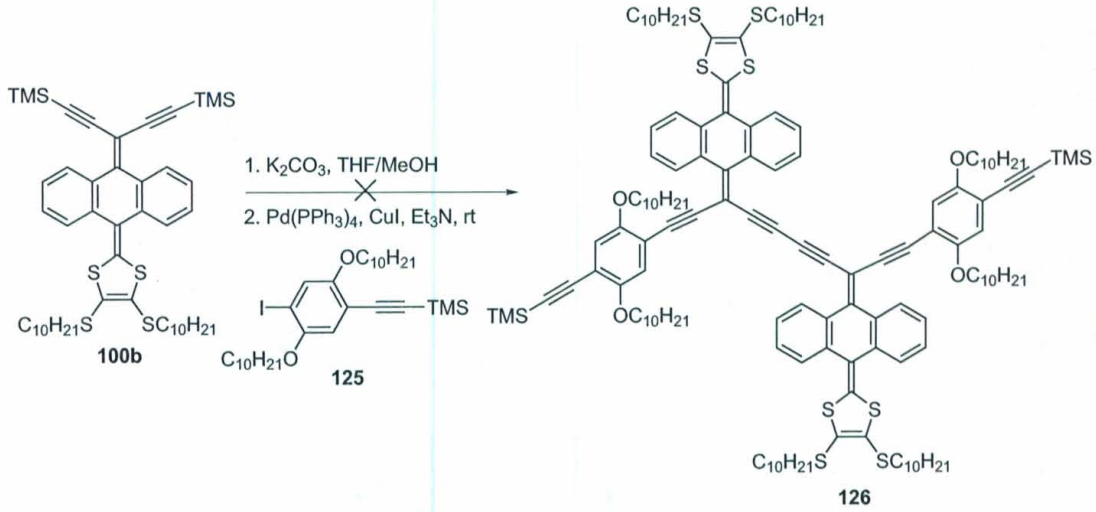

Scheme 2.15: Attempted synthesis of ex-TTFAQ **126** via cross-homo-coupling reaction.

herein.

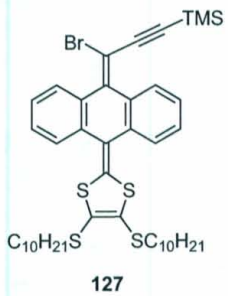

Figure 2.5: Structure of compound **127**.

To seek the possibility of enhancing the stability by employing different alkynyl substituents, two Sonogashira reactions were tested on dibromide **101b** using phenylacetylene or 4-ethynylbenzonitrile as the alkyne counterpart. In these two reactions, significant amounts of mono cross-coupling products were not isolated. It was thus concluded that the monoalkynyl-substituted product was

unstable and should be converted to a more stable form in situ. Following this rationalization, a Sonogashira cross coupling between **101b** and a 1:1 mixture of TMSA/phenylacetylene was next attempted. Surprisingly, this reaction afforded compound **124** as the only product (see Scheme 2.16). This result suggested that phenylacetylene reacted much faster than TMSA in Sonogashira coupling with dibromide **101b**.

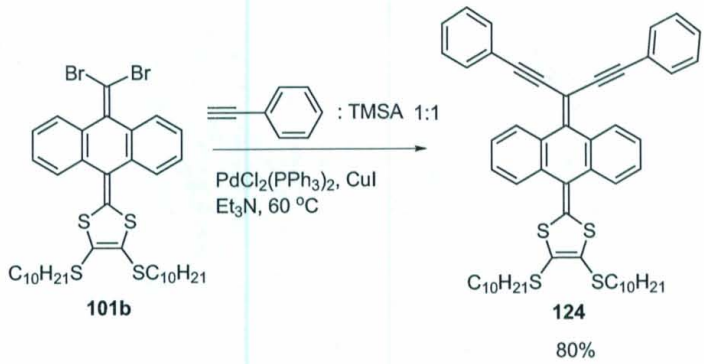

Scheme 2.16: Sonogashira coupling reaction of **101b** with 1:1 TMSA/phenylacetylene.

When phenylacetylene was added after TMSA had reacted with the alkyne at rt for 1 day, the desired product **128** was separated in 14% yield as shown in Scheme 2.17. Further modification of the reaction conditions was made by adding a mixture of 1 equiv of phenylacetylene and excess TMSA to **101b** at once. The best result attained so far was using 1:6 phenylacetylene/TMSA (see Scheme 2.18). Under these conditions, the yield of product **128** was improved to 30%. Although such a yield was not high, it was still reckoned as acceptable since another product of the reaction, dialkyne **114b**, could also serve as a useful precursor for the synthesis of ex-TTFAQs. With **128** in hand, a trimeric ex-TTFAQ was envisaged to be accessible through

a Sonogashira coupling reaction between desilylated **128** and a dihalide compound. Different donor/acceptor endcapping groups, theoretically, could be introduced as substituents on phenylacetylene. However, the reactivity of alkynes with endgroups should be comparable to TMSA to afford acceptable yields. At this stage, this synthetic strategy has been demonstrated to be very promising, but further efforts are required to streamline it.

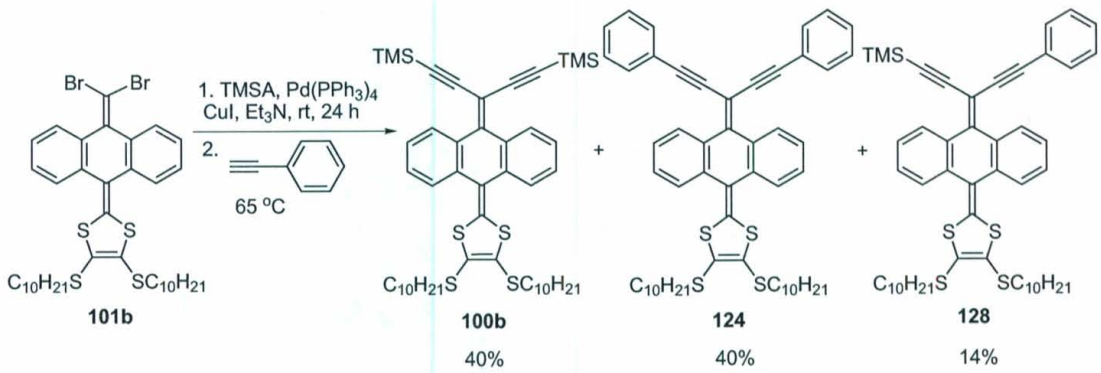

Scheme 2.17: Synthesis of mono-TMSA substituted compound **128**.

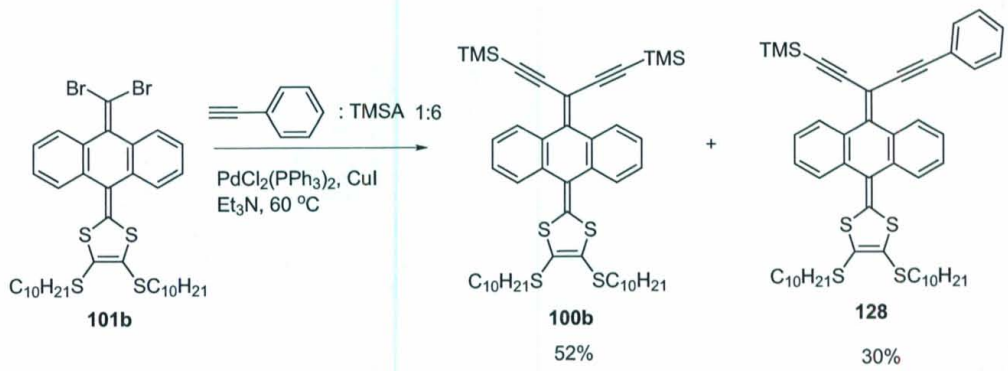

Scheme 2.18: Modified synthesis of mono-substituted compound **128**.

2.2.1.9 An Unknown Product Formed in the Sonogashira Coupling Reaction of 101b and Phenylacetylene

During the synthesis of **124** via a Sonogashira coupling reaction of dibromo compound **101b** with phenylacetylene, a purple substance was obtained in a quantity nearly the same as **124**. MALDI-TOF MS analysis indicated that this unknown product has the same molecular mass as **124**. However, its ^{1}H NMR spectrum showed a complicated set of proton signals in the aromatic region, pointing to an unsymmetrical molecular structure that is more complex than **124**. It is known that the Pd catalyst can induce hydroarylations of alkynes, and the cyclizations of compounds with similar structures to **124** are well documented.[115–117] If the reaction occurred in a way similar to the reported ones, the structure of the unknown compound could be **130** (see Scheme 2.19). The ^{13}C NMR spectrum of **130** did not provide sufficient information for structural elucidation of the unknown due to limited solubility. Thus, the proposed cyclization is uncertain and awaits further study. It should be noted that there are two observations contradicting the cyclization reaction. First, when compound **124** was subjected to the same reaction conditions for 1 day, no reaction occurred. Second, when diyne **115b** reacted with iodobenzene to form **124**, the unknown compound was not formed. Mostly likely, the unknown substance was formed by a competing reaction to the Sonogashira coupling, rather than a follow-up reaction.

To better understand the reaction leading to the unknown product, the structure of the unknown needs to be clearly confirmed. One difficulty preventing structural identification of the unknown is the complex ^{1}H NMR spectral pattern in the aromatic region. To acquire a better resolved ^{1}H NMR spectrum, reducing the number of

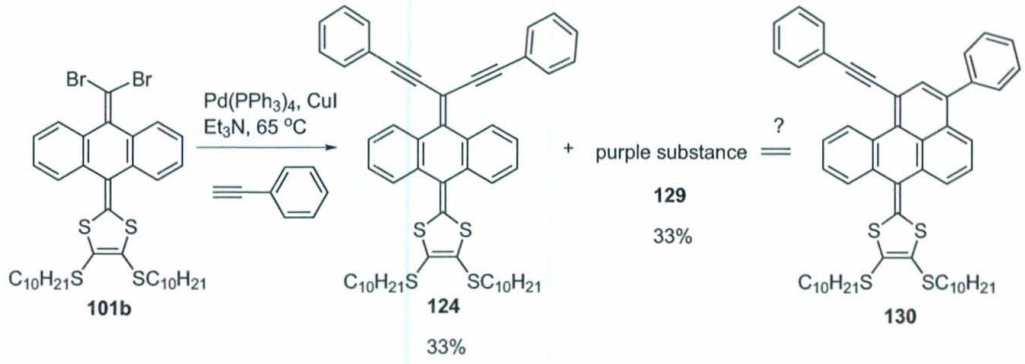

Scheme 2.19: Sonogashira reaction of **101b** with phenylacetylene.

aromatic protons on the phenylacetylene substituents would be beneficial. Upon this consideration, Sonogashira reactions of **101b** with 4-methoxyphenylacetylene/4-nitrophenyleacetylene were performed. The use of these substituents was expected to simplify the signals of the phenyl protons and to make the spectral assignment easier. Interestingly, only the cross coupling reaction of **101b** with 4-methoxyphenylacetylene yielded a blue substance as a byproduct in a comparable yield to the cross-coupling product (Scheme 2.20), whereas the cross coupling of **101b** with 4-nitrophenylacetylene ended with mainly cross-coupling product. This result suggested that the side reaction is substituent sensitive. The signals of aromatic protons for the unknown product **132** in Scheme 2.20 were better resolved, but still not good enough to allow clear structure identification. Because the crude product of the blue substance contained some inseparable impurities, no further characterization was done. Understanding of this unexpected side reaction will require further experimental efforts; in particular, it will be of great value if single crystals of the unknown suitable for X-ray stucture analysis can be obtained.

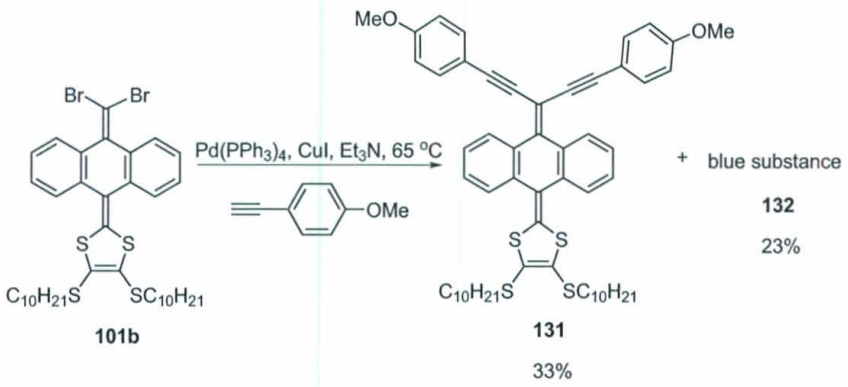

Scheme 2.20: Sonogashira reaction of **101b** with 4-methoxyphenylacetylene.

2.2.1.10 Structural Properties of Macrocyclic TTFAQ Analogue 98b

Single crystals of **98b** were obtained by slow diffusion of MeOH into a $CHCl_3$ solution of **98b** at 4 °C. The structure of **98b** was then investigated by single crystall X-ray diffraction. Two structurally similar polymorphs were observed in the single crystal of **98b**. Figure 2.6(a) shows the ORTEP plot highlighting the geometric features of the conjugated molecular skeletons for one of the polymorphs. Compound **98b** displays a substantially bent S-shaped structure, in which the central macrocyclic enyne core assumes a planar conformation, while the two dithiole rings are in a nearly perpendicular orientation versus the central cyclic enyne plane. The interplanar angle between the two planes of adjacent dithiole and anthracene units is 15.5°, while the angle between the dithiole ring and central cyclic enyne plane is at 79.3°. These angles are in line with the bend parameters observed in the crystal structures of quinonedimethane-type exTTFs reported in the literature.[118,119]

The nonplanarity of the central structure between the two dithiole rings could arise mainly from the significant steric interactions among the anthryl units and macrocylic enyne moieties. Interestingly, to release the steric hindrance, the two anthryl units

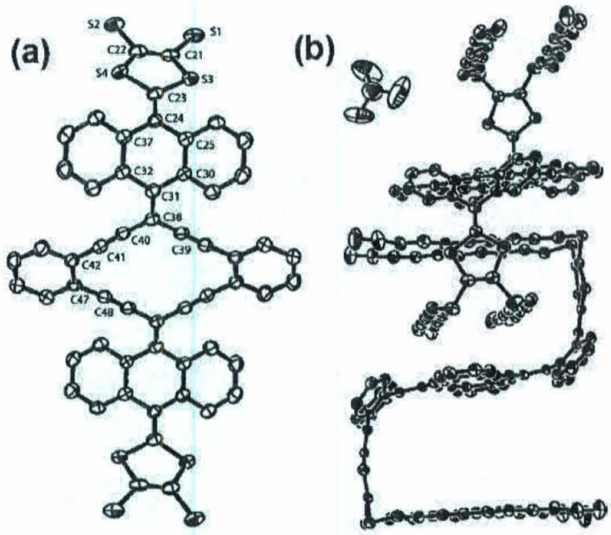

Figure 2.6: (a) ORTEP drawing of compound **98b** at the 50% probability level (*n*-decyl chains were removed for clarity). (b) Solid-state packing of two molecules of **98b** in the unit cell. Note that solvent $CHCl_3$ molecules are present in the ORTEP plots. Selected bond lengths (Å): C23-C24 1.361(5), C24-C37 1.474(6), C32-C37 1.410(5), C31-C32 1.478(7), C31-C38 1.374(7), C38-C40 1.431(5), C40-C41 1.189(5), C41-C42 1.439(5), C42-C47 1.429(7). Selected bond angles (deg): C25-C24-C37 114.9(3), C30-C31-C32 113.8(4), C39-C38-C40 113.9(4), C38-C40-C41 117.3(6), C40-C41-C42 175.2(5), C41-C42-C47 121.1(4). CCDC 680314.

bend to the opposite sides of the central cyclic enyne plane. This is different from the scenario observed on the anthraquinone central plane, that is, the steric hindrance is released when the dithiole ring and macrocyclic enyne core bend to the same side of the antraquinone plane. A possible explanation is that this avoids steric interactions between alkyl chains and maximizes the π-alkyl interactions.

In the crystal lattice, two molecules of **98b** are closely positioned in the manner depicted in Figure 2.6(b). The long *n*-decyl chains and the central bisbenzo-cyclic enyne moiety adopt a π-alkyl-alkyl-π intermolecular stacking, interlocking the two molecules orthogonally with respect to one another.

2.2.1.11 Electronic Properties of Macrocyclic TTFAQ Analogue 98b and Related Compounds

UV-Vis absorption spectra of macrocycle exTTF **98b**, acyclic exTTF dimer **123**, monomer **124** and TTFAQ derivative **133** were measured (Figure 2.8). Compound **98b** exhibits three significant absorption bands at 528, 419 and 387 nm, while its "half structure", monomer **124**, shows only two bands at 464 and 367 nm. An acyclic counterpart to **98b**, exTTF **123**, also shows two bands at 510 and 367 nm. The broad absorption of **98b** between 370–420 nm may arise from interactions between the dithiole rings and the central macrocycle. Compared to monomer **124**, the longest wavelength absorptions of exTTF **98b** and **123** are significantly redshifted, as a result of their further extended conjugated pathways between the two dithiole rings. Interestingly, the longest wavelength absorption of monomer **124** is redshifted compared to TTFAQ derivative **133**, probably due to a push and pull effect.

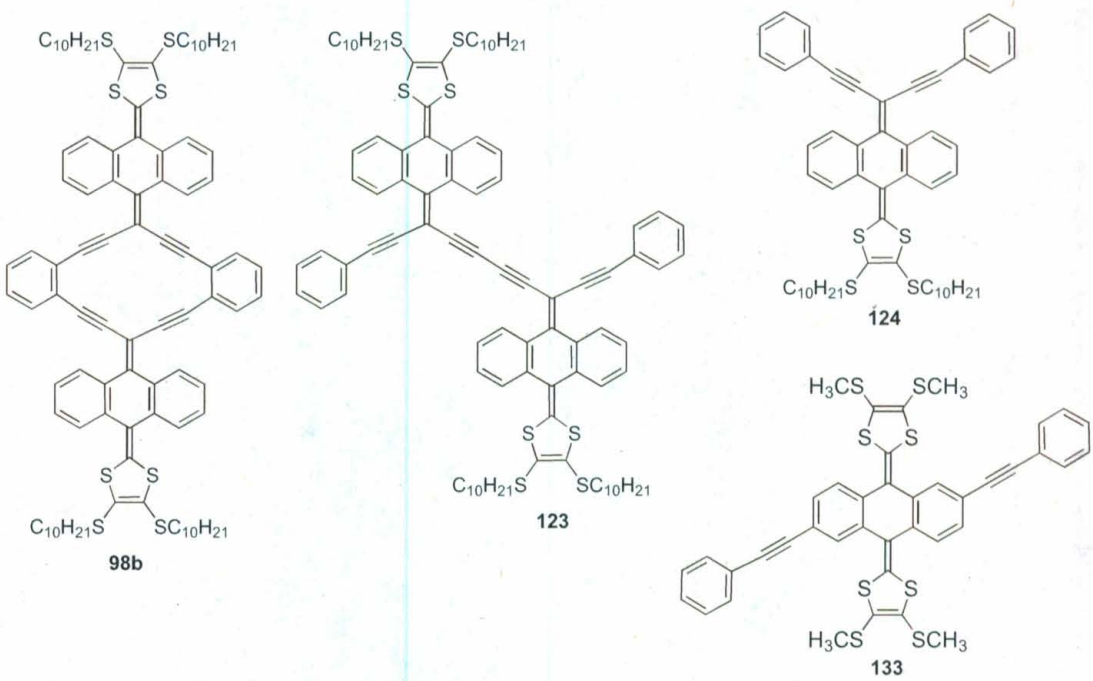

Figure 2.7: Structures of macrocycle exTTF **98b**, acyclic exTTF **123**, monomer **124**, and TTFAQ derivative **133**.

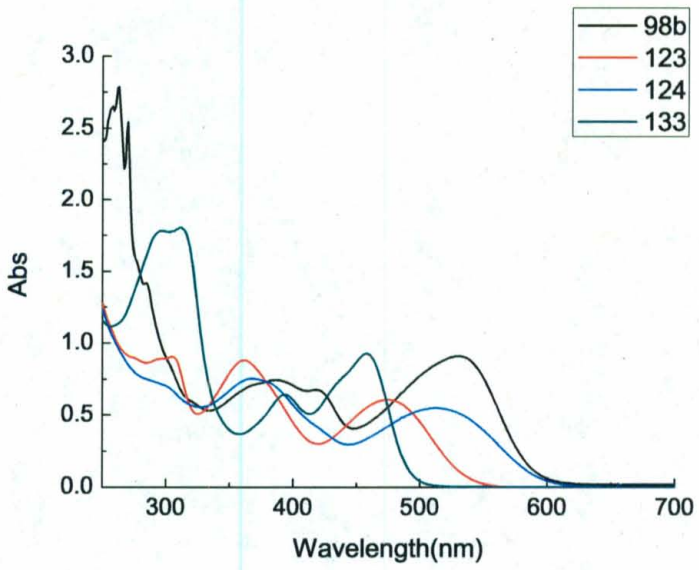

Figure 2.8: UV-vis spectra of compounds **98b**, **123**, **124**, and **133** measured in $CHCl_3$.

The fluorescent properties of **98b** and monomer **124** are delineated in Figure 2.9. The maximum emission peak (λ_{em}) of **98b** appears at 628 nm, a wavelength redshifted by 44 nm versus that of **124**. This observation is consistent with the UV-vis results, suggesting that **98b** has a smaller HOMO-LUMO gap than does **124**. The fluorescence quantum yield of **98b** ($\phi = 0.13$) is about double that of its half-structure **124** ($\phi = 0.064$), which can be due to the rigid central enyne core.

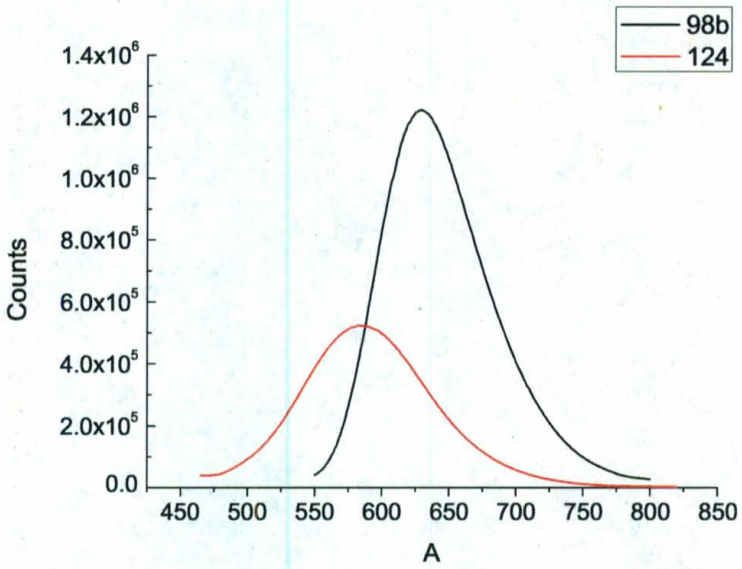

Figure 2.9: Fluorescence spectra of **98b** ($\lambda_{ex} = 531$ nm) and monomer **124** ($\lambda_{ex} = 447$ nm) measured in $CHCl_3$.

2.2.1.12 Electrochemical Redox Properties of 98b and 124

Cyclic voltammetric analyses were performed on macrocycle **98b** and monomer **124**, and their cyclic voltammograms are shown in Figure 2.10. As can be seen, both compounds showed an irreversible reduction and two irreversible oxidation

processes. The similar redox behaviors of macrocycle **98b** and compound **124** suggest insignificant electronic communications between the two dithiole rings through the $\pi-$conjugated macrocyclic bridge in compound **98b**. The irreversible reductions of **98b** and **124** occur at similar potentials, about -0.2 V. The exact origin of this reduction is not clear and waits for further investigation. At this juncture, it is tentatively assigned to the reduction of the exocyclic alkene on the anthracene units based on two rationales. First, the exocylic alkenes are expected to show electron-withdrawing ability facilitated by the C≡C bonds of the central enyne macrocycle. Second, the reduced species may be stabilized by the aromatic structure of the anthraquinoid moiety. It is noted that the reduction potential of macrocycle **98b** is slightly lower than that of **124**. This observation agrees with the empirical estimation that the macrocyclic enyne core has a better electron withdrawing ability than the acyclic enyne framework in **124**.

2.2.1.13 Oxidative Titration and Spectroelectrochemistry of TTFAQ Analogue 98b

To further investigate the electronic properties of macrocyle **98b** in both neutral and oxidized states, an oxidative titration experiment using $PhI(OAc)_2/CF_3SO_3H$ as the oxidant was carried out. The progress of the titration was monitored by UV-vis absorption spectroscopy.[120,121] As shown in Figure 2.11, four isosbestic points are clearly seen in the titration process, indicating clean oxidations of **98b** to cationic species. With increasing addition of the oxidant, the intensity of the absorption peaks at 370 and 530 nm decreased and the absorption at 450 nm increased. Unlike the oxidative titration of TTFAQ derivatives reported in the literature,[122,123] no

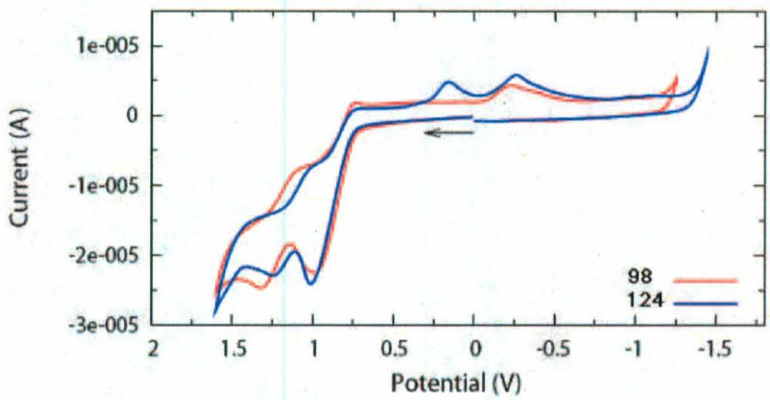

Figure 2.10: Cyclic voltammograms of **98b** and **124** measured in $CHCl_3/CH_3CN$ (4:1, v/v) at room temperature. Bu_4NBF_4 (0.1 M) as the supporting electrolyte, glassy carbon as the working electrode, Pt wire as the counter electrode, and Ag/AgCl as the reference. Scan rate: 100 mV s^{-1}.

distinctive new low-energy band significantly emerged as a result of the formation of cationic **98b**. Possibly, the absorption of the cationic species resulting from oxidative titration is weak in intensity and merged with the broad featureless absorption profile in the range of 500-600 nm. Nonetheless, a long absorption tail above 600 nm is still discernible and can be associated with the oxidized species.

Spectroelectrochemistry of **98b** was also studied (see Figure 2.12). In the experiments, UV-vis absorption spectra of **98b** were determined at various applied potentials in the range from +300 to +1500 mV. The spectral variations are essentially the same as those in oxidative titration. The drifting of spectral baselines at high potentials is likely due to system error caused by the evaporation or electrolysis of solvent.

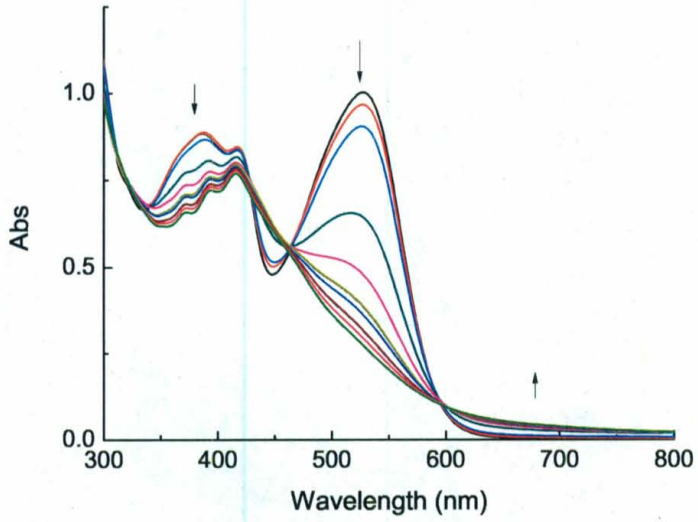

Figure 2.11: UV-vis spectra of macrocycle **98b** upon addition of oxidant (0 to 1 equiv.) measured in $CHCl_3$.

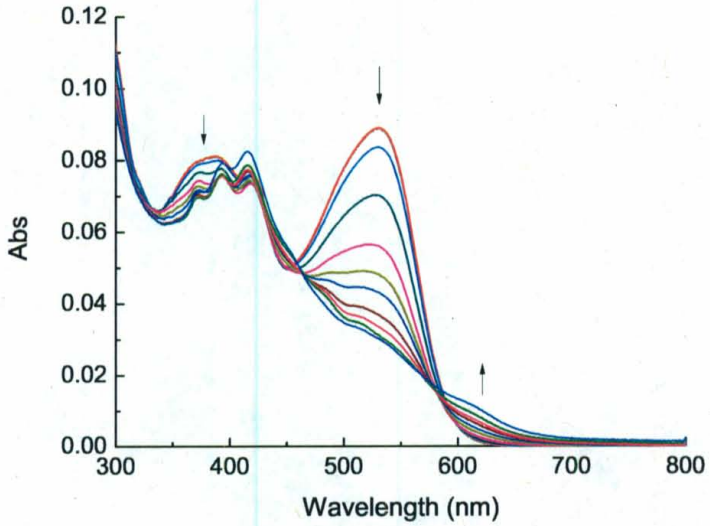

Figure 2.12: UV-Vis spectra of **98b** determined at potentials from +0.3 to +1.5 V. Experimental conditions: supporting electrolyte: Bu_4NBF_4 (0.1 M); solvent: $CHCl_3$; working electrode: Pt mesh; counter electrode: Pt; reference electrode: Ag/AgCl.

2.2.1.14 Summary

A new synthetic methodology has been developed and applied to the synthesis of a class of highly $\pi-$extended TTFAQ analogues containing a macrocyclic enyne core. Insertion of the macrocyclic enyne π-spacer into TTFAQ has brought about some interesting solid-state packing and electronic absorption/emission properties to **98b**. However, as indicated by the CV data **98b** is a weaker electron-donor than TTFAQ as a result of its prolonged π-spacer length and highly bent molecular shape.

2.2.2 Synthesis and Characterization of TTFAQ Analogue 99

2.2.2.1 Retrosynthetic Analysis

Following the synthesis of TTFAQ analogue **98b**, a planar macrocyclic enyne bridged TTFAQ analogue **99** was targeted. The retrosynthetic analysis of **99** is shown in 2.21. By a strategy similar to TTFAQ analogue **98b**, disconnection of the central macrocyclic enyne structure led to two precursors **134** and **135**. Similar to the successful macrocyclization reaction in the synthesis of **98b**, a four-fold Sonogashira reaction of desilylated **134** and diiodo **135** was envisaged to afford the desired product. Precursor **134** could be prepared from ketone **136**. An HWE reaction of ketone **136** and phosphonate **105** or phosphonium salt **137** would then furnish **134**. The synthesis of diiodide **135**, ketone **136**, phosphonate **105**, phosphonium **137** are all well-documented in the literature.

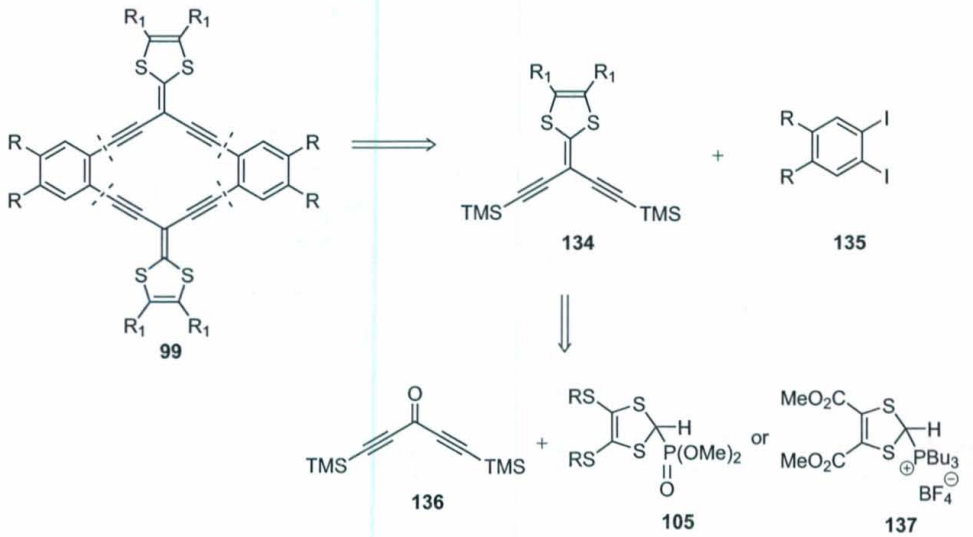

Scheme 2.21: Retrosynthetic analysis of TTFAQ analogue **99**.

2.2.2.2 Synthesis of Ketone 136

Ketone **136** was synthesized according to known procedures.[124–127] The detailed steps are described in Scheme 2.22. The synthesis started with treatment of propargyl alcohol **138** with *n*-BuLi in THF cooled in a dry ice-acetone bath. The lithium acetylide generated in situ was then treated with TMSCl, followed by aqueous workup, to give compound **139** in 75% yield. PCC oxidation of alcohol **139** afforded aldehyde **140**, which was then subjected to nucleophilic attack by lithium trimethylsilylacetylide to afford alcohol **141**. In addition to this stepwise manner, alcohol **141** could also be prepared by one-pot addition of lithium trimethylsilylacetylide to methyl formate. PCC oxidation of alcohol **141** then furnished ketone **136** in 35% yield.

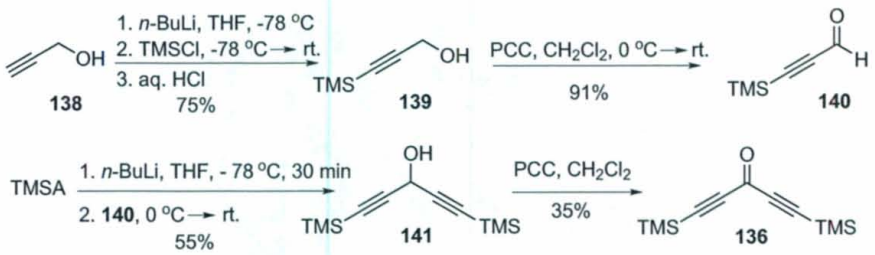

Scheme 2.22: Synthesis of ketone **136**.

With ketone **136** in hand, two routes could be possibly employed to construct TTFAQ analogue **99**. The first route is depicted in the retrosynthetic analysis in Scheme 2.21, while the second one starts from a Sonogashira coupling between a diiodide and ketone **136** to form a macrocyclic diketone, which is next subjected to a two-fold Wittig-type olefination. In this thesis work, both synthetic routes were investigated. The second route was soon abandoned, since desilylation of ketone **136**

with K_2CO_3 in THF/MeOH or TBAF ended up with only decomposed substances, indicating very poor stability of desilylated **136**.

2.2.2.3 Synthesis of Dithiafulvenes 134a,b

Using ketone **136** as the precursor, compounds **134a,b** were prepared by the HWE or Wittig reactions depicted in Scheme 2.23. In the synthesis, phosphonate **105a** and phosphonium salt **137**[128] were first deprotonated by *t*-BuLi. The resulting ylides were reacted with ketone **136** to afford compounds **134a,b**[87] respectively in moderate yields. It is worth noting that ketone **136** showed limited stability in some organic solvents. For instance, after dissolving ketone **136** in dry THF, the solution became dark brown with 5 min. TLC analysis indicated the presence of several new compounds, likely stemming from some decomposition reactions. When ketone **136** was dissolved in CH_2Cl_2, however, it afforded a stable pale yellow solution. Apparently, the stability of **136** in solution is solvent dependent.

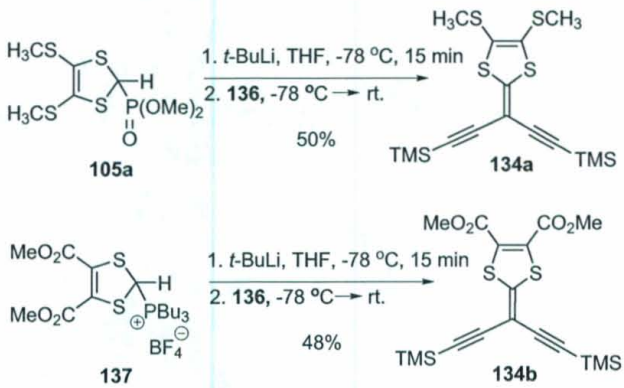

Scheme 2.23: Synthesis of DTF precursor **134a,b**.

2.2.2.4 Synthesis of Diiodoarenes 135b,c

To construct the target macrocyles through the Sonogashira strategy, 1,2-diiodobenzenes were chosen as the building blocks. In addition to 1,2-diiodobenzene (**135a**) which is commercially available, alkyloxy and crown ether-appended diiodobenzenes **135b,c** were also prepared so as to impart better solubility or more functionality to the target compounds. The syntheses of **135b,c** were performed according to known procedures. As shown in Scheme 2.24 diiodobenzene **135b** was prepared from catechol by a two-step synthesis involving an alkylation of catechol followed by an iodination with $I_2/Hg(OAc)_2$.[129]

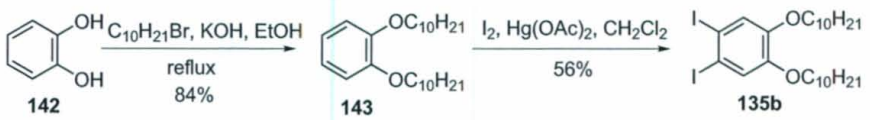

Scheme 2.24: Synthesis of diiodobenzene **135b**.

Crown ether-annulated diiodobenzene **135c** was prepared by two different routes. In route 1 (Scheme 2.25), catechol was protected with acetone to form acetal **146** in the presence of P_2O_5. Iodination of **146** with $I_2/Hg(OAc)_2$, followed by deprotection of the resulting diiodo compound **147** in a refluxing, acidic, aqueous solution, furnished diiodonated catechol **148**. Compound **148** was then cleanly converted to diiodo crown ether **135c** by a reaction with ditosylate **145** in the presence of NaOH and a phase transfer catalyst, Bu_4NBr.[130,131] Ditosylate **145** was prepared by a reaction of tetraethyleneglycol with TsCl in THF using Et_3N as base.[132] In route 2 (Scheme 2.25), catehol was reacted with ditosylate **145** in the presence of NaOH and Bu_4NBr. The resulting crown ether **149** was iodinated with H_5IO_6/I_2 in

acidic conditions to afford **135c** which was purified by recrystallization from hexanes. Iodination of **149** under other conditions such as using $I_2/Hg(OAc)_2$ or ICl was tried, but these reactions afforded mixtures of substituted benzenes, making purification of the desired product unsuccessful. Overall, route 2 has been found to be more concise and productive.

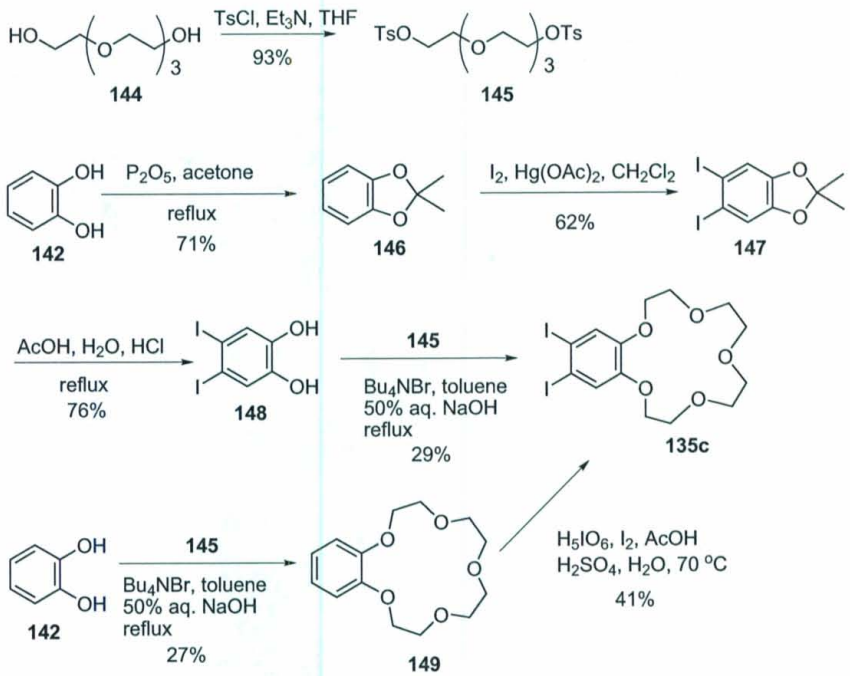

Scheme 2.25: Synthesis of crown ether-annulated diiodobenzene **135c**.

2.2.2.5 Synthesis of TTFAQ Analogues 99a-c

The synthesis of macrocyclic TTFAQ analogues **99a-c** is described in Scheme 2.26. Compound **134a** was first desilylated with K_2CO_3 in THF/MeOH. Since the resulting terminal alkyne was not stable in the solid state, it was directly used in the following cyclization reactions without further purification. The cyclization used

a one-pot coupling strategy as in the synthesis of TTFAQ analogue **98b**. As shown in Scheme 2.26, desilylated **134a** was reacted with diiodobenzenes **135a-c** respectively to give cyclic products **99a** in 20% yield, **99b** in 7% yield, and **99c** only in a trace amount. In all the three reactions, the formation of acyclic oligomers was prominent. In the reaction for **99c**, deiodination and decomposition of the catalyst were also observed. Electron-donating subsitituents could slow down Sonogashira reactions, which partially accounts for the extremely low yield of **99c**. Addition of NaCl to the synthesis of **99c** was tried with the hope that the electron-donating ability of the crown ether could be reduced by coordinating Na^+ with the crown ether. Nevertheless, this method did not lead to significantly improved yields. Deiodination and decomposition of the catalyst became trivial under these conditions. Furthermore, other solvent/base systems, such as THF/Et_3N (1:1), and toluene/DBU, have been investigated, but they did not give any better results.

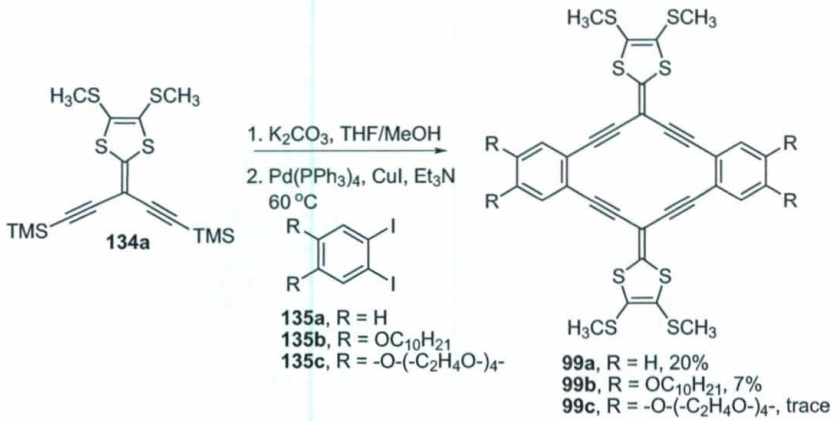

Scheme 2.26: Synthesis of TTFAQ analogues **99a-c** by a one-pot macrocyclization.

Aside from **134a**, compound **134b** (for structure, see Scheme 2.23) was also tested as a building block for making macrocylic TTFAQ analogues similar to **99**,

but carrying ester pendant groups instead of SCH_3 groups on the dithiole rings. In the synthesis, desilylation of **134b** with K_2CO_3 in THF/MeOH failed, but the use of TBAF was able to accomplish the task successfully. The resulting diyne was then subjected to a four-fold Sonogashira reaction with 1,2-diiodobenzene using the conditions described above. Although the desired macrocycle product was detected by MALDI-TOF MS analysis, separation of it from byproducts, mostly acyclic oligomers, was unsuccessful. At this juncture, the applicability of **134b** as a building block for constructing macrocyclic TTFAQs did not appeare to be promising.

Parallel with the one-pot cyclization strategy, a step-wise ring closure approach was also pursued in the hope of obtaining higher yields. As shown in Scheme 2.27, the syntheses started with the Sonogashira reactions of desilylated **134a** with excess diiodo compounds **135a**,**b** respectively. Cyclization of intermediates **150a**,**b** to form the final macrocylic products is theoretically a favorable choice due to the less entropic penalty than that of the one-pot strategy. Experimentally, the syntheses of **150a**,**b** ended with very poor yields, making this strategy not so promising. The low yields could come from the inherent instability of desilylated **134a** under Sonogashira reaction conditions, which would also explain the extremely low yield in the formation of macrocycle TTFAQ analogue **99**.

2.2.2.6 Single Crystal Structural Properties of Macrocyclic TTFAQ Analogue 99b

Attempts to grow single crystals of TTFAQ analogue **99a** in various organic solvents were not very successful. However, high-quality crystals of **99b** were formed accidentally when a solution of **99b** in $CHCl_3/CH_3CN$ (4:1, v/v) in the presence

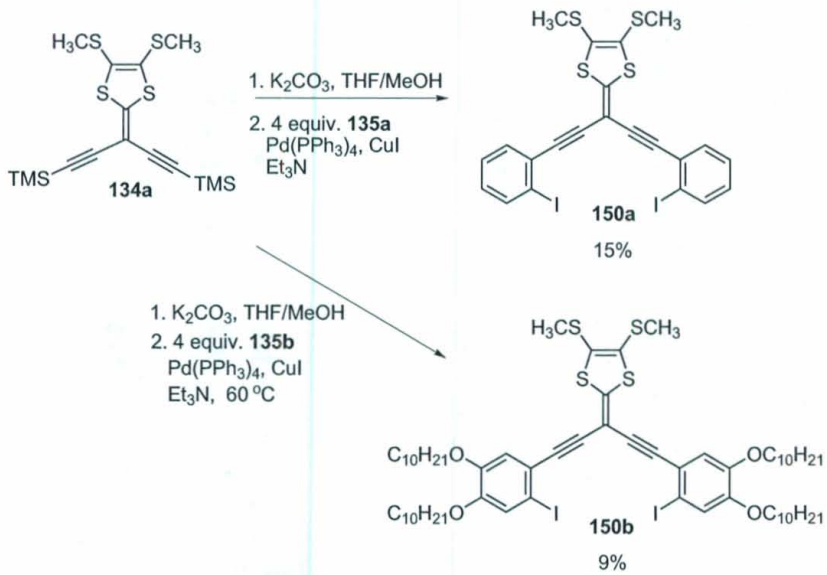

Scheme 2.27: Synthesis of compounds **150a** and **150b**.

of Bu_4NBF was stored at ca. 4 °C. Originally, the mixture was prepared for cyclic voltammetry study. After storing in a fridge for more than one month, single crystals grew slowly at the bottom of the sample vial. X-ray diffraction analysis on one of these crystals was carried out, and the single crystal structural properties of **99b** are illustrated in Figure 2.13.

As can be seen in Figure 2.13(A) and (B), the single crystal structure of **99b** adopts a planar conformation. The central enyne macrocycle is coplanar with adjacent phenyls and dithiole rings, as a result of the removal of steric hindrance caused by the anthraquinone moiety in TTFAQ analogue **98b**. A closer comparison of crystallographic data of **99b** to **98b** shows that the bond length alternation (BLA) index (δ_{BLA}) of **99b** (0.155 Å) is slightly shorter than that of TTFAQ analogue **98b** (δ_{BLA} = 0.165 Å). The variation in BLA suggests that the cyclic enyne segment in **99b** possesses a higher degree of π-delocalization than TTFAQ **98b**, resulting

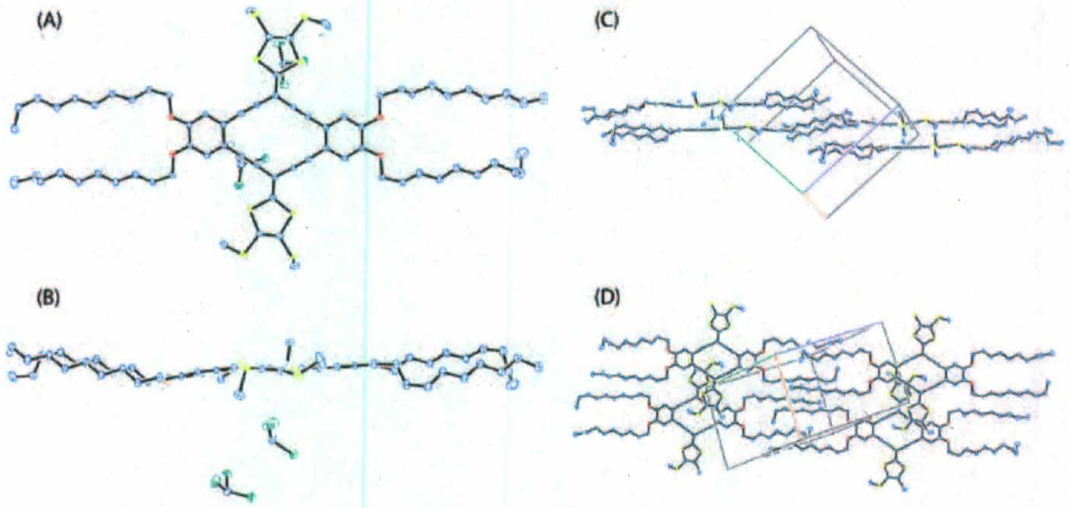

Figure 2.13: Single-crystal structure of TTFAQ analogue **99b**: (A) front view of ORTEP plots. (B) side view of ORTEP plot. (C) side view of crystal packing diagram, and (D) front view of crystal packing diagram. Ellipsolid probability at 30% level. Note that solvent $CHCl_3$ molecules are present in the ORTEP plots. CCDC 726951.

from stronger electronic interactions between the dithiole rings and the central enyne macrocylce.

As shown in Figure 2.13(C) and (D), the molecules of **99b** pack in a columnar fashion in the crystal lattice where the electron-rich dithiole rings directly overlap with the relatively electron-deficient macrocyclic enyne core, affording a slipped face-to-face stacking. This solid-state packing feature is markedly different from the crystal packing of non-planar TTFAQ analogue **98b**. The distance between the mean planes of two adjacent molecules is measured at 3.73 Å, and the close proximity between the donor (dithiole) and acceptor (enyne ring) is suggestive of intermolecular charge-transfer interactions. The planar framework of **99b** is important to the formation of efficient π-stacking in the solid state, which could benefit its electronic and optoelectronic applications.

2.2.2.7 Electronic Properties of Macrocyclic TTFAQ Analogues 99a,b and Related Compounds

The UV-Vis absorption and fluorescence emission properties of **99a**,**b** were studied and the results are shown in Figures 2.14 and 2.16.

In Figure 2.14, compound **99a** shows two characteristic low-energy absorption bands at 480 and 453 nm, which are nearly identical to those of **99b** at 483 and 457 nm. These absorptions are substantially redshifted in comparison to the maximum absorption band (λ_{max}) of dithiole precursor **134a** at 380 nm, indicating the presence of significant electronic interactions between the dithiole rings and the central macrocyclic enyne units in **99a**,**b**. The slight but noticeable redshift of absorption bands in the spectra of **99b** to **99a** does not follow the expectation, since decyloxy

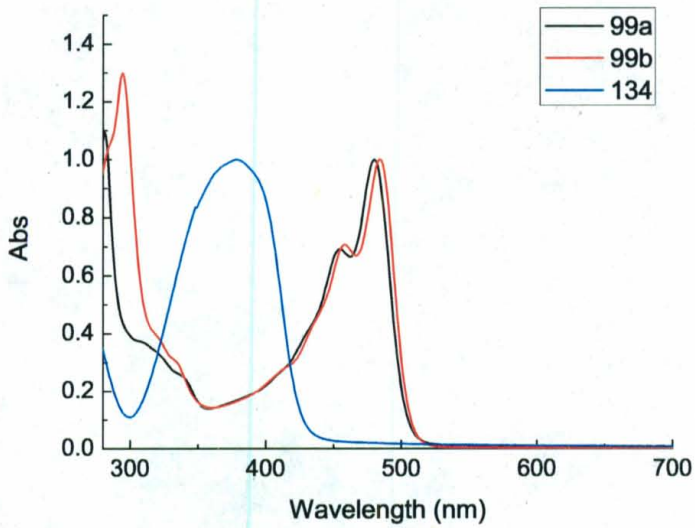

Figure 2.14: UV-Vis absorption spectra of compounds **134a** and **99a**,**b** measured in $CHCl_3$.

chains are supposed to increase the electron density of the central $\pi-$chromophore and cause a blueshift to the longest-wavelength absorption if it is a π-π^* transition. The UV-Vis absorption of **99b** shows interesting solvent-dependant behavior (Figure 2.15), where the solvatochromic effect is particularly significant in oxygen-containing solvents, such as EtOAc and THF.

The fluorescence spectra for **99a**,**b** are shown in Figure 2.16, in which both compounds exhibit a similar broad and structureless emission profile. The maximum emission wavelength (λ_{em}) of **99b** bearing decyloxy chain appears at 510 nm, which is slightly blueshifted relative to that of **99a** at 522 nm.

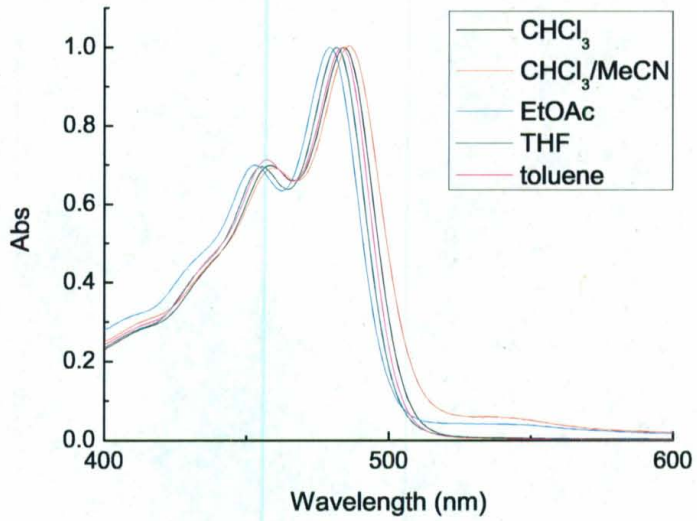

Figure 2.15: UV-Vis absorption spectra of **99b** measured in different solvents.

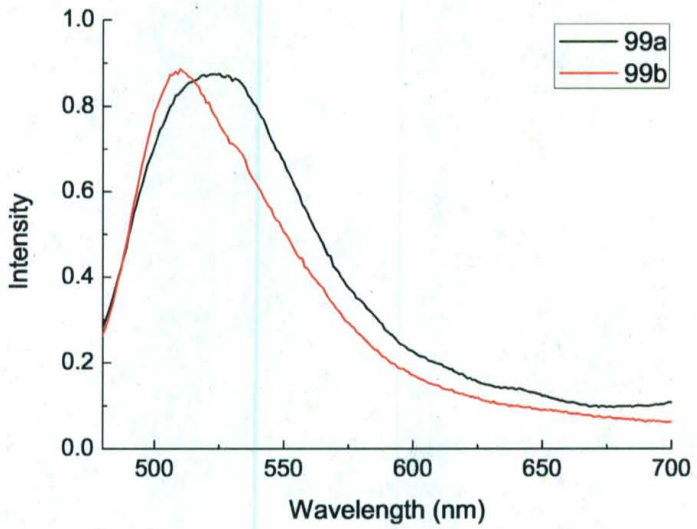

Figure 2.16: Fluorescence spectra of **99a,b** measured in $CHCl_3$ (λ_{ex} = 400 nm).

2.2.2.8 Electrochemical Redox Properties of 98b, 134a and 150b

The electrochemical redox behavior of compound **99b** was studied by cyclic voltammetry while efforts to characterize **99a** by the same technique failed due to its limited solubility. The cyclic voltammograms of **99b** shown in Figure 2.18 were determined over varied ranges of potential scans at 0 °C. The lower potential limit was chosen at -0.5 V just in case reduction of the oxidized species might occur at low potentials due to the energy requirement for conformational change. In the scan range of -0.5 to +0.72 V, the voltammogram shows a pair of redox waves at $E_{pa1} = +0.67$ V and $E_{pc1} = +0.53$ V. Given the fact that the separation between the two peaks is +0.14 V and the peak positions are scan rate dependant, this redox wave pair is considered as quasi-reversible and its origin is tentatively assigned to a simultaneous two-electron oxidation at the dithiole rings of **99b**. The value of the first oxidation potential is similar to those reported for TTFAQ (+0.44 V vs SCE in CH_2Cl_2)[133] but much lower than that of non-planar TTFAQ analogue **98b** (+0.98 V). This result suggests that the acetylene expanded macrocyclic spacer in **99b** mediates electronic communication between the two dithiole rings to an extent that is comparable to the anthraquinoid spacer in a typical TTFAQ. When scanned from -0.5 to +0.9 V, a second anodic current peak emerged at $E_{pa2} = +0.76$ V, which is associated with a relatively sharp cathodic current peak at $E_{pc2} = +0.65$ V. When the switching potentials are from -0.5 to +1.2 V, two anodic peaks at +0.64 and +0.76 V along with one broad cathodic peak at +0.62 V were observed in the voltammogram. In the range of -0.5 to +1.5 V, a third anodic peak at +1.32 V appeared, while there is no noticeable cathodic current observed in the voltammogram. The irreversible pattern here may be rationalized by

an EC mechanism, where an electrochemically promoted reaction swiftly follows up the oxidation of **99b**. Different pulse voltammetric analysis (see the inset of Figure 2.13) also corroborates that **99b** undergoes three distinct oxidation steps at +0.59, +0.71, and +1.13 V, respectively.

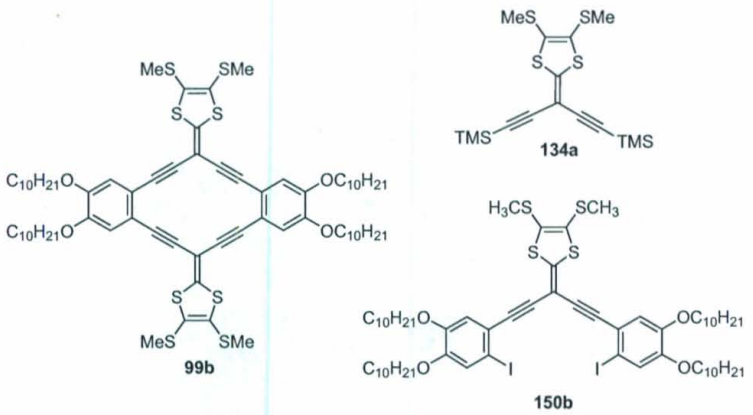

Figure 2.17: Structures of compounds **99b**, **134a**, and **150b**.

Compared with **99b**, monomer **134a** displays relatively simple redox properties. As shown in Figure 2.19, the CV profile gives an irreversible oxidation with a large anodic peak current and a small cathodic peak current. Since a blue film was observed on the electrode surface after scanning, the irreversible behavior is likely correlated to a deposition process. The oxidation occurs at about +0.95 V, which is much higher than both 1st and 2nd oxidation potentials of **99b**. In other words, the electron-donating ability of **99b** is much higher than monomer **134a**, which is consistent with the general expectation for TTF. It also serves as evidence that this macrocyclic core allows significant electron communication between two dithiole rings. The oxidation profile of **134a** is similar to the first oxidation of non-planar TTF **98b** bearing an extra anthraquinoid structure. This observation indicates the anthraquinoid structure

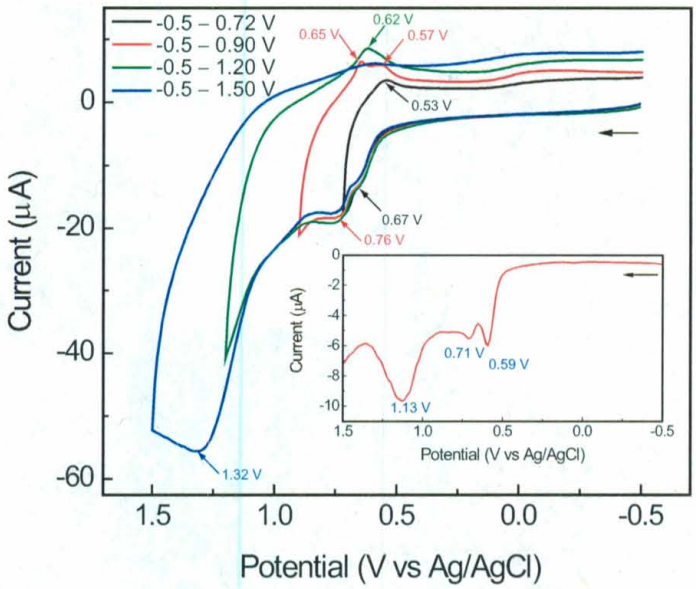

Figure 2.18: Cyclic voltammograms of TTFAQ analogue **99b** measured in varied potential scan windows at 0 °C. Experimental conditions: solvent: CH_2Cl_2; electrolyte: Bu_4NBF_4 (0.1 M); working electrode: glassy carbon; counter electrode: Pt; reference electrode: Ag/AgCl; scan rate: 500 mV/s. Inset: differential pulse voltammogram of **99b** measured at 0 °C.

in **98b**, in fact, has little influence on the electron-donating ability of dithiole rings.

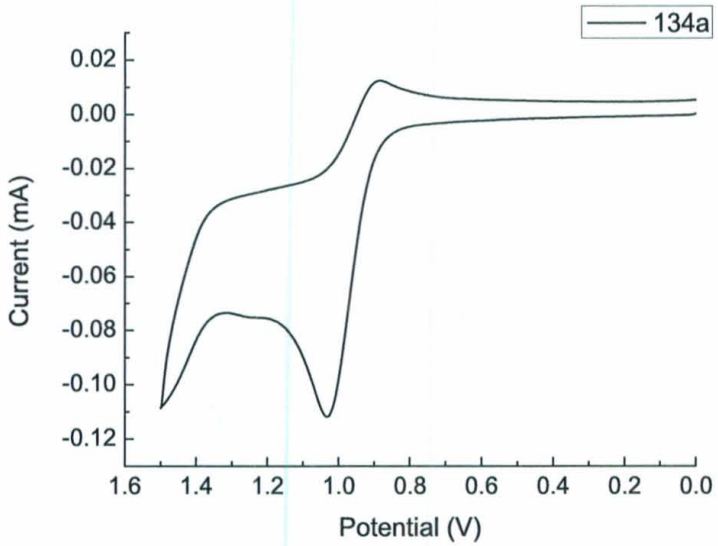

Figure 2.19: Cyclic voltammogram of compound **134a**. Experimental conditions: solvent: CH_2Cl_2; electrolyte: Bu_4NBF_4 (0.1 M); working electrode: glassy carbon; counter electrode: Pt; reference electrode: Ag/AgCl; scan rate: 200 mV/s.

The redox behavior of **150b** is relative complex. As shown in Figure 2.20, the voltammogram displays three oxidations at +0.83, +1.19 and +1.38 V, respectively. The first oxidation is similar to that of **134a**, thus it is ascribed to the oxidation of dithiole rings. The first oxidation potential of **150b** is lower than **134a**, corresponding to an enhanced electron-donating ability. An explanation for this can be that either the electron density on dithiole ring is increased or the oxidized product is stabilized by the substituent effect. Compared with **99b**, the first oxidation potential of **150b** is much higher, suggesting that the macrocyclic core in **99b** provides further stabilization to the resulting cations. The second oxidation potential of **150b** is

similar to the third oxidation peak of **99b**, and hence they may be of the same origin; that is, the oxidation of ethynylated benzo units. The oxidation of **150b** shows reversible character but **99b** does not. The different behavior may be rationalized by a possible following chemical reaction when **99b** is oxidized at the electrode surface. The reaction might involve the whole macrocylic unit; however, the detailed transformation is not clear at the moment. The third oxidation of **150b** is barely recognizable due to significant overlap with the oxidation peak of solvent. Its origin may be attributed to the oxidation of the iodobenzo units, which normally requires a high potential to take place. No characteristic reduction processes of **150b** are observed in the voltammogram. By comparing the structural differences between **150b** and **98b**, the reduction features of non-planar **98b** (see Figure 2.10) can be reasonably correlated to the antraquinoid structure, which is absent in the structure of **150b**.

2.2.2.9 Spectroelectrochemistry of TTFAQ Analogue 99b and Monomer 134a

Spectroelectrochemistry of **99b** and monomer **134a** were determined using the same methods as for TTFAQ analogue **98b**. Figures 2.21 and 2.22 show the detailed spectroelectrochemical data. The UV-Vis absorption bands of **99b** at 483 and 457 nm decrease as the compound is gradually oxidized. In the meantime, an absorption tail emerges, starting from 500 nm and extending to 800 nm, which can be associated with the formation of cationic species resulting from electrochemical oxidation. Importantly, isosbestic points are observed for absorptions at low potentials, indicating clean reversible oxidation. However, at high potentials, the

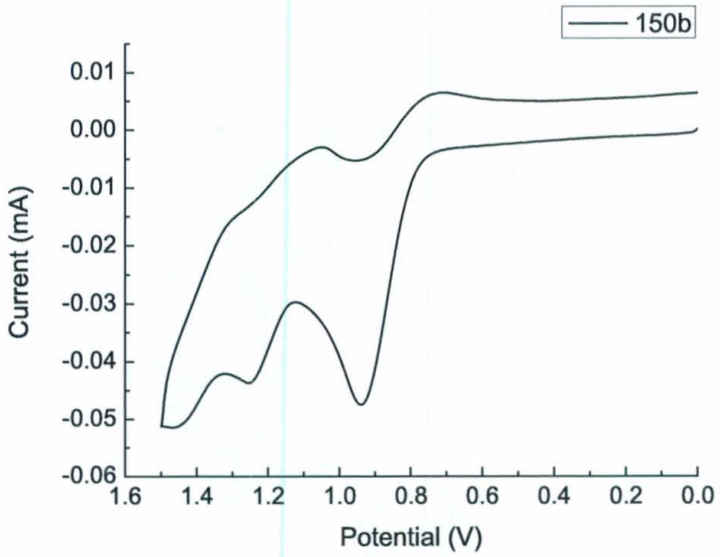

Figure 2.20: Cyclic voltammogram of compound **150b**. Experimental conditions: solvent: CH_2Cl_2; electrolyte: Bu_4NBF_4 (0.1 M); working electrode: glassy carbon; counter electrode: Pt; reference electrode: Ag/AgCl; scan rate: 200 mV/s.

isosbestic points disappear possibly due to the formation of complex oxidized species by follow-up chemical reactions. This observation is consistent with the cyclic voltammetric data in that once the third oxidation occurs, cathodic peaks are no longer observed. In contrast the spectroelectrochemical data for **99b**, the absorption spectra of **134a** give two isosbestic points throughout the whole range of applied potentials, which is indicative of a clean oxidation. Based on this observation, the irreversible behavior of **134a** is ascribed to a partial deposition of insoluble oxidized species on the electrode instead of a follow-up reaction. This assignment is also supported by the fact that a blue film of low solubility was observed on the electrode surface after measurements.

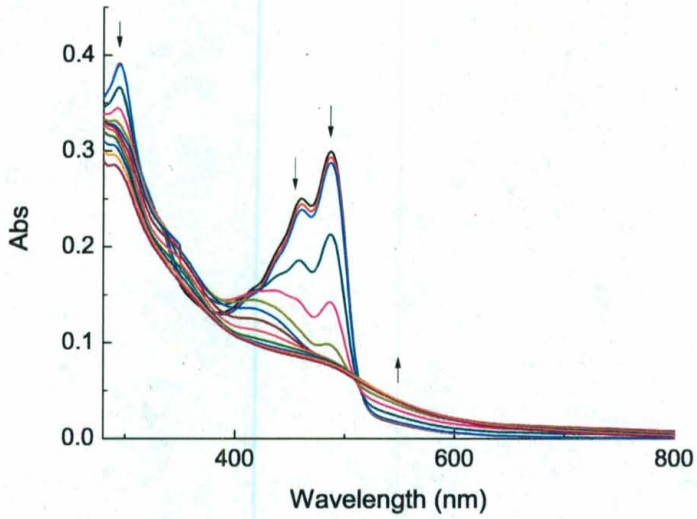

Figure 2.21: UV-Vis spectra of macrocycle **99b** determined at potentials from +0.3 to +1.5 V. Experimental conditions: supporting electrolyte: Bu_4NBF_4 (0.1 M); solvent: CH_2Cl_2; working electrode: Pt mesh; counter electrode: Pt; reference electrode: Ag/AgCl.

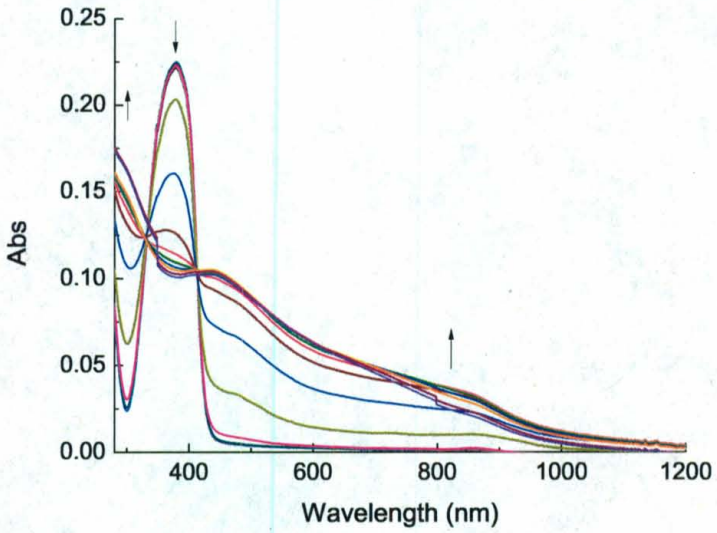

Figure 2.22: UV-Vis spectra of monomer **134a** determined at potentials from +0.3 to +1.5 V. Experimental conditions: supporting electrolyte: Bu_4NBF_4 (0.1 M); solvent: CH_2Cl_2; working electrode: Pt mesh; counter electrode: Pt; reference electrode: Ag/AgCl.

2.2.2.10 Summary

The first examples of planar acetylene-expanded TTFAQ analogues have been synthesized and characterized. Success in the synthesis proves the efficiency of one-pot Sonogashira cyclization protocol in constructing shape-persistent macrocyclic enyne structures. The simplified planar structures compared to the previously designed TTFAQ analogue **98** indeed improve the electron communication between two dithiole rings and thus increase its electron-donating ability. In addition, the solid-state packing is significantly changed as a result of the planar molecular shape. Based on

their efficient solid-state packing and electrochemical activities, the planar TTFAQ analogues are envisioned to be potentially useful materials for organic electronic devices.

2.3 Experimental

General Procedures

Chemicals were purchased from commercial suppliers and used directly without purification. CH_2Cl_2 was distilled from CaH_2 before its use in Corey-Fuchs reactions. Et_3N was distilled from LiH prior to use in Sonogashira couplings. THF was distilled from benzophenone/Na before its use in HWE reactions. All reactions were conducted in standard, dry glassware and under an inert atmosphere of nitrogen unless otherwise noted. Evaporation and concentration were carried out with a water-aspirator. Flash column chromatography was performed using 240-400 mesh silica gel obtained from VWR International. Thin-layer chromatography (TLC) was carried out with silica gel 60 F254 covered on plastic sheets and visualized by UV light. Melting points (m.p.) were measured with a Fisher-Jones melting point apparatus and are uncorrected. ^{1}H NMR and ^{13}C NMR spectra were measured on a Bruker Avance 500 MHz spectrometer. Chemical shifts are reported in ppm downfield from the signal of the internal reference $SiMe_4$. Coupling constants (J) are given in Hz. Infrared spectra (IR) were recorded on a Bruker Tensor 27 spectrometer equipped with a ZnSe ATR module. APCI mass spectra (MS) were measured on an Agilent 1100 series LCMSD spectrometer, and MALDI-TOF MS were measured on an Applied Biosystems Voyager instrument using dithranol as the matrix. Positive-mode high-

resolution mass spectra (HRMS) were measured on a Waters GCT premier instrument equipped with an electron ionization (EI) ion source and a QSTAR XL hybrid quadrupole/TOF mass spectrometer equipped with an o-MALDI ion source (Applied Biosystems). Single crystal X-ray diffraction data were collected on a Rigaku Saturn CCD area detector equipped with a SHINE optic with MoK_α radiation ($\lambda = 0.71075$ Å). UV-Vis spectra were measured on a Cary 6000i UV-Vis-NIR spectrophotometer, and fluorescence spectra were measured on a Photon Technology International (PTI) Quantamaster spectrofluorometer. Cyclic voltammetric (CV) and differential pulse voltammetric (DPV) experiments were carried out in a standard three-electrode setup controlled by a BASi epsilon workstation. Spectroelectrochemistry was investigated through the following protocol: In a 1 mm quartz cuvette were placed a Pt mesh as working electrode, Ag/AgCl as reference electrode, and Pt wire as counter electrode. The applied potential (V) was increased in steps through controlled potential electrolysis (CPE). In each potential step, the electrolysis was first performed for ca. 1.5 min until the electrical current remained constant then a UV-Vis spectrum was obtained.

Decyl Macrocycle TTFAQ analogue (98b).

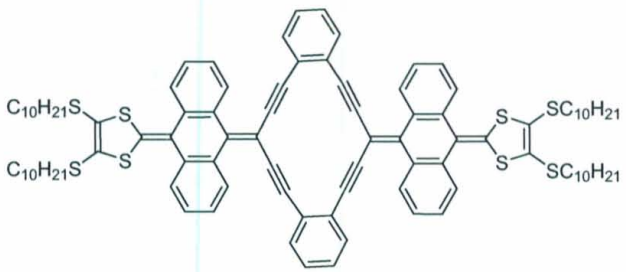

98b

Compound **100b** (133 mg, 0.160 mmol) was dissolved in THF/MeOH (20 mL, 1:1). K_2CO_3 (200 mg, 1.45 mmol) was added and the mixture was stirred for 30 min. The mixture was diluted with Et_2O, washed with H_2O, dried over $MgSO_4$, and concentrated in vacuo to about 10 mL. 1,2-Diiodobenzene (50 mg, 0.16 mmol) and CuI (12 mg, 0.063 mmol) were mixed in a 100 mL rbf, and Et_3N (40 mL) was added. The mixture was degassed and then $Pd(PPh_3)_4$ (20 mg, 0.017 mmol) was added. The mixture was heated to 65 °C. The solution of desilylated **114b** was purged with N_2 for 5 min and added dropwise in the reaction mixture over 3 h (5 mL of the solution was added over 0.5 h, and then the mixture was allowed to stir for 1.5 h before another 5 mL of the solution was added over 1h.) The mixture was stirred overnight. Then it was diluted with CH_2Cl_2, washed with NH_4Cl and H_2O, dried over $MgSO_4$, and chromatographed with 10% CH_2Cl_2 in hexanes to afford crude product **98b**, which was further purified by recrystallization from 1:1 MeOH/$CHCl_3$ as a black-red solid (32 mg, 0.021 mmol, 27%). M.p. 140-142 °C; ^{1}H NMR (500 MHz, $CDCl_3$): δ = 8.50-8.40 (m, 4H), 7.71 (d, J = 6.4 Hz, 4H), 7.47-7.36 (m, 12H), 7.31-7.27 (m, 4H), 2.90-2.72 (m, 8H), 1.65-1.56 (m, 8H), 1.45-1.33 (m, 8H), 1.30-1.15 (m, 48H), 0.90-0.80 (m, 12H); ^{13}C NMR (125 MHz, $CDCl_3$): δ = 136.1, 133.4, 132.1, 128.3, 128.1, 126.9, 125.73, 125.68, 125.3 (five sp^2 carbon peaks not observed due to coincidental overlap), 99.8, 91.9, 36.7, 32.1, 29.9, 29.74, 29.72, 29.5, 29.3, 28.7, 22.9, 14.3; FTIR (neat) 3060, 2958, 2927, 2853, 1572, 1531, 1485 cm^{-1}; MS (MALDI-TOF) m/z calcd for $C_{96}H_{108}S_8$, 1516.62 found 1518.82 $[M + H]^+$).

TTFAQ analogue (99a).

To a solution of dithiafulvene monomer **134a** (47 mg, 0.12 mmol) in THF/MeOH (10 mL, 1:1) was added K_2CO_3 (200 mg, 1.45 mmol). The mixture was stirred for

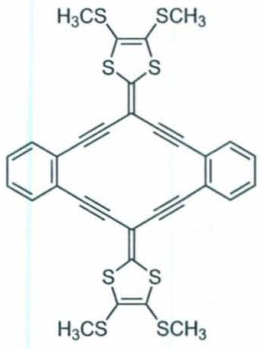

99a

30 min at rt and then diluted with Et_2O, washed with H_2O, dried over $MgSO_4$, and concentrated in vacuo to about 5 mL. $Pd(PPh_3)_4$ (32 mg, 0.028 mmol), CuI (10 mg, 0.053 mmol), *o*-diiodobenzene (30 mg, 0.091 mmol), and Et_3N (15 mL) were mixed and deoxygenated. The mixture was heated to 60 °C. The solution of desilylated **134a** was purged with N_2 for 5 min and added into the reaction mixture over 1 h. The mixture was stirred overnight. Then it was diluted with Et_2O, washed with NH_4Cl and H_2O, dried over $MgSO_4$, and purified by column chromatography (40% CH_2Cl_2 in hexanes) to afford **99a** as an orange solid (6 mg, 0.009 mmol, 20%). M.p. 208-210 °C; ^{1}H NMR (500 MHz, $CDCl_3/CS_2$): δ = 7.36 (dd, J = 5.8, 3.3 Hz, 4H), 7.18 (dd, J = 5.8, 3.3 Hz, 4H), 2.48 (s, 12H); Meaningful ^{13}C NMR was not obtained due to limited solubility; FTIR (neat) 2956, 2924, 2854, 1733, 1462, 1261, 1080, 967 cm^{-1}; MS (MALDI-TOF) m/z calcd for $C_{32}H_{20}S_8$ 659.93, found 661.53 $[M + H]^+$; EI-HRMS calcd for $C_{32}H_{20}S_8$ 659.9331, found 659.9339 $[M]^+$.

TTFAQ analogue 99b.

To solution of dithiafulvene monomer **134a** (51 mg, 0.13 mmol) in THF/MeOH (10 mL, 1:1) was added K_2CO_3 (200 mg, 1.45 mmol). The mixture was stirred for 30 min at rt and then diluted with Et_2O, washed with H_2O, dried over $MgSO_4$, and

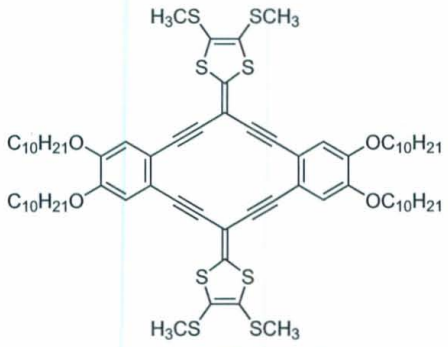

99b

concentrated in vacuo to about 5 mL. $Pd(PPh_3)_4$ (31 mg, 0.027 mmol), CuI (10 mg, 0.053 mmol), diiodo compound **39b** (68 mg, 0.11 mmol), and Et_3N (30 mL) were mixed and deoxygenated. The mixture was heated to 60 °C. The solution of desilylated **134a** was purged with N_2 for 5 min and added into the reaction mixture over 1 h. The mixture was stirred overnight, and then diluted with Et_2O, washed with NH_4Cl and H_2O, dried over $MgSO_4$, and purified by column chromatography (40% CH_2Cl_2 in hexanes) to afford **99b** as an orange solid (5 mg, 0.004 mmol, 7%). M.p. 180 °C (dec.); ^{1}H NMR (500 MHz, $CDCl_3$): δ = 6.90 (s, 4H), 4.02 (t, J = 6.6 Hz, 8H), 2.49 (s, 12H), 1.86-1.78 (m, 8H), 1.53-1.44 (m, 8H), 1.40-1.22 (m, 48H), 0.88 (t, J = 6.9 Hz, 12H); ^{13}C NMR (125 MHz, $CDCl_3$): δ = 150.8, 149.4, 129.7, 118.0, 115.5, 99.8, 96.2, 88.8, 69.6, 32.2, 29.86, 29.82, 29.7, 29.6, 29.5, 26.3, 22.9, 19.5, 14.3; FTIR (neat) 2956, 2924, 2852, 1597, 1510, 1468, 1404, 1251 cm^{-1}; MS (MALDI-TOF) m/z calcd for $C_{72}H_{100}O_4S_8$ 1284.54, found 1285.60 $[M + H]^+$.

(3-(10-(4,5-Bis(methylthio)-1,3-dithiol-2-ylidene)anthracen-9(10H)-ylidene)penta-1,4-diyne-1,5-diyl)bis(trimethylsilane)(100a).

Dibromo compound **101a** (210 mg, 0.387 mmol), $Pd(PPh_3)_4$ (45 mg, 0.039 mmol), and CuI (22 mg, 0.074 mmol) were mixed in a 100 mL rbf. Et_3N (100 mL) was added

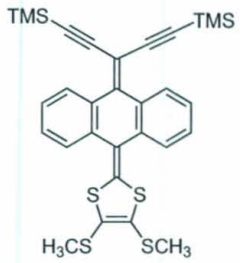

100a

and the mixture was deoxygenated. TMSA (6.0 mL, 42 mmol)) was added and the mixture was heated to 60 °C and stirred for 2 days. The mixture was diluted with CH_2Cl_2, washed with NH_4Cl and H_2O, dried over $MgSO_4$, and chromatographed with 5% CH_2Cl_2 in hexanes to afford **100a** as a red-brown oil (105 mg, 0.182 mmol, 47%). M.p. 165-167 °C; ^{1}H NMR (500 MHz, $CDCl_3$): δ = 8.29 (d, J = 7.8 Hz, 2H), 7.61 (d, J = 7.7 Hz, 2H), 7.36 (td, J = 7.7, 0.8 Hz, 2H), 7.24 (td, J = 7.8, 0.7 Hz, 2H), 2.43 (s, 6H), 0.23 (s, 18H); ^{13}C NMR (125 MHz, $CDCl_3$): δ = 148.3, 135.7, 132.9, 132.8, 128.1, 128.0, 126.4, 125.7, 125.1, 123.3, 103.9, 99.8, 99.7, 19.5, 0.16; FTIR (neat) 2958, 2127, 1573, 1525, 1494, 1449, 1249, 1211, 956, 842, 767, 720, 671 cm^{-1}; MS (APCI) m/z calcd for $C_{30}H_{32}S_4Si_2$ 576.1, found 577.0 (100, $[M + H]^+$).

(3-(10-(4,5-Bis(decylthio)-1,3-dithiol-2-ylidene)anthracen-9(10H)-ylidene)penta-1,4-diyne-1,5-diyl)bis(trimethylsilane) (100b).

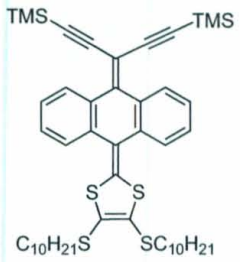

100b

Dibromo compound **101b** (400 mg, 0.503 mmol), $PdCl_2(PPh_3)_2$ (18 mg, 0.026 mmol), and CuI (14 mg, 0.074 mmol) were mixed in a 50 mL rbf. Et_3N (30 mL) was added and the mixture was deoxygenated. TMSA (2.0 mL, 14 mmol) was added and the mixture was heated to 60 °C and stirred for 2 days. The mixture was diluted with CH_2Cl_2, washed with NH_4Cl and H_2O, dried over $MgSO_4$, and chromatographed with 5% CH_2Cl_2 in hexanes to afford **100b** as a red-brown oil (400 mg, 0.482 mmol, 96%). ^{1}H NMR (500 MHz, $CDCl_3$): δ = 8.27 (d, J = 7.8 Hz, 2H), 7.62 (d, J = 7.7 Hz, 2H), 7.34 (t, J = 7.8 Hz, 2H), 7.21 (t, J = 7.7 Hz, 2H), 2.88-2.73 (m, 4H), 1.67-1.60 (m, 4H), 1.45-1.35 (m, 4H), 1.34-1.18 (m, 24H), 0.89-0.84 (t, J = 6.8 Hz, 6H), 0.22 (s, 18H); ^{13}C NMR (125 MHz, $CDCl_3$): δ = 148.4, 135.8, 133.3, 132.9, 128.1, 128.0, 126.8, 125.6, 125.1, 122.4, 104.0, 99.8, 99.5, 36.6, 32.1, 30.0, 29.77, 29.76, 29.5, 29.4, 28.8, 22.9, 14.3, 0.1; FTIR (neat) 3060, 2924, 2853, 1491, 1458, 1446, 770, 754, 690 cm^{-1}; MS (MALDI-TOF) m/z calcd for $C_{48}H_{68}S_4Si_2$ 828.37, found 829.40 ([M + H]$^+$).

4,5-Bis(methylthio)-2-(10-(dibromomethylene)anthracen-9(10H)-ylidene)-1,3-dithiol (101a).

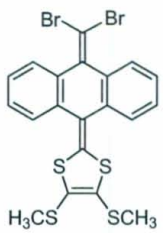

101a

Dithiafulvalene ketone **102a** (282 mg, 0.731 mmol) and CBr_4 (987 mg, 2.98 mmol) were mixed in a 100 mL oven-dried rbf. The mixture was flame-dried under vacuum

for 5 min before dry CH_2Cl_2 (20 mL) was added. Then a solution of PPh_3 (1.60 g, 6.10 mmol) in CH_2Cl_2 was added and the mixture was stirred overnight. The mixture was then loaded on a 40 cm silica column and eluted with hexanes to afford product **101a** as an orange crystalline solid (248 mg, 0.458 mmol, 63%). M.p. 140 °C (dec.); ^{1}H NMR (500 MHz, $CDCl_3$): δ = 7.87 (d, J = 7.6 Hz, 2H), 7.60 (d, J = 7.6 Hz, 2H), 7.32 (td, J = 7.6, 1.0 Hz, 2H), 7.25 (td, J = 7.6, 1.0 Hz, 2H), 2.42 (s, 6H); ^{13}C NMR (125 MHz, $CDCl_3$): δ = 139.9, 136.2, 134.0, 132.6, 128.1, 127.6, 126.2, 126.1, 125.2, 122.5, 90.0, 19.3; FTIR (neat) 3059, 2919, 1682, 1534, 1499, 1448, 1428, 1313, 1328, 773, 736, 675 cm^{-1}; MS (APCI) m/z calcd for $C_{20}H_{14}{}^{79}Br_2S_4$ 539.8, found 539.8 (34, $[M]^+$).

4,5-Bis(decylthio)-2-(10-(dibromomethylene)anthracen-9(10H)-ylidene)-1,3-dithiol (101b).

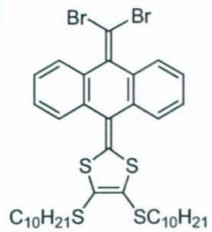

101b

Dithiafulvalene ketone **102b** (1.21 g, 1.89 mmol) and CBr_4 (2.7 g, 8.2 mmol) were mixed in a 100 mL oven-dried rbf. The mixture was flame-dried under vacuum for 10 min before dry CH_2Cl_2 (30 mL) was added. A solution of PPh_3 (4.2 g, 16 mmol) in CH_2Cl_2 was added. The mixture was stirred overnight. The mixture was then filtered through a short silica plug and then concentrated in vacuo. The residue was purified by column chromatography using 10% CH_2Cl_2 in hexanes as eluent to afford

101b as a yellow oil (1.36 g, 1.71 mmol, 91%). ^{1}H NMR (500 MHz, $CDCl_3$): δ = 7.87 (dd, J = 7.7, 0.8 Hz, 2H), 7.62 (d, J = 7.6 Hz, 2H), 7.33-7.28 (m, 2H), 7.26-7.21 (m, 2H), 2.88-2.77 (m, 4H), 1.67-1.61 (m, 4H), 1.43-1.35 (m, 4H), 1.34-1.20 (m, 24H), 0.87 (t, J = 6.8 Hz, 6H); ^{13}C NMR (125 MHz, $CDCl_3$): δ = 139.9, 136.3, 134.0, 133.1, 128.1, 127.6, 126.6, 125.9, 125.1, 121.5, 89.8, 36.5, 32.1, 29.9, 29.76, 29.74, 29.5, 29.4, 28.8, 22.9, 14.3; FTIR (neat) 3061, 2924, 2852, 1951, 1538, 1496, 1449, 1282, 1051, 770, 747, 674 cm^{-1}; MS (APCI) m/z calcd for $C_{38}H_{50}{}^{79}Br_2S_4$ 794.1, found 794.2 (38, $[M]^+$)

10-(4,5-Bis(methylthio)-1,3-dithiol-2-ylidene)anthracen-9(10H)-one (102a).

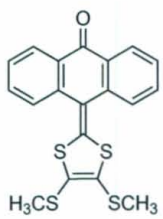

102a

$P(OEt)_3$ (20 mL) was deoxygenated and heated to 155 °C before anthraquinone (1.2 g, 5.6 mmol) was added. A solution of methyl thione **104a** (3.0 g, 6.3 mmol) in xylenes (10 mL) was added over 40 min. After the addition of thione **104a** started for 20 min, a second portion of anthraquinone (0.80 g, 3.8 mmol) was added. The mixture was stirred for 1 h and then concentrated in vacuo at 95 °C to about 6 mL. The residue was purified by column chromatography (25 cm column) with gradient elution (30% CH_2Cl_2 in hexanes, and then 80% CH_2Cl_2 in hexanes) to afford product **102a** as a red solid (320 mg, 0.83 mmol, 13%). M.p. 209-210 °C; ^{1}H NMR (500 MHz,

$CDCl_3$): δ = 8.27 (dd, J = 7.8, 0.9 Hz, 2H), 7.78 (d, J = 7.8 Hz, 2H), 7.65 (td, J = 7.8, 1.2 Hz, 2H), 7.45 (t, J = 7.8 Hz, 2H), 2.42 (s, 6H); ^{13}C NMR (125 MHz, $CDCl_3$): δ = 183.7, 140.3, 138.9, 132.1, 130.9, 127.5, 127.2, 127.1, 126.4, 119.6, 19.5; FTIR (neat) 2918, 1647, 1593, 1484, 1466, 1426, 1334, 1311, 1169, 771, 688 cm^{-1}; MS (APCI) m/z calcd for $C_{19}H_{14}OS_4$ 386.0, found 387.0 (100, $[M + H]^+$), 298.0 (15).

10-(4,5-Bis(decylthio)-1,3-dithiol-2-ylidene)anthracen-9(10H)-one (102b).

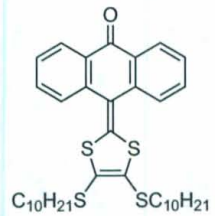

102b

$P(OEt)_3$ (25 mL) was deoxygenated and heated to 155 °C before anthraquinone (1.5 g, 6.7 mmol) was added. A solution of decyl thione **104b** (3.0 g, 6.3 mmol) in xylenes (2.5 ml) was added over 2 h. After the addition of thione started for 1 h, a second portion of anthraquinone (0.50 g, 3.3 mmol) was added. The mixture was allowed to stir for 0.5 h and then filtered through a silica plug (30 cm) and washed with CH_2Cl_2. The filtrate was concentrated in vacuo and subjected to distillation at reduced pressure. The residue was chromatographed with gradient elution (20% CH_2Cl_2 in hexanes, and then 40% CH_2Cl_2 in hexanes) to afford product **102b** as a red oil, which solidified to a red solid under vacuum (2.0 g, 3.1 mmol, 50%). M.p. 48-50 °C; ^{1}H NMR (500 MHz, $CDCl_3$): δ = 8.28 (dd, J = 7.8, 1.1 Hz, 2H), 7.79 (d, J = 7.8 Hz, 2H), 7.65 (td, J = 7.8, 1.4 Hz, 2H), 7.44 (t, J = 7.6 Hz, 2H), 2.81 (t, J

= 7.4 Hz, 4H), 1.63-1.54 (m, 4H), 1.42-1.35 (m, 4H), 1.32-1.20 (m, 24H), 0.87 (t, J = 7.1 Hz, 6H); ^{13}C NMR (125 MHz, $CDCl_3$): δ = 183.7, 140.9, 139.0, 132.0, 130.9, 127.6, 127.5, 127.0, 126.4, 119.0, 36.7, 32.1, 29.9, 29.8, 29.7, 29.5, 29.3, 28.7, 22.9, 14.3; FTIR (neat) 2924, 2853, 1658, 1596, 1485, 1466, 1298, 1170, 932, 772, 689 cm^{-1}; MS (APCI) m/z calcd for $C_{37}H_{50}OS_4$ 638.3, found 639.2 (100, $[M + H]^+$), 640.3 (45), 641.3 (28).

4,5-Bis(methylthio)-1,3-dithiol-2-thione (104a).

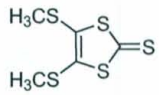

104a

To a solution of **106** (0.52 g, 0.72 mmol) in acetone (40 mL) was added MeI (0.200 mL, 3.21 mmol). The mixture was refluxed for 2 h and filtered. The residue was washed with acetone. The filtrate was evaporated and the residue was quenched with H_2O (80 mL). The mixture was extracted with CH_2Cl_2. The organic layer was washed with H_2O, dried over $MgSO_4$, and evaporated under vacuum. The residue was recrystallized from MeOH (33 mL) to afford **104a** as an orange crystalline solid (0.24 g, 1.1 mmol, 74%). ^{1}H NMR (500 MHz, $CDCl_3$): δ = 2.49 (s, 6H). The data are consistent with the literature report.[134]

4,5-Bis(decylthio)-1,3-dithiol-2-thione (104b).

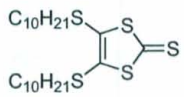

104b

To a solution of compound **106** (2.00 g, 2.78 mmol) in acetone (80 mL) was added $C_{10}H_{21}Br$ (2.80 g, 12.7 mmol). The mixture was refluxed for 2 h and then filtered. The solid residue was washed with acetone (5 mL × 3). To the resulting filtrate, acetonitrile (100 mL) was added. The mixture was then cooled with an ice-water bath. A precipitate was formed and collected by vacuum filtration. The solid was washed with acetonitrile to afford **104b** as a yellow flake-like solid (1.60 g, 3.34 mmol, 60%). ^{1}H NMR (500 MHz, $CDCl_3$): δ = 2.87 (t, J = 7.5 Hz, 4H), 1.71-1.61 (m, 4H), 1.45-1.15 (m, 28H), 0.91-0.85 (t, J = 7.0 Hz, 6H). The data are consistent with the literature report.[134]

***S*-Methyl phosphonate (105a).**

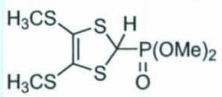

105a

To a solution of **109a** (6.1 g, 22 mmol) in MeCN (50 mL) was added NaI (4.0 g, 27 mmol) under N_2. $P(OMe)_3$ (3.3 mL, 28 mmol) was added. The mixture was stirred for 3 h and then evaporated in vacuo. To the residue were added H_2O and CH_2Cl_2. The organic layer was washed with H_2O, dried over $MgSO_4$, and evaporated in vacuo to afford a dark red liquid **105a** (4.6 g, 15 mmol, 69 %). (In some cases the product was not pure enough and it was chromatographed with EtOAc/hexanes.) ^{1}H NMR (500 MHz, $CDCl_3$): δ 4.73 (d, J = 5.6 Hz, 1H), 3.89 (d, J = 10.7 Hz, 6H), 2.42 (s, 6H). The data are consistent with the literature report.[134]

***S*-Decyl phosphonate (105b).**

To a solution of **109b** (200 mg, 0.385 mmol) in MeCN (20 mL) was added NaI

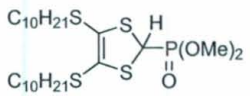

105b

(110 mg, 0.733 mmol), followed by $P(OMe)_3$ (0.1 mL, 0.6 mmol). The mixture was stirred for 2.5 h and then evaporated in vacuo. To the residue were added H_2O and CH_2Cl_2. The organic layer was washed with H_2O, dried over $MgSO_4$, and evaporated in vacuo to afford **105b** as a pale brown liquid (146 mg, 0.269 mmol, 70%). ^{1}H NMR (500 MHz, $CDCl_3$): $\delta = 4.75$ (d, $J = 5.4$ Hz, 1H), 3.88 (d, $J = 10.6$ Hz, 6H), 2.90-2.81 (m, 2H) 2.79-2.71 (m, 2H), 1.71-1.61 (m, 4H), 1.45-1.35 (m, 4H), 1.35-1.16 (m, 24H), 0.88 (t, $J = 7.1$ Hz, 6H). The data are consistent with the literature report.[134]

Bis(tetraethylammonium) bis(1,3-dithiole-4,5-dithiolate)zincate (106).

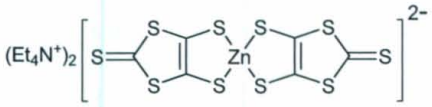

106

A mixture of Na (6.80 g, 0.300 mol) and CS_2 (60 mL, 1.0 mol) was refluxed for 20 min under N_2 protection. Dried DMF (20 mL) was added dropwise over a period of 20 min. The mixture was refluxed for 2 h and then concentrated under vacuum at 30 °C. MeOH (40 mL) was added to the residue under cooling in an ice-water bath. After filtration, a solution of $ZnCl_2$ (7.00 g, 51.3 mmol) in 1:1 MeOH/$NH_3 \cdot H_2O$ (120 mL) was added carefully to the filtrate. To the resulting mixture, Et_4NBr (20 g, 95 mmol) in H_2O (80 mL) was then added. Then the mixture was left standing overnight. After filtration the residue was sequentially washed with H_2O and Et_2O to yield **106** as a red-colored solid (24 g, 33 mmol, 88%). M.p. 203-204 °C. M.p. is

consistent with reported data.[78]

4,5-Bis(methylthio)-1,3-dithiol-2-ium tetrafluoroborate (107a).

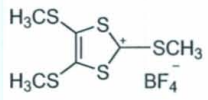

107a

A mixture of thione **104a** (6.75 g, 29.8 mmol) and DMS (15.0 mL, 158 mmol) was heated to 100 °C and stirred for 1.5 h. The mixture was cooled in an ice bath, and $HBF_4{\cdot}Et_2O$ (0.30 mL, 2.5 mmol) was added. AcOH (15 mL, 342 mmol) was then added. After 10 min, Et_2O (100 mL) was added. The product was collected by filtration and washed with Et_2O to afford **107a** as a light brown solid (9.80 g, 29.2 mmol, 100%). ^{1}H NMR (300 MHz, $CDCl_3$): $\delta = 3.23$ (s, 3H), 2.76 (s, 6H). The data are consistent with the literature report.[134]

4,5-Bis(decylthiol)-1,3-dithiol-2-ium tetrafluoroborate (107b).

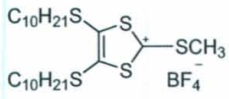

107b

A mixture of DMS (1.5 mL, 15 mmol) and thione **104b** (1.01 g, 2.11 mmol) was heated to 100 °C and stirred for 2 h under N_2. The resulting solution was cooled in an ice-water bath and $HBF_4{\cdot}Et_2O$ (1.0 mL, 8.0 mmol) was added. Et_2O (3 mL) was added and the mixture was stirred for another 20 min. More Et_2O (20 mL) was added afterwards, which resulted in a precipitate immediately. The solid formed was collected by filtration and washed with ice-cooled Et_2O to afford **107b** as a white

solid (1.20 g, 2.07 mmol, 98%). ^{1}H NMR (300 MHz, $CDCl_3$): δ = 3.23 (s, 3H), 3.17 (t, J = 7.3 Hz, 4H), 1.80-1.67 (m, 4H), 1.53-1.38 (m, 4H), 1.37-1.16 (m, 24H), 0.88 (t, J = 6.8 Hz, 6H). The data are consistent with the literature report.[134]

4,5-Bis(methylthio)-2-(methylthio)-1,3-dithiole (108a).

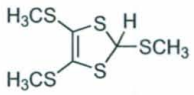

108a

To a solution of compound **107a** (9.8 g, 30 mmol) in EtOH (80 mL) was added $NaBH_4$ (2.8 g, 74 mmol) in an ice-water bath. After 15 min the mixture was warmed up to rt and kept stirring for another 3 h. The mixture was then evaporated under vacuum. H_2O (20 mL) was added to the residue. The product was collected by filtration to yield **107a** as a pale orange solid (6.4 g, 26.4 mmol, 88%). (In most cases, the product found at this stage was solid. However, it could be a liquid. If that was the case, the product could be extracted with CH_2Cl_2, dried over $MgSO_4$, and evaporated under vacuum to afford **108a** as a dark-red liquid, which solidified in a fridge.) ^{1}H NMR (500 MHz, $CDCl_3$): δ = 5.80 (s, 1H), 2.42 (s, 6H), 2.27 (s, 3H). The data are consistent with the literature report.[134]

4,5-Bis(decylthio)-2-(methylthio)-1,3-dithiole (108b).

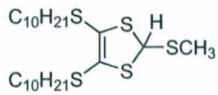

108b

To a solution of compound **107b** (1.20 g, 2.07 mmol) in EtOH (25 mL) cooled

with an ice-water bath was added $NaBH_4$ (200 mg, 5.29 mmol). The mixture was stirred for 2.5 h and then evaporated under vacuum. To the residue H_2O and CH_2Cl_2 were added. The organic layer was washed with H_2O, dried over $MgSO_4$, and then evaporated under vacuum to afford **108b** as a yellow liquid (0.80 g, 1.6 mmol, 78%). ^1H NMR (300 MHz, $CDCl_3$): $\delta = 5.73$ (s, 1H), 2.98-2.88 (m, 2H), 2.75-2.63 (m, 2H), 2.25 (s, 3H), 1.72-1.58(m, 4H), 1.45-1.1 (m, 28H), 0.88 (t, $J = 6.8$ Hz, 6H). The data are consistent with the literature report.[134]

***S*-Methyl dithiolium salt (109a).**

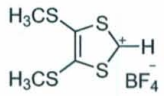

109a

Ac_2O (50 mL, 0.53 mol) was mixed with thiol **108a** (6.4 g, 26 mmol) in an ice-water bath under N_2. After 10 min, $HBF_4{\cdot}Et_2O$ (5.0 mL, 40 mmol) was added. After another 30 min, Et_2O (100 mL) was added. The product was collected by filtration and washed with Et_2O to afford **109a** as a yellow solid (6.1 g, 22 mmol, 83%). ^1H NMR (300 MHz, $CDCl_3$): $\delta = 11.30$ (s, 1H), 2.83 (s, 6H). ^1H NMR data are consistent with those reported.[134]

***S*-Decyl dithiolium salt (109b).**

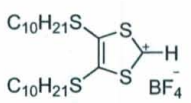

109b

To thiol **108b** (1.00 g, 2.02 mmol) that was cooled in an ice-water bath was added

Ac_2O (8.0 mL, 85 mmol). After 5 min, $HBF_4{\cdot}Et_2O$ (1.0 mL, 8.0 mmol) was added. After another 15 min, Et_2O (20 mL) was added. The formed slurry was filtered, and the solid residue was washed with Et_2O. The filtrate was cooled in a freezer overnight. The resulting yellow crystalline solids were filtered and washed with ice-cooled Et_2O to afford pure product **109b** (0.748 g, 1.40 mmol, 70%). ^1H NMR (300 MHz, $CDCl_3$): $\delta = 11.36$ (s, 1H), 3.21 (t, $J = 7.2$ Hz, 4H), 1.83-1.68 (m, 4H), 1.53-1.40 (m, 4H), 1.37-1.13 (m, 24H), 0.88 (t, $J = 6.5$ Hz, 6H). The data are consistent with the literature report.[134]

Acyclic exTTF 123 and monomer 124.

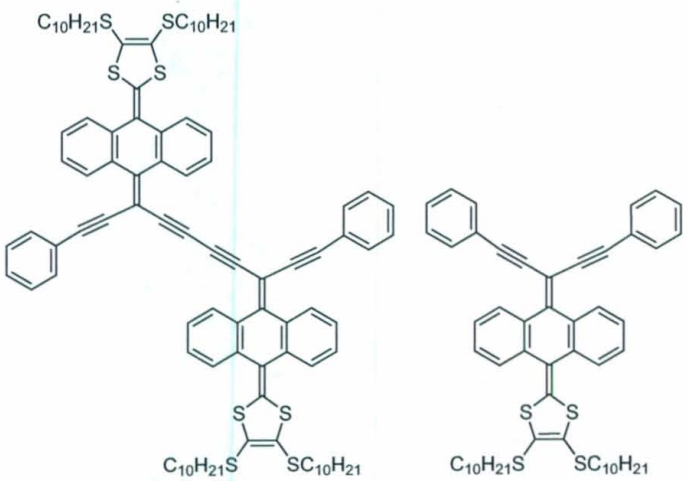

123 **124**

Compound **100b** (38 mg, 0.046 mmol) was dissolved in THF/MeOH (15 mL, 1:1). K_2CO_3 (200 mg, 1.45 mmol) was added and the mixture was stirred for 30 min. The mixture was diluted with Et_2O, washed with H_2O, dried over $MgSO_4$, and concentrated in vacuo to about 5 mL. Iodobenzene (9.5 mg, 0.047 mmol), and CuI (3 mg, 0.016 mmol) were mixed in a 50 mL rbf, and Et_3N (15 mL) was added. The

mixture was deoxygenated and then $Pd(PPh_3)_4$ (5 mg, 0.004 mmol) was added. To the mixture was added a N_2-purged desilylated **100b** solution in Et_2O. The mixture was stirred overnight. Then it was diluted with CH_2Cl_2, washed with aq. NH_4Cl solution and H_2O, dried over $MgSO_4$, and chromatographed with 5% CH_2Cl_2 in hexanes to afford **124** as an orange oil monomer (10 mg, 0.017 mmol, 51%), and **123** as a red oil (14 mg, 0.0092 mmol, 39%).

123. ^{1}H NMR (500 MHz, $CDCl_3$): δ = 8.38 (d, J = 7.8 Hz, 2H), 8.32-8.23 (m, 2H), 7.68 (t, J = 7.8 Hz, 4H), 7.51-7.46 (m, 4H), 7.45-7.37 (m, 4H), 7.36-7.30 (m, 10H), 2.91-2.73 (m, 8H), 1.67-1.56 (m, 8H), 1.44-1.33 (m, 8H), 1.30-1.18 (m, 48H), 0.90-0.78 (m, 12H); ^{13}C NMR (125 MHz, $CDCl_3$): δ = 149.3, 135.84, 135.76, 134.2, 133.00, 132.95, 132.92, 131.8, 128.8, 128.6, 128.3, 127.8, 126.91, 126.88, 126.3, 125.8, 125.3, 123.2, 122.1, 99.8, 98.8, 94.1, 88.4, 83.4, 78.8, 78.6, 36.66, 36.65, 32.1, 29.93, 29.92, 29.90, 29.79, 29.76, 29.74, 29.59, 29.54, 29.53, 29.40, 29.36, 28.76, 28.74, 22.9, 14.3; FTIR (neat) 3060, 2924, 2853, 1572, 1525, 1492, 1457, 782, 754, 690 cm^{-1}; MS (MALDI-TOF) m/z calcd for $C_{96}H_{110}S_8$ 1518.64, found 1520.33 ([M + H]$^+$).

124. ^{1}H NMR (500 MHz, $CDCl_3$): δ = 8.40 (dd, J = 7.8, 1.2 Hz, 2H), 7.68-7.65 (m, 2H), 7.51-7.48 (m, 4H), 7.41-7.31 (m, 10H), 2.90-2.73 (m, 4H), 1.66-1.58 (m, 4H), 1.43-.133 (m, 4H), 1.32-1.18 (m, 24H), 0.86 (t, J = 7.0 Hz, 6H); ^{13}C NMR (125 MHz, $CDCl_3$): δ = 146.6, 136.0, 133.5, 133.4, 131.8, 128.7, 128.6, 128.0, 127.9, 126.8, 125.9, 125.3, 123.4, 122.4, 99.8, 93.3, 89.5, 36.6, 32.1, 29.9, 29.76, 29.74, 29.5, 29.4, 28.8, 22.9, 14.3; FTIR (neat) 3060, 2924, 2853, 1574, 1531, 1496, 1448, 1284, 957, 842, 762, 693 cm^{-1}; MS (MALDI-TOF) m/z calcd for $C_{54}H_{60}S_4$ 836.36, found 837.54 ([M + H]$^+$).

Mono-substituted compound 128.

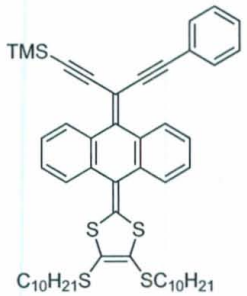

128

Dibromo compound **101b** (51 mg, 0.064 mmol), $Pd(PPh_3)_4$ (10 mg, 0.0086 mmol), CuI (8 mg, 0.042 mmol), and Et_3N (20 mL) were mixed in a 50 mL rbf under N_2. Phenylacetylene (0.010 mL, 0.069 mmol) and TMSA (0.050 mL, 0.40 mmol)) was added and the mixture was heated to 60 °C and stirred overnight. The mixture was diluted with CH_2Cl_2, washed with NH_4Cl and H_2O, dried over $MgSO_4$, and chromatographed with 5% CH_2Cl_2 in hexanes to afford **128** as a red-brown oil (16 mg, 0.019 mmol, 30%). ^{1}H NMR (500 MHz, $CDCl_3$): δ = 8.34 (t, J = 8.0 Hz, 2H), 7.67-7.60 (m, 2H), 7.48-7.44 (m, 2H), 7.38-7.24 (m, 7H), 2.89-2.72 (m, 4H), 1.70-1.55 (m, 4H), 1.42-1.35 (m, 4H), 1.30-1.21 (m, 24H), 0.92-0.80 (m, 6H), 0.25 (s, 9H); ^{13}C NMR (125 MHz, $CDCl_3$): δ = 147.5, 136.0, 135.9, 133.4, 133.3, 133.0, 131.7, 131.5, 128.6, 128.5, 128.0, 127.95, 127.93, 126.9, 126.7, 125.8, 125.6, 125.2, 125.1, 123.5, 122.4, 104.0, 99.7, 99.6, 93.3, 89.4, 36.6, 32.12, 32.11, 29.96, 29.93, 29.91 ,29.78, 29.76, 29.74, 29.54, 29.52, 29.38, 29.37, 28.79, 28.76, 22.9, 14.3, 0.2; FTIR (neat) 3060, 2955, 2924, 2853, 1573, 1530, 1493, 1448, 1250, 943, 845, 768, 755, 689 cm$^-$1; MS (MALDI-TOF) m/z calcd for $C_{51}H_{64}S_4Si$ 832.37, found 833.06 ($[M + H]^+$).

Unknown substance 130. Dibromo compound **101b** (46 mg, 0.058 mmol), $Pd(PPh_3)_4$ (8 mg, 0.007 mmol), CuI (4 mg, 0.02 mmol), phenylacetylene (0.60 mL, 4.2 mmol), and Et_3N (20 mL) were mixed and deoxygenated. The mixture was

heated to 60 °C and stirred overnight. Then it was diluted with CH_2Cl_2, washed with aq. NH_4Cl solution and H_2O, dried over $MgSO_4$, and purified with column chromatography (5% CH_2Cl_2 in hexanes) to afford **130** as a purple solid (16 mg, 0.019 mmol, 33%). ^{1}H NMR (500 MHz, $CDCl_3$): δ = 8.08-8.05 (m, 1H), 8.01-7.98 (m, 1H), 7.93 (d, J = 7.4 Hz, 2H), 7.69-7.60 (m, 4H), 7.47-7.38 (m, 8H), 7.33 (t, J = 7.3 Hz, 2H), 2.81-2.75 (m, 4H), 1.62-1.55 (m, 4H), 1.39-1.33 (m, 4H), 1.31-1.18 (m, 24H), 0.89-0.83 (m, 6H); ^{13}C NMR (125 MHz, $CDCl_3$): δ = 150.1, 139.2, 137.5, 135.4, 134.68, 134.64, 132.71, 132.67, 131.8, 128.88, 128.85, 128.7, 128.3, 128.0, 127.9, 127.8, 127.5, 127.3, 127.21, 127.18, 127.1, 126.5, 126.4, 125.1, 123.6, 122.2, 118.9, 101.8, 98.7, 89.1, 36.7, 32.1, 29.93, 29.91, 29.8, 29.7, 29.5, 29.3, 28.73, 28.72, 22.9, 14.3; FTIR (neat) 3063, 2954, 2924, 2853, 2018, 1733, 1598, 1517, 1487, 1463, 1442, 1279, 1159 cm^{-1}; MS (MALDI-TOF) m/z calcd for $C_{54}H_{60}S_4$ 836.36, found 838.00 ($[M + H]^+$).

Dithiafulvene monomer 134a.

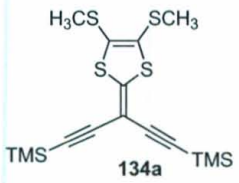

134a

To a solution of phosphonate **105a** (0.192 g, 0.631 mmol) in THF (20 mL) cooled under a dry ice bath was added t-BuLi (0.42 mL, 1.7 M, 0.71 mmol). The mixture was stirred for 15 min. Ketone **136** (140 mg, 0.631 mmol) in THF (10 mL) was added. The mixture was warmed to rt and stirred overnight. The resulting black brown solution was evaporated in vacuo. To the black residue were added CH_2Cl_2

and H_2O. The organic layer was separated, washed with H_2O, dried over $MgSO_4$. It was puriefied by column chromatography (20% CH_2Cl_2 in hexanes) to afford **134a** as a light yellow liquid, which solidified in a fridge to a yellow solid (125 mg, 0.313 mmol, 50%). M.p. 72-73 °C; ^{1}H NMR (500 MHz, $CDCl_3$): δ = 2.44 (s, 6H), 0.22 (s, 18H); ^{13}C NMR (125 MHz, $CDCl_3$): δ = 157.8, 129.5, 103.3, 100.2, 87.9, 19.3, 0.2; FTIR (neat) 2959, 2923, 2138, 2132, 1509, 1461, 1428, 1248, 1215, 963, 839, 755 cm^{-1}; MS (APCI) m/z (%) 401 $[M+H]^+$ (100); EI-HRMS calcd for $C_{16}H_{24}S_4Si_2$ 400.0299, found 400.0295 $[M]^+$.

Dithiafulvene monomer 134b.

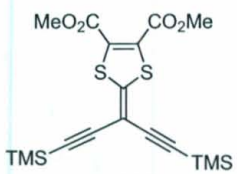

134b

To a solution of phosphonium salt **137** (248 mg, 0.503 mmol) in THF (20 mL) cooled in a dry ice bath was added *n*-BuLi (0.25 mL, 2.5 M, 0.63 mmol). The mixture was stirred for 0.5 h. A solution of ketone **40** (110 mg, 0.498 mmol) in THF (10 mL) was added dropwise over 5 min. The mixture was stirred overnight. It was evaporated in vacuo. To the residue were added H_2O and CH_2Cl_2. The organic layer was separated, washed with H_2O, dried over $MgSO_4$, and purified by column chromatography (30% CH_2Cl_2 in hexanes) to afford **134b** as a yellow solid (101 mg, 0.238 mmol, 48%). ^{1}H NMR (500 MHz, $CDCl_3$): δ = 3.87 (s, 6H), 0.23 (s, 18H); ^{13}C NMR (125 MHz, $CDCl_3$): δ = 159.8, 154.9, 132.7, 104.3, 99.6, 89.1, 53.68, 0.08; MS (APCI) m/z (%) 514 (100), 425 $[M+H]^+$ (98). The data are consistent with the the

literature report.[8]

1,2-Bis(decyloxy)-4,5-diiodobenzene 135b.

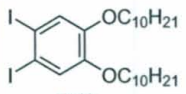

135b

Compound **143** (1.50 g, 3.84 mmol), I_2 (2.17 g, 8.54 mmol), $Hg(OAc)_2$ (2.56 g, 8.03 mmol), and CH_2Cl_2 (60 mL) were mixed. The mixture was stirred at rt overnight. It was filtered through a 1 cm diatomaceous earth plug and washed with CH_2Cl_2. The filtrate was washed with $Na_2S_2O_3$ (aq), $NaHCO_3$ (aq), H_2O, brine, and dried over $MgSO_4$. It was evaporated in vacuo. The residue was recrystallized from EtOH to afford **135b** as a white solid (1.40 g, 2.17 mmol, 57%). ^{1}H NMR (500 MHz, $CDCl_3$): $\delta = 7.25$ (s, 2H), 3.92 (t, $J = 6.6$ Hz, 4H), 1.82-1.73 (m, 4H), 1.46-1.40 (m, 4H), 1.37-1.22 (m, 12H), 0.88 (t, $J = 6.9$ Hz, 6H). The data are consistent with the literature report.[129]

Diiodo crown ether 135c.

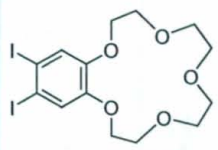

135c

Method 1: Compound **148** (0.481 g, 1.33 mmol), Bu_4NBr (0.206 g, 0.638 mmol), toluene (15 mL), and NaOH (50%, 5 mL) were mixed and stirred at 50 °C for 0.5 h. To the mixture was added a solution of ditosylate **145** (0.419 g, 1.35 mmol) in toluene (15 mL). The mixture was heated to 110 °C and stirred overnight. The

resulting mixture was diluted with toluene. The organic layer was separated, washed with H_2O, dried over $MgSO_4$, and evaporated in vacuo. The residue was extracted with hot hexanes (15 mL × 3). The resulting solution of extract was evaporated to afford **135c** as a white solid (0.210 g, 0.404 mmol, 30%).

Method 2: Crown ether **149** (1.210 g, 4.515 mmol), I_2 (1.010 g, 3.976 mmol), H_5IO_6 (0.384 g, 1.68 mmol), AcOH (12 mL), H_2SO_4 (0.4 mL), and H_2O (4 mL) were mixed and heated to 70 °C. The mixture was stirred overnight. The resulting mixture was poured into an aq. $NaHSO_3$ solution. The residue was dissolved in CH_2Cl_2/EtOAc. The combined mixture was extracted with CH_2Cl_2, dried over $MgSO_4$ and then filtered through a short silica plug (4 cm) using CH_2Cl_2 as eluent. The filtrate, a light yellow solution, was evaporated. The brown residue was extracted with hot hexanes (30 mL × 2). After cooling, pure **135c** was crystallized as a white crystal (0.973 g, 1.87 mmol, 41%). ^{1}H NMR (500 MHz, $CDCl_3$): δ = 7.26 (s, 2H), 4.09-4.05 (m, 4H), 3.89-3.85 (m, 4H), 3.75-3.70 (m, 8H); MS (APCI) m/z (%) 520.8 (78) $[M+H]^+$, 537.8 (100) $[M+H_2O]^+$. The data are consistent with the literature report.[135,136]

1,5-Bis(trimethylsilyl)penta-1,4-diyn-3-one 136.

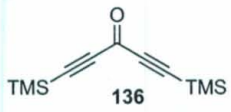

136

To a cooled solution of PCC (1.60 g, 7.40 mmol) in CH_2Cl_2 (30 mL) was added a solution of alcohol **141** (1.24 g, 5.56 mmol) in CH_2Cl_2 (10 mL). The mixture was allowed to warm to rt and stirred for 5 h. It was purified by column chromatography

(CH_2Cl_2) to yield **136** as a yellow liquid (1.13 g, 5.11 mmol, 92%). ^{1}H NMR (500 MHz, $CDCl_3$): $\delta = 0.27$ (s, 18H). The data are consistent with the literature report.[137]

3-(Trimethylsilyl)prop-2-yn-1-ol 139.

139

To a solution of propargyl alcohol (5.00 mL, 85.0 mmol) in THF (80 mL) cooled in a dry ice bath was added *n*-BuLi (75.0 mL, 2.5 M, 190 mmol) over 30 min. The mixture was stirred at this temperature for 1 h. TMSCl (33.0 mL, 260 mmol) was added over 15 min. The mixture was stirred for 5 h. HCl (100 mL, 2M) was added and the mixture was stirred for 1 h. The aqueous layer was extracted with Et_2O. The combined organic layer was washed with H_2O, dried over $MgSO_4$, concentrated in vacuo and purified by column chromatography (using hexanes as eluent until the product came out, then 80% CH_2Cl_2 in hexanes) to afford **139** as a clear colorless liquid (8.30 g, 62.9 mmol, 74%). ^{1}H NMR (500 MHz, $CDCl_3$): $\delta = 4.27$ (d, $J = 4.7$ Hz, 2H), 1.57 (s, 1H), 0.18 (s, 9H). The data are consistent with the literature report.[138]

3-(Trimethylsilyl)propiolaldehyde 140.

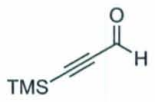

140

Alcohol **139** (3.38 g, 25.6 mmol) in CH_2Cl_2 (20 mL) was added over 8 min into a mixture of PCC (6.10 g, 28.2 mmol) and CH_2Cl_2 cooled under an ice-water bath.

The mixture was stirred for 8 h. It was then filtered though a short silica plug and washed with CH_2Cl_2 to **140** as a light yellow liquid (3.03 g, 23.3 mmol, 91%). ^{1}H NMR (500 MHz, $CDCl_3$): $\delta = 9.17$ (s, 1H), 0.27 (s, 9H). The data are consistent with the literature report.[138]

1,5-Bis(trimethylsilyl)penta-1,4-diyn-3-ol 141.

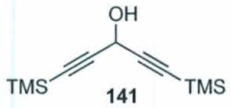

141

To a solution of TMSA (3.10 mL, 23.0 mmol) in THF (70 mL) cooled in a dry ice bath was added *n*-BuLi (10.0 ml, 2.5 M, 25.0 mmol) over 10 min. The mixture was stirred for 40 min. A solution of aldehyde **140** (3.00 g, 23.0 mmol) in THF (10 mL) was added over 10 min. The mixture was stirred for 4 h. To the resulting solution was added an aq. NH_4Cl (50 mL) solution. The mixture was stirred for 10 min. Then it was extracted with Et_2O (30 mL $\times$2). The combined organic layer was washed with H_2O, brine, dried over $MgSO_4$, and purified by column chromatography (40% CH_2Cl_2 in hexanes) to afford **141** as a brown liquid (2.82 g, 12.8 mmol, 55%). ^{1}H NMR (500 MHz, $CDCl_3$): $\delta = 5.10$ (d, $J = 7.5$ Hz, 1H), 2.17 (d, J= 7.4 Hz, 1H), 0.17 (s, 18H). The data are consistent with the literature report.[137]

1,2-Bis(decyloxy)benzene 143.

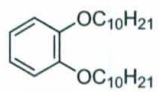

143

Catechol (5.06 g, 46.0 mmol), KOH (6.50 g, 116 mmol), EtOH (100 mL), and

$C_{10}H_{21}Br$ (25 mL) were mixed. The resulting grey mixture was heated to 90 °C and refluxed overnight. It was then diluted with CH_2Cl_2, washed with aq. NH_4Cl solution, H_2O, brine, and dried over $MgSO_4$. It was filtered through a short silica plug and washed with hexanes. The filtrate was concentrated in vacuo. To the residue was added EtOH (150 mL) and white crystals formed. The mixture was chilled for 30 min then filtered. The resulting white crystals were washed with EtOH to afford pure product **143** (12.3 g, 31.5 mmol, 69%). ^{1}H NMR (500 MHz, $CDCl_3$): δ = 6.88 (m, 4H), 3.99 (t, J = 6.7 Hz, 4H), 1.85-1.76 (m, 4H), 1.50-1.43 (m, 4H), 1.37-1.23 (m, 28H), 0.88 (t, J = 7.0 Hz, 6H). The data are consistent with the literature report.[129]

Ditosylate 145.

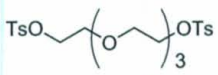

145

To a solution of TsCl (19.00 g, 100.0 mmol) in THF (50 mL) was added tetraethylene glycol (8.00 ml, 46.0 mmol), and Et_3N (15.00 ml, 107.7 mmol). The mixture was stirred for 1 day. It was then evaporated in vacuo. The residue was diluted with EtOAc, washed with H_2O, dried over $MgSO_4$, and purified with column chromatography (with CH_2Cl_2 until all TsCl was removed and then with EtOAc as eluents) to afford product **145** as a colorless liquid (12.80 g, 41.2 mmol, 89%). ^{1}H NMR (500 MHz, $CDCl_3$): δ = 7.79 (d, J = 8.2 Hz, 4H), 7.34 (d, J = 8.1 Hz, 4H), 4.17-4.13 (m, 4H), 3.69-3.65 (m, 4H), 3.58-3.54 (m, 8H), 2.44 (s, 6H). The data are consistent with the literature report.[132]

2,2-Dimethylbenzo[d][1,3]dioxole 146.

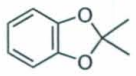

146

Catechol (11.07 g, 100.1 mmol), P_2O_5 (14.40 g, 101.0 mol), acetone (7.50 mL, 0.100 mol) and toluene (100 ml) were mixed and heated to 65 °C. The mixture was stirred overnight. The solution was poured into aq. $NaHCO_3$ solution under an ice-water bath. The organic layer was separated, washed with aq. $NaHCO_3$ solution until aqueous layer was clear colorless. Then it was washed with H_2O, brine, dried over $MgSO_4$. The resulting mixture was filtered through a short silica plug, and washed with CH_2Cl_2. The filtrate was evaporated to give **146** as a light yellow liquid (10.7 g, 71.3 mmol, 71%). ^{1}H NMR (500 MHz, $CDCl_3$): δ = 6.79-6.72 (m, 4H), 1.67 (s, 6H). The data are consistent with the literature report.[135]

5,6-Diiodo-2,2-dimethylbenzo[d][1,3]dioxole 147.

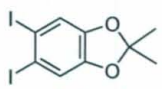

147

Compound **146** (2.01 g, 13.4 mmol), I_2 (7.45 g, 29.0 mol), $Hg(OAc)_2$ (9.35 g, 29.0 mmol), and CH_2Cl_2 (150 mL) were mixed and stirred for 2 days. The mixture was filtered, washed with aq. Na_2SO_3 solution, H_2O, dried over $MgSO_4$, and evaporated in vacuo. The residue was recrystalized from EtOH to give **147** as a pale yellow solid (3.60 g, 8.96 mmol, 67%). ^{1}H NMR (500 MHz, $CDCl_3$): δ = 7.21 (s, 2H), 1.65 (s, 6H). The data are consistent with the literature report.[135]

4,5-Diiodocatechol 148.

Compound **147** (1.63 g, 4.05 mmol), AcOH (100 mL), H_2O (45 mL), and aq. HCl

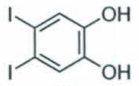

148

(50%, 15 mL) were mixed and refluxed for 3 h. The resulting yellow solution was extracted with CH_2Cl_2, washed with H_2O, filtered through a short silica plug, and washed with EtOAc. The filtrate was purified by column chromatography (CH_2Cl_2) to give **148** as a pale brown solid (1.12 g, 3.09 mmol, 76%). ^{1}H NMR (500 MHz, $CDCl_3$): δ = 7.35 (s, 2H), 1.78 (s, 2H). ^{1}H NMR data are consistent with those reported.[135]

Crown ether 149.

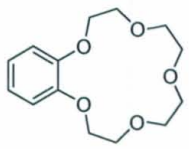

149

To a mixture of catechol (1.833 g, 16.65 mmol), Bu_4NBF_4 (2.743 g, 8.508 mmol) and toluene (100 mL) was added aq. NaOH solution (35 mL, 50%). The mixture was heated to 50 °C and stirred for 30 min. A solution of ditosylate **145** (5.150 g, 16.61 mmol) in toluene (100 mL) was added. The resulting mixture was refluxed overnight. It was then washed with H_2O, dried over $MgSO_4$, and evaporated in vacuo. The residue was extracted with hot hexanes (100 mL). Upon cooling, white crystals were formed and collected by filtration as pure product **149** (1.210 g, 4.515 mmol, 27%). ^{1}H NMR (500 MHz, $CDCl_3$): δ = 6.93-6.86 (m, 4H), 4.16-4.12 (m, 4H), 3.94-3.90 (m, 4H), 3.78-3.76 (m, 8H). The data are consistent with the literature report.[139]

Diiodo compound 150a.

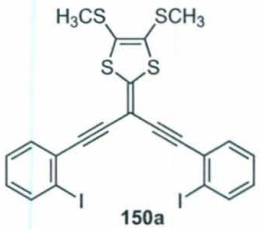

150a

To solution of compound **135a** (45 mg, 0.11 mmol) in THF/MeOH (10 mL, 1:1 v/v) was added K_2CO_3. The mixture was stirred for 30 min. The mixture was diluted with Et_2O, washed with H_2O, dried over $MgSO_4$, and concentrated in vacuo to ca. 5 mL. $PdCl_2(PPh_3)_2$ (12 mg, 0.018 mmol), CuI (10 mg, 0.053 mmol), 1,2-diiodobenzene (150 mg, 0.465 mmol), and Et_3N (20 mL) were mixed, deoxygenated, and heated to 60 °C. The solution of desilylated **135a** was purged with N_2 for 5 min and added into the reaction mixture over 1 h. The mixture was stirred overnight. Then it was diluted with Et_2O, washed with NH_4Cl and H_2O, dried over $MgSO_4$, and purified with column chromatography (30% CH_2Cl_2:hexane) to afford a yellow oil **150a** (10 mg, 0.016 mmol, 15%). ^{1}H NMR (500 MHz, $CDCl_3$): δ = 7.86 (d, J = 8.0 Hz, 2H), 7.50 (dd, J = 7.7, 1.4 Hz, 2H), 7.31 (t, J = 8.0 Hz, 2H), 6.99 (td, J = 7.5, 1.9 Hz, 2H), 2.47 (s, 6H); ^{13}C NMR (125 MHz, $CDCl_3$): δ = 157.1, 139.0, 132.6, 130.0, 129.5, 129.3, 128.0, 100.2, 99.1, 89.2, 87.2, 19.4; FTIR (neat) 3058, 2957, 2921, 2854, 2362, 2337, 2180, 1579, 1510, 1467, 1448, 1427, 1259, 1015 cm^{-1}; HR MALDI-TOF MS m/z calcd for $C_{22}H_{14}I_2S_4$ 659.8068, found 659.8059 $[M]^+$.

Diiodo compound 150b.

To a solution of compound **134a** (40 mg, 0.10 mmol) in THF/MeOH (15 mL, 1:1 v/v) was added K_2CO_3. The mixture was stirred for 30 min. The mixture was diluted with Et_2O, washed with H_2O, dried over $MgSO_4$, and concentrated in vacuo to ca.

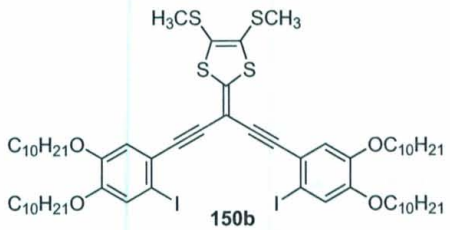

150b

5 mL. $Pd(PPh_3)_4$ (16 mg, 0.014 mmol), CuI (11 mg, 0.057 mmol), diiodo compound **101b** (230 mg, 0.360 mmol), and Et_3N (30 mL) were mixed and deoxygenated. The mixture was heated to 60 °C. The solution of desilylated **134a** was purged with N_2 for 5 min and added into the reaction mixture over 1.5 h. The mixture was stirred overnight. Then it was diluted with Et_2O, washed with aq. NH_4Cl solution and H_2O, dried over $MgSO_4$, and purified with column chromatography (30% CH_2Cl_2 in hexanes) to afford **150b** as a yellow oil (12 mg, 0.0093 mmol, 9%). ^1H NMR (500 MHz, $CDCl_3$): δ = 7.24 (s, 2H), 6.99 (s, 2H), 3.97 (td, J = 6.5, 1.4 Hz, 8H), 2.46 (s, 6H), 1.85-1.75 (m, 8H), 1.50-1.40 (m, 8H), 1.39-1.20 (m, 48H), 0.92-0.84 (m, 12H) ; ^{13}C NMR (125 MHz, $CDCl_3$): δ = 154.9, 150.1, 149.2, 129.2, 123.2, 122.1, 117.1, 99.1, 89.8, 87.6, 87.5, 69.6, 32.1, 29.84, 29.82, 29.80, 29.79, 29.61, 29.57, 29.34, 29.29, 26.20, 26.16, 22.9, 19.3, 14.3; FTIR (neat) 3058, 2955, 2920, 2851, 2359, 2180, 1588, 1502, 1461, 1333, 1257, 1198, 1047 cm^{-1}; HR MALDI-TOF MS m/z calcd for $C_{62}H_{94}I_2O_4S_4$ 1284.4119, found 1284.4162 $[M]^+$.

Chapter 3

Oligoyne Centered $\pi-$Extended Tetrathiafulvalenes and Tetrathialfulvalene Vinylogues

3.1 Introduction

Oligoynes are linearly conjugated carbon chains composed of alternating single and triple carbon-carbon bonds. The incorporation of an oligoyne unit in between the two dithiole rings of TTF generates a class of interesting $\pi-$extended TTFs. As shown in Figure 3.1, the bis(dithiafulvenyl)-endcapped conjugated 1,3-butadiyne **151**, reported in 1990 by Gorgues and co-workers, presents the first example of a butadiyne centered exTTF in the literature.[140,141] Synthetically, compound **151** was acquired by a Wittig-Horner reaction using phosphonates and acetylenecarbodialdehydes as the precursors. Later in 2007, a longer homolog, namely 1,3,5,7-octatetrayne centered

exTTF **152** (see Figure 3.1), was successfully prepared by Nielsen and co-workers using a Cu-catalyzed alkynyl homocoupling reaction as the key step.[142] Besides these two examples, other similar oligoyne centered exTTFs such as diyne and tetrayne centered exTTFs **153** and **154** have been prepared and investigated by Diederich and Nielsen.[8,87] Unlike **151** and **152**, exTTFs **153** and **154** bear acetylenic units outside the central $\pi-$moiety to form a cross-conjugated motif. In addition to diyne and tetrayne units, Nielsen and co-workers also successfully synthesized a hexayne centered exTTF **155** in good yield via the Hay coupling.[142] Owing to its bulky triisopropylsilyl (TIPS) endcapping groups, exTTF **155** showed satisfactory chemical stability that is in contrast to many unstable hexayne species. Note that methyl ester groups are commonly used substituents on the dithiole rings in making oligyne centered exTTFs, because of their easy accessibility in synthesis and electron-withdrawing effect that stabilizes the exTTF products.

The combination of oligoynes with TTF units can produce two major benefits in terms of material design. First, the oligoyne moieties can provide stabilization to oxidized TTF species as a result of extended $\pi-$conjugation. Second and more importantly, this design strategy can lead to materials with novel optoelectronic properties and unique solid-state reactivities. Especially, oligoyne compounds as a class of fascinating one-dimensional carbon building blocks have attracted growing attention in the development of carbon-rich functional nanomaterials in recent years. For instance, the nonlinear optical susceptibilities of oligoynes were found to increase exponentially with increasing number of acetylenic repeat units,[143,144] while topochemical polymerization of oligoynes tended to result in highly conjugated polymer networks[145–148] and ordered carbon-based nanomaterials.[149–152] Moreover,

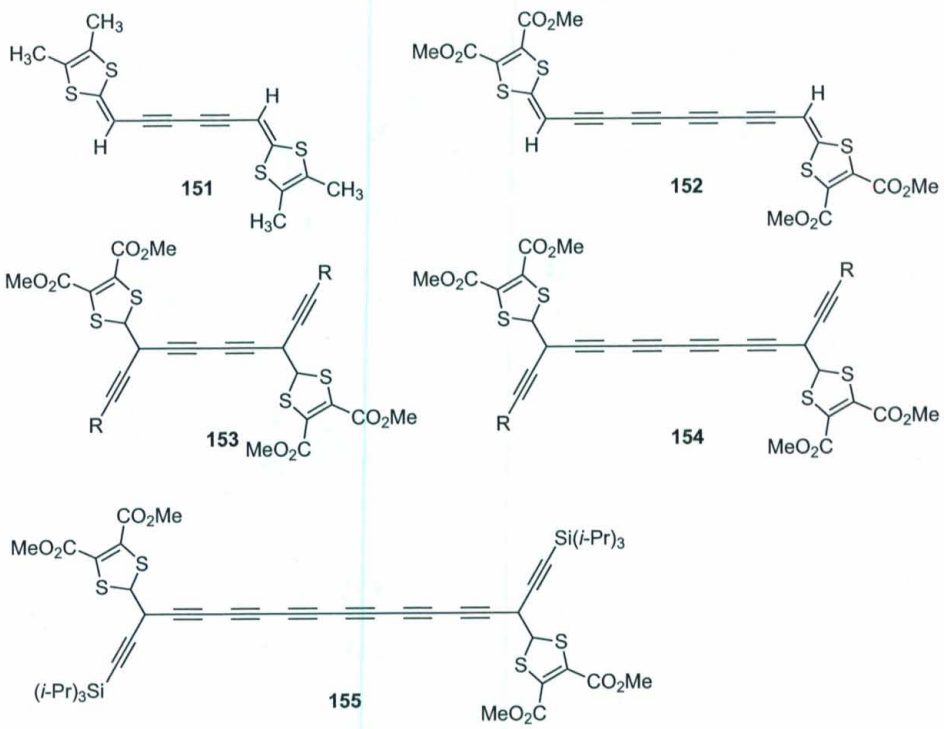

Figure 3.1: Structures of oligoyne centered exTTFs **151-155**.

the "wire-like" sp carbon chains of conjugated oligoynes are the substructures of an intriguing carbon allotrope, carbyne, whose mystical structural and electronic properties have been under debate for a long time.

Oligoyne-centered exTTFs have been synthesized and studied for nearly two decades; however, they still remain a quite small group in the vast family of exTTF derivatives. Given the limited number of oligoyne centerd exTTFs in the present literature, continued synthesis and characterization of new oligoyne-exTTFs are indispensable and beneficial from both fundamental and practical aspects. Upon this consideration, a series of unprecedented oligoyne-centered exTTFs **156** was targeted in this thesis. As shown in Scheme 3.1, the basic structure of **156** is akin to those of exTTFs **151** and **152**; however, the insertion of a benzene ring between the dithiafulvalene (DTF) and alkynyl groups not only elongates π-conjugation, but also adds valuable reactivity. DTF molecules monosubstituted with aryl groups, regardless of the electronic nature of the substituents on the aryl groups, have been known to undergo oxidative dimerizations to form tetrathiafulvalene vinylogues (TTFVs). The details of this kind of dimerization are discussed in Section 1.3. In view of this reactivity, it is conceivable that the two phenyl-DTF units in oligoyne exTTF **156** may serve useful synthetic handles for construction of intriguing conjugated polymer materials, such as **158**. Also of interest is alkynyl-TTFV **157**, which is a structural isomer of **156**. Complementary to the oxidative polymerization approach, **157** undergoing alkynyl homocoupling would also lead to poly[**157**] that structurally resembles polymer **158**. Detailed synthesis and properties characterization of these new exTTF derivatives are discussed in the first part of this chapter.

As with many TTFV derivatives, diphenyl-substituted TTFV **157** possesses

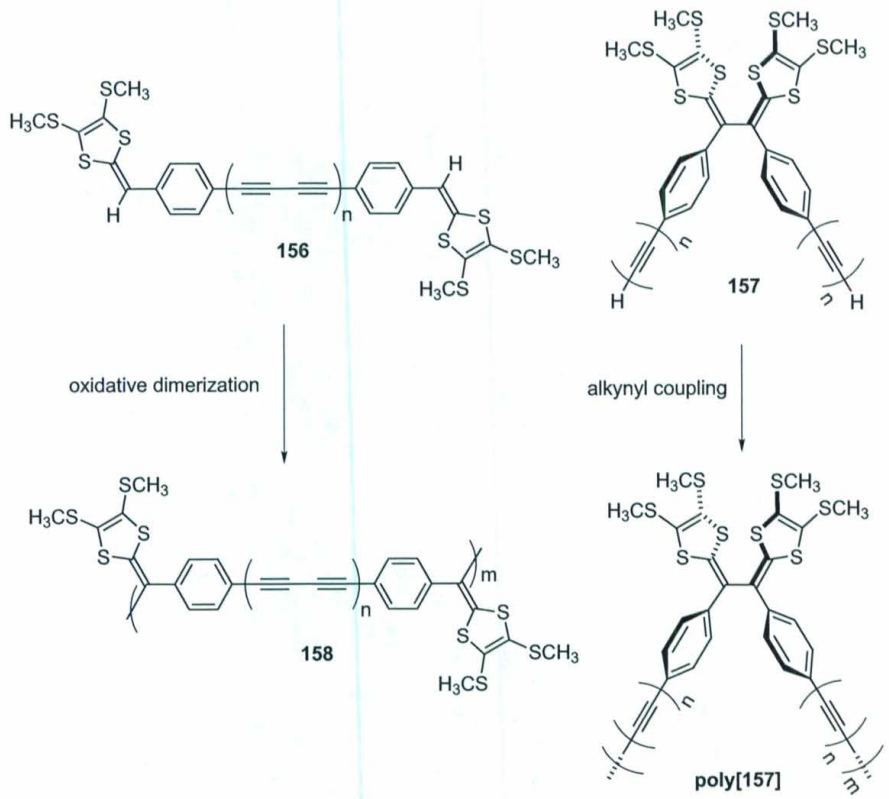

Scheme 3.1: Structures of oligoyne TTF **156**, TTFV **157**, polymer **158**, and poly[**157**].

interesting conformational switching properties. As shown in Scheme 3.2, in the neutral state the two phenyl groups are oriented in a *cis*, V-shaped conformation governed by steric crowding, whereas upon oxidation the dication of phenyl-TTF assumes a *trans* conformation where the two phenyl groups point outward in a linear fashion as a result of the on-site Coulombic repulsion between the two cationic dithiolium rings. Taking advantage of the conformational switching behavior, this thesis covers the synthesis and characterization of a number of TTFV based donor/acceptor derivatives **159**.[153–155] The design of these compounds was aimed at chemical sensing applications, while the detailed results are described in the second part of this chapter.

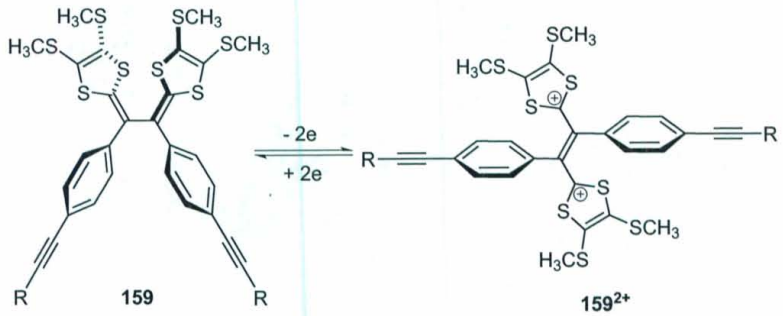

Scheme 3.2: Conformational switching of TTFV derivatives **159** upon oxidation.

3.2 Results and Discussion

3.2.1 Synthesis and Characterization of Oligoyne Centered TTF 156 and Related TTFV Derivatives

3.2.1.1 Retrosynthetic Analysis

Scheme 3.3 outlines the retrosynthetic analysis of the target TTFV compounds. A straightforward bond disconnection at the central oligoyne units of **156a-c** and TTFV **157a-b** leads to handy synthons, acetylenic phenyl-DTF **160a-c**. Alternatively, a retro-oxidative dimerization at the TTFV moieties of **157a,b** readily unveils DTF precursors **160a,b**. DTF **160a-c** can be prepared from aldehyde **161** and phosphonate **105a** according to the synthetic method mentioned in Section 2.2.1.3. While the dithiole ring can be made by an HWE reaction between aldehyde **161** and phosphonate **105a**, extension of alkynyl bonds can be accomplished by Hay coupling of desilylated DTF with excess TMSA.

In planning the synthesis of oligoyne-TTFV analogues, the redox-controlled *cis*-to-*trans* conformational switching of the TTFV moiety was taken as an important factor that determins the structures of polymeric derivatives associated with the oligoyne-TTFVs. In particular, structural extension based on synthon **160a-c** was anticipated to generate macromolecules of different conformations, depending on the detailed synthetic sequences and conditions. Taking into account the V-shape of neutral diphenyl-TTFV and the linear shape of oligoyne and dicationic [phenyl-TTFV]$^{2+}$ units, three major synthetic consequences are readily perceived as illustrated in Figure 3.2, namely linear cationic polymer chains **162**$^{n+}$, helical foldamers **162**, and shape-

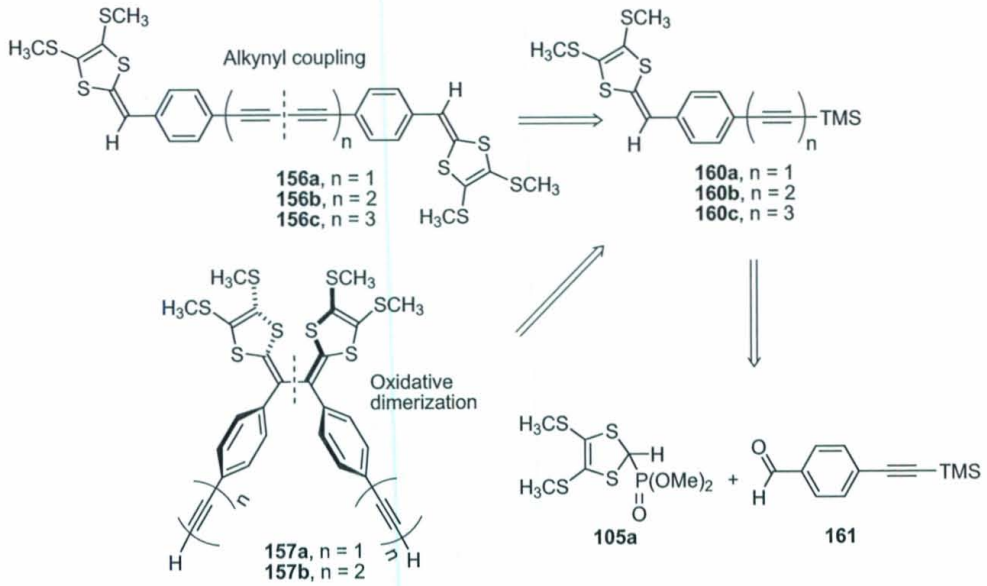

Scheme 3.3: Retrosynthetic analysis of oligoyne TTFs **156a-c** and TTFVs **157a,b**.

persistent macrocycles **163**. These oligoyne-TTFV related macromolecules were not known in the literature prior to this work.

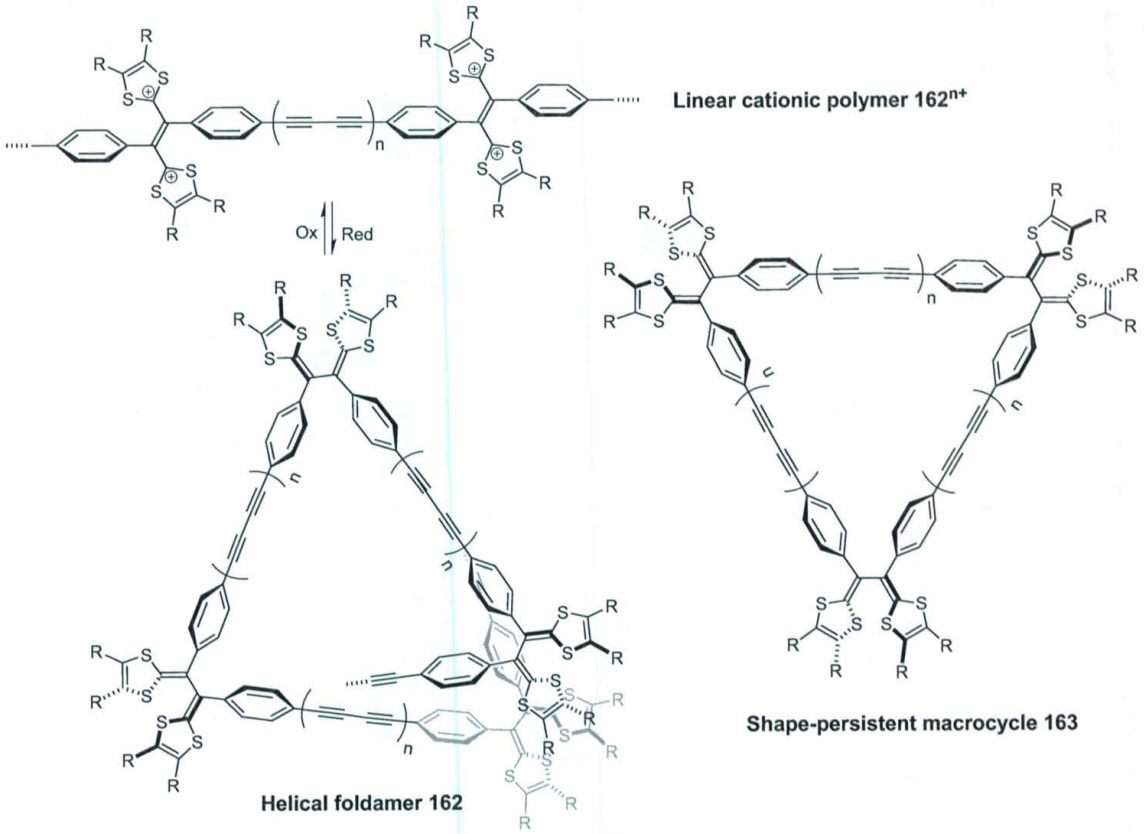

Figure 3.2: Various macromolecular systems possibly derived from acetylenic phenyl-DTF **160**.

3.2.1.2 Synthesis of Oligoyne exTTFs 156a-c

The synthesis of DTFs **160a-c** and **156a-c** is described in Scheme 3.4. The synthetic route followed the methods developed by a former group member, Ilias Mahmud,[156] with modifications of some reaction conditions. The synthesis started with a Sonogashira reaction of 4-bromobenzaldehyde with TMSA using $PdCl_2(PPh_3)_2$/CuI as catalyst in Et_3N. The isolated yield of aldehyde **161** was 93%, which was slightly higher than the yield attained in benzene/DBU (88%). Next, aldehyde **161** was subjected to an HWE reaction with phosphonate **105a** to afford DTF alkyne **160a** in 80% yield as a yellow liquid, which solidified upon storage in a fridge. DTF **160a** was desilylated with K_2CO_3 to afford a free terminal alkyne intermediate, which was subjected to Hay coupling with excess TMSA (ca. 14 equiv mol) to form diyne-attached phenyl-DTF **160b** in 82% yield. Note that the Hay coupling reactions were catalyzed by CuI/TMEDA in CH_2Cl_2, instead of the commonly reported catalytic conditions of CuCl/TMEDA in acetone/CH_2Cl_2 (1:1). The yields obtained under the two catalytic conditions were, however, quite comparable. Repetition of the same desilylation/Hay coupling sequence on **160b** led to the formation of triyne-substituted phenyl-DTF **160c**. In this Hay coupling reaction, because of the fast homocoupling reaction of desilylated diyne **160b**, a considerably large excess of TMSA (ca. 38 equiv mol) was added to ensure a satisfactory yield of **160c**, 60%.

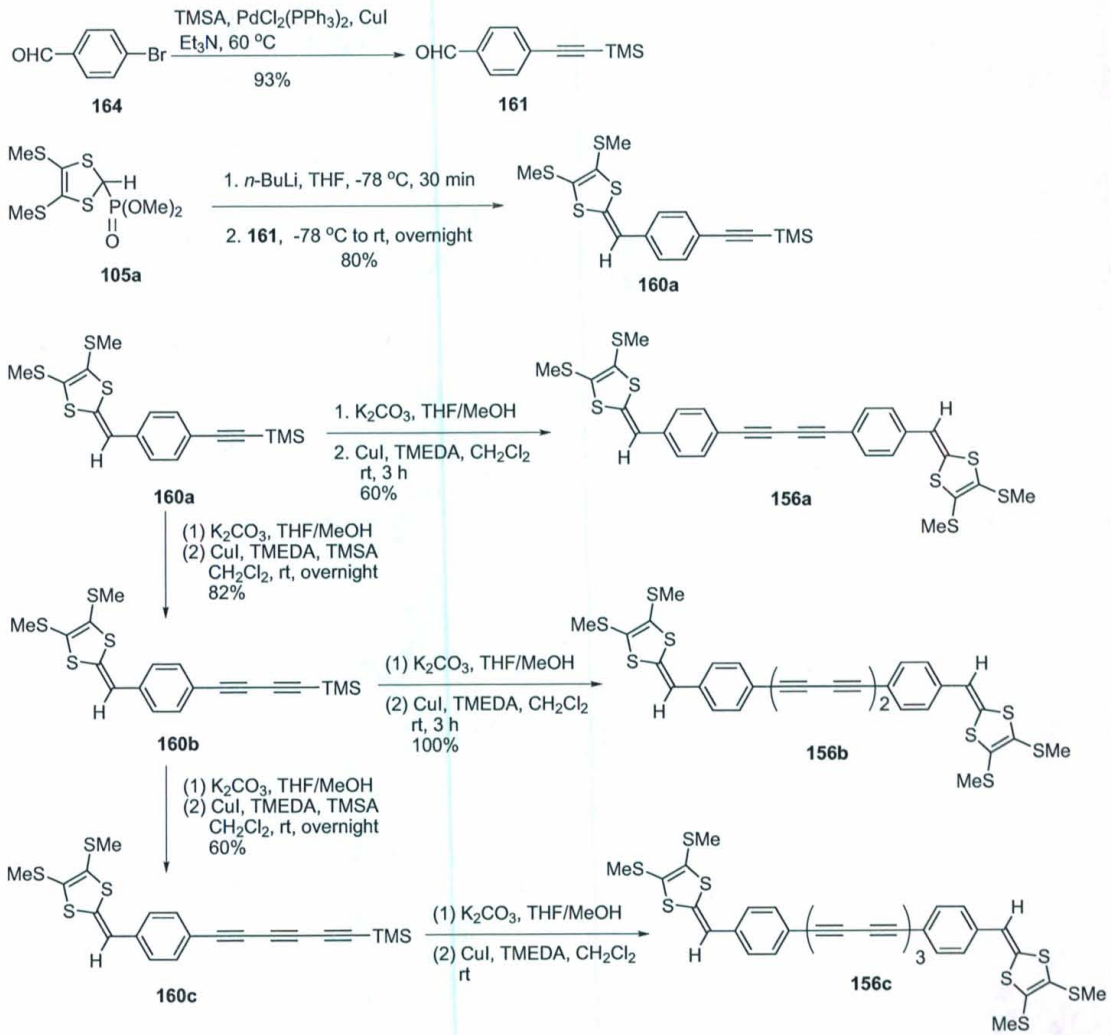

Scheme 3.4: Synthesis of DTFs **160a-c** and oligoyne TTFs **156a-c**.

With the acetylenic DTF precursors **160a-c** in hand, a straightforward oxidative homocoupling strategy was then implemented to produce the desired oligoyne-centered exTTFs. As shown in Scheme 3.4, desilylation of DTF **160a** with K_2CO_3 followed by oxidative homocoupling in the presence of CuI/TMEDA afforded diyne-centered exTTF **156a** in 60% yield. Under the same conditions, homocoupling of desilylated diyne-DTF **160b** proceeded more rapidly and efficiently, resulting in tetrayne-centered exTTF **156b** in a quantitative yield. Tetrayne-centered exTTF **156b** has solubility significantly lower than that of **156a**, and it precipitated out from the reaction solution. Homocoupling of desilylated triyne-DTF **160c** also proceeded smoothly to form hexayne-exTTF **156c** in dilute solution as evident by TLC. MALDI-TOF MS analysis clearly showed the molecular ion at $m/z = 709.9461$ corresponding to $[\mathbf{156c}]^+$ (709.9487 calcd for $C_{36}H_{22}S_8$), validating the formation of hexayne-exTTF **156c**. The isolation of hexayne-exTTF **156c** was, however, unsuccessful due to its extremely poor chemical stability in the solid state. Actually, upon evaporation of the solvent under vacuum, the orange solution of **156c** was instantaneously changed into a purplish substance insoluble in any organic solvents. The insolubility of the solid products hampered meaningful structural characterization. Nonetheless, it is reasonable to assume that topochemical polymerization of the hexayne moiety of **156c** accounts for the solid-state reactivity. Previously, Tykwinski and co-workers synthesized a diphenyl-endcapped hexayne which was separated as a relatively stable orange solid.[143] In hexayne-exTTF **156c**, the dramatically reduced stability can be ascribed to the endcapping DTF groups that may induce optimal solid-state packing geometry via strong S-S contact to facilitate topochemical polymerization.

3.2.1.3 Synthesis of TTFV 157a,b

Phenyl-DTFs **160a,b** were respectively subjected to an iodine-promoted oxidative dimerization reaction, yielding cationic dimerized products which were subsequently treated with $Na_2S_2O_3$ to afford neutral acetylenic phenyl-TTFVs **165a,b** in the same yield of 60% (see Scheme 3.5). Although I_2 was reported as a cheap but less efficient oxidant for the dimerization of DTF with common yields around 40%, it gave promising yields under optimized conditions for the synthesis of **165a,b**. Although in the dimerization process 1 equiv of I_2 is theoretically sufficient to oxidize DTF and the resulting TTFV *in situ*, the use of 3 equiv of I_2 was found to result in the best yield. It is likely that the reduction potential of I_2 is comparable to the oxidation potential of DTF, thus an excess amount of I_2 can maintain a suitable concentration of I_2 in solution to ensure efficient oxidative power. The equilibrium in the first oxidation step was evidenced by the recovery of some DTF starting material after workup. The addition of a large excess of I_2 did not further improve the yield, since such conditions would trigger some undesireable side reactions such as addition of I_2 to unsaturated carbon-carbon bonds. Besides the amount of I_2, reaction times for the two steps were also found to be crucial factors to reaction yields. A longer reaction time of the oxidation step was necessary for the dimerization to go to completion, while the reaction time for the reduction step had to be relatively shorter. Otherwise, unidentified side products could be observed by TLC analysis. It should be noted that TTFVs **165a,b** are not very stable when adsorbed on silica. This was evidenced by the observation that the yellow-colored spot of TTFVs **165a,b** loaded on TLC plates turned to a green-bluish color in less than 1 min. For this reason,

column chromatographic separation was conducted as rapidly as possible to prevent decomposition. According to the color change, it was speculated that the TTFV compounds, on contact with the acidic surface of silica gel and air, could be readily oxidized into cationic species.

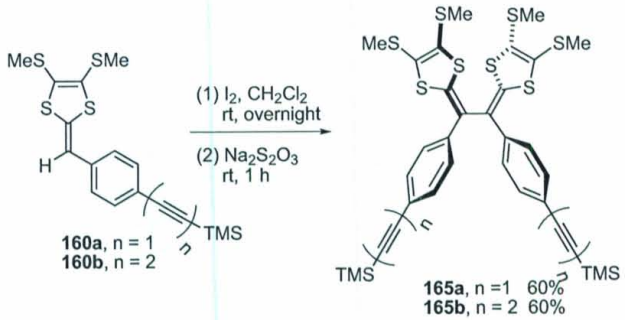

Scheme 3.5: Synthesis of TTFVs **165a,b**.

3.2.1.4 Synthesis of Shape Persistent Macrocyles 163a,b by Alkynyl Coupling of TTFV Precursors

The synthesis of TTFV shape persistent macrocycles is outlined in Scheme 3.6. Desilylation of TTFV **165a** with K_2CO_3 followed by a Pd/Cu-catalyzed homocoupling reaction under dilute conditions (ca. 2.8 mM) in refluxing acetone resulted in a series of cyclic oligomers ranging from trimer to pentamer, as manifested by MALDI-TOF MS analysis (Figure 3.3). By flash column chromatography, trimeric macrocycle **163a** was isolated as the major product in 18% yield, while other byproducts were not readily separable due to their low amounts. The addition of $PdCl_2(PPh_3)_2$ was crucial to the formation of macrocycles, because the use of CuI/TMEDA as catalyst only resulted in some unidentified products which appeared

only on the baseline of TLC. A plausible rationalization is that the two adjacent dithiole rings of TTFV bind to Pd through S-Pd interactions, which pre-organize the TTFV in a conformation that requires little structural change to form the macrocycle products, in particular, trimeric macrocycle **163a**. Unlike TTFV **165a**, macrocycle **163a** did not change its yellow color when loaded on TLC plate, indicating a better chemical stability. The stability can be accounted for by the relatively higher oxidation potential of **163a** than TTFV **165a**, owing to the relative rigid conformation of macrocycle. In the ^{1}H-NMR spectrum, the *S*-methyl groups of **163a** gave two singlet signals at 2.44 and 2.45 ppm with different integration value. In the ^{13}C NMR spectrum of **163a** the *S*-methyl gave rise to only one signal at 19.1 ppm. Close inspection of the ^{13}C NMR of **163a** also revealed a signal assigned to two alkenyl carbons in the 5-membered ring overlapping at 138.1 ppm. This observation may suggest a high degree of symmetry existing in the macrocylic core as well as the dithiole rings.

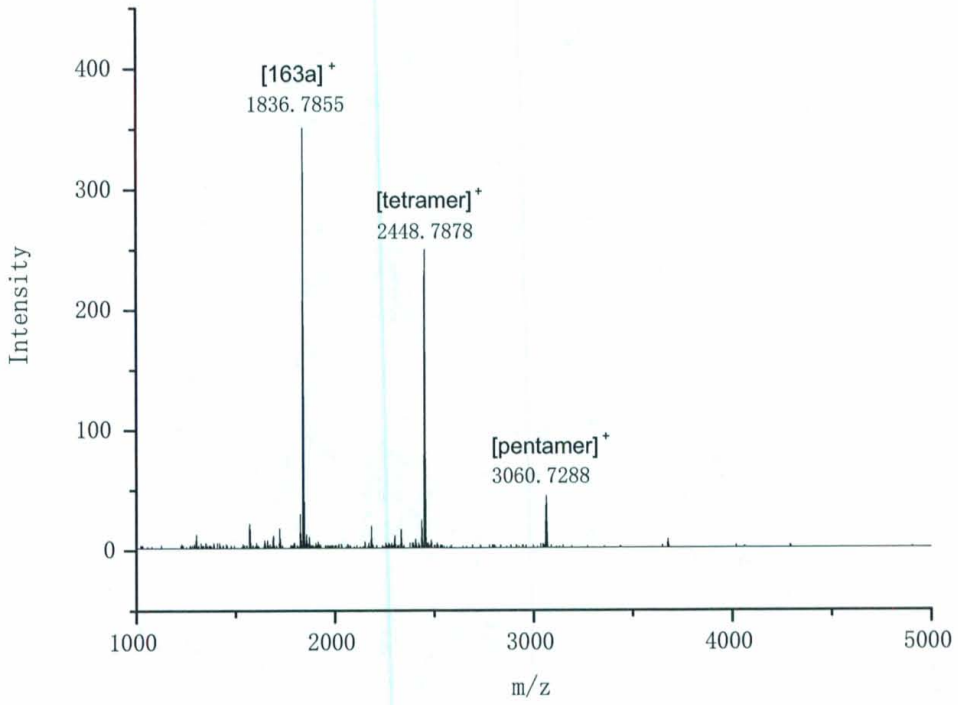

Figure 3.3: MALDI-TOF MS analysis on the macrocylization crude products showing the presence of macrocycle **163a** and other higher macrocyles.

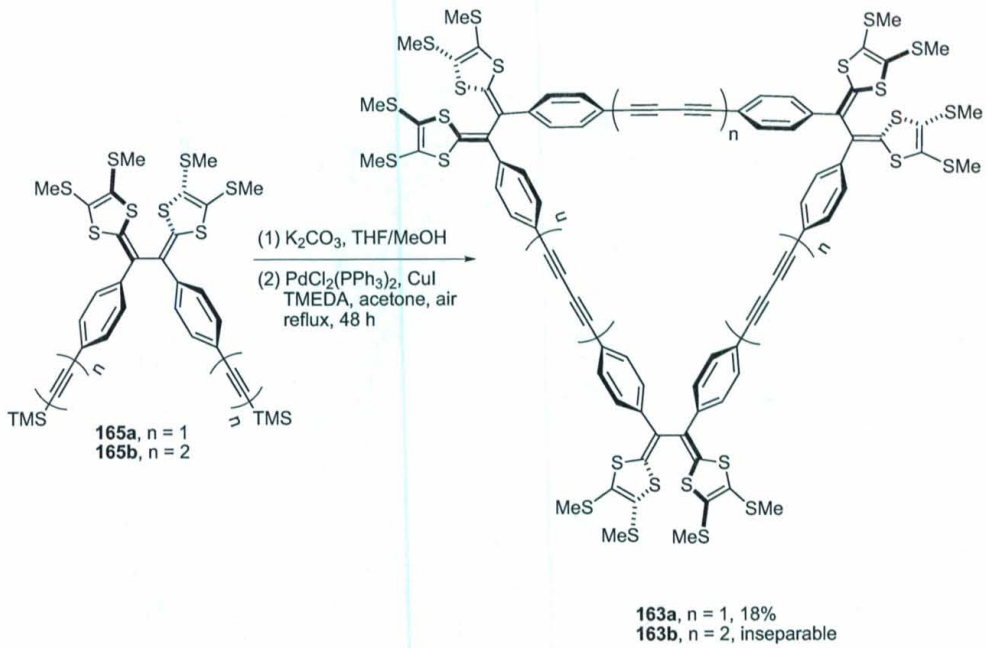

Scheme 3.6: Synthesis of shape persistent macrocycles **163a,b**.

In a similar manner, TTFV **165b** was desilylated and then subjected to macrocyclization reactions under the catalysis of Pd/Cu in refluxing acetone (Scheme 3.6). MALDI-TOF MS analysis clearly indicated the formation of macrocycle **163b** as the major product of the macrocyclization (Figure 3.4). However, efforts to isolate pure **163b** by flash column chromatography failed because of the very similar R_f value of **163b** to some intractable byproducts.

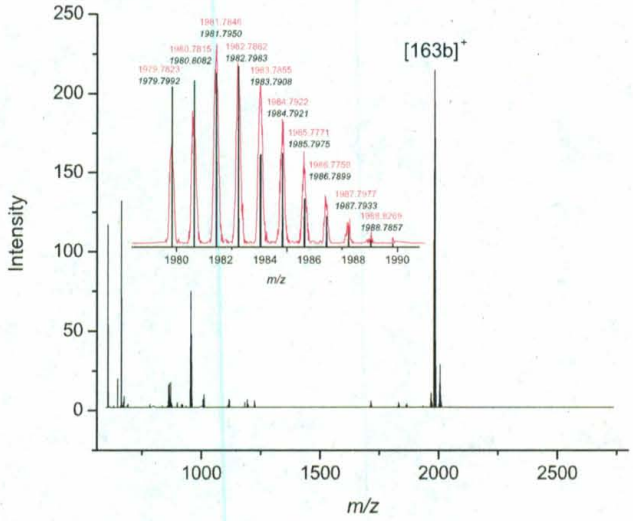

Figure 3.4: MALDI-TOF MS analysis on the macrocyclization products showing the presence of macrocycle **163b**.

3.2.1.5 Synthesis of TTF Polymers from 156a,b by Chemical and Electrochemical Methods

The two phenyl-DTF units in oligoyne-exTTFs **156a**,**b** upon oxidative dimerization were expected to cross link into "chain-like" oligomer and polymer wires. The oxidative coupling of DTF groups could be conducted by either chemical or

electrochemical means. As shown in Scheme 3.7, chemical polymerization was performed by treating the solution of **156a,b** with I_2 in CH_2Cl_2 at ambient temperature for ca. 12 h. Afterwards, the resulting polymers were reduced by $Na_2S_2O_3$ to afford neutral polymer products **158a,b** respectively. Both **158a,b** were orange solids and readily soluble in non-polar organic solvents such as CH_2Cl_2 and chloroform. MALDI-TOF MS analysis on the samples of **158a,b** revealed the presence of oligomers of short chain lengths (m = 2–8 for **158a** and m = 2–4 for **158b**). The relative low degrees of oligomerization observed are not surprising for two reasons. First, they are the results of the moderate yields of the DTF coupling in the solution phase using I_2 as the oxidant. Second, the oxidation potentials of the DTF should increase as the chain length of the oligomer increases, because the formed TTFV moieties in the reaction solution are dicationic and electron-withdrawing in nature. With a weak oxidant like I_2, the DTF units in longer oligomers may not be readily oxidized. As such, the reaction rate slows down with increasing polymer chain length and eventually stops at a certain degree of polymerization.

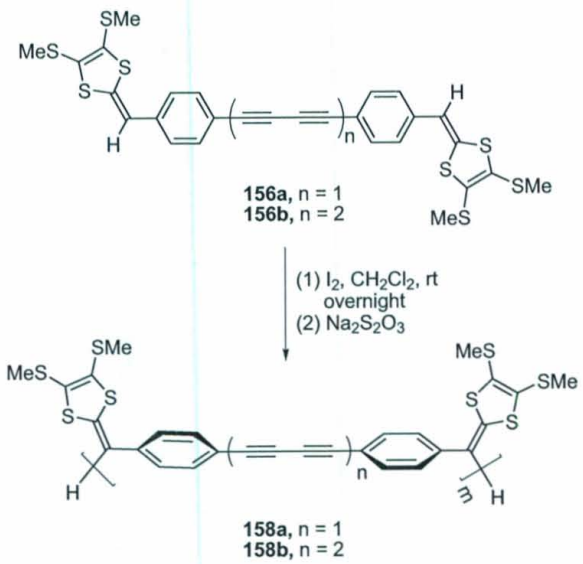

Scheme 3.7: Synthesis of poly(oligoyne-TTFV)s **158a**,**b** via DTF oxidative coupling.

3.2.1.6 X-Ray Single Crystal Structure of Oligoyne exTTFs 156a,b

Single crystals of diyne-exTTF **156a** and tetrayne-exTTF **156b** were grown by slow evaporation of their solutions in CH_2Cl_2 at low temperature (4 °C), and their detailed molecular and solid-state structures were characterized by single crystal X-ray diffraction. As can bee seen from Figure 3.5, both diyne-exTTF **156a** and tetrayne-exTTF **156b** show nearly planar π-conjugated backbones in the molecular structures (Figure 3.5A,B), with the DTF rings slightly deviated from the planes of phenyl rings by ca. 15–20°, presumably due to steric hindrance between the sulfur atoms and adjacent phenyl protons.

In the crystal lattice, molecules of diyne-exTTF **156a** are closely packed at a distance of d = 5.35 Å with an inclination angle Φ = 57.2° between the axes of molecules and the packing axis (Figure 3.5C,E), while the distances between the alkynyl carbons in adjacent molecules (C1'-C2 4.779 Å, C1'-C4 4.574 Å) are beyond the range of van der Waals contact (ca. 3.4 Å). Such packing geometries are moderately deviated from the optimal arrangements for diacetylene 1,4-addition (d = 4.9 Å, Φ = 45°) polymerization and therefore suggest a low probability for diyne **156a** to undergo topochemically controlled polymerization in the solid state. The single crystals of tetrayne-exTTF **156b** show a packing distance d = 5.34 Å similar to that of diyne **156a**, but a relatively smaller inclination angle Φ = 48.8°. Of note is that the C1' to C4 distance (4.30 Å) is considerably shorter than those of C1' to C2 and C1' to C6, which implies a higher probability for topochemical polymerization in a 1,4-addition fashion. In addition to the ordered alignment of oligoyne moieties, intimate S-S interactions give another notable feature in the solid-state structure.

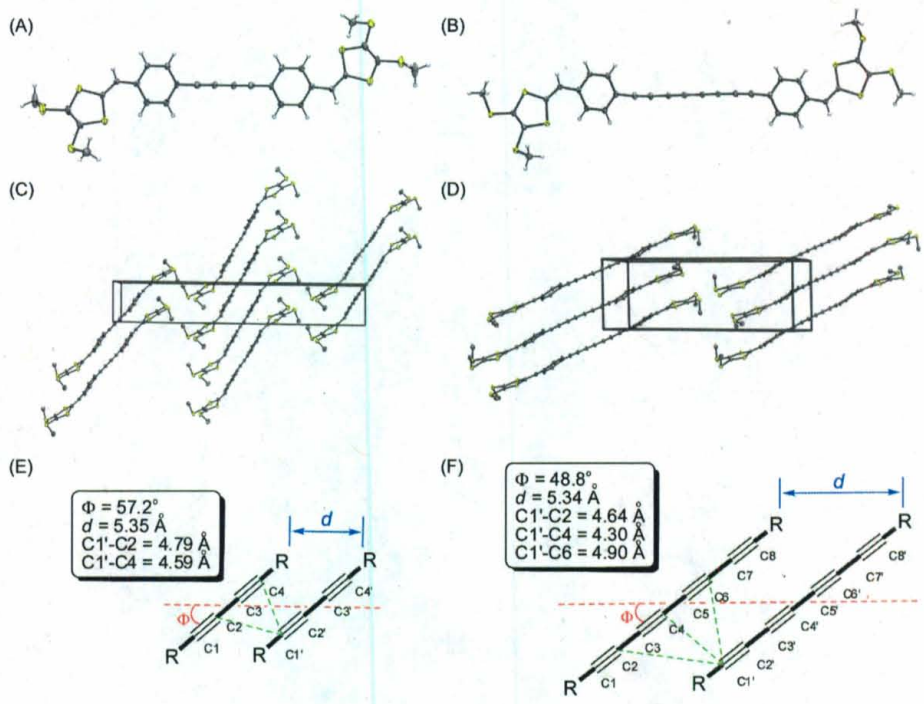

Figure 3.5: ORTEP drawing of (A) diyne-exTTF **156a**, and (B) tetrayne-exTTF **156b** (30% probability thermal ellipsoids). Crystal packing of (C) diyne-exTTF **156a**, and (D) tetrayne-exTTF **156b**, viewed perpendicular to the *b*-axis. Packing geometries of (E) diyne-exTTF **156a**, and (F) tetrayne-exTTF **156b** in the solid state. CCDC 749087 (diyne-exTTF **156a**), 804971 (tetrayne-exTTF **156b**).

In the crystal of diyne-exTTF **156a**, the shortest S-S distances between adjacent molecules are 3.51 Å, while for tetrayne-exTTF **156b** the close S-S contacts are 3.99 and 4.04 Å. The weak S-S interaction in **156b** can be viewed as one of the driving force for the topochemical polymerization. Clearly, the DTF rings play an important role in dictating the solid-state packing properties of oligoyne-exTTFs, which in turn affect their solid-state reactivity. Indeed, the close S-S interactions are believed to be responsible for the extremely poor stability of hexayne-exTTF **156c** in the solid state.

3.2.1.7 Solid-State Reactivities of Oligoyne-exTTF 156a,b

To further explore the solid-state reactivities of oligoyne-exTTFs **156a**,**b** differential scanning calorimetry (DSC) and thermogravimetric analysis (TGA) were undertaken. As shown in Figure 3.6A, the DSC trace of diyne **156a** shows a sharp endothermic peak at 206.8 °C (ΔH = -40.3 kJ/mol) which is attributed to melting. A prominent exothermic peak emerges at 244.5 °C (ΔH = 171.4 kJ/mol), and TGA measurement shows no significant weight loss below 275 °C. The thermal analysis suggests that the exothermic peak is due to thermally induced diacetylene cross-linking reaction. Given the relatively broad peak width and moderate reaction heat, the thermal cross-linking may have occurred in a random and disordered manner rather than topochemical polymerization. The DSC trace of tetrayne **156b** (Figure 3.6B) shows a noticeable endothermic transition at 137 °C and an intense sharp exothermic peak at 226.9 °C (ΔH = 249.7 kJ/mol). TGA data reveals a slight weight loss (ca. 10%) at this temperature. Collectively, the thermal data suggests that tetrayne **156b** might have undergone a much ordered cross-linking reaction in the solid state. According to the

crystallographic data, the solid-state reaction is mostly like through a 1,4-addition pathway (Scheme 3.8).

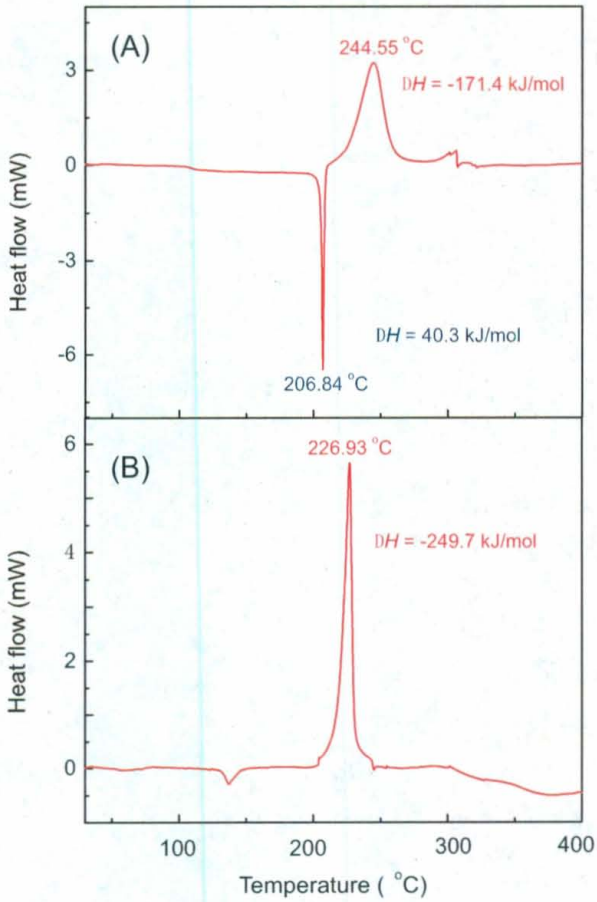

Figure 3.6: DSC of (A) diyne-exTTF **156a**, (B) tetrayne-exTTF **156b**.

3.2.1.8 Electronic Properties of Oligoyne exTTFs 156a-c and DTFs 160a-c

The electronic absorption properties of oligoyne-exTTFs **156a-c** were investigated by UV-Vis spectroscopy. For comparison purposes, the UV-Vis spectra of acetylenic DTF precursors **160a-c** were also determined. Detailed spectroscopic results are

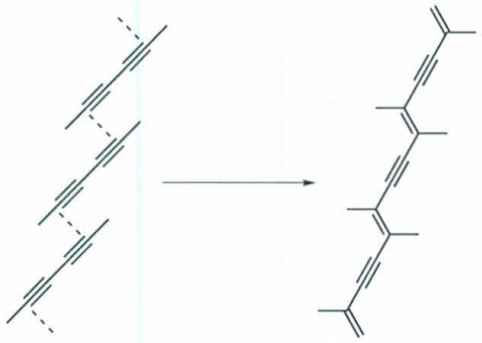

Scheme 3.8: Proposed pathway for a topochemical 1,4-addition.

given in Figure 3.7 and summarized in Table 3.1. The UV-Vis absorption spectrum of diyne-exTTF **156a** (Figure 3.7A) features a strong low-energy absorption band at 423 nm and a relatively weak band at 332 nm, which can be assigned to the $\pi \rightarrow \pi^*$ transitions at the phenyl-DTF moiety. In the spectrum of tetrayne-exTTF **156b**, the lowest-energy absorption band (λ_{max} = 467 nm) is notably redshifted by ca. 40 nm compared to that of diyne **156a**, as a result of extended π-conjugation. Additionally, a relatively strong high-energy absorption peak emerges at 307 nm in the spectrum of **156b**, the origin of which is likely due to transitions at the phenyl-butadiyne-phenyl framework. The UV-Vis absorption spectrum of hexayne-exTTF **156c** was measured from the solution obtained after a brief aqueous workup of the reaction solution. Since TLC analysis showed that the crude product solution contained only small amounts of impurities, the spectrum was deemed acceptable in offering a qualitative characterization of the electronic absorption properties of hexayne-exTTF **156c**. In contrast to the structureless low-energy profiles observed in the spectra of diyne **156a** and tetrayne **156b**, the absorption of hexayne **156c** gives rise to spectral patterns with more distinctive fine structures. In the low-energy region, three sharp absorption peaks can be seen along with a shoulder at 431, 458, 467, and 506 nm. The intensities

Table 3.1: Summary of electronic properties of oligoyne-exTTFs **156a-c**. Optical energy gap (E_g) obtained from the intersection between the tangential line and the base line of the lowest-energy absorption profile.

Entry	λ_{abs}, nm (ε, 10^4 M^{-1} cm^{-1})	E_g(eV)
156a	423 (6.69), 332 (2.23)	2.61
156b	467 (8.39), 307 (6.58)	2.39
156c	506, 467, 458, 431, 346, 326, 303, 283(sh), 264(sh)	2.25

of these are relatively weak in comparison to the bands in the high-energy range. The spacings of the three low-energy peaks are determined to be 2371 and 1778 cm^{-1}. The significant difference in these spacing values implies that the sharp absorption bands mostly likely originate from various electronic transitions rather than a vibronic progression. In the high-energy region, three sharp absorption peaks are clearly seen at 303, 326, and 346 nm, respectively. The spacings of these peaks (1827 and 1884 cm^{-1}) are nearly identical and consistent with the characteristic vibronic progressions observed in other conjugated hexaynes and longer polyyne systems.[157]

3.2.1.9 Electronic Properties of Macrocycle 163a, TTFV 165a, and Polymers 158a,b

The UV-Vis absorption properties of TTFV-based macrocycle **163a**, TTFV precursor **165a**, and polymers **158a,b** are compared in Figure 3.8. The absorption spectrum of macrocycle **163a** shows three $\pi \rightarrow \pi^*$ transition bands at 400, 335, and 260 nm. The lowest-energy band is redshifted by ca. 20 nm relative to that of TTFV precursor **165a** (λ_{max} = 380 nm) as a result of extended π-conjugation. The spectrum of

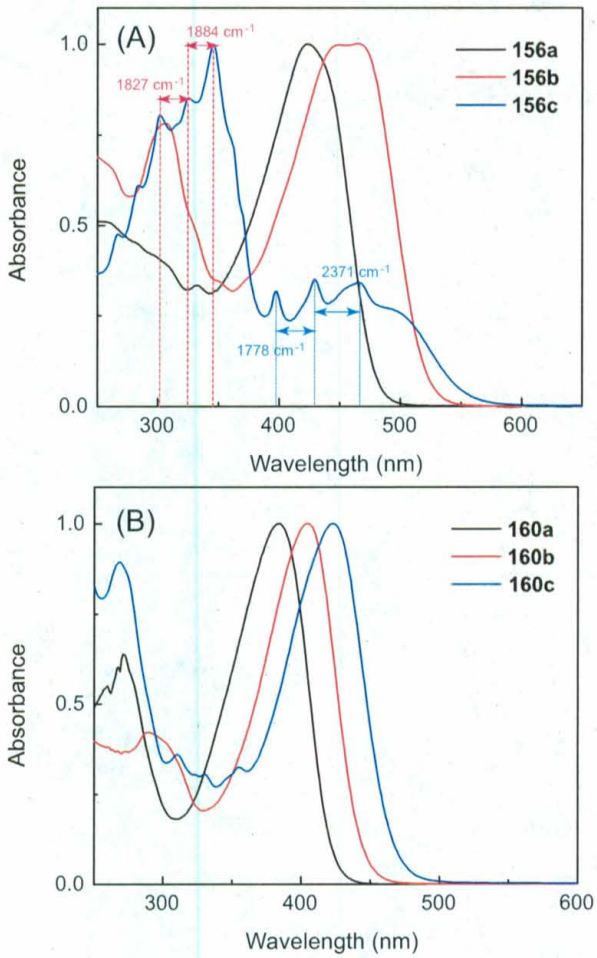

Figure 3.7: Normalized UV-Vis spectra of (A) oligyne-exTTFs **156a-c**, (B) DTFs **160a-c** measured in $CHCl_3$.

polymer **158a**, which is structurally the acyclic analogue of macrocycle **163a**, shows three absorption bands at 422, 331, and 298 nm. The lowest-energy absorption peak of **158a** is redshifted by 22 nm in comparison with macrocycle **163a**. It is interesting to note that the low-energy cutoff edges of **163a** and **158a** are nearly superimposable, which is indicative of the same optical band gap energies for the two species. This observation suggests rather insignificant electronic delocalization across the π-framework of **158a**. It is reasonable to assume that the TTFV units of **158a** take *cis* conformation in the neutral state to form foldamers. Such a helical orientation hence attenuates the electronic communication between each conjugated repeat segments in the polymer backbone. The UV-Vis spectrum of **158b** shows three absorption bands at 444, 348, and 304 nm, respectively. Compared with **158a**, the λ_{max} value of **158b** is redshifted by 22 nm as a result of further extended oligyne length in the repeat unit. In addition to the significant $\pi \rightarrow \pi^*$ features, the spectra of **158a**,**b** both show a weak long-wavelength hump in the Vis-NIR region, peaking at 566 nm for **158a** and 738 nm for **158b**. The origins of these peaks can be ascribed to trace amounts of cationic TTFV moieties due to incomplete reduction during the polymer preparation process. This assignment is evidenced by UV-Vis spectroelectrochemical studies (vide infra).

3.2.1.10 Electrochemical and UV-Vis Spectroelectrochemical Properties of Oligoyne exTTFs and Related Derivatives

The electrochemical redox properties of oligoyne-exTTFs and related compounds were investigated by cyclic voltammetric (CV) analysis, and the detailed voltammograms are illustrated in Figure 3.9. The CV profile of diyne-exTTF **156a** (Figure 3.9A)

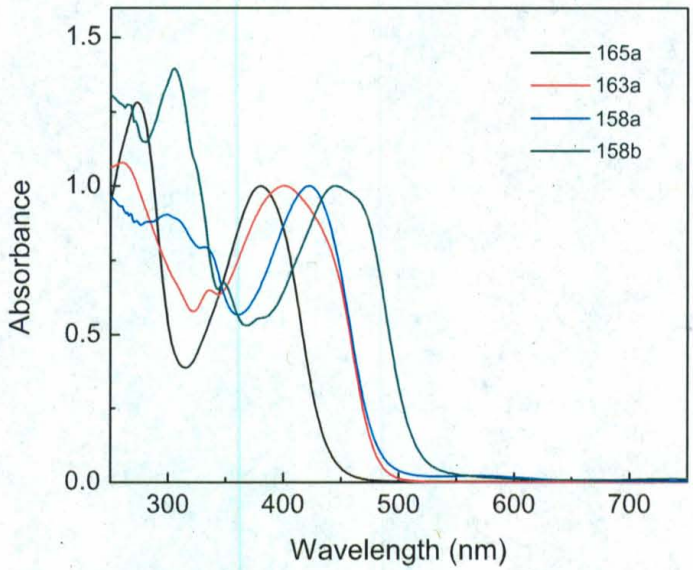

Figure 3.8: UV-Vis absorption spectra of macrocycle **163a**, TTFV **165a**, and polymers **158a**,**b** measured in $CHCl_3$.

shows an anodic peak at E_{pa} = + 0.75 V and a cathodic peak at E_{pc} = +0.55 V on the first cycle of scan. The anodic wave originates from the oxidation of the DTF moieties in **156a** to $[DTF]^{+\bullet}$. The cathodic peak, however, is not due to a reversible reduction process of $[DTF]^{+\bullet}$. Instead, it is assigned to the simultaneous two-electron reduction on $[TTFV]^{2+}$ that results from a rapid dimerization reaction of $[DTF]^{+\bullet}$ on the electrode surface. The assignment is evidenced by the dramatically changed voltammogram patterns observed on the second cycle of CV scan, in which a new anodic peak emerges at +0.62 V preceding the anodic peak at +0.75 V. Compared with the cyclic voltammogram of TTFV precursor **165a** (Figure 3.9C), the reversible couple at E_{pa} = +0.62 V and E_{pc} = +0.55 V can be reasonably attributed to the redox processes taking place at TTFV units. In the succeeding scan cycles, the cathodic peak due to $[DTF]^{+\bullet}$ formation (at ca. +0.75 V) shows a gradual decrease

in intensity, whereas the redox wave pair related to the TTFV groups are seen to steadily increase in intensity. This observation is indicative of electropolymerization of **156a** on the surface of the working electrode to form multiple layers of conductive polymer. Indeed, after a number of CV scans, a smooth and uniform thin film was deposited on the surface of working electrode. In Figure 3.9A, it is also notable in that the redox wave pairs associated with TTFV moiety show gradually increased quasi-reversible behavior with increasing number of CV scans. Tetrayne-exTTF **156b** gives very similar CV patterns (Figure 3.9B) to those of diyne-exTTF **156a**, and affords a high-quality conductive polymer thin film on the working electrode surface after successive CV scans. The voltammogram of macrocycle **163a** shows a quasi-reversible oxidation at $E_{pa} = +0.78$ V and $E_{pc} = +0.56$ V (Figure 3.9D). Compared with the voltammogram of TTFV **165a**, the redox potentials of **163a** are shifted anodically by ca. 0.1 V. The shift is due to the conformation constraint in macrocycle **163a** that prohibit the TTFV moiety from stretching into a trans TTFV dication upon oxidation. Similar effects have been found in a series of poly(ethylene glycol) tethered TTFV macrocycles reported by Lorcy and co-workers.[108]

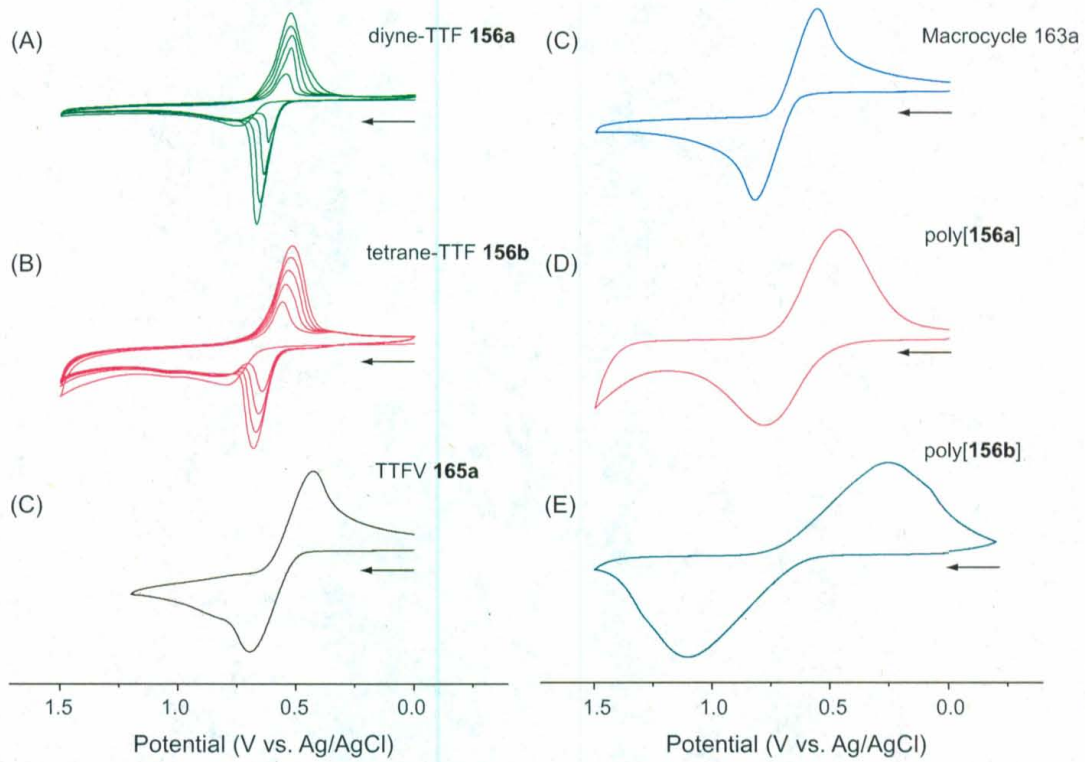

Figure 3.9: Cyclic voltammograms of: (A) Diyne-exTTF **156a** (10^{-3} M), scan rate: 200 mV s^{-1}, working electrode: glassy carbon; (B) Tetrayne-exTTF **156b** (10^{-3} M), scan rate: 200 mV s^{-1}, working electrode: glassy carbon; (C) TTFV **165a** (10^{-3} M), scan rate: 50 mV s^{-1}, working electrode: glassy carbon; (D) Macrocycle **163a** (10^{-3} M), scan rate: 50 mV s^{-1}, working electrode: glassy carbon; (E) poly[**156a**] thin film, scan rate: 50 mV s^{-1}, working electrode: ITO glass; (F) poly[**156b**] thin film, scan rate: 50 mV s^{-1}, working electrode: ITO glass. Experimental conditions: supporting electrolyte: Bu_4NBF_4 (0.1 M); solvent: CH_2Cl_2; counter electrode: Pt; reference electrode: Ag/AgCl. The arrows indicate the potential scan direction.

In addition to voltammetric studies, UV-Vis spectroelectrochemical analysis on the exTTFs and related TTFV macromolecules was also conducted in order to probe their optical responses to electrochemical redox processes. In the experiments, each UV-Vis spectral scan was performed after the electrolysis of an analyte at a controlled voltage for at least 90 seconds to ensure the electric current attained a constant value. As such, the systems examined by UV-Vis spectroscopy can be deemed as having arrived at equilibrium. The detailed results of spectroelectrochemistry are given in Figure 3.10.

Upon increasing oxidation, the lowest-energy absorption band of diyne-exTTF **156a** at 423 nm decreases steadily and a new broad band grows at 660 nm with relatively weak intensity (Figure 3.10A). The new long-wavelength band is assigned to the characteristic absorption of $[TTFV]^{2+}$.[108] The trend of UV-Vis spectral changes in the spectroelectrochemical analysis of **156a** is similar to that of TTFV precursor **165a** (Figure 3.10C), hence corroborating the formation of TTFV species in the process of electrochemical oxidation of diyne-exTTF **156a**. For tetrayne-exTTF **156b**, a substantial decrease of the absorption peak at 647 nm along with an increasing broad band at 668 nm can be observed (Figure 3.10B). The trend is similar to that of diyne **156a**, indicating the electrochemical polymerization through the formation of TTFV units. Unlike the spectroelectrochemical data for diyne **156a**, the UV-Vis absorption profile of tetrayne **156b** shows three sharp bands at 347, 377, and 408 nm when the oxidation arrives at a high degree. The spacings between these bands are 2293 and 2015 cm^{-1} are consistent with a vibronic progression arising from carbon triple bond stretching mode. The vibronic spectral pattern is also clearly discernible in the UV-Vis absorption spectrum of oxidized (cationic) poly[**156b**] thin film, where three

sharp bands can be seen at 353, 383, and 415 nm, respectively. These spectral results imply that oxidized (cationic) poly[**156b**] possess more rigid polymeric backbone than its neutral form.

The spectroelectrochemical data for macrocycle **163a** is shown in Figure 3.9D. As oxidation progresses, the lowest-energy band at ca. 422 nm drops in intensity along with a moderate degree of redshift, while the absorption in the high-energy region (ca. 322 nm) is slightly increased. The most notable spectral feature, however, is the substantial rise of a broad absorption tail from ca. 500 to 750 nm with a barely distinguishable peak at 600 nm, which are markedly different from those of acyclic TTF species **156a**,**b** and **165a**. The pronounced low-energy tail in the spectrum of oxidized macrocycle **163a** is correlated to the electronic absorptions of $[TTFV]^{2+}$. Given the unique conformation constraint in macrocycle **163a**, the TTFV moieties must retain *cis*-conformation even after being oxidized into $[TTFV]^{2+}$ dications. In this sense, macrocycle **163a** offers a convenient model to unravel the unique electronic absorption properties of *cis*-$[TTFV]^{2+}$.[108]

The solution-phase UV-Vis studies have revealed that compounds carrying TTFV groups are electronically transparent in the Vis-NIR region of the spectrum (500 to 800 nm) in the neutral state, and they become quite absorbing in this spectral range after being oxidized. Also the oxidation and reduction processes on the TTFV moieties are chemically reversible. Collectively, these spectral and electrochemical properties point to potential applications in electrochromism and electrochromic devices.[158–160] To further investigate the electrochromic properties in the solid state, the UV-Vis absorption spectra of polymer films prepared by electrodeposition of diyne-exTTF **156a** and tetrayneexTTF **156b** on ITO glass were characterized in both neutral and

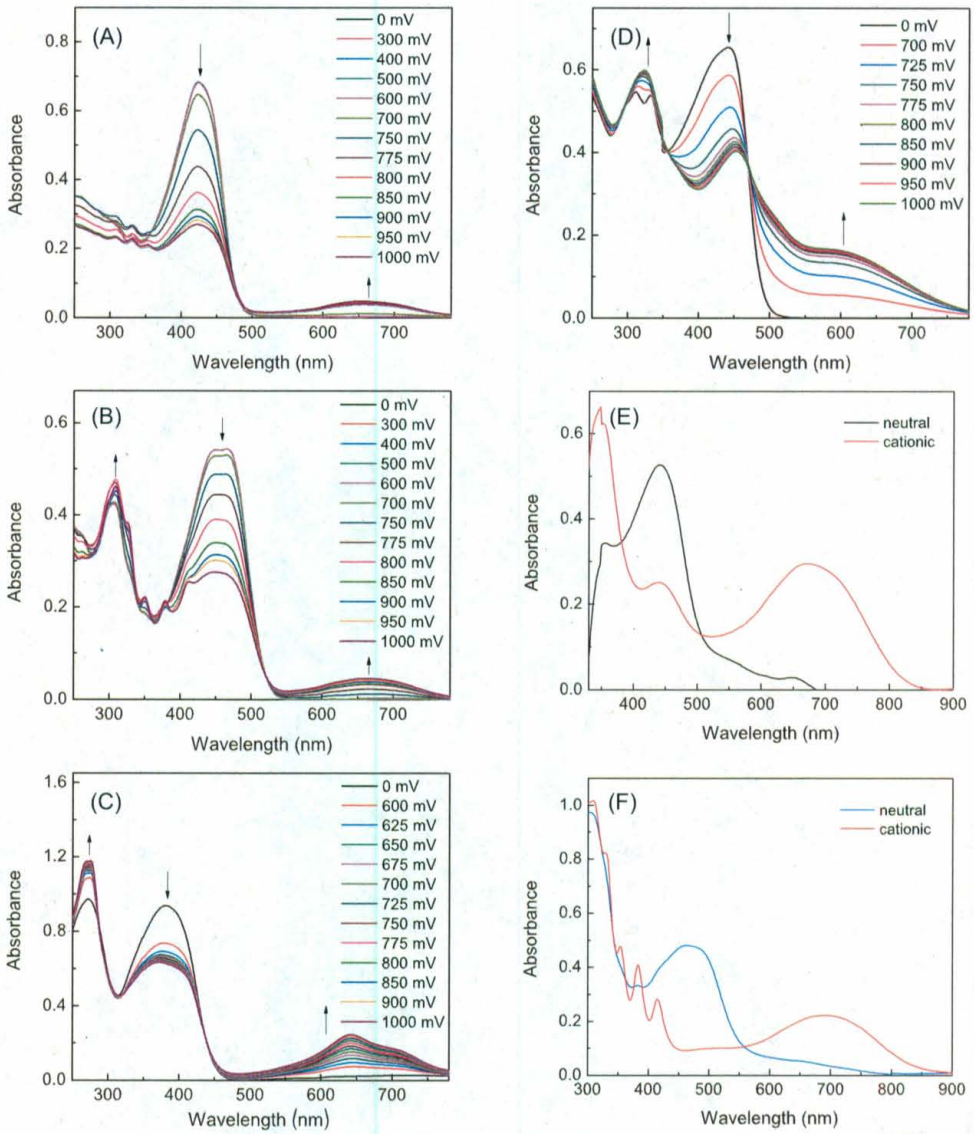

Figure 3.10: UV-Vis spectroelectrochemistry of (A) diyne-exTTF **156a**, (B) tetrayne-exTTF **156b**, (C) TTFV **165a**, and (D) macrocycle **163a**. Experimental conditions: supporting electrolyte: Bu_4NBF_4 (0.1 M); solvent: CH_2Cl_2; working electrode: Pt mesh; counter electrode: Pt; reference electrode: Ag/AgCl. UV-Vis absorption spectra of (E) poly[**156a**], (F) poly[**156b**] on ITO glass in the neutral (blue trace) and cationic (red trace) states.

oxidized states. As shown in Figure 3.10E, the thin film of poly[**156a**] shows a strong absorption $\pi \rightarrow \pi^*$ transition band at 441 nm. In addition, a weak absorption tail is observed in the range of ca. 500–700 nm, which is likely arising from trace amounts unreduced $[TTFV]^{2+}$ moieties (doping) in the polymer film. In charging the polymer thin films in an electrolysis setup at +0.9 V for 1 min, the color of poly[**156a**] was observed to gradually changed from yellow to dark green. The UV-Vis spectrum of oxidized poly[**156a**] shows a strong broad low-energy band covering the spectral range of 500 to 850 nm and peaking at 670 nm, while the absorption peak at 441 nm is greatly attenuated. In UV-Vis spectrum of neutral poly[**156b**] thin film (Figure 3.10F), a strong absorption band at 464 nm and a long absorption tail extending from ca. 550 to 800 nm are observed. Upon oxidation, the peak at 464 nm disappears, while a broad band appears in the Vis-NIR region (ranging from 550 to 900 nm and peaking at 691 nm) together with three distinctive vibronic bands at 415, 383, and 353 nm in the high-energy region.

3.2.1.11 Summary

The redox-controlled conformational switching behavior of phenyl-substituted TTFV is the key to the versatile synthesis of extended $\pi-$conjugated molecular and macromolecular structures with different topologies and dimensions, ranging from "rod-like" oligoyne-exTTFs to TTFV-containing shape persistent macrocycles and conducting polymer wires. The optical gaps of oligoyne-exTTFs show a reducing trend and do not converge as the oligoyne chain length increases from diyne to hexayne. The oligoyne-exTTFs can be efficiently polymerized through DTF oxidative coupling reactions and the polymer thin films resulting from electropolymerization show intriguing conductivity and redox activities. Furthermore, the polymer films exhibit redox-switchable coloration in the Vis-NIR region of the spectrum, suggesting potential applications in electrochromic devices. The synthetic access to TTFV oliogyne shape-persistent macrocycles **163a**,**b** has not only added new members to the family of phenylacetylene-based cyclophanes, but provided useful models for further understanding the effect of conformational constraint on the electronic properties of TTFV-embedded macromolecular systems. It is also envisaged that the nearly flat arrangement of the acetylene-rich ring framework of **163a** could render it a unique supramolecular hosts for certain metal ions and aromatic molecular guests. Finally, solid-state structural and thermal analyses have shown that tetrayne-exTTF **156b** can undergo topochemical polymerization more readily than diyne-exTTF **156a**. This finding hints to a possibility that macrocycle **163b** and electrochemically-induced polymer, poly[**156b**], if assuming they adopt folding conformation, may be further cross-linked through solid-state tetrayne cross-linking reactions to form defined and

organized 3-dimensional polymer networks.

3.2.2 Synthesis and Characterization of TTFV Based Tweezers and Crown Ether Hybrids

3.2.2.1 Synthetic Strategy towards Novel TTFV Derivatives

The synthetic targets to be discussed the section are TTFV based tweezers and crown ether hybrids derived directly from precursor TTFV **165a**. The retrosynthesis illustrated in Scheme 3.9 clearly reveals the synthetic strategies to such compounds. Basically, desilylated **165a** can afford alkyne-linked TTFV derivatives by Sonogashira reactions with suitable aryl halides to give a type of tweezer-like TTFV derivatives **159**. In addition, taking advantage of the efficient "click" chemistry enabled by terminal alkynes, TTFV **165a** was expected to cyclize with a chain-like diazido tether to form triazole-linked TTFV-crown ether hybrids such as compound **166**.

3.2.2.2 Synthesis of TTFV Tweezers

The construction of a TTFV-dianthraquinone tweezers **159a** is described in Scheme 3.10. In the synthesis, TTFV **165a** was first desilylated with K_2CO_3, and then subjected to Sonogashira cross coupling with 2-iodoanthraquinone **167**, to afford molecular tweezers **159a**. Due to the low solubility of **159a** in Et_3N, the product precipitated out of the reaction solution and was readily separated by filtration. The resulting crude product was rinsed with Et_3N and purified by silica gel column chromatography to afford pure product **159a** in 66% yield. Note that compound **159a** is an acceptor-donor-acceptor triad in electronic structure and hence is referred

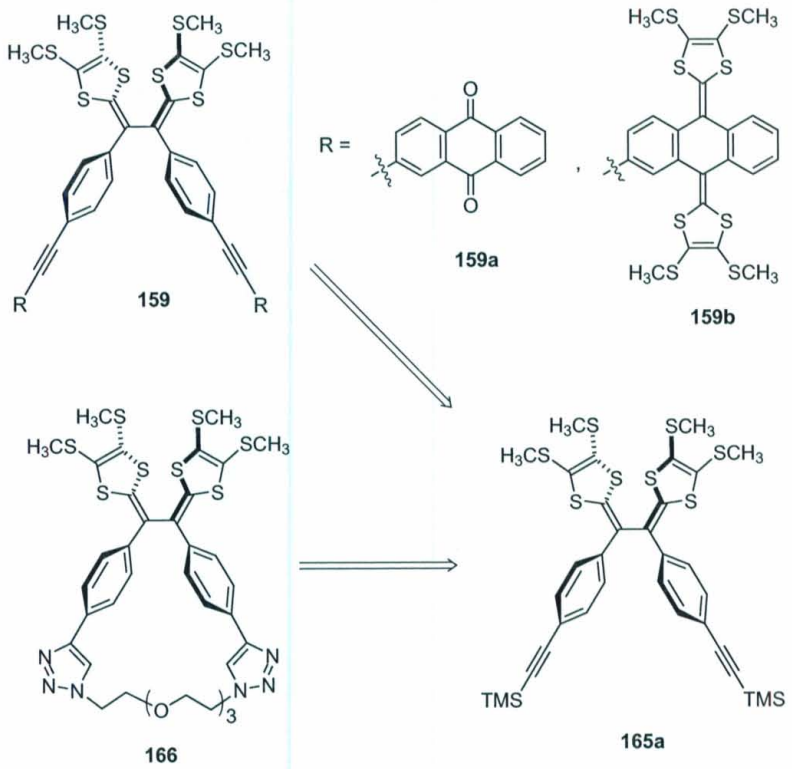

Scheme 3.9: Synthetic strategy for some new TTFV analogues derived from **165a**.

to as AQ-TTFV-AQ in the following discussions.

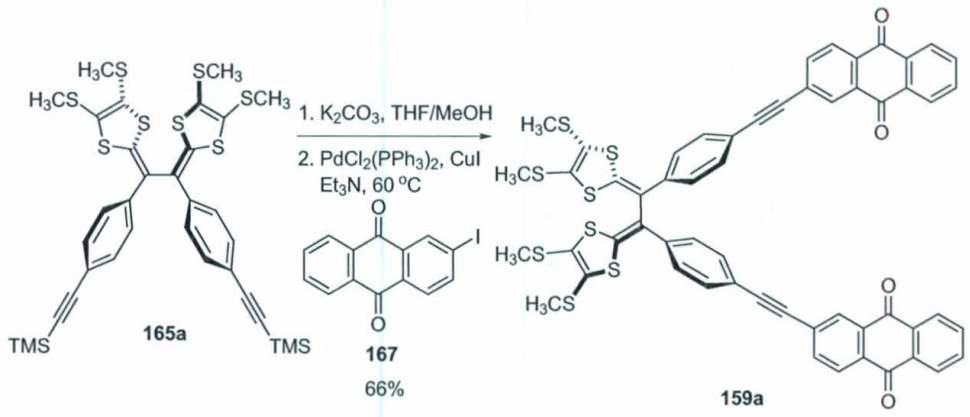

Scheme 3.10: Synthesis of AQ-TTFV-AQ **159a** by a Sonogashira reaction.

With compound **159a** in hand, a TTFAQ-tipped molecular tweezer **159b** was considered to be readily accessible through a 4-fold HEW reaction between **159a** and suitable phosphonate precursors. As shown in Scheme 3.11, phosphonate **105a** was first treated with a strong base, *n*-BuLi, at low temperature to form phosphonate ylide. AQ-TTFV-AQ **160a** was next added to react with the *in situ* generated phosphonate ylide, affording the desired molecular tweezers **159b** which is a TTFAQ-TTFV-TTFAQ triad. The HWE reaction produced **160b** in reasonable yields; however, purification of **159b** by column chromatography was found tedious and tricky. Similar to TTFV **165a**, compound **159b** was unstable in contact with silica gel. However, the existence of numerous byproducts in the 4-fold HWE reaction required a slow chromatographic procedure. As such, the isolated yields of **159b** were highly dependent on the silica gel column separation conditions. In particular, the yield appeared to be significantly influenced by the duration of column chromatography.

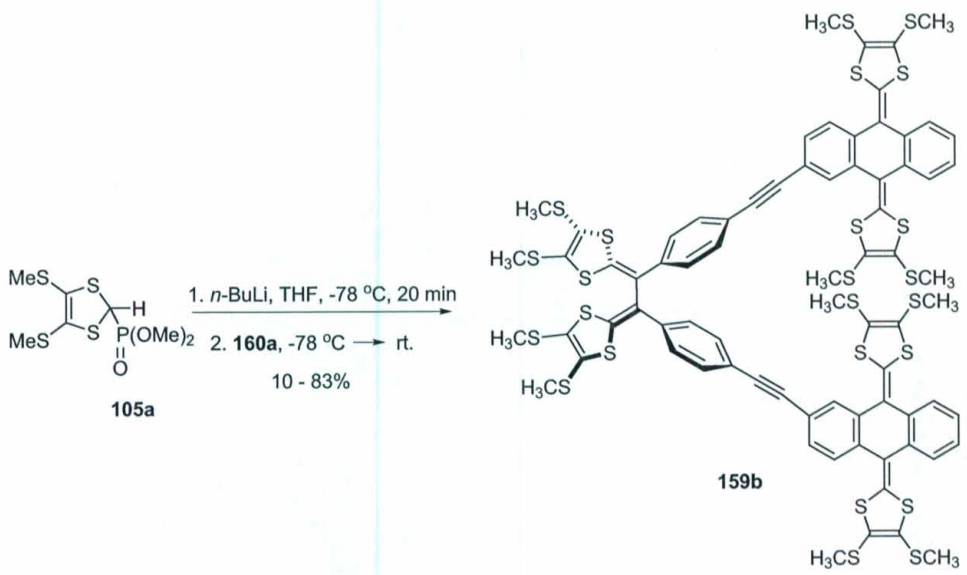

Scheme 3.11: Synthesis of TTFAQ-TTFV-TTFAQ **159b** by an HWE reaction.

In addition to the HWE strategy, an alternative Sonogashira coupling route was explored for the synthesis of compound **159b**. As shown in Scheme 3.12, a monoiodinated TTFAQ precursor **168** was first prepared by a $P(OEt)_3$-promoted olefination reaction between 2-iodoanthraquinone **167** and thione **104a** in toluene at 100 °C. The reaction gave the desired product **168** in 43% yield, along with the formation of two incomplete olefination byproducts **169** and **170**. A higher yield of **169** than **170** indicated a faster reaction rate of the ketone close to the electron-withdrawing iodide atom. All these compounds were readily separated and purified by column chromatography. Cross coupling of **168** with desilylated TTFV **165a** under the catalysis of Pd/Cu afforded compound **159b** (see Scheme 3.13), which precipitated out upon addition of MeOH into the reaction mixture. The precipitated product could then be easily purified by flushing through a short silica plug with $CHCl_3$, giving pure **159b** in a yield of 62%. The short separation time on column chromatography considerably reduced the undesirable decomposition of **159b** in contact with silica gel, therefore ensuring more consistent and reproducible yields for the reaction.

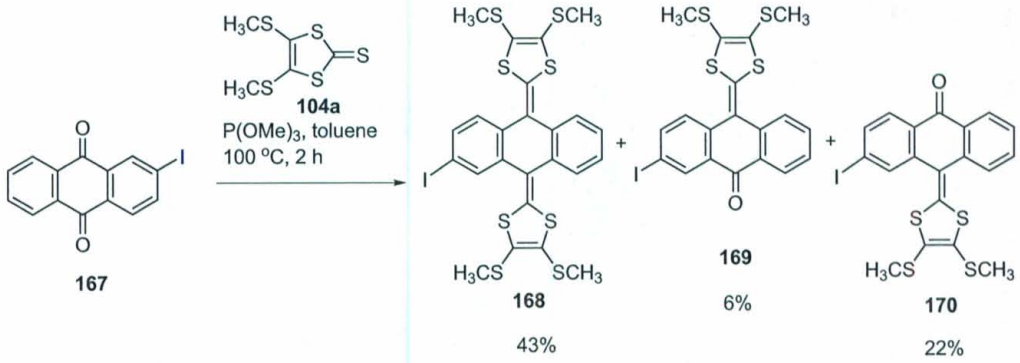

Scheme 3.12: Synthesis of monoiodinated TTFAQ **168** by a phosphate-mediated coupling.

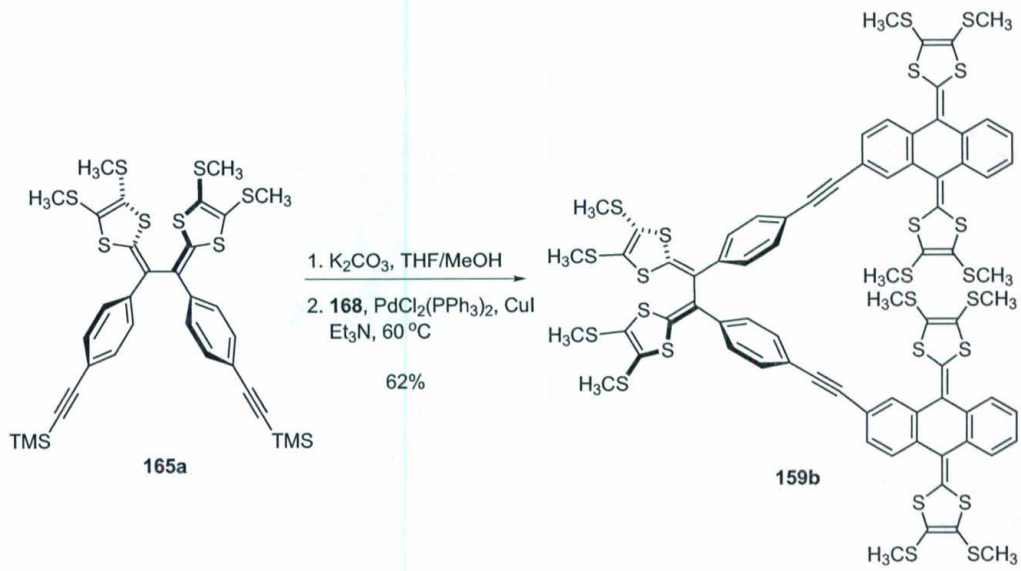

Scheme 3.13: Synthesis of TTFAQ-TTFV-TTFAQ **159b** by a Sonogashira reaction.

3.2.2.3 Synthesis of a TTFV Crown Ether Hybrid

The synthesis of a TTFV crown ether hybrid **166** was achieved by an alkyne-azide [3+2] cycloaddition (click reaction) between diazide **171** and desilylated **165a** in the presence of $CuSO_4 \cdot 5H_2O$/sodium ascorbate in DMF (see Scheme 3.14). After aqueous workup, the crude product was precipitated out as viscous oil, which was further purified by column chromatography. The use of $MgSO_4$ as drying agent was avoided as the product was found to be strongly bound to $MgSO_4$ through the complexation of the crown ether moiety with Mg^{2+} ion. The high yield of this cyclization (73%) was attributed to a template effect by Na^+. The reaction outcome may serve as a springboard to further synthetic exploration on other TTFV crown ether hybrids in future work.

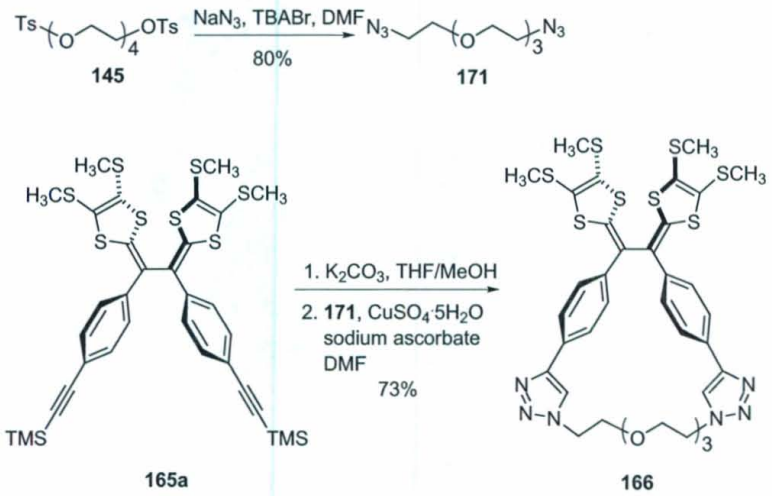

Scheme 3.14: Synthesis of TTFV crown ether hybrid **166** by a click reaction.

3.2.2.4 Electronic Properties of TTFV Tweezers 160a,b and Crown Ether Hybrid 166

The electronic absorption properties of molecular tweezers **159a,b** and crown ether **166** were investigated by UV-Vis absorption spectroscopy. Figure 3.11 compares the absorption spectra of **159a,b**, **166**, and **165a**. In the spectrum, TTFV **165a** shows an absorption band at 380 nm in the low-energy region. In the spectrum of AQ-TTFAQ-AQ **159a**, a notable absorption shoulder at 460 nm along with a broad long-wavelength absorption tail extending to ca. 580 nm are observed. To clarify the origin of the band, UV-Vis spectrum of a 1:2 mixture of TTFV **165a** and anthraquinone **172** was determined and compared with the spectrum of **160a**. The absence of a low-energy absorption band in the UV-Vis profile of the mixture of **165a** and **172** confirms that the long-wavelength shoulder and tail in the spectrum of **159a** is due to intramolecular charge transfer (ICT). The absorption spectrum of TTFAQ-TTFV-TTFAQ **159b** shows a broad low-energy band peaking at 416 nm, the origin of the band can be assigned to overlapped $\pi \rightarrow \pi^*$ transition bands of TTFV and TTFAQ. Interestingly, the longest wavelength absorption of crown ether hybrid **166** is blueshifted compared to TTFV **165a**. The observation indicates a decrease in effective $\pi-$conjugation in changing the $\pi-$bridge from acytylene to triazole.

3.2.2.5 Electrochemical Redox Properties of TTFV Tweezers 159a,b and TTFV Crown Ether Hybrid 166

The electrochemical redox properties of TTFV-hinged tweezers **159a,b** and crown ether hybrid **166** were investigated by cyclic voltammetric analysis. Figure 3.12

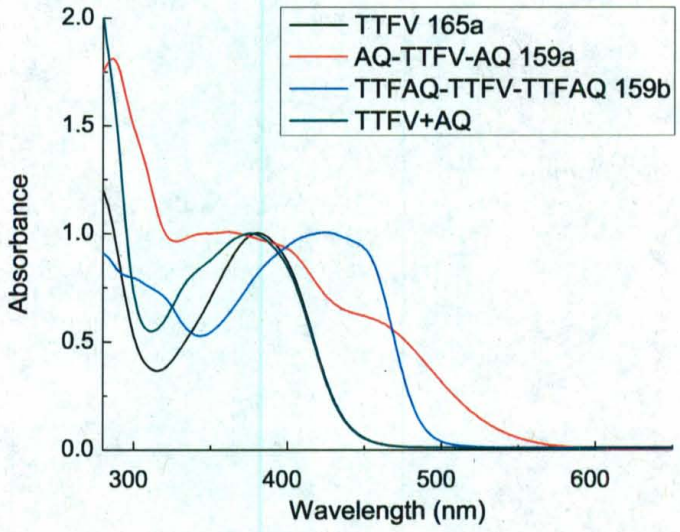

Figure 3.11: UV-Vis absorption spectra of TTFV tweezers **159a**,**b**, TTFV crown ether hybrid **166**, TTFV **165a**, and a mixture of **165a** and **172** (in 1:2 molar ratio). Spectra were measured in CH_2Cl_2.

shows the detailed cyclic voltammograms of these compounds, and for comparison purpose the CV profile of TTFV **165a** is also included in Figure 3.12.

From Figure 3.12A, it can be seen that TTFV **165a** gives a quasi-reversible redox couple at E_{pa} = +0.67 V and E_{pc} = +0.46 V, which are attributed to a simultaneous two-electron process. In the CV profile of AQ-TTFV-AQ **159a** (Figure 3.12B), the TTFV-originated redox wave pair is also reversible. With E_{pa} at a less positive potential of +0.61 V and E_{pc} at a more positive potential of +0.54 V, the peak separation of **159a** is much smaller than TTFV **165a**. The oxidation potential of **159a** is only slightly higher than that of TTFV **165a**, despite the electron-withdrawing nature of the AQ groups in conjugation with TTFV unit. This observation is consistent with those reported examples showing little or no change in the oxidation potentials of TTFV moieties regardless the nature of substituents on the aryl groups. In fact, it was considered as a merit allowing elaboration on the aryl moiety without affecting the redox behavior of the TTFV unit. In the negative potential window, two reversible redox wave pairs are observed, which are typical of the successive two-step reduction of anthraquinone and indicate no electronic communication between the two AQ groups. Of interest is the cyclic voltammogram of TTFAQ-TTFV-TTFAQ **159b** (Figure 3.12C). In the anodic scan, only one oxidation peak is observed at +0.68 V. The current intensity of this peak suggests it arise from simultaneous oxidation at the central TTFV and the two TTFAQ moieties with total 6 electrons. In the cathodic scan, however, two reduction peaks are seen at +0.55 V and +0.23 V respectively. The former is assigned to the reduction at the TTFV core (2 electrons), while the latter is due to the reduction of the two TTFAQ moieties (4 electrons). The assignment is supported by the current intensities of the two cathodic

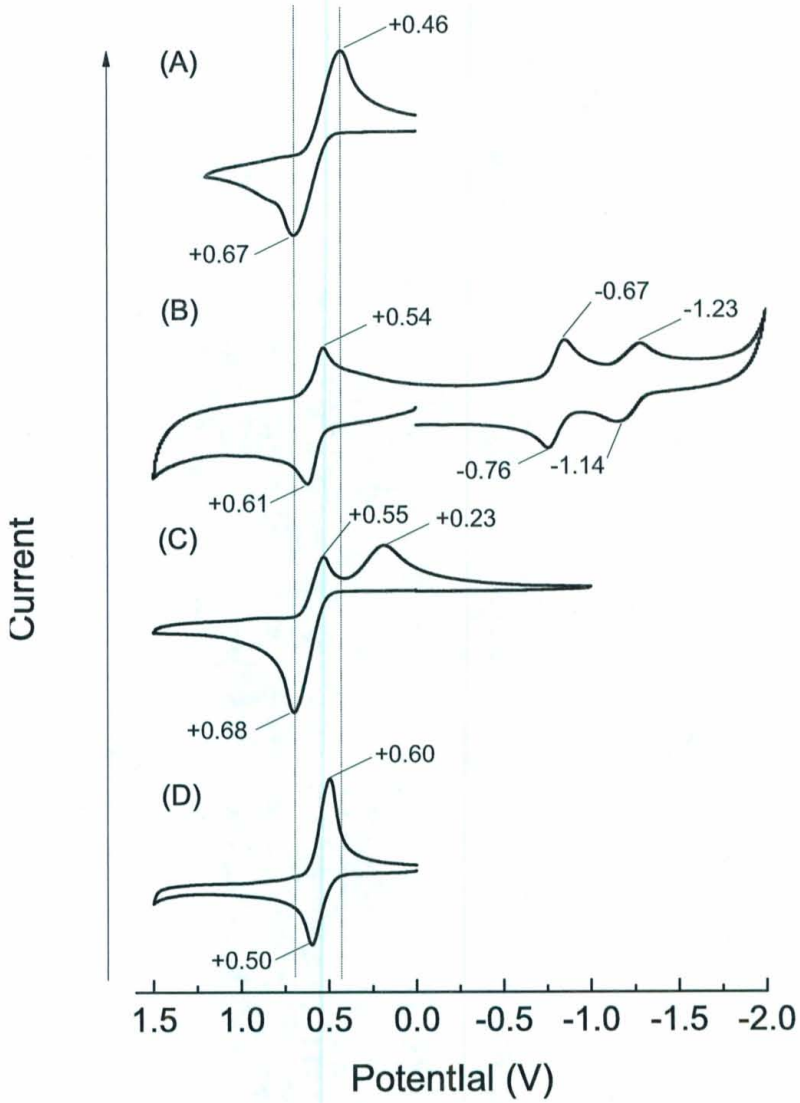

Figure 3.12: Cyclic voltammograms of (A) TTFV **165a**, (B) AQ-TTFV-AQ **159a**, (C) TTFAQ-TTFV-TTFAQ **159b**, and (D) TTFV crown ether **166**. Experimental conditions: analyte (ca. 10^{-3} M); Bu_4NBF_4 (0.1 M) as supporting electrolyte; CH_2Cl_2 as solvent; glassy carbon as working electrode; Pt wire as counter electrode; Ag/AgCl as reference; scan rate 0.1 V s^{-1}.

peaks. The CV patterns of **159b** indicate a significant degree of intramolecular electronic interaction between the TTFV and TTFAQ groups. Also, the large peak separation of the oxidation of TTFAQ indicates the process is accompanied by a dramatic conformational change. The redox behavior of crown ether hybrid **166** resembles that of **159a**, showing one reversible oxidation with E_{pa} at +0.60 V and E_{pc} at +0.50 V. With no increase in the oxidation potential, it is assumed that the crown ether chain is long enough to allow the TTFV unit to undergo conformational change upon oxidation.

3.2.2.6 Spectroelectrochemistry of TTFV Tweezers 159a,b

To gain a deeper insight into the redox process, UV-Vis spectroelectrochemical analyses were performed on TTFV tweezers **159a,b**. Detailed experimental results are given in Figure 3.13. For convenience of dicussion and comparison purposes, the spectroelectrochemistry data of **165a** is reiterated as follows. With increasing applied potential the absorption band of TTFV **165a** at 380 nm decreases, while a new long-wavelength absorption band emerges with a peak at 642 nm and a shoulder at 713 nm. The new bands are assigned to the characteristic absorption of dication $[TTFV]^{2+}$. In the spectroelectrochemical measurements of AQ-TTFV-AQ **159a**, a similar long-wavelength band is observed to grow with increasing applied potential, indicating the formation of $[TTFV]^{2+}$. The ICT band of **159a** at 380 nm steadily reduces as the oxidation of TTFV progresses, while the absorption due to AQ at ca. 360 nm remains unchanged. For TTFAQ-TTFV-TTFAQ **159b**, a broad band peaking at 650 nm grows with increasing applied potential. Concomitantly, the absorption band at 416 shows a significant decrease and a band at ca. 330 increases notably. According to the CV data, these spectral changes are attributed to the simultaneous formation of $[TTFV]^{2+}$ and $[TTFAQ]^{2+}$ in compound **160b**.

3.2.2.7 Preliminary Study on the Sensing Properties of TTFV Tweezers 159a,b and Crown Ether Hybrid 166

It was expected TTFV tweezers **159a,b** would show some binding affinity for C_{60} on the ground of two considerations. First, anthraquinone and TTFAQ have been known to bind with C_{60} through $\pi-$stacking forces. Second, *cis* TTFV should bring

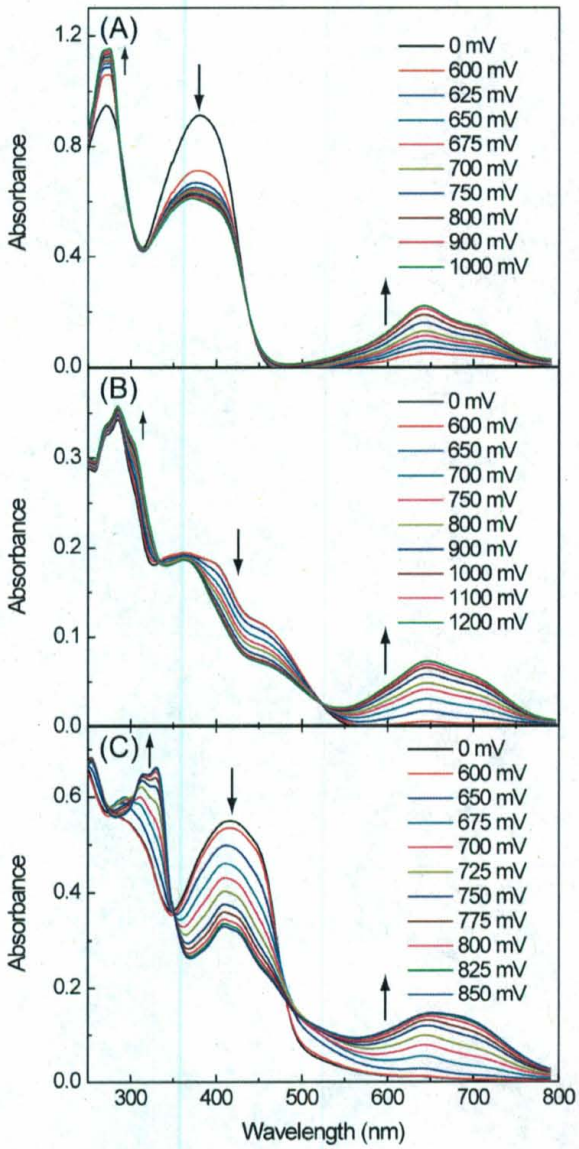

Figure 3.13: UV-Vis spectral changes with increasing applied potential steps during electrolysis. (A) TTFV **165a**. (B) AQ-TTFV-AQ **159a**. (C) TTFAQ-TTFV-TTFAQ **159b**. Experimental conditions: Bu_4NBF_4 (0.1 M) as supporting electrolyte; CH_2Cl_2 as solvent; Pt mesh as working electrode; Pt wire as counter electrode; Ag/AgCl as reference.

the appendant groups on both sides in a close proximity, which may facilitate the formation of a cavity favoring cooperative binding motifs. Experimentally, no change was observed in the UV-Vis absorption spectra and cyclic voltammograms upon titration of C_{60} into the solutions of **159a,b**. Various solvent systems have been tested, including toluene, benzene, *o*-dichlorobenzene, $CHCl_3$, and 1:1 $CHCl_3/CS_2$, and **159a,b** did not show binding to C_{60} in any of them. This result suggests that TTFV tweezers **159a,b** do not form binding cavity suitable for C_{60} as expected. The binding cavity might be either too small or too big, the latter being more likely, since it was reported that the bulkiness of aryl group could effect the twisting angle of the molecule. In addition, the rigid structure of alkynyl linkage could prevent the self-fitting of the tweezers to C_{60} host.

The UV-Vis absorption spectra of **159a,b** upon addition of different metal ions were also determined to test their potential as colorimetric chemosensors. It was found that Zn^{2+}, Pd^{2+}, Ag^{+} showed slight binding with both molecules, as evidenced by a slight decrease in the absorption of TTFV and a barely noticeable increase of absorption around 700 nm. The active binding sites are proposed to be the TTFV moiety due to the characteristic color change, which is similar to the oxidation of TTFV. In fact, TTFV **165a** showed, although to a small extent, color change towards green-yellowish upon addition of Zn^{2+} ions. It is proposed that the chromic effect come from the alteration of the twisting angle of the TTFV moiety in binding with metal ions. The colorimetric responses to metal ions become even more prominent in the case of TTFV crown ether hybrid **166**. After adding $ZnCl_2$ to the organic solution of **166**, a new layer was found to be immediately deposited on the surface of the insoluble inorganic salt and turned to blue color within seconds. In addition

to binding with transition metal ions, TTFV crown ether **166** can also bind with alkaline metal ions through its crown ether receptors. It was observed that **166** in contact with $MgSO_4$ formed a yellow colored complex.

3.2.2.8 Summary

Two TTFV based tweezers and a crown ether hybrid were successfully prepared. Sonogashira couplings and click reactions have been proven powerful in synthesizing such type of TTFV derivatives. The electronic properties and redox behaviors of these TTFV derivatives were studied by UV-Vis spectroscopic and voltammetric methods. The results suggest that the redox behavior of TTFV core is insensitive to appended side groups, and this behavior may be useful to the development of electrochemically actuated molecular switching devices. In addition, the side groups attached to the TTFV core may affect the orientation of the dithiole rings of TTFV, affording another means (input) to exert control over the switching of TTFV at the molecular level.

3.3 Experimental

General Procedures

Chemicals were purchased from commercial suppliers and used directly without purification. Et_3N was distilled from LiH prior to use in Sonogashira couplings. THF was distilled from benzophenone/Na before its use in HWE reactions. All reactions were conducted in standard and dry glassware unless otherwise noted. Evaporation and concentration were carried out with a water-aspirator. Flash column chromatography was performed using 240-400 mesh silica gel obtained from VWR

International. Thin-layer chromatography (TLC) was carried out with silica gel 60 F254 covered on plastic sheets and visualized by UV light. Melting points (m.p.) were measured with a Fisher-Jones melting point apparatus and are uncorrected. ^{1}H and ^{13}C NMR spectra were measured on a Bruker Avance 500 MHz spectrometer. Chemical shifts are reported in ppm downfield from the signal of the internal reference $SiMe_4$. Coupling constants (J) are given in Hz. Infrared spectra (IR) were recorded on a Bruker Tensor 27 spectrometer equipped with a ZnSe ATR module. Positive-mode high-resolution mass spectra (HRMS) were measured on a Waters GCT premier instrument equipped with an electron ionization (EI) ion source and a QSTAR XL hybrid quadrupole/TOF mass spectrometer equipped with an o-MALDI ion source (Applied Bio-systems). Single crystal X-ray diffraction data were collected on a Rigaku Saturn CCD area detector equipped with a SHINE optic with MoK_α radiation (λ = 0.71075 Å). UV-Vis absorption spectra were measured on a Cary 6000i spectrophotometer. Cyclic voltammetric analyses were carried out in a standard three-electrode setup controlled by a BASi epsilon workstation. Spectroelectrochemistry was investigated through the following protocol: In a 1 mm quartz cuvette were placed a Pt mesh as working electrode, and Ag/AgCl as reference electrode, and Pt wire as counter electrode. The applied potential (V) was increased in steps through controlled potential electrolysis (CPE). In each potential step, the electrolysis was first performed for ca. 1.5 min until the electrical current remained constant then a UV-Vis spectrum was then determined. Thermogravimetric analysis (TGA) was conducted on a TA Instruments Q500 thermogravimetric analyzer, and differential scanning calorimetric (DSC) analysis was performed on a Mettler Toledo DSC 1 instrument. All samples were placed under a nitrogen atmosphere during the

thermal analysis.

Diyne-exTTF 156a.

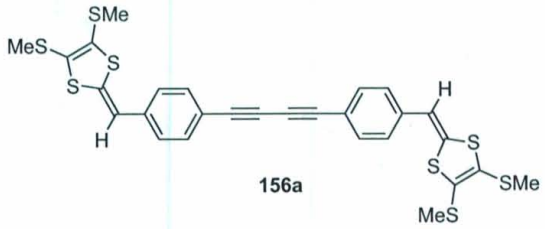

156a

To a solution of DTF **160a** (107 mg, 0.283 mmol) in THF/MeOH (1:1, 30 mL) was added K_2CO_3 (200 mg, 1.45 mmol). The mixture was stirred at rt for 30 min, and then diluted with CH_2Cl_2, washed with H_2O, dried over $MgSO_4$, and concentrated *in vacuo* to ca. 2 mL. The residue was redissolved in CH_2Cl_2 (30 mL) and to the resulting yellow solution was added a solution of CuI (200 mg, 1.05 mmol) and TMEDA (0.20 mL) in CH_2Cl_2 (3 mL). The mixture was stirred at rt under air for 3 h, then washed with H_2O, dried over $MgSO_4$, and concentrated *in vacuo*. The residue was subjected to silica flash column chromatography (10% CH_2Cl_2 in hexanes) to give diyne-exTTF **156a** (57 mg, 0.093 mmol, 66%) as a yellow solid. M.p. 170 °C (dec.); ^{1}H NMR (500 MHz, $CDCl_3$) δ 7.49 (d, J = 8.1 Hz, 4H), 7.16 (d, J = 8.4 Hz, 4H), 6.46 (s, 2H), 2.47 (s, 6H), 2.46 (s, 6H). The data are consistent with literature report.[156]

Tetrayne-exTTF 156b.

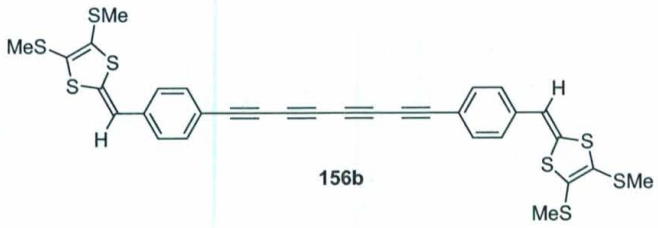

156b

To a solution of diyne-DTF **160b** (71 mg, 0.18 mmol) in THF/MeOH (1:1, 20 mL) was added K_2CO_3 (200 mg, 1.45 mmol). The mixture was stirred at rt for 30 min and then was diluted with Et_2O, washed with H_2O, and dried over $MgSO_4$. After vacuum evaporation, the residue was redissolved in CH_2Cl_2 (20 mL). To the solution was then added a solution of CuI (60 mg, 0.31 mmol) and TMEDA (0.10 mL) in CH_2Cl_2 (3 mL). The mixture was stirred at rt under air for 3 h. Then another portion of CH_2Cl_2 (130 mL) was added to dissolve all the solids formed during the reaction. The solution was washed with H_2O, dried over $MgSO_4$, and filtered through a short silica plug to afford pure tetrayne-exTTF **156b** (58 mg, 0.88 mmol, 100%) as a golden flake. M.p. 200 °C (dec); ^{1}H NMR (500 MHz, $CDCl_3$) δ 7.50 (d, J = 8.3 Hz, 4H), 7.15 (d, J = 8.3 Hz, 4H), 6.45 (s, 2H), 2.45 (s, 6H), 2.44 (s, 6H). The data are consistent with literature report.[156]

Poly(diyne-TTFV)s 158a.

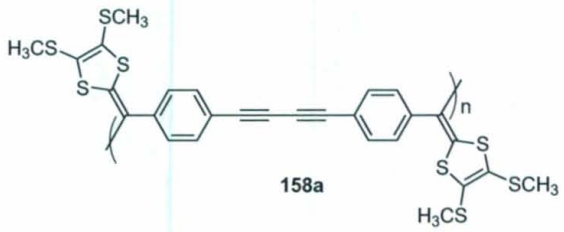

158a

To a solution of diyne exTTF **156a** (43 mg, 0.070 mmol) in CH_2Cl_2 (50 mL) was added I_2 (46 mg, 0.18 mmol). The mixture was stirred at rt overnight, resulting in a pale yellow solution with dark green precipitates. To this mixture was added satd $Na_2S_2O_3$ solution (aq. 20 mL), and the content was kept under stirring for 1 h. The resulting yellow organic layer was separated, washed with H_2O, and dried

over $MgSO_4$. Filtration followed by evaporation in vacuo afforded **158a** as a yellow solid (39 mg, crude yield 91%). HRMS (MALDI-TOF) *m/z* found 1225.9014 (n = 2), 1837.8391 (n = 3), 2450.7645 (n = 4), 3063.6956 (n = 5), 3681.4704 (n = 6), 4902.6271 (n = 8).

Poly(tetrayne-TTFV)s 158b.

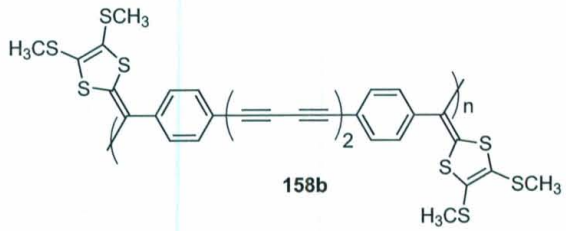

158b

To a solution of TTF tetrayne **156b** (26 mg, 0.040 mmol) in CH_2Cl_2 (40 mL) was add I_2 (30 mg, 0.12 mmol). The mixture was stirred at rt overnight, and then satd $Na_2S_2O_3$ solution was added. The mixture was stirred for another 1.5 h, and then washed with H_2O, dried over $MgSO_4$, and evaporated in vacuo to afford **158b** (24 mg, crude yield 80%). HRMS (MALDI-TOF) *m/z* found 1321.8988 (n = 2), 1983.8686 (n = 3), 2643.7519 (n = 4).

AQ-TTFV-AQ 159a.

To a solution of TTFV **165a** (43 mg, 0.057 mmol) in THF/MeOH (30 mL, 1:1) was added K_2CO_3. The mixture was stirred for 20 min. It was then diluted with CH_2Cl_2, washed with H_2O, dried over $MgSO_4$, and evaporated *in vacuo*. To the residue was added 2-iodoanthraquinone **172** (83 mg, 0.25 mmol) and Et_3N (50 mL). The mixture was purged with N_2 for 20 min. Then $PdCl_2(PPh_3)_2$ (14 mg, 0.020 mmol) and CuI (10 mg, 0.052 mmol) were added. The mixture was stirred overnight. During the

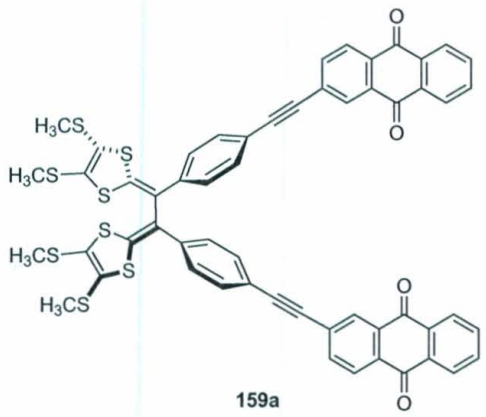

159a

reaction, red precipitate were formed. The mixture was filtered. The residue was washed with Et_3N, redissolved in CH_2Cl_2, washed with aq. NH_4Cl solution, H_2O, dried over $MgSO_4$, and purified with chromatography using CH_2Cl_2 as eluent to afford **159a** as a red solid (38 mg, 0.037 mmol, 66%). M.p. 290 °C; ^{1}H NMR (500 MHz, $CDCl_3$): δ = 8.42 (s, 2H), 8.34-8.30 (m, 4H), 8.29 (d, J = 8.1 Hz, 2H), 7.88 (dd, J = 8.1, 0.8 Hz, 2H), 7.83-7.78 (m, 4H), 7.53 (d, J = 8.5 Hz, 4H), 7.45 (d, J = 8.5 Hz, 4H),2.46 (s, 6H), 2.40 (s, 6H); ^{13}C NMR (125 MHz, $CDCl_3$): δ = 182.9, 182.7, 139.2, 137.7, 136.6, 134.5, 134.4, 133.8, 133.7, 133.6, 132.51, 132.46, 130.4, 129.9, 129.0, 127.6, 127.55, 127.52, 126.6, 125.6, 123.4, 120.4, 94.8, 89.1, 19.2, 19.1; FTIR (neat) 2919, 2854, 2209, 1672, 1588, 1516, 1477, 1323, 1282, 974, 929, 850 cm^{-1}; HRMS (MALDI-TOF) m/z calcd for $C_{56}H_{34}O_4S_8$ 1026.0223, found 1026.0163 $[M]^+$.

TTFAQ-TTFV-TTFAQ 159b

Method 1. To a solution of phosphonate **105a** (50 mg, 0.16 mmol) in dry THF (20 mL) cooled by a dry ice bath was added n-BuLi (0.10 mL, 0.25 mmol, 2.5 M in hexanes). The mixture was stirred for 20 min. Then a solution of AQ-TTFV-AQ **160a** (16 mg, 0.016 mmol) in dry THF (20 mL) was added. The mixture was allowed to warm to rt and stirred overnight. The resulting mixture was evaporated,

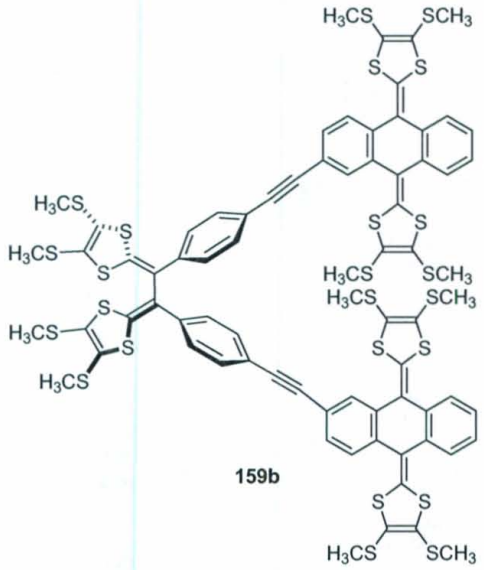

159b

diluted with CH_2Cl_2, washed with H_2O until the aqueous layer was clear colorless. The organic layer was dried over $MgSO_4$ and purified with chromatography using 70% CH_2Cl_2 in hexanes to afford **159b** as an orange solid (14 mg, 0.0081 mmol, 51%).

Method 2. To a solution of TTFV **165a** (11 mg, 0.015 mmol) in THF/MeOH (10 mL, 1:1) was added K_2CO_3. The mixture was stirred for 20 min. It was then diluted with CH_2Cl_2, washed with H_2O, dried over $MgSO_4$, and evaporated in vacuo. To the residue was added mono-iodinated TTFAQ **168** (21 mg, 0.030 mmol) and Et_3N (20 mL). The mixture was purged with N_2 for 10 min. Then $PdCl_2(PPh_3)_2$ (6 mg, 0.009 mmol) and CuI (6 mg, 0.032 mmol) were added. The mixture was heated to 60 °C and stirred overnight. During reaction, brown solid formed. The mixture was filtered. The residue was washed with Et_3N, redissolved in CH_2Cl_2, concentrated to ca. 4 mL, and precipitated with MeOH (4 mL). The precipitate was collected by filtration, washed with MeOH, dissolved in $CHCl_3$, filtered through a short silica plug to afford product **159b** as an orange solid (16 mg, 0.0093 mmol, 62%).

M.p. 230-231 °C; ^{1}H NMR (500 MHz, $CDCl_3$): δ = 7.66 (d, J = 1.5 Hz, 2H), 7.57-7.54 (m, 4H), 7.53 (d, J = 8.1 Hz, 2H), 7.50 (d, J = 8.4 Hz, 4H), 7.45-7.38 (m, 6H), 7.32 (dd, J = 5.6, 3.2 Hz, 4H), 2.46-2.43 (m, 6H) 2.42-2.37 (m 30H); ^{13}C NMR (125 MHz, $CDCl_3$): δ = 138.2, 137.0, 135.0, 134.69, 134.67, 133.0, 132.23, 132.22, 129.7, 129.1, 128.8, 128.4, 126.7, 126.6, 126.5, 126.43, 126.36, 126.2, 126.0, 125.7, 125.63, 125.57, 125.4, 123.8, 123.4, 123.0, 121.5, 121.4, 90.48, 90.45, 19.3, 19.2, 19.1; FTIR (neat) 2919, 2854, 1672, 1530, 1492, 1418, 1310, 1215, 964, 891, 837 cm^{-1}; HRMS (MALDI-TOF) m/z calcd for $C_{76}H_{58}S_{24}$ 1737.7836, found 1737.7771 $[M]^+$.

Alkyne-DTF 160a.

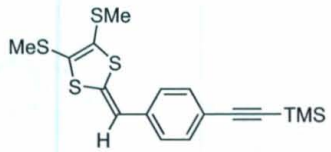

160a

To a solution of phosphonate **105a** (900 mg, 2.96 mmol) in THF (60 mL) cooled by a dry ice bath was added n-BuLi (1.50 mL, 2.5 M in THF, 3.8 mmol). The mixture was stirred for 20 min and then 4-(trimethylsilylethynyl)benzaldehyde **161** (530 mg, 2.62 mmol) in THF (20 mL) was added. The mixture was allowed to be slowly warmed up to rt and stirred overnight. The resulting dark brown yellow solution was diluted with Et_2O, washed with H_2O, and dried over $MgSO_4$. After concentration in vacuo, the residue was subjected to column chromatography (10% CH_2Cl_2 in hexanes) affording compound **160a** (800 mg, 2.12 mmol, 80%) as a light yellow liquid, which slowly solidified into a yellow solid in a fridge. M.p. 90-91 °C; ^{1}H NMR (500 MHz, $CDCl_3$) δ 7.43 (d, J = 8.3 Hz, 2H), 7.12 (d, J = 8.3 Hz, 2H), 6.44 (s, 1H), 2.44 (s,

3H), 2.43 (s, 3H), 0.25 (s, 9H). The data are consistent with literature report.[156]

Diyne-DTF 160b.

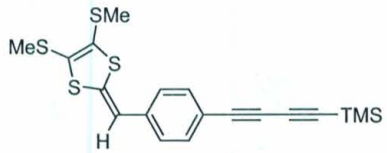

160b

To a solution of DTF **160a** (95 mg, 0.25 mmol) in THF/MeOH (1:1, 20 mL) was added K_2CO_3 (200 mg, 1.45 mmol). The mixture was stirred at rt for 30 min. Then the mixture was diluted with CH_2Cl_2, washed with H_2O, dried over $MgSO_4$, and concentrated in vacuo to ca. 1 mL. The residue was diluted with CH_2Cl_2 (20 mL), and to this solution was then added TMSA (0.50 mL, 3.4 mmol) and a solution of CuI (90 mg, 0.47 mmol) and TMEDA (0.10 mL) in CH_2Cl_2 (3 mL). The mixture was stirred at rt under air for 3 h. Then it was washed with H_2O, dried over $MgSO_4$, and purified with column chromatography with 10% CH_2Cl_2 in hexanes to give DTF **160b** (0.83 mg, 0.21 mmol, 82%) as a yellow solid. M.p. 85-86 °C; ^{1}H NMR ($CDCl_3$, 500 MHz) δ 7.45 (d, J = 8.4 Hz, 2H), 7.13 (d, J = 8.4 Hz, 2H), 6.43 (s, 1H), 2.43 (s, 3H), 2.42 (s, 3H), 0.23 (s, 9H). The data are consistent with literature report.[156]

Triyne-DFT 160c.

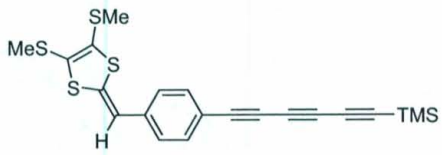

160c

To a solution of diyne-DTF **160b** (220 mg, 0.55 mmol) in THF/MeOH (1:1, 30

mL) was added K_2CO_3 (200 mg, 1.45 mmol). The mixture was stirred at rt for 20 min. Then the mixture was diluted with Et_2O, washed with H_2O, and dried over $MgSO_4$. After vacuum evaporation, the residue was redissolved in CH_2Cl_2 (20 mL). In the mean time, a solution of CuI (300 mg, 1.57 mmol) and TMEDA (0.30 mL) in CH_2Cl_2 (27 mL) was prepared. To this mixture was slowly added a pre-mixed solution of desilylated DTF diyne **160b** and TMSA (3.00 mL, 20.7 mmol) at rt under air over a period of 4 h. Then the reaction mixture was stirred for another 0.5 h, then washed with H_2O, dried over $MgSO_4$, and purified by column chromatography (10% CH_2Cl_2 in hexanes) to afford triyne-DTF **160c** (138 mg, 0.324 mmol, 59%) as a yellow solid. M.p. 117-118 °C; ^{1}H NMR (500 MHz, $CDCl_3$) δ 7.48 (d, J = 8.4 Hz, 2H), 7.14 (d, J = 8.4 Hz, 2H), 6.44 (s, 1H), 2.44 (s, 3H), 2.43 (s, 3H), 0.22 (s, 9H). The data are consistent with literature report.[156]

Macrocycle TTFV 163a.

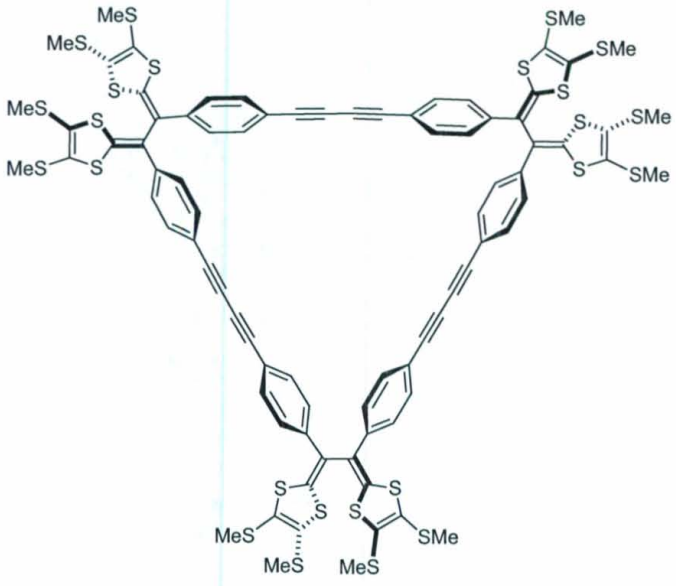

163a

To a solution of TTFV **165a** (64 mg, 0.085 mmol) in THF/MeOH (1:1, 30 mL) was added K_2CO_3 (300 mg, 2.17 mmol). The mixture was stirred at rt for 20 min, and then diluted with CH_2Cl_2, washed with H_2O, dried over $MgSO_4$, and concentrated in vacuo to ca. 2 mL. The residue was redissolved in CH_2Cl_2/acetone (1:1, 30 mL). To the resulting yellow solution was sequentially added a solution of CuI (60 mg, 0.31 mmol) and TMEDA (0.10 mL), and then $PdCl_2(PPh_3)_2$ (10 mg, 0.015 mmol) in CH_2Cl_2 (2 mL). The mixture was refluxed under air for 5 days, and then washed with H_2O, dried over $MgSO_4$, and concentrated in vacuo. The residue was dissolved in CS_2 (2 mL) and purified with flash column chromatography (40% CH_2Cl_2 in hexanes) to afford compound **163a** (9.0 mg, 0.0049 mmol, 18%) as a yellow solid. M.p. 210 °C (dec); IR (neat) 2921, 2253, 1522, 1430, 905, 730 cm^{-1}; ^1H NMR (500 MHz, $CDCl_3$) δ 7.34-7.28 (m, 24H), 2.45 (s, 18H), 2.43 (s, 18H); ^{13}C NMR (125 MHz, $CDCl_3$) δ 138.1, 133.0, 128.4, 126.7, 125.6, 123.8, 120.2, 82.8, 75.3, 19.1 (only one alkenyl signal and one SCH_3 signal were observed due to overlap); HRMS (MALDI-TOF) m/z calcd for $C_{84}H_{60}S_{24}$ 1835.7992, found 1835.8222 $[M]^+$.

Macrocycle 163b.

To a solution of TTFV **165b** (31 mg, 0.039 mmol) in THF/MeOH (1:1, 20 mL) was added K_2CO_3 (200 mg, 1.45 mmol). The mixture was stirred at rt for 20 min, and then diluted with CH_2Cl_2 (20 mL), washed with H_2O, dried over $MgSO_4$, and concentrated in vacuo to ca. 3 mL. The residue was redissolved in CH_2Cl_2/acetone (1:1, 40 mL), and to the resulting solution was added a solution of CuI (60 mg, 0.31 mmol) and TMEDA (0.10 mL) in CH_2Cl_2 (3 mL). Then $PdCl_2(PPh_3)_2$ (10 mg, 0.15 mmol) was added. The mixture was refluxed under air for 5 days. The mixture was diluted with CH_2Cl_2, washed with satd NH_4Cl (aq) and H_2O sequentially, and then

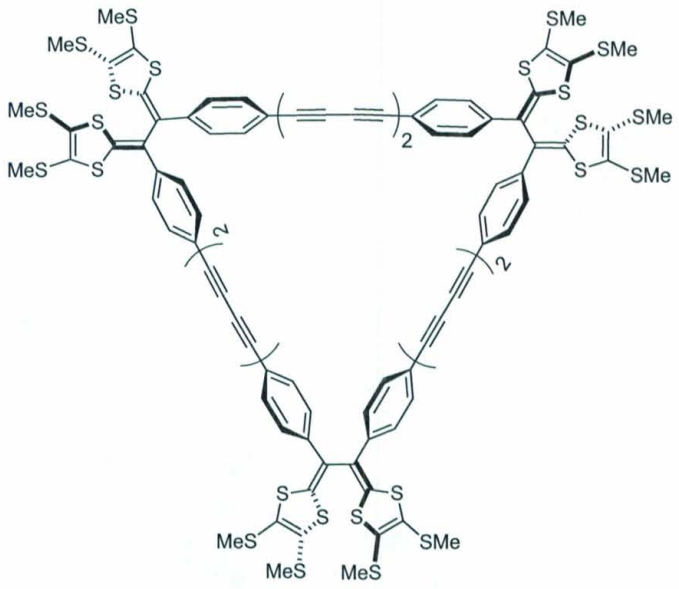

163b

dried over $MgSO_4$. After vacuum evaporation, the residue was subjected to silica flash column chromatography (35% CH_2Cl_2 in hexanes) to afford crude product of **163b**. The presence of some inextricable oligomer byproducts thwarted its complete purification.

TTFV 165a.

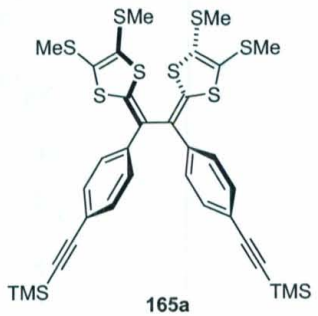

165a

To a solution of DTF **160a** (107 mg, 0.283 mmol) in CH_2Cl_2 (20 mL) was added I_2 (260 mg, 1.02 mmol). The resulting black greenish mixture, after being stirred at

rt overnight, was quenched with $Na_2S_2O_3$ solution (20 mL, aq., satd.). The content was kept under stirring for another 1 h, then the yellow organic layer was separated, washed with H_2O, dried over $MgSO_4$, and concentrated in vacuo. The residue was dissolved in CS_2 (2 mL) and then subjected to flash column chromatography (15% CH_2Cl_2 in hexanes) to give compound **165a** (64 mg, 0.085 mmol, 60%) as a yellow liquid, which solidified into a yellow solid in fridge. M.p. 180-181 °C; IR (neat) 2919, 2849, 2153, 1523, 1425, 1247, 839, 861 cm^{-1}; ^1H NMR (500 MHz, $CDCl_3$) δ 7.38 (d, J = 8.4 Hz, 4H), 7.30 (d, J = 8.4 Hz, 4H), 2.42 (s, 6H), 2.37 (s, 6H), 0.23 (s, 18H); ^{13}C NMR (125 MHz, $CDCl_3$) δ 138.0, 137.2, 132.5, 128.7, 126.5, 125.4, 123.8, 121.4, 105.3, 95.2, 19.13, 19.07, 0.2; HRMS (MALDI-TOF) m/z calcd for $C_{34}H_{38}S_8Si_2$ 758.0278, found 758.0272 $[M]^+$.

TTFV 165b.

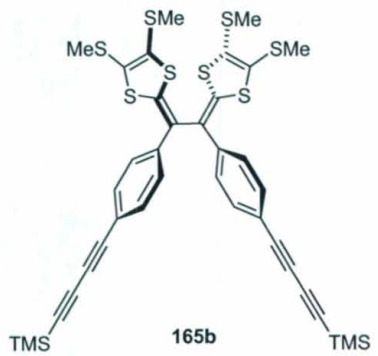

165b

To a solution of diyne-DTF **160b** (56 mg, 0.14 mmol) in CH_2Cl_2 (30 mL) was added I_2 (137 mg, 0.54 mmol). The mixture was stirred at rt under air overnight, then a $Na_2S_2O_3$ solution (20 mL, aq., satd.) was added. The mixture was stirred for another 1 h. The organic layer was separated, washed with H_2O, dried over $MgSO_4$, and concentrated in vacuo. The residue was subjected to silica column

chromatography (20% CH_2Cl_2 in hexanes) to afford compound **165b** as a yellow solid (32 mg, 0.040 mmol, 60%). M.p. 125-127 °C; IR (KBr): 2959, 2921, 2200, 2101, 1596, 1520, 1503 cm^{-1}; ^1H NMR (500 MHz, $CDCl_3$) δ 7.41 (d, J = 8.2 Hz, 4H), 7.32 (d, J = 8.2 Hz, 4H), 2.43 (s, 6H), 2.38 (s, 6H), 0.23 (s, 18H); ^{13}C NMR (125 MHz, $CDCl_3$) δ 139.5, 137.7, 133.2, 129.1, 126.4, 125.5, 123.1, 119.4, 99.8, 91.3, 88.2, 75.0, 19.16, 19.05, -0.2; HRMS (MALDI-TOF) m/z calcd for $C_{38}H_{38}S_8Si_2$ for 806.0278, found 806.0280 $[M]^+$.

TTFV Crown ether 166.

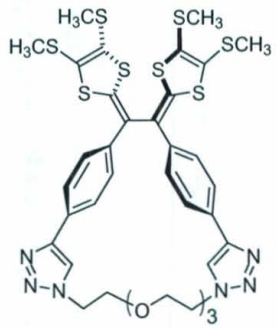

166

To a solution of TTFV **165a** (27.4 mg, 0.036 mmol) in THF/MeOH (1:1, 30 mL) was added K_2CO_3 (100 mg, 0.73 mmol). The mixture was stirred at rt for 20 min, and then diluted with CH_2Cl_2, washed with H_2O, dried over $MgSO_4$, and concentrated in vacuo to ca. 2 mL. The residue was redissolved in DMF (10 mL) and purged with N_2 for 10 min. To the yellow solution was sequentially added $CuSO_45H_2O$ (18 mg, 0.072 mmol), a solution of azide **171** (7.4 mg, 0.030 mmol) in DMF (1 mL), and sodium ascorbate (26 mg, 0.13 mmol). The mixture was heated to 50 °C and stirred overnight. The mixture was then filtered. The filtrate was diluted with CH_2Cl_2 (5

mL), washed with H_2O (50 mL $\times$5), and brine (10 mL). To the organic portion was added MeOH (25 mL). The resulting sticky film deposited on the bottom of glassware was washed with MeOH, redissolved in $CHCl_3$, and concentrated in vacuo to yield pure product **166** (19 mg, 0.022 mmol, 73%) as a yellow oil. ^{1}H NMR (500 MHz, $CDCl_3$) δ 7.85 (s, 2H), 7.74 (d, J = 8.4 Hz, 4H), 7.48 (d, J = 8.3 Hz, 4H), 4.44-4.29 (m, 4H), 3.73-3.66 (m, 4H), 3.51-3.42 (m, 8H), 2.44-2.36 (m, 12H); ^{13}C NMR (125 MHz, $CDCl_3$) δ 147.3, 136.9, 136.8, 129.3, 128.4, 127.2, 126.1, 125.3, 124.2, 121.2, 70.6, 70.5, 69.5, 50.4, 19.2, 19.1; HRMS (MALDI-TOF) m/z calcd for $C_{35}H_{36}N_6O_3S_8$ for 844.0615, found 844.0619 $[M]^+$.

Mono-iodinated TTFAQ 168, byproducts 169 and 170.

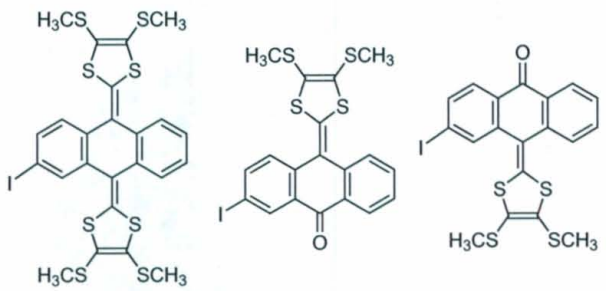

A solution of thione **104a** (71 mg, 0.314 mmol) and 2-iodoanthraquinone **167** (105 mg, 0.314 mmol) in toluene (10 mL) was purged with N_2 for 5 min. $P(OEt)_3$ was added. The mixture was stirred for 1 h. Then thione **104a** (70 mg, 0.310 mmol) was added. The mixture was stirred for 1.5 h. It was directly loaded on a silica column (30 cm), and developed with CH_2Cl_2 to afford pure **168** as a yellow solid (58 mg, 0.084 mmol, 27%) and a fraction of solution containing **168**, **189** and **170**. The fraction was evaporated and then subjected to chromatography using 80% CH_2Cl_2 in

hexanes as eluent to afford **168** as a yellow solid (36 mg, 0.052 mmol, 17%),**169** as a red solid (9 mg, 0.02 mmol, 6%), and **170** as a red solid (36 mg, 0.070 mmol, 22%).

168. M.p. 190 °C (dec); FTIR (neat) 2991, 2919, 2853, 1670, 1574, 1495, 1453, 1423, 1312, 1268, 1215, 968, 889, 821 cm^{-1}; ^{1}H NMR (500 MHz, $CDCl_3$): δ = 7.84 (d, J = 1.6 Hz, 1H), 7.61 (dd, J = 8.1, 1.5 Hz, 1H), 7.55-7.51 (m, 2H), 7.31 (dd, J = 5.7, 3.2 Hz 2H), 7.28 (d, J = 8.2 Hz, 1H), 2.43-2.37 (m, 12H); ^{13}C NMR (125 MHz, $CDCl_3$): δ = 136.8, 135.2, 134.55, 134.45, 134.3, 134.1, 132.8, 132.0, 127.7, 127.1, 126.7, 126.5, 126.1, 125.9, 125.7, 125.6, 122.9, 122.2, 111.2, 91.4, 19.4, 19.32, 19.31, 19.30; HRMS (MALDI-TOF) m/z calcd for $C_{24}H_{19}IS_8$ 689.8297, found 689.8253 $[M]^+$.

169. M.p. 224-225 °C; FTIR (neat) 3062, 2920, 2852, 1650, 1595, 1481, 1463, 1397, 1261, 1164, 966, 827, 821 cm^{-1}; ^{1}H NMR (500 MHz, $CDCl_3$): δ = 8.59 (d, J = 1.9 Hz, 1H), 8.26 (dd, J = 7.8, 1.0 Hz, 1H), 7.94 (dd, J = 8.3, 2.0 Hz, 1H), 7.77 (d, J = 7.9 Hz 1H), 7.67 (td, J = 7.6, 1.4 Hz 1H), 7.54 (d, J = 8.3 Hz, 1H), 7.45 (td, J = 7.8, 0.9 Hz 1H), 2.43 (s, 3H), 2.42 (s, 3H); ^{13}C NMR (125 MHz, $CDCl_3$): δ = 182.3, 141.6, 140.5, 138.6, 138.0, 136.3, 132.4, 132.2, 130.5, 128.1, 127.6, 127.43, 127.37, 127.2, 126.4, 118.6, 91.8, 19.55, 19.54; HRMS (MALDI-TOF) m/z calcd for $C_{19}H_{13}IOS_4$ 511.8894, found 511.8867 $[M]^+$.

170. M.p. 210-212°C; FTIR (neat) 3062, 2994, 2918, 1648, 1540, 1481, 1426, 1294, 1261, 1179, 1099, 967, 931, 840 cm^{-1};^{1}H NMR (500 MHz, $CDCl_3$): δ = 8.24 (dd, J = 7.8, 1.0 Hz, 1H), 8.11 (d, J = 1.4 Hz, 1H), 7.94 (d, J = 8.2 Hz, 1H), 7.78 (dd, J = 8.2, 1.5 Hz, 1H), 7.74 (dd, J = 7.9, 0.5 Hz 1H), 7.66 (td, J = 7.6, 1.5 Hz 1H), 7.45 (td, J = 7.8, 1.0 Hz 1H), 2.44(s, 3H), 2.42 (s, 3H); ^{13}C NMR (125 MHz, $CDCl_3$): δ = 183.1, 142.1, 140.0, 138.5, 135.9, 135.1, 132.3, 130.6, 130.0, 128.8, 127.6, 127.5, 127.21, 127.19, 126.4, 117.9, 100.2, 19.6, 19.5; HRMS (MALDI-TOF) m/z calcd for

$C_{19}H_{13}IOS_4$ 511.8894, found 511.8865 $[M]^+$.

Azide 171.

171

To a solution of **145** (1.238 g, 3.98 mmol) in DMF (20 mL) was added NaN_3 (1.030 g, 15.9 mmol) and TBABr (60 mg). The mixture was heated to 80 °C and stirred overnight. Et_2O was added. The mixture was filtered and the filtrate was diluted with EtOAC, washed thoroughly with H_2O, dried over $MgSO_4$, and concentrated to azide **171** (685 mg, 3.17 mmol, 80%) as a yellow liquid. ^1H NMR (500 MHz, $CDCl_3$): δ = 3.71-3.65 (m, 12H), 3.41-3.37 (m, 4H). The data are consistent with literature report.[161]

Chapter 4

Conclusions and Future Work

This thesis work aims at the development of new exTTFs with acetylenic conjugated structures. The synthetic methodologies are expected to benefit relevant research on the structural tailoring of TTF. The property studies of target molecules may help for a better understanding of structure-property relationships as well as further designs of exTTFs to meet the different needs of various device applications.

In the first project, two types of macrocyclic acetylenic TTFAQ analogues were successfully synthesized. A one-pot, 4-fold Sonogashira coupling strategy has been proven to be efficient in the construction of shape-persistent macrocyclic enyne core. Although the methodology failed with heavily substituted precursors, more complex acetylenic TTFAQ analogues could possibly be derived from simple TTFAQ analogues, similar to the functionalization of TTFAQs. Both types of TTFAQ analogues have very different molecular conformations and solid-state ordering. The second type of TTFAQ analogues adopts a planar conformation owing to the absence of steric hindrance in the structure. Its columnar $\pi-$stacking may render it useful for

the research on organic conductors/semiconductors. Regarding the electron-donating ability, extension of conjugated structures has opposite effects on both types of TTFAQ analogues. For the stabilization of TTF dications, it is crucial that the conjugated systems achieve planar conformation upon oxidaiton, such as those in the second type of TTFAQ analogues.

In the second project, acetylenic TTFV derivatives, oligoyne-TTFs, were synthesized. The high efficiency of Hay coupling in the preparation of oligoyne systems was demonstrated. Also, TTFV oligomers/polymers and macrocyclic TTFVs were selectively formed by different synthetic routes, taking advantage of the *cis* to *trans* conformational change of TTFV moiety upon oxidation. Oligoyne-TTFs show solid-state reactivity upon heating. More interestingly, they undergo electropolymerization to form thin films which display electrochromic behavior. Thus, it is expected these compounds may find applications in related areas. Acetylenic TTFV derivatives show reversible oxidations with substantial conformational changes. In addition, the acetylenic groups on aryl rings are suitable for further elaborations. Thus, acetylenic TTFVs may be useful building blocks for the construction of molecular redox switches, or other complex macromolecular systems. Following this idea, a side project was started. A series of TTFV tweezers and a TTFV-crown ether hybrid were synthesized by Sonogashira coupling and click reactions. The reaction conditions can be applicable for subsequent preparation of TTFV derivatives. The preliminary results of spectroscopic responses to metal ion complexation show promising aspects for the further design of synthetic receptors and chemosensors.

Bibliography

[1] Frei, M.; Diederich, F.; Tremont, R.; Rodriguez, T.; Echegoyen, L. *Helv. Chim. Acta* **2006**, *89*, 2040–2057.

[2] Dumur, F.; Gautier, N.; Gallego-Planas, N.; Sahin, Y.; Levillain, E.; Mercier, N.; Hudhomme, P.; Masino, M.; Girlando, A.; Lloveras, V.; Vidal-Gancedo, J.; Veciana, J.; Rovira, C. *J. Org. Chem.* **2004**, *69*, 2164–2177.

[3] Siqot, Y.; Frere, P.; Nozdryn, T.; Cousseau, J.; Salle, M.; Jubault, M.; Orduna, J.; Garin, J.; Gorgues, A. *Tetrahedron Lett.* **1997**, *38*, 1919–1922.

[4] Jeppesen, J. O.; Takimiya, K.; Jensen, F.; Brimert, T.; Nielsen, K.; Thorup, N.; Becher, J. *J. Org. Chem.* **2000**, *65*, 5794–5805.

[5] Crivillers, N.; Oxtoby, N. S.; Mas-Torrent, M.; Veciana, J.; Rovira, C. *Synthesis* **2007**, 1621.

[6] Ketcham, R.; Hoernfeldt, A. B.; Gronowitz, S. *J. Org. Chem.* **1984**, *49*, 1117–1119.

[7] Sugimoto, T.; Awaji, H.; Sugimoto, I.; Misaki, Y.; Kawase, T.; Yoneda, S.; Yoshida, Z.; Kobayashi, T.; Anzai, H. *Chem. Mater.* **1989**, *1*, 535–547.

[8] Nielsen, M. B.; Utesch, N. F.; Moonen, N. N. P.; Boudon, C.; Gisselbrecht, J.-P.; Concilio, S.; Piotto, S. P.; Seiler, P.; Gunter, P.; Gross, M.; Diederich, F. *Chem. Eur. J.* **2002**, *8*, 3601–3613.

[9] Yamashita, Y.; Kobayashi, Y.; Miyashi, T. *Angew. Chem. Int. Ed. Engl.* **1989**, *28*, 1052–1053.

[10] Hansen, T. K.; Lakshmikantham, M. V.; Cava, M. P.; Niziurski-Mann, R. E.; Jensen, F.; Becher, J. *J. Am. Chem. Soc.* **1992**, *114*, 5035–5039.

[11] Fraser, A. T.; Clegg, W.; Hursthouse, M. B.; Karaulov, A. I. *Angew. Chem. Int. Ed. Engl.* **1990**, *29*, 1450–1452.

[12] Roncali, J. *J. Mater. Chem.* **1997**, *7*, 2307–2321.

[13] Wudl, F.; Wobschall, D.; Hufnagel, E. J. *J. Am. Chem. Soc.* **1972**, *94*, 670–672.

[14] Jerome, D. *Chem. Rev.* **2004**, *104*, 5565–5592.

[15] Bryce, M. R. *Adv. Mater.* **1999**, *11*, 11–23.

[16] Jerome, D. *Solid State Sciences* **2008**, *10*, 1692–1700.

[17] Williams, J. M.; Kini, A. M.; Wang, H. H.; Carlson, K. D.; Geiser, U.; Montgomery, L. K.; Pyrka, G. J.; Watkins, D. M.; Kommers, J. M. *Inorg. Chem.* **1990**, *29*, 3272–3274.

[18] Murata, T.; Morita, Y.; Yakiyama, Y.; Fukui, K.; Yamochi, H.; Saito, G.; Nakasuji, K. *J. Am. Chem. Soc.* **2007**, *129*, 10837–10846.

[19] Kobayashi, Y.; Yoshioka, M.; Saigo, K.; Hashizume, D.; Ogura, T. *J. Am. Chem. Soc.* **2009**, *131*, 9995–10002.

[20] Liu, H.; Li, J.; Lao, C.; Huang, C.; Li, Y.; Wang, Z. L.; Zhu, D. *Nanotechnol.* **2007**, *18*, 495704.

[21] Savy, J.-P.; de Caro, D.; Valade, L.; Legros, J.-P.; Auban-Senzier, P.; Pasquier, C. R.; Fraxedas, J.; Senocq, F. *EPL* **2007**, *78*, 37005.

[22] de Caro, D.; Malfant, I.; Savy, J.-P.; Valade, L. *J. Phys.: Condens. Matter.* **2008**, *20*, 184012.

[23] Tanaka, K.; Kunita, T.; Ishiguro, F.; Naka, K.; Chujo, Y. *Langmuir* **2009**, *25*, 6929–6933.

[24] Puigmarti-Luis, J.; Laukhin, V.; Perez del Pino, A.; Vidal-Gancedo, J.; Rovira, C.; Laukhina, E.; Amabilino, D. *Angew. Chem. Int. Ed.* **2007**, *46*, 238–241.

[25] Hou, Y.; Yang, M.; Wan, X.; Mao, J.; Ma, Y.; Huang, Y.; Chen, Y. *Macromol. Chem. Phys.* **2009**, *210*, 1044–1051.

[26] Liu, Y.; Wang, C.; Li, M.; Lai, G.; Shen, Y. *Macromolecules* **2008**, *41*, 2045–2048.

[27] Hou, Y.; Wan, X.; Yang, M.; Ma, Y.; Huang, Y.; Chen, Y. *Macromol. Rapid Commun.* **2008**, *29*, 719–723.

[28] Liu, Y.; Wang, C.; Li, M.; Lai, G.; Shen, Y. *New J. Chem.* **2008**, *32*, 505–510.

[29] Geng, Y.; Wang, X.-J.; Chen, B.; Xue, H.; Zhao, Y.-P.; Lee, S.; Tung, C.-H.; Wu, L.-Z. *Chem. Eur. J.* **2009**, *15*, 5124–5129.

[30] Torrance, J. B. *Acc. Chem. Res.* **1979**, *12*, 79–86.

[31] Rovira, C. *Chem. Rev.* **2004**, *104*, 5289–5318.

[32] Gao, X.; Wu, W.; Liu, Y.; Jiao, S.; Qiu, W.; Yu, G.; Wang, L.; Zhu, D. *J. Mater. Chem.* **2007**, *17*, 736–743.

[33] Aleveque, O.; Frere, P.; Leriche, P.; Breton, T.; Cravino, A.; Roncali, J. *J. Mater. Chem.* **2009**, *19*, 3648–3651.

[34] Noda, B.; Wada, H.; Shibata, K.; Yoshino, T.; Katsuhara, M.; Aoyagi, I.; Mori, T.; Taguchi, T.; Kambayashi, T.; Ishikawa, K.; Takezoe, H. *Nanotechnol.* **2007**, *18*, 424009.

[35] Shibata, K.; Wada, H.; Ishikawa, K.; Takezoe, H.; Mori, T. *Appl. Phys. Lett.* **2007**, *90*, 193509.

[36] Xian, X.; Yan, K.; Zhou, W.; Jiao, L.; Wu, Z.; Liu, Z. *Nanotechnol.* **2009**, *20*, 505204.

[37] Martin, N.; Sanchez, L.; Herranz, M. A.; Illescas, B.; Guldi, D. M. *Acc. Chem. Res.* **2007**, *40*, 1015–1024.

[38] Oswald, F.; Chopin, S.; de la Cruz, P.; Orduna, J.; Garin, J.; Sandanayaka, A. S. D.; Araki, Y.; Ito, O.; Delgado, J. L.; Cousseau, J.; Langa, F. *New J. Chem.* **2007**, *31*, 230–236.

[39] Hou, Y.; Chen, Y.; Liu, Q.; Yang, M.; Wan, X.; Yin, S.; Yu, A. *Macromolecules* **2008**, *41*, 3114–3119.

[40] Pauliukaite, R.; Malinauskas, A.; Zhylyak, G.; Spichiger-Keller, U. *Electroanal.* **2007**, *19*, 2491–2498.

[41] Cao, Z.; Jiang, X.; Xie, Q.; Yao, S. *Biosen. Bioelectronics* **2008**, *24*, 222 – 227.

[42] Cano, M.; Palenzuela, B.; Avila, J. L.; Rodriguez-Amaro, R. *Electroanal.* **2007**, *19*, 973–977.

[43] Cano, M.; Avila, J. L.; Mayen, M.; Mena, M.; Pingarron, J.; Rodriguez-Amaro, R. *J. Electroanal. Chem.* **2008**, *615*, 69–74.

[44] Liao, J.-Y.; Ho, K.-C. *Sen. Actuat. B: Chem.* **2008**, *130*, 343–350.

[45] Balandier, J.-Y.; Belyasmine, A.; Salle, M. *Eur. J. Org. Chem.* **2008**, 269–276.

[46] Li, J.; Zhang, G.; Zhang, D.; Zheng, R.; Shi, Q.; Zhu, D. *J. Org. Chem.* **2010**, *75*, 5330–5333.

[47] Zhao, Y.-P.; Wang, X.-J.; Wang, J.-J.; Si, G.; Liu, Y.; Tung, C.-H.; Wu, L.-Z. *New J. Chem.* **2009**, *33*, 813–817.

[48] Zhao, B.-T.; Blesa, M.-J.; Derf, F. L.; Canevet, D.; Benhaoua, C.; Mazari, M.; Allain, M.; Salle, M. *Tetrahedron* **2007**, *63*, 10768–10777.

[49] Park, J. S.; Le Derf, F.; Bejger, C. M.; Lynch, V. M.; Sessler, J. L.; Nielsen, K. A.; Johnsen, C.; Jeppesen, J. O. *Chem. Eur. J.* **2010**, *16*, 848–854.

[50] Song, M.; Wang, X.; Liu, W.; Zuo, J. *J. Coll. Interf. Sci.* **2010**, *343*, 48–51.

[51] Canevet, D.; Salle, M.; Zhang, G.; Zhang, D.; Zhu, D. *Chem. Commun.* **2009**, 2245–2269.

[52] Zhang, Y.; Cai, L.-Z.; Wang, C.-Y.; Lai, G.-Q.; Shen, Y.-J. *New J. Chem.* **2008**, *32*, 1968–1973.

[53] Zhang, X.; Wang, C.; Lai, G.; Zhang, L.; Shen, Y. *New J. Chem.* **2010**, *34*, 318–324.

[54] Nielsen, K. A.; Levillain, E.; Lynch, V. M.; Sessler, J. L.; Jeppesen, J. O. *Chem. Eur. J.* **2009**, *15*, 506–516.

[55] Ashton, P. R.; Balzani, V.; Becher, J.; Credi, A.; Fyfe, M. C. T.; Mattersteig, G.; Menzer, S.; Nielsen, M. B.; Raymo, F. M.; Stoddart, J. F.; Venturi, M.; Williams, D. J. *J. Am. Chem. Soc.* **1999**, *121*, 3951–3957.

[56] Aprahamian, I.; Dichtel, W. R.; Ikeda, T.; Heath, J. R.; Stoddart, J. F. *Org. Lett.* **2007**, *9*, 1287–1290.

[57] Nygaard, S.; Leung, K. C.-F.; Aprahamian, I.; Ikeda, T.; Saha, S.; Laursen, B. W.; Kim, S.-Y.; Hansen, S. W.; Stein, P. C.; Flood, A. H.; Stoddart, J. F.; Jeppesen, J. O. *J. Am. Chem. Soc.* **2007**, *129*, 960–970.

[58] Zhao, Y.-L.; Dichtel, W. R.; Trabolsi, A.; Saha, S.; Aprahamian, I.; Stoddart, J. F. *J. Am. Chem. Soc.* **2008**, *130*, 11294–11296.

[59] Aprahamian, I.; Olsen, J.-C.; Trabolsi, A.; Stoddart, J. F. *Chem. Eur. J.* **2008**, *14*, 3889–3895.

[60] Nygaard, S.; Hansen, S. W.; Huffman, J. C.; Jensen, F.; Flood, A. H.; Jeppesen, J. O. *J. Am. Chem. Soc.* **2007**, *129*, 7354–7363.

[61] Tomcsi, M. R.; Stoddart, J. F. *J. Org. Chem.* **2007**, *72*, 9335–9338.

[62] Saha, S.; Flood, A. H.; Stoddart, J. F.; Impellizzeri, S.; Silvi, S.; Venturi, M.; Credi, A. *J. Am. Chem. Soc.* **2007**, *129*, 12159–12171.

[63] Guo, X.; Zhou, Y.; Feng, M.; Xu, Y.; Zhang, D.; Gao, H.; Fan, Q.; Zhu, D. *Adv. Funct. Mater.* **2007**, *17*, 763–769.

[64] Enoki, T.; Miyazaki, A. *Chem. Rev.* **2004**, *104*, 5449–5478.

[65] Day, P.; Kurmoo, M. *J. Mater. Chem.* **1997**, *7*, 1291–1295.

[66] Gonzalez, M.; Segura, J. L.; Seoane, C.; Martin, N.; Garin, J.; Orduna, J.; Alcala, R.; Villacampa, B.; Hernandez, V.; Lopez Navarrete, J. T. *J. Org. Chem.* **2001**, *66*, 8872–8882.

[67] Liu, C.-G.; Guan, W.; Song, P.; Yan, L.-K.; Su, Z.-M. *Inorg. Chem.* **2009**, *48*, 6548–6554.

[68] Wang, L.; Park, S.-J.; Lee, S.-H.; Kim, Y.-J.; Kook, Y.-B.; Kuo, S.-W.; Van Horn, R. M.; Cheng, S. Z. D.; Lee, M.-H.; Jeong, K.-U. *Chem. Mater.* **2009**, *21*, 3838–3847.

[69] Wang, L.; Jeong, K.-U.; Lee, M.-H. *J. Mater. Chem.* **2008**, *18*, 2657–2659.

[70] Chahma, M.; Hassan, N.; Alberola, A.; Stoeckli-Evans, H.; Pilkington, M. *Inorg. Chem.* **2007**, *46*, 3807–3809.

[71] Balandier, J.-Y.; Chas, M.; Dron, P. I.; Goeb, S.; Canevet, D.; Belyasmine, A.; Allain, M.; Salle, M. *J. Org. Chem.* **2010**, *75*, 1589–1599.

[72] Zheng, P.; Guo, Y.-J.; Liu, W.; Li, Y.-Z.; Zuo, J.-L.; You, X.-Z. *Trans. Met. Chem.* **2008**, *33*, 767–773.

[73] Asakawa, D.; Chen, L. C.; Hiraoka, K. *J. Mass Spectrom.* **2008**, *43*, 1494–1501.

[74] Hudhomme, P.; Salle, M.; Gautier, N.; Belyasmine, A.; Gorgues, A. *ARKIVOC* **2006**, *iv*, 49–72.

[75] Zayed, S. E.; Hason, M. E. D.; Ragab, R. *Phosphorus, Sulfur, and Silicon* **2007**, *182*, 1945–2007.

[76] Bendikov, M.; Wudl, F.; Perepichka, D. F. *Chem. Rev.* **2004**, *104*, 4891–4946.

[77] Blanchard, P.; Salle, M.; Duguay, G.; Jubault, M.; Gorgues, A. *Tetrahedron Lett.* **1992**, *33*, 2685–2688.

[78] Steimecke, G.; Sieler, H. J.; Kirmse, R.; Hoyer, E. *Phosphor. Sulf.* **1979**, *7*, 49–55.

[79] Parg, R. P.; Kilburn, J. D.; Ryan, T. G. *Synthesis* **1994**, 195–198.

[80] Moore, A. J.; Bryce, M. R. *Tetrahedron Lett.* **1992**, *33*, 1373–1376.

[81] Svenstrup, N.; Becher, J. *Synthesis* **1995**, 215–235.

[82] Gorgues, A.; Hudhomme, P.; Salle, M. *Chem. Rev.* **2004**, *104*, 5151–5184.

[83] Green, D. C. *J. Org. Chem.* **1979**, *44*, 1476–1479.

[84] Simonsen, K. B.; Svenstrup, N.; Lau, J.; Simonsen, O.; Kristensen, G. J.; Becher, J. *Synthesis* **1996**, 407–418.

[85] Lau, J.; Simonsen, O.; Becher, J. *Synthesis* **1995**, 521–526.

[86] Moore, A. J.; Bryce, M. R. *J. Chem. Soc. Perkin Trans. 1* **1991**, 157–168.

[87] Nielsen, M. B.; Moonen, N. N. P.; Boudon, C.; Gisselbrecht, J.-P.; Seiler, P.; Gross, M.; Diederich, F. *Chem. Commun.* **2001**, 1848–1849.

[88] Kato, S.-i.; Diederich, F. *Chem. Commun.* **2010**, *46*, 1994–2006.

[89] Illescas, B. M.; Santos, J.; Wielopolski, M.; Atienza, C. M.; Martin, N.; Guldi, D. M. *Chem. Commun.* **2009**, 5374–5376.

[90] Illescas, B. M.; Santos, J.; Diaz, M. C.; Martin, N.; Atienza, C. M.; Guldi, D. M. *Eur. J. Org. Chem.* **2007**, 5027–5037.

[91] Yang, X.; Zhang, G.; Zhang, D.; Zhu, D. *Langmuir* **2010**, *26*, 11720–11725.

[92] Santos, J.; Grimm, B.; Illescas, B. M.; Guldi, D. M.; Martin, N. *Chem. Commun.* **2008**, 5993–5995.

[93] Shao, M.; Zhao, Y. *Tetrahedron Lett.* **2009**, *50*, 6897–6900.

[94] Shao, M.; Zhao, Y. *Tetrahedron Lett.* **2010**, *51*, 2508–2511.

[95] Shao, M.; Zhao, Y. *Tetrahedron Lett.* **2010**, *51*, 2892–2895.

[96] Shao, M.; Dongare, P.; Dawe, L. N.; Thompson, D. W.; Zhao, Y. *Org. Lett.* **2010**, *12*, 3050–3053.

[97] Bryce, M. R.; Coffin, M. A.; Skabara, P. J.; Moore, A. J.; Batsanov, A. S.; Howard, J. A. K. *Chem. Eur. J.* **2006**, *6*, 1955–1962.

[98] Guerro, M.; Lorcy, D. *Tetrahedron Lett.* **2005**, *46*, 5499–5502.

[99] Osada, M.; Kumagai, T.; Sugimoto, M.; Nishida, J.; Yamashita, Y. *Synth. Met.* **2005**, *152*, 429–432.

[100] Sarhan, A. A. O.; Bolm, C. *Synthesis* **2009**, 1000–1006.

[101] Hascoat, P.; Lorcy, D.; Robert, A.; Carlier, R.; Tallec, A.; Boubekeur, K.; Batail, P. *J. Org. Chem.* **1997**, *62*, 6086–6089.

[102] Lorcy, D.; Carlier, R.; Robert, A.; Tallec, A.; Le Magueres, P.; Ouahab, L. *J. Org. Chem.* **1995**, *60*, 2443–2447.

[103] Amriou, S.; Perepichka, I. F.; Batsanov, A. S.; Bryce, M. R.; Rovira, C.; Vidal-Gancedo, J. *Chem. Eur. J.* **2006**, *12*, 5481–5494.

[104] Lorcy, D.; Guerro, M.; Pellon, P.; Carlier, R. *Chem. Commun.* **2004**, 212–213.

[105] Priego, E. M.; Sanchez, L.; Angeles Herranz, M.; Martin, N.; Viruela, R.; Orti, E. *Org. Biomol. Chem.* **2007**, *5*, 1201–1209.

[106] Guerro, M.; Carlier, R.; Boubekeur, K.; Lorcy, D.; Hapiot, P. *J. Am. Chem. Soc.* **2003**, *125*, 3159–3167.

[107] Guerro, M.; Pham, N. H.; Massue, J.; Bellec, N.; Lorcy, D. *Tetrahedron* **2008**, *64*, 5285–5290.

[108] Massue, J.; Bellec, N.; Guerro, M.; Bergamini, J.-F.; Hapiot, P.; Lorcy, D. *J. Org. Chem.* **2007**, *72*, 4655–4662.

[109] Perez, E. M.; Sierra, M.; Sanchez, L.; Torres, M. R.; Viruela, R.; Viruela, P. M.; Orti, E.; Martin, N. *Angew. Chem. Int. Ed.* **2007**, *46*, 1847–1851.

[110] Chen, G.; Wang, L.; Thompson, D. W.; Zhao, Y. *Org. Lett.* **2008**, *10*, 657–660.

[111] Chen, G.; Dawe, L.; Wang, L.; Zhao, Y. *Org. Lett.* **2009**, *11*, 2736–2739.

[112] Bryce, M. R.; Moore, A. J. *Synthesis* **1991**, 26–28.

[113] Ito, Y.; Matsuura, T. *Tetrahedron Lett.* **1975**, *31*, 1373–1380.

[114] Chen, G.; Zhao, Y. *Tetrahedron Lett.* **2006**, *47*, 5069–5072.

[115] Nevado, C.; Echavarren, A. M. *Synthesis* **2005**, 167–182.

[116] Treitel, N.; Eshdat, L.; Sheradsky, T.; Donovan, P. M.; Tykwinski, R. R.; Scott, L. T.; Hopf, H.; Rabinovitz, M. *J. Am. Chem. Soc.* **2006**, *128*, 4703–4709.

[117] Shen, H.-C.; Tang, J.-M.; Chang, H.-K.; Yang, C.-W.; Liu, R.-S. *J. Org. Chem.* **2005**, *70*, 10113–10116.

[118] Christensen, C. A.; Batsanov, A. S.; Bryce, M. R. *J. Org. Chem.* **2007**, *72*, 1301–1308.

[119] Christensen, C. A.; Bryce, M. R.; Batsanov, A. S.; Becher, J. *Org. Biomol. Chem.* **2003**, *1*, 511–522.

[120] Gautier, N.; Samuel, R.; Sahin, Y.; Levillain, E.; Leroy-Lhez, S.; Hudhomme, P. *Org. Lett.* **2004**, *6*, 1569–1572.

[121] Giffard, M.; Mabon, G.; Leclair, E.; Mercier, N.; Allain, M.; Gorgues, A.; Molinie, P.; Neilands, O.; Krief, P.; Khodorkovsky, V. *J. Am. Chem. Soc.* **2001**, *123*, 3852–3853.

[122] Shao, M.; G. Chen, G.; Zhao, Y. *SYNLETT* **2008**, 371–376.

[123] Chen, G.; Shao, M.; Wang, L.; Zhao, Y. *Asian Chem. Lett.* **2007**, *11*, 185–196.

[124] Bowling, N. P.; McMahon, R. J. *J. Org. Chem.* **2006**, *71*, 5841–5847.

[125] Sorg, A.; K., S.; Bruckner, R. *Chem. Eur. J.* **2005**, *11*, 1610–1624.

[126] Leibrock, B.; Vostrowsky, O.; Hirsch, A. *Eur. J. Org. Chem.* **2001**, 4401–4409.

[127] Lange, T.; van Loon, J.-D.; Tykwinski, R. R.; Schreiber, M.; Diederich, F. *Synthesis* **1996**, 537–550.

[128] Bryce, M. R.; Coffin, M. A.; Skabara, . P. J.; Moore, A. J.; Batsanov, A. S.; Howard, J. A. K. *Chem. Eur. J.* **2000**, *6*, 1955–1962.

[129] Zhao, Y.; Shirai, Y.; Slepkov, D. A.; Alemany, L. B.; Sasaki, . T.; Hegmann, F. A.; Tour, J. M. *Chem. Eur. J.* **2005**, *11*, 3643–3658.

[130] Bogaschenko, T.; Basok, S.; Kulygina, C.; Lyapunov, A.; Lukyanenko, N. *Synthesis* **2002**, 2266–2270.

[131] Pedersen, C. J. *J. Am. Chem. Soc.* **1967**, *89*, 7017–7036.

[132] Mohler, D. L.; Shen, G. *Org. Biomol. Chem.* **2006**, *4*, 2082–2087.

[133] Bryce, M. R.; Moore, A. J.; Hasan, M.; Ashwell, G. J.; Fraser, A. T.; Clegg, W.; Hursthouse, M. B.; Karaulov, A. I. *Angew. Chem. Int. Ed. Engl.* **1990**, *29*, 1450–1452.

[134] Chen, G. M.Sc. thesis, Memorial University, 2007.

[135] Lu, X.-X.; Li, C.-K.; Cheng, E. C.-C.; Zhu, N.; Yam, V. W.-W. *Inorg. Chem.* **2004**, *43*, 2225–2227.

[136] Klyatskaya, S. V.; Tretyakov, E. V.; Vasilevsky, S. F. *ARKIVOC* **2003**, *xiii*, 21–34.

[137] Anthony, J.; Boldi, A. M.; Rubin, Y.; Hobi, M.; Gramlieha, V.; Knobler, C. B.; Seilerd, P.; Diederich, F. *Helv. Chim. Acta.* **1995**, *78*, 13–45.

[138] Harris, N. J.; Gajewski, J. J. *J. Am. Chem. Soc.* **1994**, *116*, 6121–6129.

[139] Jiang, X.; Yang, X.; Zhao, C.; Sun, L. *J. Phys. Org. Chem.* **2009**, *22*, 1–8.

[140] Khanous, A.; Gorgues, A.; Texier, F. *Tetrahedron Lett.* **1990**, *31*, 7307–7310.

[141] Khanous, A.; Gorgues, A.; Jubault, M. *Tetrahedron Lett.* **1990**, *31*, 7311–7314.

[142] Qvortrup, K.; Jakobsen, M. T.; Gisselbrecht, J.-P.; Boudon, C.; Jensen, F.; Nielsen, S. B.; Nielsen, M. B. *J. Mater. Chem.* **2004**, *14*, 1768–1773.

[143] Luu, T.; Elliott, E.; Slepkov, A. D.; Eisler, S.; McDonald, R.; Hegmann, F. A.; Tykwinski, R. R. *Org. Lett.* **2005**, *7*, 51–54.

[144] Eisler, S.; Slepkov, A. D.; Elliott, E.; Luu, T.; McDonald, R.; Hegmann, F. A.; Tykwinski, R. R. *J. Am. Chem. Soc.* **2005**, *127*, 2666–2676.

[145] Sarkar, A.; Okada, S.; Komatsu, K.; Nakanishi, H.; Matsuda, H. *Macromolecules* **1998**, *31*, 5624–5630.

[146] Li, Z.; Fowler, F. W.; Lauher, J. W. *J. Am. Chem. Soc.* **2009**, *131*, 634–643.

[147] Lauher, J. W.; Fowler, F. W.; Goroff, N. S. *Acc. Chem. Res.* **2008**, *41*, 1215–1229.

[148] Inayama, S.; Tatewaki, Y.; Okada, S. *Polym. J.* **2010**, *42*, 201–207.

[149] Zhou, N.; Zhao, Y. *J. Org. Chem.* **2010**, *75*, 1498–1516.

[150] Ding, L.; Olesik, S. V. *Chem. Mater.* **2005**, *17*, 2353–2360.

[151] Zhou, N.; Merschrod S, E. F.; Zhao, Y. *J. Am. Chem. Soc.* **2005**, *127*, 14154–14155.

[152] Jahnke, E.; Lieberwirth, I.; Severin, N.; Rabe, J. P.; Frauenrath, H. *Angew. Chem. Int. Ed.* **2006**, *45*, 5383–5386.

[153] Chen, G.; Mahmud, I.; Dawe, L.; Zhao, Y. *Org. Lett.* **2010**, *12*, 704–704.

[154] Chen, G.; Mahmud, I.; Dawe, L. N.; Lee, D.; Zhao, Y. *J. Org. Chem.* **2011**,

[155] Chen, G.; Bouzan, S.; Zhao, Y. *Tetrahedron Lett.* **2010**, *51*, 6552–6556.

[156] Mahmud, I. Ph.D. thesis, Memorial University, 2009.

[157] Chalifoux, W. A.; Tykwinski, R. R. *Nature Chem.* **2010**, *2*, 967.

[158] Gomar-Nadal, E.; Mugica, L.; Vidal-Gancedo, J.; Casado, J.; Navarrete, J. T. L.; Veciana, J.; Rovira, C.; Amabilino, D. B. *Macromolecules* **2007**, *40*, 7521–7531.

[159] Wang, C.; Batsanov, A. S.; Bryce, M. R. *Chem. Commun.* **2004**, 578–579.

[160] Perepichka, D. F.; Bryce, M. R.; Batsanov, A. S.; McInnes, E. J. L.; Zhao, J. P.; Farley, R. D. *Chem. Eur. J.* **2002**, *8*, 4656–4669.

[161] Bonger, K. M.; van den Berg, R. J. B. H. N.; Heitman, L. H.; IJzerman, A. P.; Oosterom, J.; Timmers, C. M.; Overkleeft, H. S.; van der Marel, G. A. *Bioorg. Med. Chem.* **2007**, *15*, 4841–4856.